

**Insights into the transcriptome and ROS signaling of *Arabidopsis thaliana* root tips during Pi deficiency response**

**Dissertation**

zur Erlangung des

Doktorgrades der Agrarwissenschaften (Dr. agr.)

der

Naturwissenschaftlichen Fakultät III

Agrar- und Ernährungswissenschaften, Geowissenschaften  
und Informatik

der Martin-Luther-Universität Halle-Wittenberg



vorgelegt

von Frau Mingdan Deng

geb. am 08.05.1990 in Taiyuan, Shanxi, China

Gutachter:

I. Prof. Dr. Quint Marcel

II. Prof. Dr. Abel Steffen

III. PD Dr. Schäffner Anton R

Tag der öffentlichen Verteidigung: 20.03.2023

# TABLE OF CONTENTS

<b>SUMMARY</b> .....	<b>iv</b>
<b>LIST OF FIGURES</b> .....	<b>v</b>
<b>LIST OF TABLES</b> .....	<b>vi</b>
<b>LIST OF SUPPLEMENTARY FIGURES</b> .....	<b>vii</b>
<b>LIST OF SUPPLEMENTARY TABLES</b> .....	<b>ix</b>
<b>ABBREVIATIONS AND SYMBOLS</b> .....	<b>x</b>
<b>1. INTRODUCTION</b> .....	<b>1</b>
1.1 Importance of phosphorus .....	1
1.2 Plant adaptation to Pi deficiency.....	1
1.3 Molecular mechanisms of local Pi sensing at the root tip.....	4
1.4 ‘Omics’ approaches towards understanding local Pi sensing.....	6
1.5 Reactive oxygen species (ROS) and their role in root development .....	8
1.5.1 ROS production and scavenging .....	9
1.5.2 Tools for ROS detection .....	11
1.5.3 Role of ROS in regulating primary root growth .....	12
1.6 Aim of the present work.....	16
<b>2. RESULTS</b> .....	<b>18</b>
2.1 Analysis of Pi-dependent transcriptomes in <i>Arabidopsis thaliana</i> root tips .....	18
2.1.1 Rationale.....	18
2.1.2 The degree of differential mRNA expression correlates with genotype-dependent sensitivity to Pi limitation .....	18
2.1.3 Genotype-dependent root tip transcriptomes in Pi sufficiency.....	20
2.1.4 Identification of genotype-independent Pi-responsive genes .....	22
2.1.5 Enrichment analysis of genotype-dependent Pi-responsive genes.....	23
2.1.6 Identification of local Pi-responsive genes .....	28
2.1.7 Pi depletion alters expression of redox signaling-related genes.....	33
2.2 Functional characterization of the <i>PIP</i> gene family during the local Pi deficiency response .....	37
2.2.1 Rationale.....	37

---

2.2.2	Expression analysis of <i>PIP</i> promoter reporter lines.....	37
2.2.3	Primary root growth characterization of <i>pip</i> mutants .....	38
2.3	Analysis of ROS signaling in root tips during the local Pi deficiency response.....	40
2.3.1	Rationale.....	40
2.3.2	Analysis of select ROS-related mutants.....	40
2.3.3	Monitoring of ROS accumulation in root tips.....	41
2.3.4	Effect of diphenylene iodonium on primary root length in low Pi.....	46
2.3.5	Monitoring of cellular redox potential in root tips.....	46
<b>3.</b>	<b>DISCUSSION AND FUTURE PERSPECTIVES .....</b>	<b>52</b>
3.1	Transcriptome analysis of Pi-deficient root tips.....	52
3.1.1	Trehalose metabolism may involve in local Pi response .....	53
3.1.2	ROS may involve in local Pi response as signaling molecules.....	54
3.2	Influence of Pi deficiency on ROS generation .....	59
3.3	Role of PIPs in Pi deficiency response .....	62
<b>4.</b>	<b>MATERIALS AND METHODS.....</b>	<b>64</b>
4.1	Materials.....	64
4.1.1	Chemicals.....	64
4.1.2	Media.....	64
4.1.3	Plant materials and cultivation.....	65
4.1.3.1	Plant lines .....	65
4.1.3.2	Plant cultivation.....	67
4.1.4	Bacteria.....	67
4.2	Methods.....	67
4.2.1	Molecular biology methods.....	67
4.2.1.1	Isolation of genomic DNA for genotyping .....	67
4.2.1.2	Isolation of genomic DNA from <i>E. coli</i> .....	68
4.2.1.3	Genotyping .....	68
4.2.2	Transformation.....	69
4.2.2.1	<i>E.coli</i> heat-shock transformation .....	69
4.2.2.2	<i>Agrobacterium tumefaciens</i> cold-shock transformation.....	69
4.2.2.3	<i>Agrobacterium-mediated</i> plant stable transformation.....	69
4.2.2.4	Selection of transformed Arabidopsis plants .....	70
4.2.3	Histochemical analysis.....	70
4.2.3.1	GUS ( $\beta$ -glucuronidase) staining .....	70
4.2.3.2	NBT staining.....	70
4.2.4	Fluorescence ROS probes staining.....	70
4.2.4.1	Carboxy-H <sub>2</sub> DCFDA staining .....	71

4.2.4.2	DHE staining.....	71
4.2.4.3	BES- H <sub>2</sub> O <sub>2</sub> -Ac .....	71
4.2.4.4	HPF.....	71
4.2.5	Confocal laser scanning microscopy (CLSM) .....	72
4.2.6	Ratiometric analysis of roGFP2.....	73
4.2.7	Root length measurement assay .....	73
4.2.8	Analysis of protein from plant tissues .....	73
4.2.8.1	Protein extraction from seedlings .....	73
4.2.8.2	Sodium dodecyl sulfate polyacrylamide gel electrophoresis (SDS-PAGE) and immunoblotting.....	74
4.2.9	Diphenylene iodonium (DPI) treatment .....	74
4.2.10	RNA preparation and RNA-seq analysis.....	75
4.2.11	<i>In silico</i> data analysis .....	75
<b>5.</b>	<b>REFERENCES.....</b>	<b>77</b>
<b>6.</b>	<b>APPENDIX .....</b>	<b>93</b>
<b>7.</b>	<b>ACKNOWLEDGEMENT .....</b>	<b>134</b>
<b>8.</b>	<b>CURRICULUM VITAE.....</b>	<b>136</b>
<b>9.</b>	<b>STATUTORY DECLARATION.....</b>	<b>137</b>

## SUMMARY

*Arabidopsis thaliana* inhibits its primary root growth to promote topsoil foraging and Pi acquisition upon Pi limitation. Root tips locally sense external Pi limitation and adjust root growth by rapid inhibition of cell expansion (<2 h) and progressive arrest of cell division (<2 days). Multicopper oxidases LOW PHOSPHATE ROOT 1 (LPR1), LPR2 and single P5-type ATPase PHOSPHATE DEFICIENCY RESPONSE2 (PDR2) are key players in root tip Pi sensing, mediating the accumulation of Fe, reactive oxygen species (ROS), and callose in stem cell niche (SCN) during Pi limitation. The low Pi-induced arrest of root growth involves transcriptional reprogramming. Although a set of transcriptomic profiling studies have been performed in *Arabidopsis* roots upon Pi limitation, less is known in root tips. The identification of genes and pathways that are involved in the local Pi deficiency response in root tips and an understanding of the mechanism by which ROS work as signals were the major aims of this work.

RNA-seq analysis uncovered 373, 2343, and 15 differentially expressed genes (DEGs) in the wild-type (WT), hypersensitive *pdr2* mutant, and insensitive *lpr1lpr2* line, respectively (upon Pi limitation for one day). Among those DEGs, 267 are shared between WT and *pdr2* only. Four known systemic Pi starvation-induced genes (*SPX1*, *AT4*, *PAP17*, and *GDPD1*) were upregulated in all lines, suggesting the maintenance of systemic responses in all lines. An overrepresentation of genes that are involved in trehalose metabolism, cell wall biogenesis, ethylene and auxin response as well as regulation of transcription were induced in Pi-starved WT and *pdr2*. Moreover, numerous genes associated with ROS generation and scavenging (*PRXs*, *FSD1*, *GSTFs*, *CATs*), signaling (*ERFs*, *PDLP1*) as well as response to oxidative stress (*AER*, *DIN10*, *SIP2*), were induced in WT and/or *pdr2* upon Pi limitation. Additionally, 11 ROS-related transcription factors were identified that were commonly induced in Pi-starved WT and *pdr2*.

PLASMA MEMBRANE INTRINSIC PROTEIN 1;4 (PIP1;4) has been proposed to transport H<sub>2</sub>O<sub>2</sub> from apoplast into cytosol to influence callose deposition. Analysis of RNA-seq and promoter-reporter lines revealed that some PIPs were differentially expressed in Pi-starved root tips of WT and/or *pdr2*. However, no obvious root length phenotypes were observed in all 13 *pip* single mutants and *pip1;3 pip1;4* upon Pi deficiency. PIPs seem not essential for low Pi-induced primary root growth inhibition and ROS signaling mediated callose deposition. In line with the RNA-seq results, a burst of ROS was detected in the SCN of WT and *pdr2* after exposed to low Pi for one day. In addition, Pi limitation increased the superoxide level in the root apical meristem of WT and *pdr2*. RNA-seq analysis point to the role of ROS in regulating callose deposition, cell wall dynamics and SCN regeneration as signaling molecules upon Pi limitation.

## LIST OF FIGURES

Fig. 1-1: Arabidopsis root architectural adaptation to phosphate limitation and root tip structure .....	3
Fig. 1-2: Model of local Pi sensing at Arabidopsis root tips .....	5
Fig. 1-3: An overview of the major ROS production enzymes and processing pathways in plants .....	10
Fig. 2-1: Primary root growth inhibition during Pi deficiency and sample collection for RNA-seq analysis	19
Fig. 2-2: Statistical analysis of comparative gene expression analysis.....	20
Fig. 2-3: GO biological process term analysis of upregulated genes specific for <i>pdr2</i> vs. WT under +Pi condition.....	21
Fig. 2-4: Comparison of differentially expressed genes in <i>pdr2</i> and <i>lpr1lpr2</i> vs. WT.....	22
Fig. 2-5: Comparison of Pi-dependent differentially expressed genes in WT, <i>pdr2</i> and <i>lpr1lpr2</i> .....	23
Fig. 2-6: Heatmap of select local and systemic Pi response gene expression in WT, <i>pdr2</i> and <i>lpr1lpr2</i> root tips. ....	24
Fig. 2-7: GO biological process term analysis of Pi-responsive genes in WT.....	25
Fig. 2-8: GO biological process term analysis of Pi-responsive genes in <i>pdr2</i> .....	27
Fig. 2-9: GO biological process term analysis of Pi-responsive genes in <i>lpr1lpr2</i> .....	28
Fig. 2-10: Hierarchical clustering analysis of Pi-responsive genes in WT and <i>pdr2</i> .....	29
Fig. 2-11: STRING network analysis of Pi-responsive genes identified from hierarchical clustering analysis .....	32
Fig. 2-12: Pi deficiency induced the expression of oxidative stress-responsive genes in WT and <i>pdr2</i> .....	34
Fig. 2-13: Transcript level heat map of <i>PIPs</i> in WT, <i>pdr2</i> and <i>lpr1lpr2</i> during Pi deficiency .....	36
Fig. 2-14: Transcript level heat map of callose-related genes in WT, <i>pdr2</i> and <i>lpr1lpr2</i> during Pi deficiency .....	37
Fig. 2-15: Tissue-specific expression analysis of <i>PIPs</i> .....	38
Fig. 2-16: Comparison of primary root inhibition among all <i>pip</i> single mutants and WT seedlings .....	39
Fig. 2-17: Comparison of primary root inhibition among <i>pip</i> higher order mutants and WT seedlings.....	40
Fig. 2-18: Comparison of primary root inhibition among oxidative stress-related mutants and WT seedlings .....	41
Fig. 2-19: ROS accumulation in Pi-sufficient and Pi-deprived root tips.....	42
Fig. 2-20: Distribution of superoxide in root tips visualized by NBT staining during low Pi response .....	43
Fig. 2-21: Distribution of superoxide in root tips visualized by DHE staining during low Pi response.....	44
Fig. 2-22: H <sub>2</sub> O <sub>2</sub> levels in root tips during low Pi response .....	45

---

Fig. 2-23: Distribution of $\cdot\text{OH}$ in root tips during low Pi response .....	45
Fig. 2-24: Effect of a superoxide scavenger on the primary root growth during low Pi response.....	46
Fig. 2-25: 405 nm triggered autofluorescence and detection of Grx1-roGFP2 in response to Pi deficiency .....	47
Fig. 2-26: Response of cytosolic Grx1-roGFP2 to Pi deficiency in the RAM of WT.....	49
Fig. 2-27: Response of cytosolic Grx1-roGFP2 to Pi deficiency in the RAM of <i>lpr1lpr2</i> and <i>pdr2</i> .....	50
Fig. 2-28: Response of cytosolic Grx1-roGFP2 to Pi deficiency in the QC of WT.....	51
Fig. 4-1: Scheme of the experiment procedure.....	72



## LIST OF TABLES

Tab. 1-1: Overview of ROS detection tools .....	12
Tab. 2-1: All differentially expressed genes in <i>lpr1lpr2</i> vs. WT. ....	22
Tab. 2-2: Commonly regulated genes in WT, <i>pdr2</i> and <i>lpr1lpr2</i> in response to Pi deficiency. ....	23
Tab. 2-3: Select genes that may regulate local Pi response. ....	33
Tab. 2-4: All ROS related transcription factors that were commonly regulated in WT and <i>pdr2</i> . ....	35
Tab. 2-5: Select oxidative stress responsive genes that were studied further. ....	41
Tab. 4-1: Media composition .....	64
Tab. 4-2: Mutants analyzed in this study .....	65
Tab. 4-3: Transgenic lines analyzed in this study .....	66
Tab. 4-4: Components of PCR reaction .....	68
Tab. 4-5: PCR program.....	69
Tab. 4-6: Composition of SDS-PAGE Gel.....	74

## LIST OF SUPPLEMENTARY FIGURES

Fig. S6-1: KEGG pathway analysis of Pi-responsive genes in <i>pdr2</i> .....	93
Fig. S6-2: Analysis of low Pi-responsive genes that were shared between WT and <i>pdr2</i> .....	94
Fig. S6-3: Comparison of primary root inhibition between <i>upb1</i> and WT .....	94
Fig. S6-4: Expression analysis of <i>PIPs</i> in seedlings by GUS staining.....	95
Fig. S6-5: 405 nm triggered autofluorescence in root tips of WT .....	95
Fig. S6-6: Response of cytosolic Grx1-roGFP2 to Pi deficiency in the QC of WT, related to Fig. 2-28 .....	96

## LIST OF SUPPLEMENTARY TABLES

Tab. S6-1: GO-enrichment analysis of 259 genes that were upregulated in <i>pdr2</i> vs. WT under +Pi condition.....	96
Tab. S6-2: GO-enrichment analysis of 288 genes that were upregulated in Pi-starved WT.....	97
Tab. S6-3: GO-enrichment analysis of 85 genes that were downregulated in Pi-starved WT.....	98
Tab. S6-4: GO-enrichment analysis of 1472 genes that were upregulated in Pi-starved <i>pdr2</i> .....	98
Tab. S6-5: GO-enrichment analysis of 871 genes that were downregulated in Pi-starved <i>pdr2</i> .....	100
Tab. S6-6: GO-enrichment analysis of 14 genes that were upregulated in Pi-starved <i>lpr1lpr2</i> .....	101
Tab. S6-7: Differentially expressed oxidative stress responsive genes in Pi-starved WT and <i>pdr2</i> and in <i>pdr2</i> compared to WT under +Pi condition.....	101
Tab. S6-8: 5 clusters of genes that were identified in hierarchical clustering analysis.....	103
Tab. S6-9: 68 differentially expressed ROS related transcription factors in Pi-starved WT and <i>pdr2</i> and expression level of <i>PSK5</i> and <i>WOX5</i> .....	120
Tab. S6-10: 42 predicted differentially expressed transcription factors in Pi-starved WT and <i>pdr2</i> that may regulate <i>PRXs</i> .....	122
Tab. S6-11: Expression levels of 13 <i>PIPs</i> in WT, <i>pdr2</i> and <i>lpr1lpr2</i> .....	123
Tab. S6-12: Differentially expressed callose related genes in Pi-starved WT and <i>pdr2</i> .....	123
Tab. S6-13: Differentially expressed <i>TPS</i> and <i>TPP</i> in WT and <i>pdr2</i> .....	124
Tab. S6-14: Expression levels of select local and systemic low Pi responsive genes in WT, <i>pdr2</i> and <i>lpr1lpr2</i> .....	124
Tab. S6-15: KEGG pathway analysis of up- and down-regulated genes in Pi-starved WT.....	125
Tab. S6-16: GO-enrichment analysis of 218 genes that were upregulated in both WT and <i>pdr2</i> upon Pi limitation.....	125
Tab. S6-17: GO-enrichment analysis of 146 genes that were more highly induced in Pi-starved <i>pdr2</i> compared to WT.....	126
Tab. S6-18: Primers used for genotyping.....	126

## ABBREVIATIONS AND SYMBOLS

$^1\text{O}_2$	Singlet oxygen
ACHT5	ATYPICAL CYS HIS RICH THIOREDOXIN 5
Al	Aluminum
ALMT1	ALUMINUM-ACTIVATED MALATE TRANSPORTER1
APX	Ascorbate peroxidase
ASC	Ascorbate acid
<i>At</i> [gene name]	<i>Arabidopsis thaliana</i> [gene name]
ATP	Adenosine triphosphate
BG	$\beta$ -(1,3)-glucanase
BR	Brassinosteroid
CalS	Callose synthase
Carboxy-H2DCFDA	5-(and 6)-carboxy-2',7'-dichlorodihydrofluorescein diacetate
CAT	Catalase
cDNA	Complementary deoxyribonucleic acid
ChIP	Chromatin immunoprecipitation
CML41	CALMODULINLIKE41
Col-0	Columbia-0
DAB	Diaminobenzidine
DEGs	Differentially expressed genes
DHE	Dihydroethidium
DMTU	Dimethylthiourea
DNA	Deoxyribonucleic acid
e.g.	exempli gratia – for example
EDTA	Ethylenediaminetetraacetic acid
$E_{GSH}$	Glutathione redox potential
ER	Endoplasmic reticulum

ERF	ETHYLENE RESPONSE FACTOR
et al.	et alii- and others
EZ	Elongation zone
FC	Fold change
Fe	Iron
FER1	FERRETIN 1
FPKM	Fragments Per Kilobase of transcript sequence per Million base pairs sequenced
FRD3	FERRIC REDUCTASE DEFECTIVE 3
GFP	Green fluorescent protein
GO	Gene ontology
GR	Glutathione reductase
GRX	Glutaredoxin
GSH	Glutathione
GSSG	Oxidized glutathione
GSTF	GLUTATHIONE-S-TRANSFERASE
GUS	B-glucuronidase
h	Hour(s)
H <sub>2</sub> O <sub>2</sub>	Hydrogen peroxide
H <sub>2</sub> O <sub>2</sub> -BES-Ac	H <sub>2</sub> O <sub>2</sub> -3'-O-acetyl-6'-O-pentafluorobenzenesulfonyl-2'-7'-difluorofluorescein-Ac
HPF	Hydroxyphenyl fluorescein
IQD16	IQ67 DOMAIN 16
IRT1	IRON-RELATED TRANSPORTER 1
kDa	Kilodaltons
KEGG	Kyoto encyclopedia of genes and genomes
LPR1	LOW PHOSPHATE RESPONSE 1
LPR1	LOW PHOSPHATE ROOT 1
LSM	Laser scanning microscope
M	Molar

mg	Milligram
min	Minute(s)
mM	Milli molar
mm	Millimetre
Mr	Relative molecular mass
mRNA	Messenger ribonucleic acid
MZ	Maturation zone
NASC	Nottingham Arabidopsis Stock Centre
NBT	Nitro blue tetrazolium
NIP	NODULIN 26-LIKE INTRINSIC PROTEIN
nmol	Nano molar
NTR	NADPH-DEPENDENT THIOREDOXIN REDUCTASE
O <sub>2</sub> <sup>-</sup>	Superoxide
OH·	hydroxyl radical
P	Phosphorus
PAP	PURPLE ACID PHOSPHATASE
PCA	Principal component analysis
PDCB	PLASMODESMATA CALLOSE-BINDING PROTEIN
PDLP	PLASMODESMATA-LOCALIZED PROTEIN
PDR2	PHOSPHATE DEFICIENCY RESPONSE2
PHB3	PROHIBITIN3
PHL1	PHR1-LIKE1
PHR1	PHOSPHATE STARVATION RESPONSE 1
Pi	Inorganic phosphate
PIP	PLASMA MEMBRANE INTRINSIC PROTEIN
PlantPAN	Plant Promoter Analysis Navigator
PPC	PHOSPHOENOLPYRUVATE CARBOXYLASE
PPCK	PHOSPHOENOLPYRUVATE CARBOXYLASE KINASE

PRDX	Peroxiredoxin
PR	Primary root
PRX	Class III peroxidase
PSI	Phosphate starvation-induced
PSK	PHYTOSULFOKINE
QC	Quiescent center
RAM	Root apical meristem
RBOH	Respiratory burst oxidase homolog
ROS	Reactive oxygen species
RSA	Root system architecture
SCN	Stem cell niche
SHR	SHORT-ROOT
SOD	Superoxide dismutase
SPX	SYG1, Pho81 and XPR1
STOP1	SENSITIVE TO PROTON TOXICITY1
TF	Transcription factor
TPS	Tre6P synthase
Tre6P	Trehalose 6-phosphate
TPP	Tre6P phosphatase
TRE1	TREHALASE1
TRX	Thioredoxin
TZ	Transition zone
UPB1	UPBEAT1

# 1. INTRODUCTION

## 1.1 Importance of phosphorus

Phosphorus (P) is an essential macro element for plant growth and development. Plants only take up free inorganic phosphate (Pi), mainly in the form of  $\text{H}_2\text{PO}_4^-$  from the soil (Ullricheberius *et al.*, 1984). After absorbing the Pi, plants use it for the synthesis of organic molecules such as nucleic acids, membrane phospholipids, and ATP (Raghothama, 1999; Peret *et al.*, 2011). Pi also plays an essential role in signal transduction processes and regulation of enzyme activity (Poirier & Bucher, 2002; Chiou & Lin, 2011). In soil, 20-80% of P is present in the organic form (Schachtman *et al.*, 1998). The organic P pool comprises a variety of chemical compounds, but the main forms are inositol phosphates, sugar phosphates, phospholipids, and nucleic acids (Hinsinger *et al.*, 2015). By hydrolysis of organic P substrates, Pi is released and becomes accessible to plants (Hinsinger *et al.*, 2015). The availability of Pi (typically around 1–10  $\mu\text{M}$ ) is quite low due to the firm adsorption of the anion onto the large surface areas of clay minerals and metallic oxides (Fe, Al, Ca) (Schachtman *et al.*, 1998; Abel, 2017). Therefore, low Pi availability is a common nutritional stress for plants. Pi limits crop yield on more than 70% of the global cultivated land (Lopez-Arredondo *et al.*, 2014). To increase or maintain crop productivity, Pi-containing fertilizers are supplied in large amounts. However, the fertilization efficiency is very low. Much of the P applied to soil is bound to the soil or is lost through leaching, runoff, and erosion (Bindraban *et al.*, 2020). Over-fertilizing also accelerates soil degradation and water eutrophication. Moreover, non-renewable phosphorus stocks, the primary source of P fertilizer, will likely be depleted within the next century (Steen, 1998; Cordell *et al.*, 2009). Understanding how plants sense and respond to external Pi concentrations at the molecular level will help to breed crops with improved ability to uptake and utilize Pi.

## 1.2 Plant adaptation to Pi deficiency

To cope with Pi deficiency, plants have evolved a diverse set of adaptive responses with the aim of improving Pi acquisition and reallocation and reduction of Pi usage. Some plants can establish symbiotic associations with fungi (arbuscular mycorrhizae) to increase Pi uptake. The exudation of organic anions, such as malate and citrate, into the soil and the apoplastic space helps to solubilize Pi from insoluble Pi metal-complexes (Raghothama, 1999; Plaxton & Tran, 2011). Similarly, plants also secrete phosphodiesterases, purple acid phosphatases, nucleases, and RNases to liberate and recycle Pi from organic matter inside the plant and in the soil (Dissanayaka *et al.*, 2021). P availability usually drops



substantially with soil depth (Lynch & Brown, 2001). Many plants increase the Pi uptake through modifying their root system architecture (RSA). They usually form a shallower root system with more and longer lateral roots, and denser root hairs. The strategy is described as “topsoil foraging”, which enables roots to explore the upper layers of the soil (Lynch & Brown, 2001), which contain larger amounts of Pi. This strategy has been reported in many plant species like bean, rice, and maize as well as the model plant *Arabidopsis thaliana* (Bonser *et al.*, 1996; Lynch & Brown, 2001; Sanchez-Calderon *et al.*, 2005; Zhu *et al.*, 2005; Liu *et al.*, 2013).

## **Study of Pi deficiency responses in *Arabidopsis thaliana***

*Arabidopsis thaliana* is a member of the *Brassicaceae* family. Several features of *Arabidopsis* have made it an optimal model plant to study the molecular mechanisms of local Pi deficiency responses. Those features include a short lifecycle, prolific seed production through self-pollination, and small size that require limited growth facilities. Moreover, *Arabidopsis* has a small, fully sequenced, and well-characterized genome, efficient *Agrobacterium*-mediated transformation procedures, well-established seed libraries, and centralized database.

In *Arabidopsis*, Pi starvation responses can be separated into local and systemic responses (Chiou & Lin, 2011). The local responses generally refer to the modification of the RSA, including the inhibition of the primary root growth, increasing the number and length of lateral roots and root hairs (Fig. 1-1A). These responses are mainly regulated by the Pi availability in the soil solution surrounding the rhizosphere (Chiou & Lin, 2011; Peret *et al.*, 2011). Pi limitation in the rhizosphere is thought to be sensed in root tips to locally inform root development (Ticconi *et al.*, 2004; Svistoonoff *et al.*, 2007). *Arabidopsis* root tip consists of four distinct zones (Fig. 1-1B) (Verbelen *et al.*, 2006). Cells proliferate in the root apical meristem (RAM) and originate in the stem cell niche (SCN), which is composed of the quiescent center (QC) and the stem cells surrounding the QC (Fig. 1-1B). Cells in the QC are mitotically less active and essential for the maintenance of undifferentiated stem cell status (van den Berg *et al.*, 1997). After leaving the RAM, cells enter the transition zone (TZ), where they undergo physiological changes to prepare for their fast elongation in the elongation zone (EZ) (Fig. 1-1B) (Baluska *et al.*, 1996). In the maturation zone (MZ), cells progressively slow down their elongation and root hairs are formed (Fig. 1-1B) (Le *et al.*, 2004). Pi deprivation-induced arrest of primary root growth begins with a rapid reduction of cell elongation in the transition zone followed by the progressive exhaustion of the RAM (Ticconi *et al.*, 2009; Müller *et al.*, 2015; Balzergue *et al.*, 2017). The local response of the primary root to Pi limitation depends on, and is

modulated by, external iron (Fe) availability (Svistonoff *et al.*, 2007; Ward *et al.*, 2008; Ticconi *et al.*, 2009). Removing Fe from the medium rescues the short primary root phenotype upon Pi deficiency (Svistonoff *et al.*, 2007; Ward *et al.*, 2008; Müller *et al.*, 2015). Furthermore, our recent study showed that low Fe availability (2.5-25  $\mu\text{M}$ ) in Pi deficiency gradually and strongly inhibited primary root growth and higher Fe supply (50-100  $\mu\text{M}$ ) cause a minor effect (Naumann *et al.*, 2022).

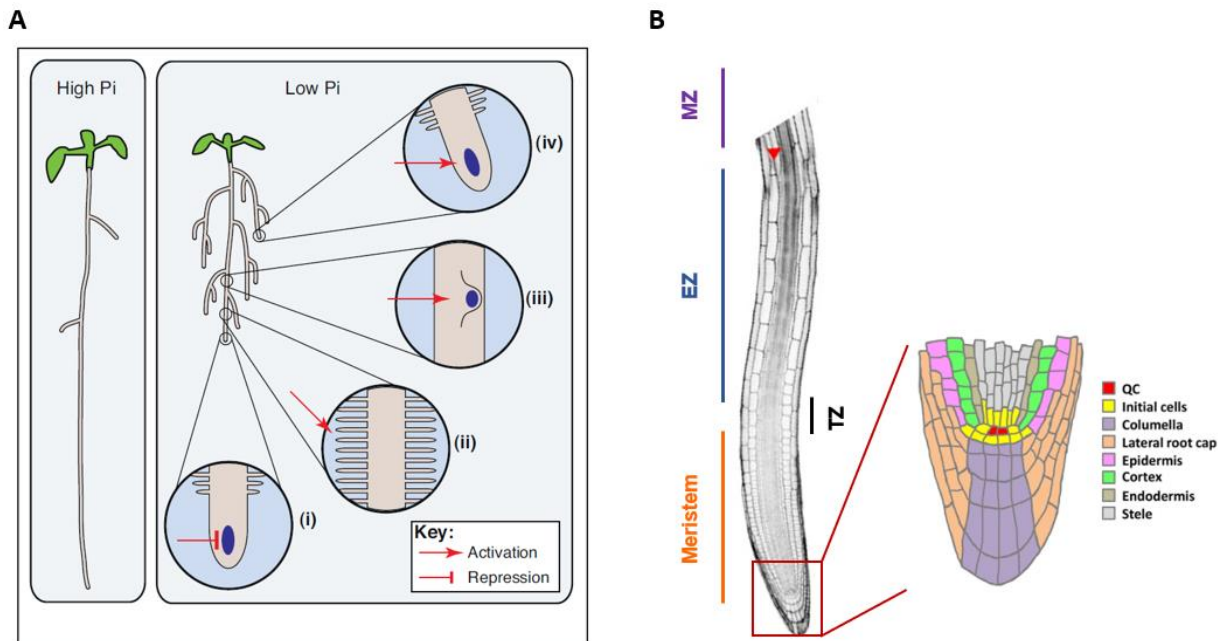


**Fig. 1-1: Arabidopsis root architectural adaptation to phosphate limitation and root tip structure**

(A) Upon Pi limitation, modification of the root system architecture includes (i) inhibition of the primary root growth, (ii) increasing the number and length of root hairs, and (iii & iv) promoting the lateral root formation and growth. Adapted from (Peret *et al.*, 2011). (B) Four distinct zones of the root tip (left figure) and organization of cells in the root tip (right figure). The red arrowhead points to the first root hair bulge. TZ, transition zone. EZ, elongation zone. MZ, maturation zone. QC, quiescent center. Adapted from (Band *et al.*, 2012; Takatsuka & Umeda, 2015).

In contrast, systemic responses depend on the internal Pi concentration and involve processes like enhancement of Pi uptake through activation of Pi transporters, recycling of Pi through catabolism of phospholipids and nucleic acids, and intense Pi recovery through secretion of phosphatases (Meyer *et al.*, 2010; Chiou & Lin, 2011; Remy *et al.*, 2012; Robinson *et al.*, 2012). These adaptations are achieved by the regulation of hundreds of phosphate starvation-induced (PSI) genes (Lan *et al.*, 2015). Several molecular players that are involved in sensing the external and internal P-status have been identified. MYB transcription factor PHOSPHATE STARVATION RESPONSE 1 (PHR1) is one of the key players. PHR1 and its closest homolog PHR1-LIKE1 (PHL1) induce the expression of most PSI genes (Rubio *et al.*, 2001; Bustos *et al.*, 2010). *PHR1* is constitutively expressed and only weakly responsive to Pi deficiency (Rubio *et al.*, 2001).

SPX domain (SYG1, Pho81 and XPR1)-containing proteins can interact with PHR1/PHL and negatively regulate their activity (Lv *et al.*, 2014; Puga *et al.*, 2014; Wang *et al.*, 2014). Under Pi sufficient condition, inositol pyrophosphates (PP-InsPs) are sensed by SPX proteins and lead to the formation of SPX–PHR/PHL complexes in the cytosol, which prevent PHR/PHL from accessing the promoters of their nuclear target genes (Wild *et al.*, 2016; Dong *et al.*, 2019; Ried *et al.*, 2021).

### **1.3 Molecular mechanisms of local Pi sensing at the root tip**

Genetic approaches identified the multicopper oxidases LOW PHOSPHATE ROOT 1 (LPR1), LPR2 and the ATPase PHOSPHATE DEFICIENCY RESPONSE2 (PDR2) as key players in root tip Pi sensing (Ticconi *et al.*, 2004; Reymond *et al.*, 2006; Svistoonoff *et al.*, 2007; Ticconi *et al.*, 2009). *LPR1* codes for a cell wall-targeted multicopper oxidase with ferroxidase activity (Svistoonoff *et al.*, 2007; Müller *et al.*, 2015; Naumann *et al.*, 2022). *PDR2* encodes the single P5-type ATPase that is localized in the endoplasmic reticulum (ER) (Ticconi *et al.*, 2009). Expression pattern of *LPR1* and *PDR2* overlap in specific cell types of the RAM (Ticconi *et al.*, 2009; Müller *et al.*, 2015). The double mutant *lpr1lpr2* is insensitive to Pi deficiency and causes unrestricted primary root growth (Müller *et al.*, 2015; Balzergue *et al.*, 2017). *PDR2* works upstream of *LPR1/LPR2* as indicated by the suppression of the hypersensitive short root phenotype of *pdr2* by *lpr1lpr2* (Ticconi *et al.*, 2009; Müller *et al.*, 2015). *PDR2* is thought to restrict *LPR1* function by unknown mechanisms (Müller *et al.*, 2015). Upon Pi limitation, cell type-specific expressed *LPR1* determines the accumulation of apoplastic Fe<sup>3+</sup> in the SCN, which is accompanied by the generation of reactive oxygen species (ROS) and callose (a  $\beta$ -1,3 glucan) at the same site (Müller *et al.*, 2015) (Fig. 1-2). Callose is a key modulator of plasmodesmata permeability and thus its deposition at the plasmodesmata neck region can influence symplastic trafficking (Amsbury *et al.*, 2017). It has been shown that callose deposition impaired the movement of SHORT-ROOT (SHR), a key transcription factor of the SCN maintenance (Helariutta *et al.*, 2000), from stele into QC and leads to a reduction of root growth (Müller *et al.*, 2015) (Fig. 1-2).

In addition to the *PDR2-LPR1/LPR2* pathway, ALUMINUM-ACTIVATED MALATE TRANSPORTER1 (ALMT1) and the transcription factor SENSITIVE TO PROTON TOXICITY1 (STOP1) also play essential roles in low Pi response. Both genes were identified by a genetic screen for insensitive, *lpr1*-like mutants (Balzergue *et al.*, 2017). They were also found in a *pdr2* suppressor screen for the rescue of the hypersensitive primary

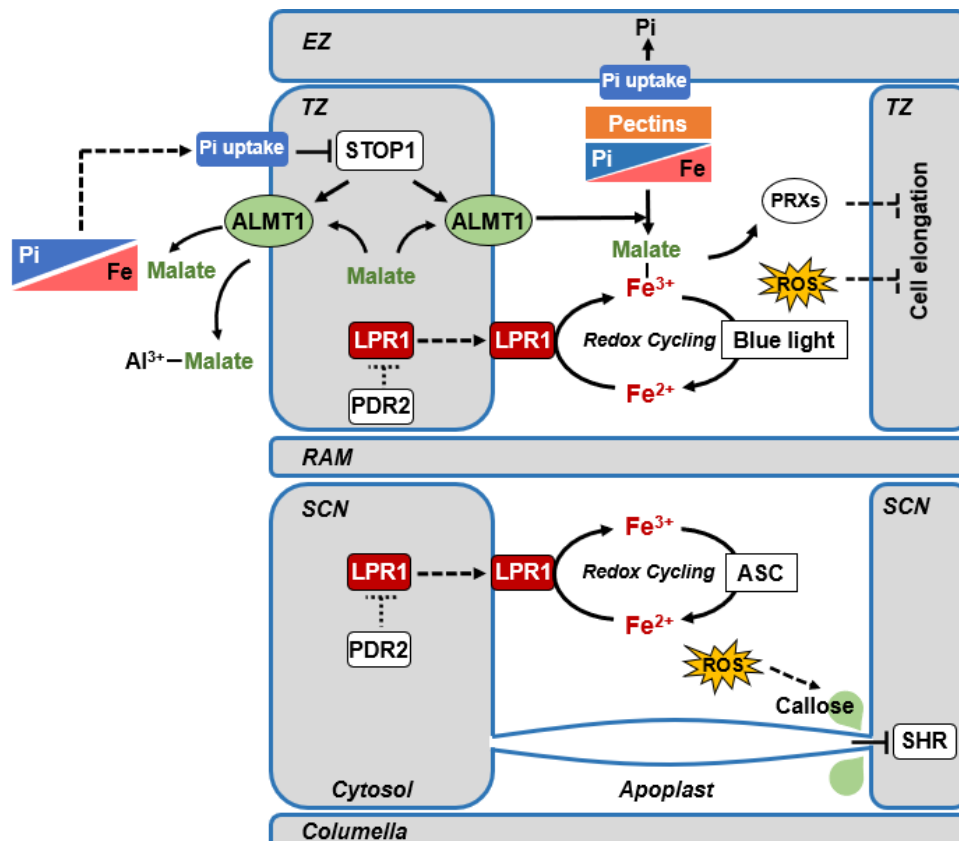


**Fig. 1-2: Model of local Pi sensing at Arabidopsis root tips**

Upon Pi limitation, cell wall localized LPR1 expresses ferroxidase activity and determines the accumulation of apoplastic Fe<sup>3+</sup> in the SCN. ER-targeted PDR2, the single P5-type ATPase, restricts the function of LPR1. It is thought that ROS is generated in the SCN via Fe redox cycling, which leads to callose deposition via unknown ROS signaling. Callose deposition impairs the movement of SHR, causing inhibition of cell division in the RAM. Ascorbate promotes the Fe redox cycle by reducing Fe<sup>3+</sup> to Fe<sup>2+</sup>. Pi limitation stimulates the accumulation of STOP1 in the nucleus, which induces ALMT1 expression. ALMT1-mediated malate release into the apoplast mobilizes Fe<sup>3+</sup> from Fe-Pi or Fe-pectin complexes. Blue light illumination of translucent agar plates promotes photo-Fenton, which reduces Fe<sup>3+</sup> to Fe<sup>2+</sup> for subsequent Fenton reaction and Fe redox cycle. Hydroxyl radicals generated via the Fenton reaction inhibit cell elongation. The STOP1-ALMT1 module and LPR1 ferroxidase activity also inhibit cell elongation by peroxidase-dependent cell wall stiffening. ALMT1-mediated malate exudation in the rhizosphere aids in the solubilization of Pi and the detoxification of Al<sup>3+</sup>. Adapted from (Abel, 2017). RAM, root apical meristem; SCN, stem cell niche; TZ, transition zone; EZ, elongation zone; ER, endoplasmic reticulum; PRXs, class III peroxidases; ASC, ascorbate.

root growth inhibition upon Pi deficiency (Ahmed, 2015). *ALMT1* encodes a malate efflux channel that is localized at the plasma membranes of root cells, which is known to facilitate Al exclusion during Al-toxicity (Hoekenga *et al.*, 2006; Kochian *et al.*, 2015). *STOP1* is a zinc finger-type transcription factor that induces the transcription of *ALMT1* by binding to its promoter, resulting in the excretion of malate to cope with Al toxicity (Tokizawa *et al.*, 2015). Recent studies report that the expression of *ALMT1* is induced by Pi limitation (Balzergue *et al.*, 2017; Mora-Macias *et al.*, 2017). While the expression of *STOP1* is not

responsive to low Pi, *STOP1* abundance is enhanced in the nucleus to activate *ALMT1* expression, which triggers malate exudation into the apoplast of root tips and rhizosphere (Balzergue *et al.*, 2017) (Fig. 1-2). Malate that is excreted into the rhizosphere is likely to mobilize Pi from soil minerals (Narang *et al.*, 2000). It is thought that release of malate into the apoplast helps to mobilize  $\text{Fe}^{3+}$  from cell wall-bound Fe-pectin or Fe-Pi complexes for reduction by ascorbate (Grillet *et al.*, 2014). ROS is generated via Fe redox cycling which may lead to callose deposition (Müller *et al.*, 2015) (Fig. 1-2). It was also proposed that blue light and Pi deficiency-caused low pH promote the reaction of  $\text{Fe}^{3+}$  with malate to produce  $\text{Fe}^{2+}$  via a photo-Fenton reaction (Zheng *et al.*, 2019) (Fig. 1-2). Subsequently, through the Fenton reaction,  $\text{Fe}^{2+}$  reacts with  $\text{H}_2\text{O}_2$  to produce  $\text{Fe}^{3+}$  and hydroxyl radicals ( $\text{OH}\cdot$ ) that then inhibits the primary root growth (Zheng *et al.*, 2019) (Fig. 1-2). Upon Pi starvation, *STOP1*-*ALMT1* modulates the rapid inhibition of cell elongation in the transition zone, whereas the reduction of the RAM is largely *STOP1*-*ALMT1* independent (Balzergue *et al.*, 2017). Moreover, it was shown that Pi limitation triggers peroxidase-dependent cell wall stiffening in the transition zone of WT, and this is absent in *stop1* and *almt1* (Balzergue *et al.*, 2017) (Fig. 1-2).

#### 1.4 ‘Omics’ approaches towards understanding local Pi sensing

‘Omics’ technologies, such as genomics, transcriptomics, proteomics, and metabolomics, have been advanced in the last few decades. ‘Omics’ approaches with the focus on the RNA levels have been utilized extensively to investigate the global gene expression changes during Pi deficiency response. Large suites of genes have been reported to be regulated by Pi. Several novel players and pathways were highlighted.

Based on a split-root experimental design and a subsequent transcriptomic analysis, Thibaud *et al.* identified groups of genes that were locally or systemically regulated by Pi deficiency in the root (Thibaud *et al.*, 2010). Among the genes that were locally upregulated by Pi limitation, over-representative genes are associated with stress-related responses (cytochrome P450 dependent monooxygenases, defense response genes), hormone-related responses (biosynthesis and response to ethylene), and oxidative processes (peroxidase, oxidoreductase, glutathione S-transferase) (Thibaud *et al.*, 2010). Transcription factors implicated in development (*MYB*, *MADS*) or stress (*WRKY*) were also induced by low Pi (Thibaud *et al.*, 2010). Besides, a set of genes involved in cell wall synthesis or cell activity were repressed upon Pi deficiency (Thibaud *et al.*, 2010). Moreover, they identified genes that were systemically upregulated by Pi deficiency, including genes related to Pi recovery or recycling (for instance high-affinity Pi transporters, phosphatases, enzymes involved in phospholipid remobilization, sulfo- and galactolipid synthesis and nucleases), Pi signaling and sensing (*SPX1*, *SPX2*, and *SPX3*) (Thibaud *et al.*, 2010). Interestingly, strong

downregulation of genes associated with metal uptake or transport was observed in the systemic regulation group (Thibaud *et al.*, 2010).

Even though several transcriptomic studies have discovered a surprisingly large number of *PSI* genes, many of these genes are not shared across studies. Through integrating four publicly available transcriptomic data, Lan *et al.* identified a group of genes that were robustly affected by Pi limitation across a wider range of conditions, which were defined as core *PSI* genes (Lan *et al.*, 2015). Those core *PSI* genes consist of 95 genes and 2 genes that were upregulated and downregulated by low Pi, respectively (Lan *et al.*, 2015). Within these 95 genes, the largest group comprises genes related to lipid metabolism and galactolipid biosynthesis (Lan *et al.*, 2015). Another group consists of Pi transporters from the PHT family and the *PHOSPHATE TRANSPORTER TRAFFIC FACILITATOR1 (PHF1)* (Lan *et al.*, 2015). Moreover, several genes that encode intracellular and secreted purple acid phosphatases (PAPs), pyrophosphorylases, and other phosphatases exist in the *PSI* core genes (Lan *et al.*, 2015). High induction was also observed for *SPXs* (*SPX1*, *SPX2*, and *SPX3*) and transcription factor *ERF070*, which were shown to be essential for root development under Pi limitation (Ramaiah *et al.*, 2014; Lan *et al.*, 2015). In addition, phosphoenolpyruvate carboxylase (PPC) kinase (PPCK) 1 and 2, which phosphorylate and thereby activate PPC during Pi starvation to contribute to malate biosynthesis, were also in core *PSI* genes (Gregory *et al.*, 2009; Shane *et al.*, 2013; Lan *et al.*, 2015).

Several mutants with compromised responses to Pi deficiency are available, allowing for comparative transcriptome/proteomics analysis. Comparative transcriptome analysis using the insensitive mutants *stop1* and *almt1* revealed a preferential loss of local transcriptional responses to Pi limitation in both mutants, which confirms the role of *STOP1* and *ALMT1* in regulating local Pi response in root tips (Mora-Macias *et al.*, 2017). A cluster of gene ontology (GO) categories related to “cell wall organization”, which has been linked to the local Pi response, was found to be significantly overrepresented in WT root tips (Mora-Macias *et al.*, 2017). This response was nearly abolished in the root tips of *stop1* and *almt1*, which suggests that the local Pi response was largely lost in both mutants (Mora-Macias *et al.*, 2017). Expression of *SPX1* and *SPX2*, systemic key regulators, were normally induced in *stop1* and *almt1* (Mora-Macias *et al.*, 2017). Among the systemic genes that were differentially expressed in the Pi-starved WT, over 60% of them remained responsive in *stop1* and *almt1* (Mora-Macias *et al.*, 2017).

Taking advantage of the opposite Pi-conditional root phenotype of *pdr2* (hypersensitive) and *lpr1/lpr2* (insensitive), our group performed transcriptome and proteome analysis to investigate the Pi dependent regulation of gene and protein expression in roots (Hoehenwarter *et al.*, 2016). The results showed that

systemic response to low Pi was maintained in the roots of *pdr2* and *lpr1lpr2* mutants. An overrepresentation of genes and proteins that are involved in the regulation of iron homeostasis were observed in all the genotypes in response to Pi deficiency (Hoehenwarter *et al.*, 2016). Among these genes, *IRON-RELATED TRANSPORTER 1 (IRT1)* was repressed by low Pi, whereas *IRT3* and *FERRETIN 1 (FER1)* were induced by low Pi (Hoehenwarter *et al.*, 2016). Further experiments showed that *FERRIC REDUCTASE DEFECTIVE 3 (FRD3)*-mediated apoplastic Fe redistribution, but not general Fe uptake and cellular storage, triggered the inhibition of primary root growth in response to Pi deficiency (Hoehenwarter *et al.*, 2016). Expression changes of several cell wall-modifying enzymes were altered by Pi limitation in all genotypes, but more pronounced in WT and *pdr2* (Hoehenwarter *et al.*, 2016). Half of those enzymes have potential function in pectin modification, mainly pectin methyl esterification (Hoehenwarter *et al.*, 2016). This was consistent with the pectin staining results, which showed that Pi limitation increased the deposition of pectin at Fe accumulation sites in WT and *pdr2*, not in *lpr1lpr2* (Hoehenwarter *et al.*, 2016). Another transcriptome study also revealed that pectin-related processes were involved in the early Pi deficiency responses (Lin *et al.*, 2011). Moreover, more than twenty class III peroxidases (*PRXs*), which are plant-specific heme oxidoreductases, were identified to be regulated on the mRNA and/or protein level in WT and/or *pdr2* in response to low Pi (Hoehenwarter *et al.*, 2016; Shigeto & Tsutsumi, 2016). *PRXs* have been shown to be involved in ROS formation and cell wall dynamics (Francoz *et al.*, 2015; Shigeto & Tsutsumi, 2016). Less than five *PRXs* were identified in Pi-starved *lpr1lpr2*. Based on proteomics analysis, Lan *et al.* found that annexin 1, a phospholipid-binding protein that has been linked with cellular defence against ROS and abiotic stress, was the highest accumulated protein in root upon Pi deficiency response (Clark *et al.*, 2010; Lan *et al.*, 2012). Other proteomic studies revealed the alteration of the antioxidant enzymes during the low Pi response, including glutathione *S*-transferase (GSTF), superoxide dismutase (SOD), ascorbate peroxidase (APX), PRX, and monodehydroascorbate reductase (Tran & Plaxton, 2008; Chevalier & Rossignol, 2011). Accumulated evidence has shown that roots regulate ROS-related processes at both RNA and protein levels to efficiently recalibrate the cellular redox state.

## **1.5 Reactive oxygen species (ROS) and their role in root development**

During plant regular aerobic metabolism, especially respiration, oxygen can be converted to reactive oxygen species (ROS) by several redox reactions (Apel & Hirt, 2004). ROS were initially described as cytotoxic for cells due to their oxidative properties that can cause damage to DNA, lipids, and proteins as well as cell death. However, they have been further shown to be signaling molecules that regulate plant development and response to biotic and abiotic stresses (Petrov *et al.*, 2015; Mhamdi & Van Breusegem,

2018; Castro *et al.*, 2021; Eljebbawi *et al.*, 2021). Many studies have reported the essential role of ROS as growth regulators during root developmental processes, such as in RAM maintenance, root elongation, lateral root formation, root hair extension, and vascular tissue differentiation (Tsukagoshi, 2016; Eljebbawi *et al.*, 2021; Mase & Tsukagoshi, 2021).

### 1.5.1 ROS production and scavenging

ROS exist in various forms including radicals that have free electrons such as superoxide ( $O_2^{\cdot-}$ ) and hydroxyl radical ( $OH\cdot$ ) as well as non-radicals like hydrogen peroxide ( $H_2O_2$ ) and singlet oxygen ( $^1O_2$ ) (Foyer & Noctor, 2009). Each type of ROS species has distinct chemical properties. Singlet oxygen, with a half-life time of 1-4  $\mu$ s, can oxidize proteins, lipids, and guanidine residues of DNA (Laloi & Havaux, 2015; Mittler, 2017; Ravanat & Dumont, 2022). Superoxide has about the same half-life time as singlet oxygen (Mittler, 2017; Waszczak *et al.*, 2018). It damages Fe- and FeS-containing proteins and reacts with various cellular constituents to form reactive radicals, such as thiyl radicals from cysteine thiols (Winterbourn, 2015; Mittler, 2017; Smirnov & Arnaud, 2019). Hydrogen peroxide is considered to be the predominant ROS involved in cellular signaling, due to its relatively long half-life (more than 1ms) and its ability to move across the plasma membrane via aquaporins (Mittler, 2017; Waszczak *et al.*, 2018). It also damages Fe- and FeS-containing proteins and oxidizes cysteine thiol and methionine residues (Smirnov & Arnaud, 2019). The hydroxyl radical is very unstable with a half-life time of 1 ns and is therefore extremely reactive and reacts with almost everything at their site of production (Mittler, 2017; Waszczak *et al.*, 2018).

In plants, intracellular ROS are mainly produced as by-products in electron transport chains or redox reactions in chloroplasts and mitochondria (Borisova *et al.*, 2012; Smirnov & Arnaud, 2019). Cell wall peroxidases and plasma membrane localized NADPH oxidases, also called respiratory burst oxidase homologs (RBOHs) in plants, are primarily responsible for apoplastic ROS generation (Torres *et al.*, 2002; Bindschedler *et al.*, 2006; Sagi & Fluhr, 2006; Orman-Ligeza *et al.*, 2016; Chapman *et al.*, 2019). Superoxide, the precursor of various ROS, is the product of the one-electron reduction of  $O_2$  that can be generated through mitochondrial respiration or by RBOHs (Fig. 1-3)(Suzuki *et al.*, 2011; Lazaro *et al.*, 2013). PRXs can also provide  $O_2^{\cdot-}$  molecules from  $H_2O_2$  when the substrates of PRXs are thiol, salicylic acid or NAD(P)H (Shigeto & Tsutsumi, 2016).  $O_2^{\cdot-}$  is converted to  $H_2O_2$  spontaneously or enzymatically via superoxide dismutase (Fig. 1-3) (Fridovich, 1997).  $H_2O_2$  can give rise to hydroxyl radical in the Haber–Weiss reaction or Fenton reaction with the aid of iron ions (Chen & Schopfer, 1999; Francoz *et al.*, 2015; Smirnov &



Arnaud, 2019). Hydroxyl radical can also be produced by PRXs in accordance with the Fenton reaction (Fig. 1-3) (Chen & Schopfer, 1999; Shigeto & Tsutsumi, 2016).

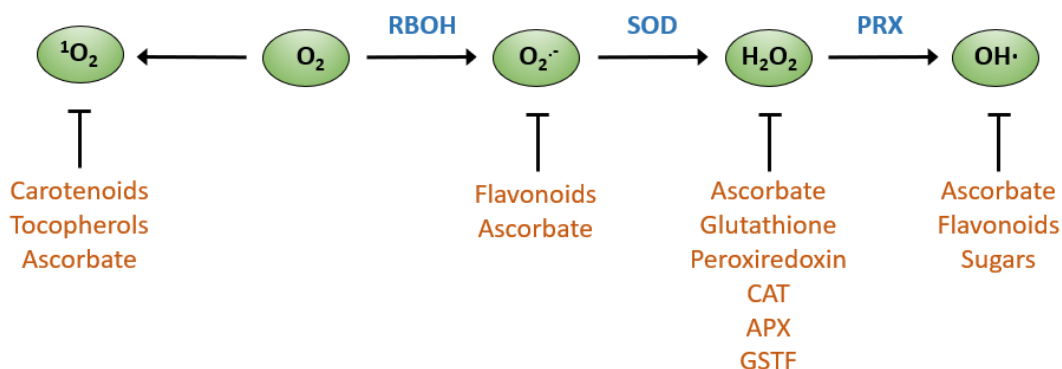


**Fig. 1-3: An overview of the major ROS production enzymes and processing pathways in plants**

Oxygen and oxygen-derived ROS are highlighted in green. The main enzymes that are involved in ROS production are shown in blue. The key ROS processing pathways are shown in blue and orange. Adapted from (Mhamdi & Van Breusegem, 2018).  $O_2$ , oxygen;  $O_2^{\cdot-}$ , superoxide;  $^1O_2$ , singlet oxygen;  $H_2O_2$ , hydrogen peroxide;  $OH\cdot$ , hydroxyl radical; RBOH, respiratory burst oxidase homolog; SOD, superoxide dismutase; PRX, class III peroxidase; CAT, catalase; APX, ascorbate peroxidase; GSTF, glutathione S-transferase.

Plants have evolved many important ROS-detoxifying machineries as a part of their evolutionary adaptations to prevent oxidative bursts and the resulting harmful damage as well as to maintain a threshold boundary between cytotoxicity and redox potential, so called ROS homeostasis (Eljebbawi *et al.*, 2021). The detoxifying machineries include enzymatic antioxidants and nonenzymatic antioxidants. A large number of antioxidative enzymes have been identified, such as SOD, catalase (CAT), APX, GSTF, peroxiredoxin (PRDX), and glutathione reductase (GR) (Willekens *et al.*, 1995; Fridovich, 1997; Asada, 1999; Wagner *et al.*, 2002; Dietz, 2003; Mittler *et al.*, 2004; Dixon & Edwards, 2010). Nonenzymatic antioxidants include ascorbate acid (ASC), glutathione (GSH), flavonoids, and carotenoids (Eltayeb *et al.*, 2007; Foyer & Noctor, 2009; Noctor *et al.*, 2012). The main superoxide-processing enzyme is SOD (Fig. 1-3) (Fridovich, 1997). Hydrogen peroxide can be processed by several enzymes, such as CAT, APX, GSTF, peroxiredoxin and PRX (Willekens *et al.*, 1995; Sharma & Dubey, 2004; Dixon & Edwards, 2010; Bhatt & Tripathi, 2011; Francoz *et al.*, 2015), as well as nonenzymatic antioxidants, such as ASC and GSH (Fig. 1-3) (Noctor *et al.*, 2012; Smirnoff & Arnaud, 2019). Singlet oxygen and hydroxyl radicals are mainly metabolized by non-enzymatic reactions (Fig. 1-3) (Triantaphylides & Havaux, 2009; Mhamdi & Van Breusegem, 2018)

## 1.5.2 Tools for ROS detection

Various methods have been used to detect and visualize ROS in plant tissues and organs. The common ROS detection tools are summarized in Tab. 1-1. Staining with nitro blue tetrazolium (NBT) and diaminobenzidine (DAB) are histochemical methods widely used to visualize superoxide and hydrogen peroxide, respectively (Bielski *et al.*, 1980; Kiernan, 2003). After interacting with intracellular superoxide, NBT forms an insoluble dark purple formazan precipitate (Bielski *et al.*, 1980). However, NBT staining is not specific for superoxide. It can also reflect the presence of ascorbate or the activity of dehydrogenases (Mhamdi & Van Breusegem, 2018). Brownish color accumulates when DAB reacts with  $H_2O_2$  in the presence of higher peroxidase activity (Kiernan, 2003). However, DAB staining is not suitable for live cell imaging.

Several fluorescent probes have been developed to monitor the real-time behavior of ROS, such as dihydroethidium (DHE),  $H_2O_2$ -3'-O-acetyl-6'-O-pentafluorobenzenesulfonyl-2'-7'-difluorofluorescein-Ac ( $H_2O_2$ -BES-Ac), 3'-(p-hydroxyphenyl) fluorescein (HPF), and 5-(and 6)-carboxy-2',7'-dichlorodihydrofluorescein diacetate (Carboxy-H2DCFDA). DHE reacts with  $O_2^-$  to produce ethidium, which can bind DNA or RNA and generate red fluorescence (Zielonka & Kalyanaraman, 2010).  $H_2O_2$ -BES-Ac is a specific indicator for intracellular  $H_2O_2$  (Maeda *et al.*, 2004). HPF is used to detect  $OH\cdot$  and it barely reacts with  $O_2^-$  and  $H_2O_2$  (Setsukinai *et al.*, 2003; Price *et al.*, 2009). Carboxy-H2DCFDA can visualize the general production of ROS (Jaenen *et al.*, 2021). Besides, Luminol, which generates chemiluminescence when oxidized, is widely used to measure extracellular  $H_2O_2$  (Winterbourn, 2014).

Most conventional fluorescent dyes are characterized by at least partial irreversibility, nonspecific behavior, and lack of compartment specificity. Genetically encoded redox probes, in which fluorescent proteins have been engineered, are the most advanced and promising tools to solve some of the problems associated with fluorescent probes (Meyer & Dick, 2010). They are noninvasive, can be targeted in specific compartments, and are suitable for quantitative and dynamic observations (Meyer & Dick, 2010). Most widely used genetically encoded sensors include Grx1-roGFP2, roGFP2-Orp1, and HyPer (Meyer *et al.*, 2007; Schwarzlander *et al.*, 2008; Nietzel *et al.*, 2019; Ugalde *et al.*, 2022). RoGFP2-Orp1 and HyPer can be used for detecting intracellular  $H_2O_2$  (Belousov *et al.*, 2006; Meyer & Dick, 2010; Nietzel *et al.*, 2019). Grx1-roGFP2 is a biosensor for the glutathione redox potential ( $E_{GSH}$ ) (Meyer & Dick, 2010). Since ROS can be partly detoxified by the glutathione-ascorbate pathway, which may transiently alter the  $E_{GSH}$ , Grx1-roGFP2 is also used to indicate ROS level (Meyer *et al.*, 2007; Foyer & Noctor, 2011; Ugalde *et al.*, 2022). A cysteine

pair have been engineered into the protein barrel of GFP (roGFP2), making roGFP2 be able to respond to the glutathione redox state in a ratiometric manner (Meyer & Dick, 2010). The two cysteine residues are close enough to form or cleave disulfide bridge depending on the redox environment of the protein, which can cause a change in the absorption properties of the protein (Meyer & Dick, 2010). Glutaredoxin (GRX) catalyzes the reversible electron transfer between GSH and roGFP2 (Meyer *et al.*, 2007). To ensure rapid and specific equilibration, human Grx1 was fused to roGFP2 (Gutscher *et al.*, 2008).

**Tab. 1-1: Overview of ROS detection tools**

ROS types	Detection tools
$O_2^{\cdot-}$	blue tetrazolium (NBT) (Bielski <i>et al.</i> , 1980), dihydroethidium (DHE) (Zielonka and Kalyanaraman, 2010)
$H_2O_2$	Diaminobenzidine (DAB) (Kiernan, 2003), $H_2O_2$ -3'-O-acetyl-6'-O-pentafluorobenzenesulfonyl-2'-7'- difluorofluorescein-Ac (BES- $H_2O_2$ -Ac) (Maeda <i>et al.</i> , 2004), Grx1-roGFP2 (Meyer and Dick, 2010), roGFP2-Orp1 (Nietzel <i>et al.</i> , 2019), HyPer (Belousov <i>et al.</i> , 2006), luminol (Winterbourn, 2014)
$OH\cdot$	3'-(p-hydroxyphenyl) fluorescein (HPF) (Setsukinai <i>et al.</i> , 2003)
General ROS	5-(and 6)-carboxy-2',7'-dichlorodihydrofluorescein diacetate (Carboxy-H2DCFDA) (Jaenen <i>et al.</i> , 2021)

### 1.5.3 Role of ROS in regulating primary root growth

ROS are generated in root cells and are needed for root growth and development (Dunand *et al.*, 2007; Yamada *et al.*, 2020). A number of reports supported the role of ROS in regulating root growth as signaling molecules. ROS have been found to affect cell division in the RAM, to regulate the transition from cell proliferation to cell differentiation, and are involved in cell elongation, in root hair development as well as in lateral root emergence. Molecular mechanisms of ROS in regulating primary root growth have been uncovered (Eljebbawi *et al.*, 2021; Mase & Tsukagoshi, 2021).

#### SCN maintenance

Multiple signal pathways mediated by ROS have been reported to be implicated in stem cell maintenance and cell fate determination (Yang *et al.*, 2018). Loss of *APP1*, which encodes a P-loop NTPase, leads to a reduction in ROS level and thus causes terminal differentiation of SCN and increased QC cell division (Yu

*et al.*, 2016). It was demonstrated that prohibitin protein PROHIBITIN3 (PHB3) maintains root SCN through the regulation of ROS homeostasis in RAM (Kong *et al.*, 2018). The *phb3* mutant displays a short-root phenotype with reduced RAM size, which can be attributed to enhanced root stem cell differentiation and increased mitotic activity in the QC (Kong *et al.*, 2018). Besides, in the RAM of *phb3* mutant, both superoxide and hydrogen peroxide were over accumulated compared to WT, leading to ectopic expression of *ETHYLENE RESPONSE FACTOR (ERF) 115*, *114*, and *109* (Kong *et al.*, 2018). Moreover, the ectopic expression of *ERFs* was independent of stem cell death signaling (Kong *et al.*, 2018). Additionally, *ERF115*, *ERF114*, and *ERF109* were further proven to directly regulate the expression of *PHYTOSULFOKINE2 (PSK2)* and *PSK5*, which are peptide hormone precursors that regulate cellular differentiation and proliferation. Thus, PHB3 is essential for the maintenance of SCN identity by restricting the spatial expression of the ROS-responsive transcription factors *ERF115*, *114*, and *109* (Kong *et al.*, 2018).

### **RAM maintenance**

Root growth and development depend on the constant generation of cells in its RAM (De Veylder *et al.*, 2007). The number of dividing cells and the duration of these divisions are controlled by the cell cycle, which governs the growth rate of the root (Gonzalez-Garcia *et al.*, 2011). To maintain RAM size and to prevent premature differentiation, a proper cell cycle is therefore highly important (Gonzalez-Garcia *et al.*, 2011). Several studies revealed the importance of redox status, adjusted by glutathione and thioredoxins (TRXs), in regulating the maintenance of RAM. Glutathione-deficient *root meristem less 1 (rml1)* mutant is inhibited in forming an active root meristem (Schnaubelt *et al.*, 2015). The level of GSH was found to be important in controlling the G1 to S cell cycle transition (Schnaubelt *et al.*, 2015). The glutathione reductase (GR) catalyzing the reduction of oxidized glutathione (GSSG) into reduced glutathione (GSH), is also essential for the maintenance of RAM. *Arabidopsis* contains two GRs, cytosol/peroxisome-localized GR1 and plastid-localized GR2 (Marty *et al.*, 2009). Researchers showed that GR2, but not GR1, is crucial for root growth and RAM maintenance. Complete loss of function of GR2 can cause embryo lethality (Tzafrir *et al.*, 2004). A weak allele of GR2 mutant, *miao*, displayed strong inhibition of primary root growth and severe defects in the RAM (Yu *et al.*, 2013). It was also proposed that the regulation of RAM maintenance by the glutathione redox status is related to auxin (Yu *et al.*, 2013). Moreover, there is an interplay between thioredoxin and glutathione pathways in regulating RAM maintenance. NADPH-dependent thioredoxin reductases (NTRs) double mutant (*ntra ntrb*) exhibited a small RAM phenotype (Reichheld *et al.*, 2007; Bashandy *et al.*, 2010). The phenotype was more severe after crossing *ntra ntrb* with glutathione biosynthesis (*rml1* and *cad2*) mutants (Reichheld *et al.*, 2007; Bashandy *et al.*, 2010).

### Cell elongation

The dividing cells in the RAM enter a new phase of cellular elongation in the elongation zone (Verbelen *et al.*, 2006), which is tightly associated to the balance between cell wall stiffening and loosening (Francoz *et al.*, 2015). Both processes are precisely controlled by ROS homeostasis (Francoz *et al.*, 2015). Cell wall targeted PRXs have antagonistic activities in regulating cell wall dynamics through adjusting ROS homeostasis. PRXs help to build a rigid cell wall through oxidizing aromatic cell wall compounds within proteins and phenolics in the presence of H<sub>2</sub>O<sub>2</sub> and thus affect its components cross-links (Marjamaa *et al.*, 2009). On the other hand, PRXs can produce hydroxyl radicals by utilizing H<sub>2</sub>O<sub>2</sub> (Chen & Schopfer, 1999). Hydroxyl radicals are able to catalyze the oxidative cleavage of xyloglucan and pectin, resulting in cell wall loosening (Schopfer *et al.*, 2001). Thus, PRXs have a dual role in regulating the cell wall status through ROS. A MYB transcription factor, *MYB30* has been identified to regulate the inhibition of root cell elongation in response to hydrogen peroxide (Mabuchi *et al.*, 2018). *MYB30* is induced by H<sub>2</sub>O<sub>2</sub> in the RAM and elongation zone (Mabuchi *et al.*, 2018). H<sub>2</sub>O<sub>2</sub> treatment can lead to a smaller RAM and inhibit the cell extension in the elongation zone in WT (Mabuchi *et al.*, 2018). The treatment did not inhibit the cell elongation in *myb30* (Mabuchi *et al.*, 2018). Besides, it was shown that *MYB30* regulates root cell elongation in response to H<sub>2</sub>O<sub>2</sub> by upregulating the expression of *LTPG1*, *LTPG2*, and *LTP5*, which encode lipid transfer proteins that transport very-long-chain fatty acids (VLCFAs) (Mabuchi *et al.*, 2018).

### Interface between proliferation and differentiation

It has been reported that superoxide mainly accumulates in the RAM and hydrogen peroxide is mainly in the elongation zone (Dunand *et al.*, 2007; Tsukagoshi *et al.*, 2010; Reyt *et al.*, 2015). The basic helix-loop-helix transcriptional factor, UPBEAT1 (UPB1) was verified to control the transition of cells from proliferation to differentiation in the root tips through regulating the ROS homeostasis between O<sub>2</sub><sup>-</sup> and H<sub>2</sub>O<sub>2</sub> (Tsukagoshi *et al.*, 2010). UPB1 inhibits expression of several PRXs and thus regulates ROS homeostasis (Tsukagoshi *et al.*, 2010). The *upb1-1* mutant has a larger RAM and accumulates more O<sub>2</sub><sup>-</sup> and less H<sub>2</sub>O<sub>2</sub> than WT, because the expression of peroxidases is not suppressed by UPB1 (Tsukagoshi *et al.*, 2010). The *UPB1* overexpression line displays the opposite phenotypes regarding RAM size and ROS levels (Tsukagoshi *et al.*, 2010).

### ROS and low Pi response

Several studies reported the involvement of ROS in primary root adaptation to Pi deficiency. As described in section 1.3, we previously showed that Pi deficiency triggered the Fe<sup>3+</sup> accumulation in the apoplast of

SCN, where *LPR1* is expressed (Müller *et al.*, 2015). At the same site, ROS generation and callose deposition was observed (Müller *et al.*, 2015). The produced callose likely interfered with symplastic communication in the SCN and modulated RAM maintenance (Müller *et al.*, 2015). Growing evidence showed that ROS and redox signaling mediate callose deposition and symplastic permeability (Benitez-Alfonso *et al.*, 2011; Tilsner *et al.*, 2016). During Pi deficiency response, ROS may trigger callose deposition (Müller *et al.*, 2015). Aquaporins facilitate the passive transport of water, small neutral solutes and gases (Maurel *et al.*, 2008). In addition, they have been also proposed to translocate H<sub>2</sub>O<sub>2</sub> among different cell compartments (Smirnov & Arnaud, 2019; Zhang *et al.*, 2019). Tian *et al.* reported the function of plasma membrane intrinsic protein (PIP) 1;4 in facilitating the transport of apoplastic H<sub>2</sub>O<sub>2</sub> into the cytoplasm to trigger callose synthesis during plant bacterial defense response in leaves (Tian *et al.*, 2016). Bacterial pathogens induced the expression of the *PIP1;4* gene in leaves, which was accompanied by H<sub>2</sub>O<sub>2</sub> accumulation in the cytoplasm and callose deposition in the apoplast (Tian *et al.*, 2016). Loss-of-function *pip1;4* mutant accumulated more H<sub>2</sub>O<sub>2</sub> in the apoplast and produced less callose, which means that removal of PIP1;4 can reduce the translocation of H<sub>2</sub>O<sub>2</sub> into the cytoplasm and thus repress the subsequent immune responses (Tian *et al.*, 2016). The Arabidopsis PIP family comprises 13 members (Johanson *et al.*, 2001). They are divided into two subgroups, PIP1 and PIP2, which consist of five PIP1 isoforms and eight PIP2 isoforms, respectively. It has been revealed that *PIP2;4* is involved in root hair elongation during Pi deficiency response (Lin *et al.*, 2011). Expression of *PIP2;4* was inhibited by low Pi (Lin *et al.*, 2011). Moreover, *pip2;4* mutant generated longer root hairs compared to WT both under Pi sufficient condition and deficient condition (Lin *et al.*, 2011). Based on these discovers, PIPs seem play a role in low Pi response.

Balzergue *et al.* reported that Pi limitation restrained the cell elongation by peroxidase-dependent cell wall stiffening (Balzergue *et al.*, 2017). Higher peroxidase activity was observed in Pi-deprived WT root tips (Balzergue *et al.*, 2017). Treatment of peroxidase inhibitors (salicylhydroxamic acid and methimazole) and DAB, a classical peroxidase substrate, restored the WT root growth under -Pi condition (Balzergue *et al.*, 2017). It was also shown that Pi limitation promoted ROS accumulation in the EZ (Balzergue *et al.*, 2017). PRXs were proposed to impede root growth via their peroxidative activity to catalyze intermolecular covalent bonds between cell wall components that consumes H<sub>2</sub>O<sub>2</sub> (Francoz *et al.*, 2015). Expression of several *PRXs* have been shown to be influenced by low Pi (Hoehenwarter *et al.*, 2016; Mora-Macias *et al.*, 2017). Moreover, it was reported that blue light and the low pH in the rhizosphere caused by Pi deficiency together promote the reaction between Fe<sup>3+</sup> and malate to produce Fe<sup>2+</sup> (via a photo-Fenton reaction) in the epidermis (Zheng *et al.*, 2019). The generated Fe<sup>2+</sup> then reacts with H<sub>2</sub>O<sub>2</sub> to produce hydroxyl radicals

and Fe<sup>3+</sup> (via a Fenton reaction) (Zheng *et al.*, 2019). A higher level of hydroxyl radicals was observed in the epidermis of Pi-starved WT root tips (Zheng *et al.*, 2019). In contrast, less H<sub>2</sub>O<sub>2</sub> was detected in the root tips, which is explained by the consumption of H<sub>2</sub>O<sub>2</sub> to produce hydroxyl radicals (Zheng *et al.*, 2019). The addition of scavengers of hydroxyl radicals, thiourea and GSH, restored the WT root growth under -Pi condition (Zheng *et al.*, 2019).

In summary, different results have been reported regarding the level, generation site, and species of ROS. Consequently, various working modes for the role of ROS in regulating primary root inhibition during Pi deficiency response have been proposed. Nevertheless, these discoveries support the contribution of ROS in moderating root response to low Pi. However, there is much more to discover about the molecular mechanism by which ROS regulate low Pi responses in root tips.

## 1.6 Aim of the present work

Root tips locally sense external Pi limitation and adjust root growth by rapid inhibition of cell expansion and progressive arrest of cell division. *PDR2-LPR1* module-mediated accumulation of Fe, ROS, and callose in the stem cell niche (SCN) lead to primary root growth inhibition upon Pi limitation (Müller *et al.*, 2015). The low Pi-induced arrest of root growth involves transcriptional reprogramming. From the reports introduced above, although extensive transcriptomes have been performed, only very few studies were carried out in root tips with the focus on early Pi deficiency response. ROS have been reported to participate in the low Pi response in root tips (Müller *et al.*, 2015; Zheng *et al.*, 2019). However, the mechanism by which ROS play a role remains unclear. The major objectives of the current study are listed below.

1) Taking advantage of the opposite Pi-conditional root phenotype of the hypersensitive *pdr2* mutant and the insensitive *lpr1lpr2* line, we aim to identify key regulators and pathways that are involved in the early Pi deficiency response through transcriptome analysis in root tips.

2) Aquaporin PIPs have been proposed to transform H<sub>2</sub>O<sub>2</sub> from apoplast into cytosol to influence callose deposition (Tian *et al.*, 2016). To study if PIPs are involved in the ROS signaling cascade during low Pi response, all thirteen PIPs with respect to the gene expression pattern and mutant phenotype in response to Pi deficiency will be investigated.

3) Questions still remain if ROS work as toxic molecules or as signals to regulate primary root inhibition in response to low Pi. Oxidative-responsive genes that maybe implicated in ROS signalling and related

mutants will be studied. Which ROS species are formed and where do ROS accumulate will be investigated in more detail using different ROS probes and genetically encoded Grx1-roGFP2.



## 2. RESULTS

### 2.1 Analysis of Pi-dependent transcriptomes in *Arabidopsis thaliana* root tips

#### 2.1.1 Rationale

Pi deficiency leading to primary root growth inhibition involves rapid inhibition of cell elongation in the elongation zone (<2 h after transfer) and progressive deterioration of the root meristem (<2 days after transfer) (Müller *et al.*, 2015; Balzergue *et al.*, 2017). Previous expression studies (DNA microarrays) carried out on whole roots by our group (Hoehenwarter *et al.*, 2016), pointed to the involvement of iron homeostasis, ROS formation, and cell wall remodeling during the local Pi deficiency response. The goal of this study was to obtain more specific and detailed information about the local Pi deficiency response at an early time point in growing root tips. Therefore, we performed RNA-seq analysis on root tips of the reference (WT), the low Pi-hypersensitive (*pdr2*), and low-Pi insensitive (*lpr1lpr2*) genotypes of *A. thaliana* to identify genes or pathways that are involved in the local Pi response.

#### 2.1.2 The degree of differential mRNA expression correlates with genotype-dependent sensitivity to Pi limitation

Using our experimental setup, we first confirmed primary root growth inhibition within 20-30 h after transfer from +Pi to -Pi condition (Fig. 2-1A and B). For RNA-seq analysis, seeds were germinated on +Pi agar plates for 5 days and subsequently transferred to +Pi or -Pi conditions. After 24 h of transfer, root tips of WT, *pdr2*, and *lpr1lpr2* seedlings were collected (Fig. 2-1C). To exclude the possibility that different tissue types may lead to changes in RNA levels, root tips were cut off between 10<sup>th</sup> to 20<sup>th</sup> root hair for all samples. RNA was extracted from root tips and further processed for RNA-seq analysis (three biological replicates for each genotype).

Principal component analysis (PCA) was performed to visualize the variation between datasets. Samples of all datasets were displayed in a 3D score plot with respect to the first three principal components. The results revealed high similarity within each replicate set and a clear separation between +Pi and -Pi samples for WT and the hypersensitive *pdr2* mutant, but not for the insensitive *lpr1lpr2* line (Fig. 2-2A). FPKM (Fragments Per Kilobase of transcript sequence per Million base pairs sequenced) was used to estimate gene expression levels. Genes with FPKM < 0.5 were not considered. Comparisons using a log<sub>2</sub> fold change (FC) cutoff of > 1 for upregulated genes and of < -1 for downregulated genes (false discovery

rate adjusted  $p$ -value  $< 0.05$ ) identified 2641 differentially expressed genes (DEGs) across all genotypes and treatments.

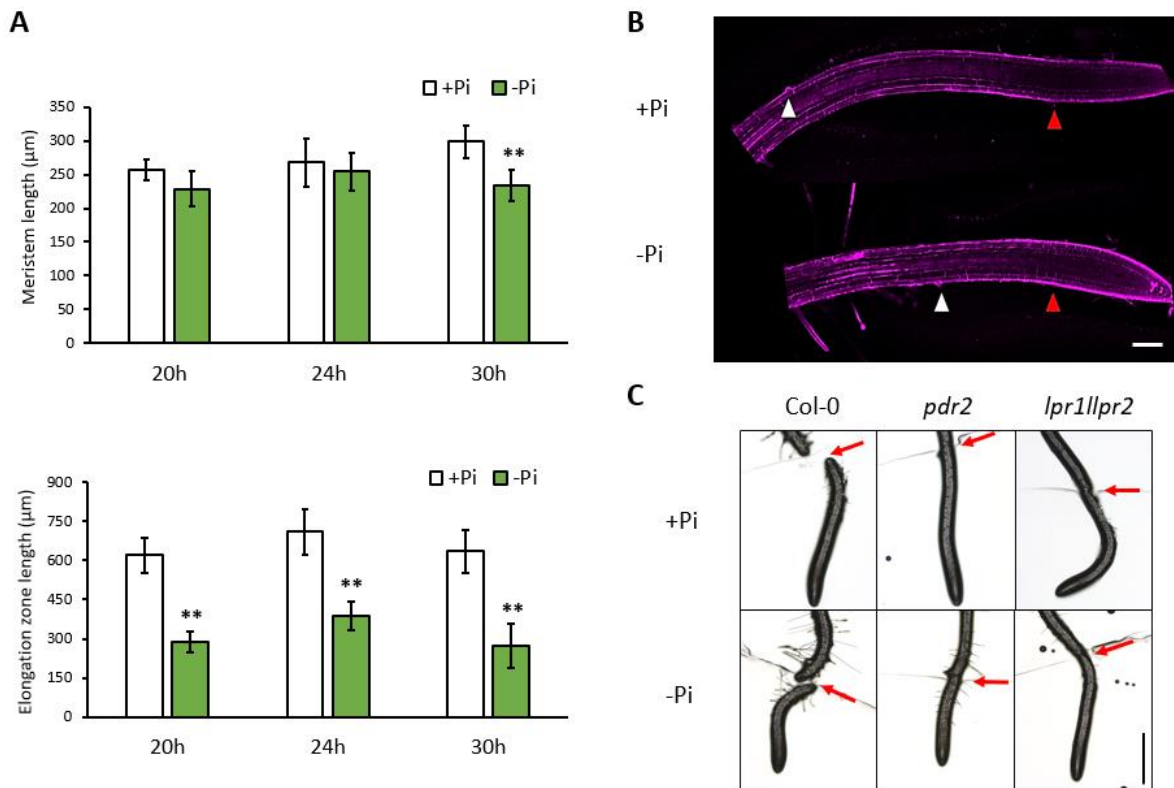


**Fig. 2-1: Primary root growth inhibition during Pi deficiency and sample collection for RNA-seq analysis**

(A) WT seeds were germinated on +Pi agar plates (25  $\mu$ M Fe) for 5 days and then transferred to +Pi (25  $\mu$ M Fe) or -Pi (25  $\mu$ M Fe) for 20 h, 24 h and 30 h prior to PI staining. Top graph: length of the root meristem. Bottom graph: length of the elongation zone. Shown is one out of two independent experiments. ( $\pm$ SD,  $n = 6-12$ , \*\* $p < 0.001$ , Student's  $t$ -test). (B) Confocal microscope images of PI-stained root tips after transfer to low Pi for 24 h. The end of the meristem (red arrowheads) and the end of the elongation zone (white arrowheads) are indicated. Scale bar represents 100  $\mu$ m. (C) Seeds were germinated on +Pi agar plates (25  $\mu$ M Fe) for 5 days, transferred to +Pi (25  $\mu$ M Fe) or -Pi (25  $\mu$ M Fe) conditions and allowed to grow for one additional day prior harvest for RNA-seq. Root tips were cut off between 10th to 20th root hair on plate. Arrows point to the site where the root tips were cut. Scale bar = 100  $\mu$ m (B); 1 mm (C).

Low Pi treatment for 24 h altered the expression of 2343 genes (1472 up-, 871 down-regulated), 373 genes (288 up, 85 down) and 15 genes (14 up, 1 down) in *pdr2*, WT, and *lpr1lpr2* root tips, respectively (Fig. 2-2B). Thus, the number of DEGs in the three genotypes correlates with the genotype-specific sensitivity of primary root growth inhibition in response to Pi deficiency. Comparing the transcriptomes of *pdr2* and *lpr1lpr2* with WT root tips under Pi sufficient condition (control condition) revealed that dysfunction of PDR2 resulted in differential expression of 293 genes (259 up, 34 down), whereas only 11 DEGs (5 up, 6 down) were detected in *lpr1lpr2* (Fig. 2-2B).

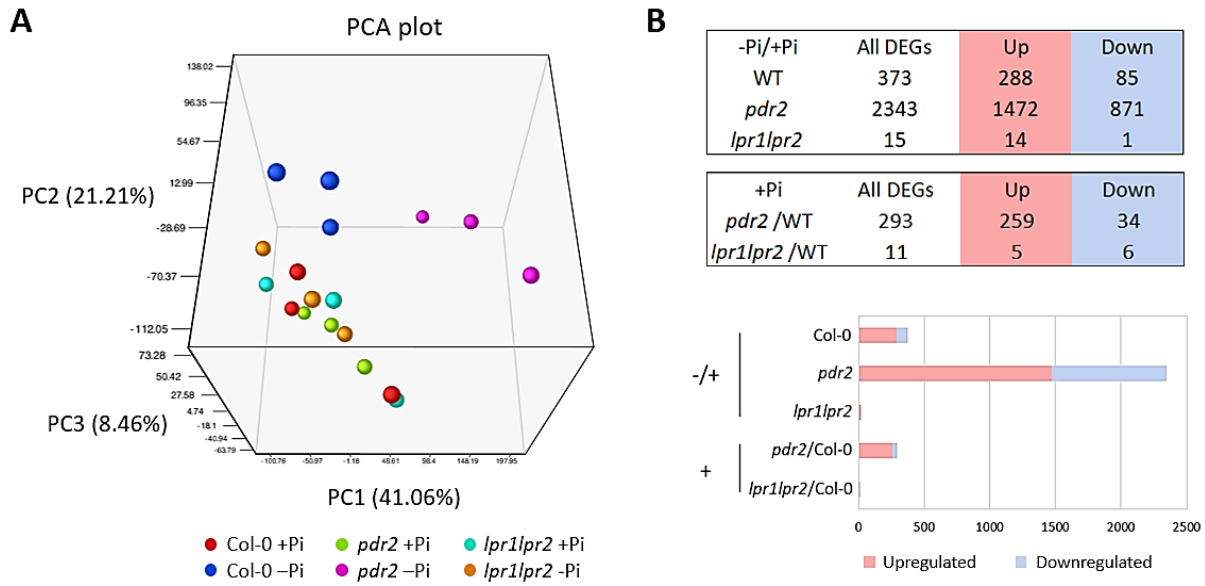


**Fig. 2-2: Statistical analysis of comparative gene expression analysis**

(A) Principal component analysis of all expressed genes in WT, *pdr2* and *lpr1lpr2* samples after transfer of 5-d-old seedlings to the +Pi or -Pi conditions for 24 h (three biological replicates). Distances in the 3D plot illustrate the degree of relationship between samples. (B) Upper boxes: Numbers of up- and down-regulated genes in WT, *pdr2* and *lpr1lpr2* root tips upon seedling transfer to +Pi or -Pi agar (-Pi/+Pi); and in *pdr2* and *lpr1lpr2* compared to WT upon transfer to +Pi medium (adjusted p-value < 0.05;  $-1 > \log_2FC > 1$ ). Lower diagram: Bar graph of the number of DEGs in the upper boxes.

### 2.1.3 Genotype-dependent root tip transcriptomes in Pi sufficiency

To get a better understanding of which role PDR2 may play under control condition, Gene Ontology (GO) enrichment analysis for the 293 DEGs of *pdr2* was performed using the Functional Annotation Tool on DAVID website (<https://david.ncifcrf.gov/>) (Fig. 2-3). GO term analysis for the biological process of the 259 upregulated genes revealed an overrepresentation of genes that are related to oxidative stress (GO terms: “response to oxidative stress”, “hydrogen peroxide catabolic process” and “glutathione metabolic process”). In addition, genes associated with cell wall (GO terms: “cell wall macromolecule catabolic process”, “suberin biosynthetic process”, “plant-type cell wall organization”, “polysaccharide catabolic process”) were highly enriched. Moreover, some defense-related categories including “response to bacterium”, “indole glucosinolate metabolic process”, “defense response to bacterium”, and “chitin catabolic process” were significantly enriched.

Analysis of the 34 downregulated genes in *pdr2* revealed only one significantly enriched GO category (“proteolysis involved in cellular protein catabolic process”). Because *pdr2* is a single point mutation

leading to dysfunctional P5-type ATPase (*pdr2-1* disrupts ATP-binding), the expression of *PDR2* is not altered in *pdr2* compared to WT, which we confirmed in our data set (Tab. S6-14).

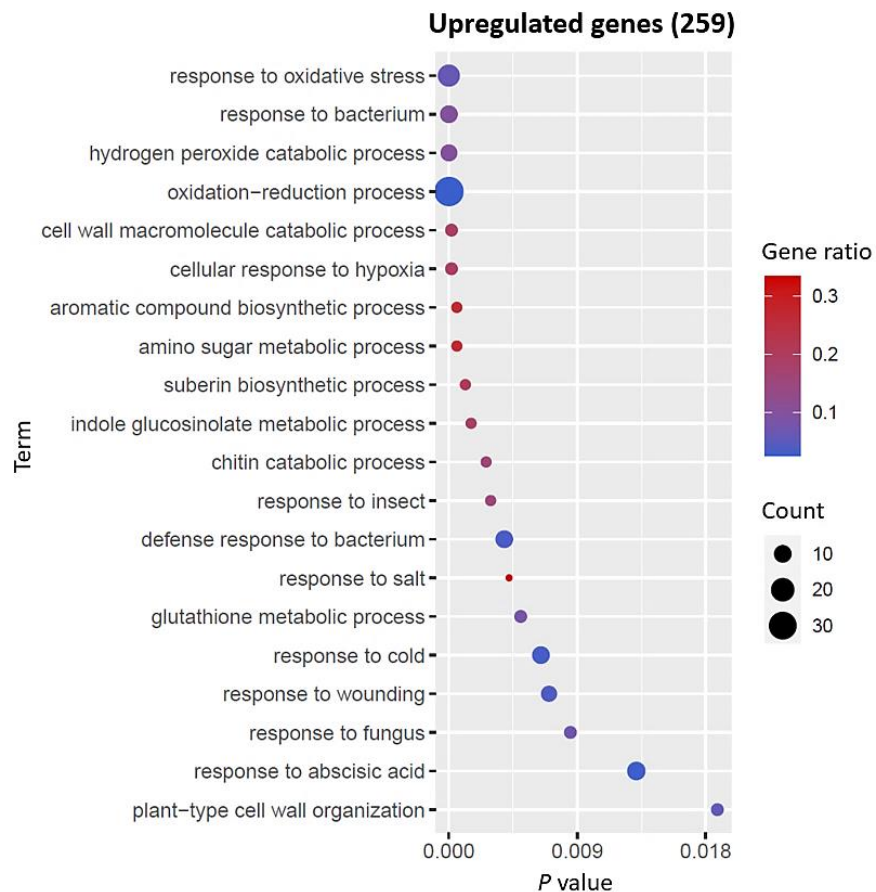


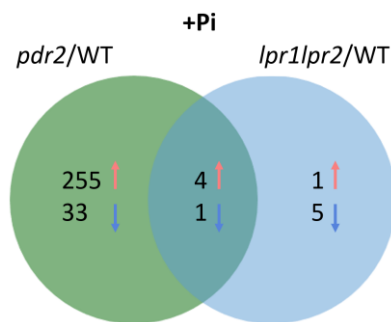
**Fig. 2-3: GO biological process term analysis of upregulated genes specific for *pdr2* vs. WT under +Pi condition**

A subset of 259 genes that were upregulated in *pdr2* compared to WT under +Pi was analyzed for GO enrichment condition (adjusted p-value < 0.05; log<sub>2</sub>FC > 1). 20 select significantly enriched terms (p-value < 0.05) were included in the dot plot. Full dataset is available in Tab. S6-1. Count: number of DEGs concerning this GO term. Gene ratio: the ratio between the number of DEGs in each GO term and all the genes that can be found involved in this GO term in GO database.

Knockout of *LPR1* and *LPR2* (Svistoonoff *et al.*, 2007) resulted in the downregulation of four additional genes, and in the upregulation of five genes (Tab. 2-1). Interestingly, five genes (4 up, 1 down) were regulated in both *lpr1lpr2* and *pdr2* root tips (Tab. 2-1, Fig. 2-4). Among those genes, *IQ67 DOMAIN 16* (*IQD16*), which participates in microtubule organization (Burstenbinder *et al.*, 2017) was upregulated in both lines, reflecting a potential role of *PDR2*, *LPR1* and *LPR2* in regulating cell shape together via *IQD16* (Burstenbinder *et al.*, 2017). In addition, the RNA abundance of *TIP2-2* and *TIP2-3*, encoding tonoplast intrinsic proteins, and of *AT4G33550*, encoding a lipid transporter, were induced in both lines.

**Tab. 2-1: All differentially expressed genes in *lpr1lpr2* vs. WT.**Adjusted p-value < 0.05;  $-1 > \log_2FC > 1$ .  $\log_2FC$  of genes that are regulated in *pdr2* compares to WT is also included.

Gene ID	Gene name	$\log_2FC$		Gene description
		<i>lpr1lpr2</i> vs WT	<i>pdr2</i> vs WT	
AT4G33550	<i>AT4G33550</i>	3.18	3.04	lipid binding; involved in lipid transport
AT4G10640	<i>IQD16</i>	2.45	2.20	IQ-domain 16, microtubule organization
AT5G47450	<i>TIP2-3</i>	2.02	1.78	Tonoplast intrinsic protein, transports ammonium (NH <sub>3</sub> ) and methylammonium
AT1G01060	<i>LHY</i>	1.98		Homeodomain-like superfamily protein; transcription factor
AT4G17340	<i>TIP2-2</i>	1.32	1.37	Tonoplast intrinsic protein 2;2; transports water and small neutral solutes
AT1G71380	<i>CEL3</i>	-1.03		Cellulase 3 (CEL3); hydrolase activity; involved in carbohydrate metabolic process
AT2G40080	<i>ELF4</i>	-1.18		Component of the central CCA1/LHY-TOC1 feedback loop in the circadian clock
AT1G22570	<i>NPF5.15</i>	-1.39		Transporter activity; involved in oligopeptide transport; located in membrane
AT3G20810	<i>JMJ30</i>	-2.16	-1.59	2-oxoglutarate (2OG) and Fe (II)-dependent oxygenase superfamily protein
AT1G71040	<i>LPR2</i>	-2.53		Multicopper oxidase
AT1G23010	<i>LPR1</i>	-2.96		Multicopper oxidase

**Fig. 2-4: Comparison of differentially expressed genes in *pdr2* and *lpr1lpr2* vs. WT**

VENN diagram shows the distribution of DEGs (adjusted p-value < 0.05;  $-1 > \log_2FC > 1$ ) between *pdr2* and *lpr1lpr2* compared to WT under +Pi control condition. Red arrows indicate up-, blue arrows indicate downregulated genes. The overlapping region contains genes that are commonly regulated in both phenotypes compare to WT.

### 2.1.4 Identification of genotype-independent Pi-responsive genes

A Venn diagram was generated to illustrate the distribution of DEGs among the three genotypes in response to Pi deficiency (Fig. 2-5). WT shared a subset of 275 and 13 low Pi-responsive genes with *pdr2* and *lpr1lpr2*, respectively. A core set of eight genes was responsive to low Pi in all three lines, and these genes were induced by Pi deficiency (Tab. 2-2). The core set comprises four known systemic response genes (*SPX1*, *AT4*, *PAP17*, and *GDPD1*) (Thibaud *et al.*, 2010). Two of the remaining genes encode tyrosine protein phosphatases. Interestingly, *MIOX4* which is involved in UDP-glucuronic acid (UDP-GlcA) biosynthesis and ascorbate metabolism, was more highly induced by low Pi in WT and *pdr2* (around 30-fold) when compared to *lpr1lpr2* (around 5-fold) (Tab. 2-2). This may reflect a role of *MIOX4* for both local and systemic Pi responses. Interestingly, a long noncoding RNA (*AT2G08820*) of unknown function was about equally highly upregulated (around 20-fold) in all three genotypes (Tab. 2-2).

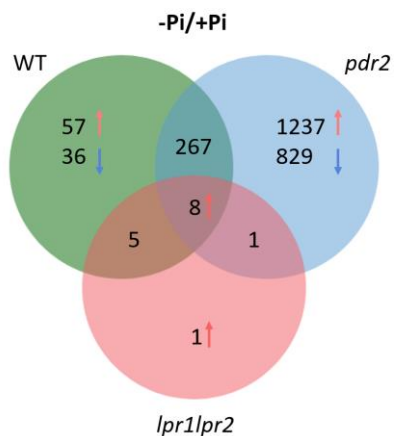


**Fig. 2-5: Comparison of Pi-dependent differentially expressed genes in WT, *pdr2* and *lpr1lpr2***

VENN diagram illustrates the distribution of Pi-responsive DEGs (adjusted p-value < 0.05;  $-1 > \log_2FC > 1$ ) among all three lines. Red arrows indicate up-, blue arrows indicate downregulated genes.

**Tab. 2-2: Commonly regulated genes in WT, *pdr2* and *lpr1lpr2* in response to Pi deficiency.**

Adjusted p-value < 0.05;  $-1 > \log_2FC > 1$ .

Gene ID	Gene name	log <sub>2</sub> FC <sub>-Pi/+Pi</sub>			Gene description
		WT	<i>pdr2</i>	<i>lpr1lpr2</i>	
AT4G26260	<i>MIOX4</i>	4.95	4.98	2.30	Myo-inositol oxygenase 4; UDP-glucuronic acid (UDP-GlcA) biosynthesis; ascorbate metabolism
AT2G08820	<i>AT2G08820</i>	4.73	4.40	4.71	lncRNA
AT3G17790	<i>PAP17</i>	4.30	2.44	4.30	Purple acid phosphatase 17; involved in Pi metabolism; has a peroxidase activity
AT5G03545	<i>AT4</i>	4.09	2.69	4.14	Pi starvation responsive, response is enhanced by the presence of IAA
AT5G20150	<i>SPX1</i>	3.09	1.89	2.06	SPX domain-containing protein 1; plays a positive role in plant adaptation to Pi starvation
AT4G03960	<i>DSP4</i>	2.03	1.10	1.69	Probable tyrosine-protein phosphatase DSP4
AT3G02040	<i>GDPD1</i>	1.97	1.08	1.21	Glycerophosphodiester phosphodiesterase 1; Pi starvation responsive
AT1G05000	<i>PFA-DSP1</i>	1.60	1.60	1.53	Phosphotyrosine protein phosphatases superfamily protein; involved in dephosphorylation

### 2.1.5 Enrichment analysis of genotype-dependent Pi-responsive genes

Genotype-specific analysis of root tip transcriptomes in response to Pi deficiency was one major goal of our study. We therefore first checked several genes known to be involved in the local and systemic Pi deficiency response. Relative expression levels of select genes are displayed in a heatmap (Fig. 2-6). It has been shown that the expression of *PDR2* and *LPR1* is not responsive to Pi deficiency (Naumann *et al.*, 2022) which we confirmed in our data set. Interestingly, *LPR2* was upregulated in *pdr2*, which may reflect a role

of *PDR2* in regulating *LPR2*. *STOP1* and *ALMT1* are two other key players of the local Pi response. Upon Pi deficiency, *STOP1* accumulates in nucleus to activate the expression of *ALMT1* (Balzergue *et al.*, 2017). Previous studies showed that the expression of *STOP1* is not altered by Pi availability, but *ALMT1* is induced by low Pi (Balzergue *et al.*, 2017; Mora-Macias *et al.*, 2017). Based on our RNA-seq data, we observed upregulation of *ALMT1* in *pdr2* and *lpr1lpr2* root tips. However, *ALMT1* was not significantly induced in WT root tips. Moreover, *PPCK1* and *PPCK2* have been shown to be induced by Pi starvation within 6 days of transfer to low Pi condition (Chutia, 2019). Interestingly, we observed induction of *PPCK1* in WT, and of *PPCK2* in *pdr2*, after low Pi treatment for 24 h. Additionally, several genes (e.g., *SPX1*, *AT4*, *IPS1*, *PAP17*, or *PHTs*), which are involved in systemic responses (Pi signaling or Pi recycling), were induced in at least one comparison, which suggests that the systemic response to Pi limitations was triggered within 24 h in all the genotypes. Taken all together, our results demonstrate that our conditions are effective to induce the local and systemic Pi deficiency response at the transcriptome level.

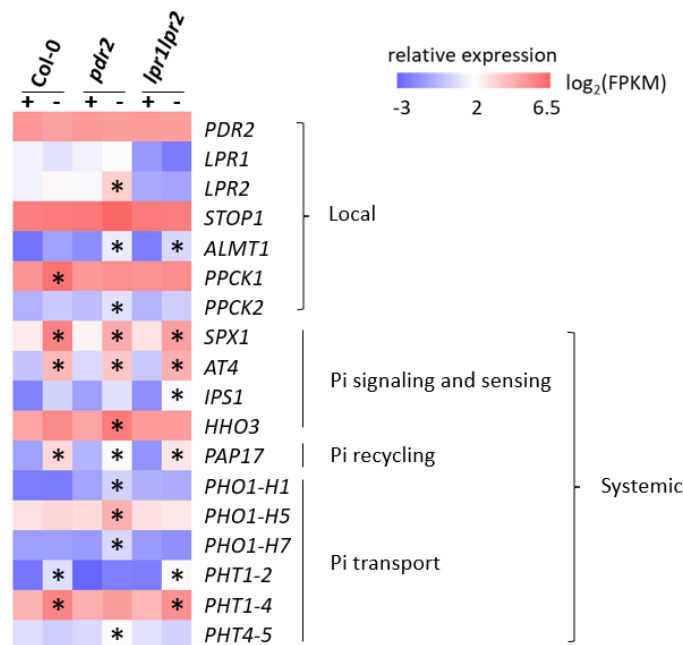


**Fig. 2-6: Heatmap of select local and systemic Pi response gene expression in WT, *pdr2* and *lpr1lpr2* root tips.**

$\log_2(\text{FPKM})$  which represents relative expression levels of select Pi-responsive genes are shown on a colour scale, blue = low expression (-3), red = high expression (6.5). "+" = +Pi, "-" = -Pi. Stars mark the DEGs (adjusted p-value < 0.05;  $-1 > \log_2\text{FC} > 1$ ) in response to Pi deficiency. Full dataset is available in Tab. S6-14.

To obtain a global view of underlying biological processes that are affected by low Pi in WT, *pdr2* and *lpr1lpr2* root tips, GO enrichment analysis and Kyoto Encyclopedia of Genes and Genomes (KEGG) pathway analysis of Pi deficiency-alerted genes were conducted using the Functional Annotation Tool on DAVID



website (<https://david.ncicrf.gov/>) and visualized with the dot plot in R software v.4.0.4. The data for WT are summarized in Fig. 2-7. Categorizing the 288 genes that were upregulated in WT revealed a pronounced overrepresentation of the GO category “trehalose metabolism in response to stress”. Several genes associated with ROS were highly enriched (GO terms: “response to oxidative stress” and “response to hydrogen peroxide”). Furthermore, the GO category “cellular phosphate ion homeostasis” was significantly enriched and thus supports the adjustment of roots to low Pi. Additional overrepresented categories contain genes involved in hormone responses (GO terms: “ethylene-activated signaling pathway” and “response to auxin”), “cell wall biogenesis”, “regulation of transcription, DNA-templated” and flavonoid biogenesis (GO terms: “flavonoid biosynthetic process”, and “flavonoid glucuronidation”).

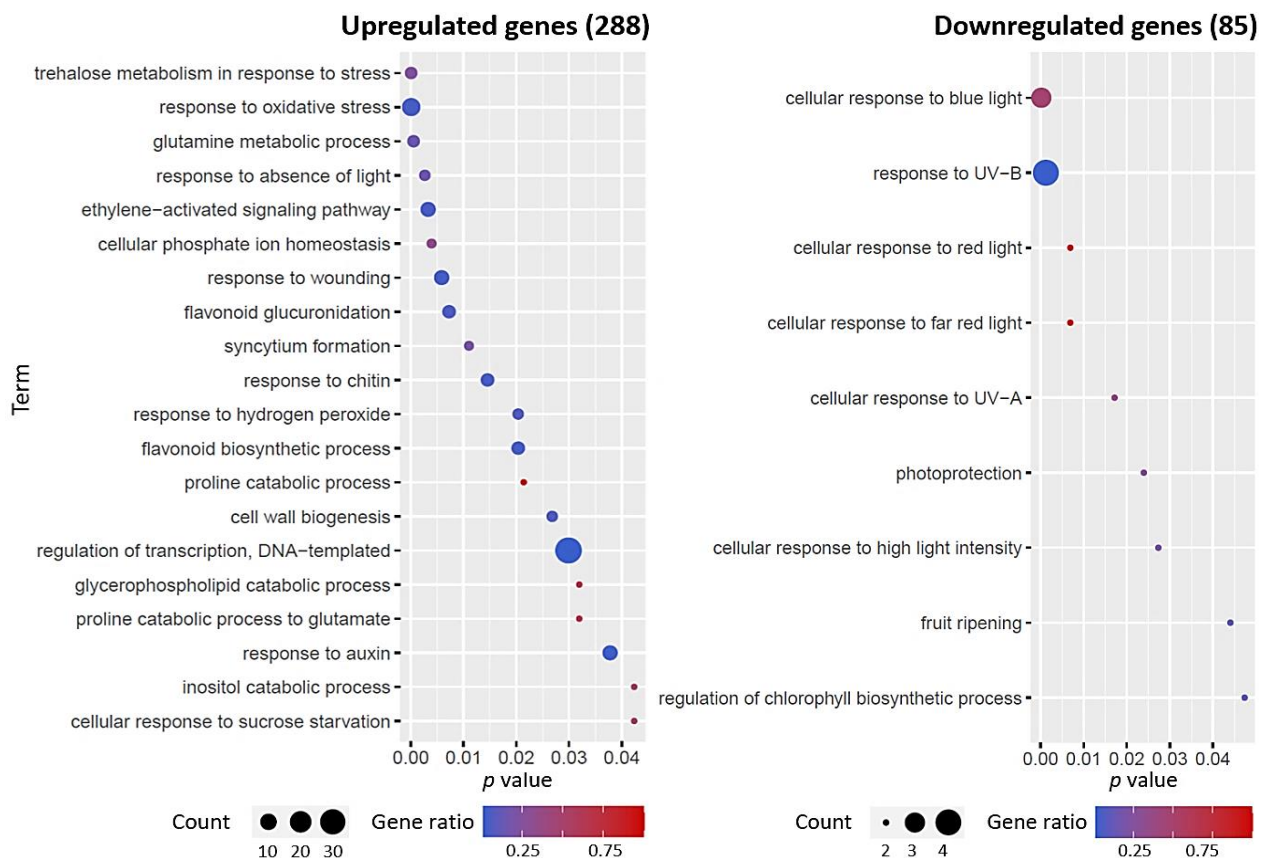


**Fig. 2-7: GO biological process term analysis of Pi-responsive genes in WT**

Pi deficiency induced genes (A) and repressed genes (B) (adjusted p-value < 0.05;  $-1 > \log_2FC > 1$ ) were analyzed for GO enrichment. The top 20 significantly enriched terms (p-value < 0.05) were included in the dot plot. Full dataset is available in Tab. S6-2 & 3. Count: number of DEGs concerning this GO term. Gene ratio: ratio between the number of DEGs in each GO term and all the genes that can be found involved in this GO term in GO database.



In terms of KEGG pathway analysis, upregulated DEGs were significantly enriched in two pathways including “Starch and sucrose metabolism”, which consist of genes that are related to trehalose metabolism process, and “ascorbate and aldarate metabolism” (Tab. S6-15).

Analysis of the 85 downregulated genes in WT revealed that they were mainly enriched in GO terms associated with photoprotection and different light-related categories that comprise similar genes (Fig. 2-7). Only one KEGG pathway was significantly enriched in downregulated genes, which contained genes involved in “cysteine and methionine metabolism” (Tab. S6-15).

For the hypersensitive *pdr2* mutant, GO analysis of the 1472 upregulated genes revealed 85 highly enriched categories (Tab. S6-4). The select 20 categories are listed in Fig. 2-8. Like WT, genes associated with “trehalose metabolism in response to stress”, “response to oxidative stress”, “hydrogen peroxide catabolic process”, “plant-type cell wall organization” and “transcription, DNA-templated” are overrepresented in the data set. Regarding ROS homeostasis, the term “glutathione metabolic process” was enriched only in the *pdr2*, but not in WT data. Furthermore, hormone-related categories were significantly enriched including “ethylene-activated signaling pathway”, “response to salicylic acid”, “response to abscisic acid”, “response to auxin”, and “response to jasmonic acid”. In addition, the upregulated DEGs were enriched in terms associated with “metal ion transport” and “cellular transition metal ion homeostasis”. Surprisingly, the upregulated genes were also highly enriched in defense-related categories (“response to chitin”, “defense response to bacterium”, “response to bacterium”) and “photosynthesis”. Accordingly, KEGG pathways like “starch and sucrose metabolism” (consisting of all the genes involved in trehalose biosynthetic process), “glutathione metabolism”, “glutathione metabolic process”, “plant-pathogen interaction”, and “photosynthesis” were significantly enriched (Fig. S6-1). Meanwhile, KEGG analysis revealed overrepresented pathway “phenylpropanoid biosynthesis” which consist of many peroxidases and cell wall related genes.

Considering the 871 downregulated genes of *pdr2*, 30 GO terms were significantly enriched (Tab. S6-5, Fig. 2-8). The most highly enriched included GO terms related to protein synthesis and processes (marked with green dots), fitting to the KEGG-overrepresentation of “ribosome”, “ribosome biogenesis in eukaryotes” and “protein processing in endoplasmic reticulum” (Fig. 2-8, Fig. S6-1). Like WT, downregulated genes were also enriched in GO terms associated with “cellular response to blue light”. Additionally, GO categories “response to auxin”, “xyloglucan metabolic process” and “cell wall macromolecule catabolic process” were highly enriched.

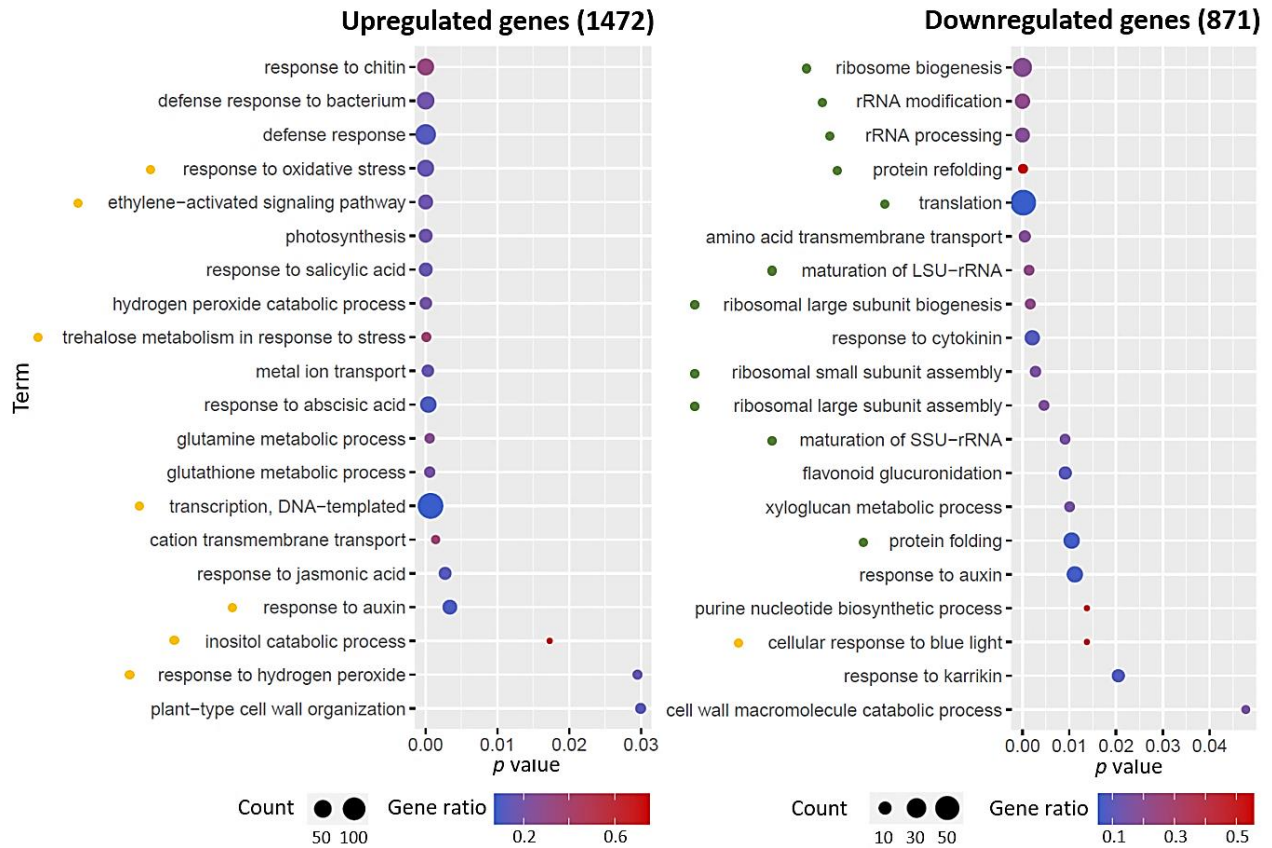


**Fig. 2-8: GO biological process term analysis of Pi-responsive genes in *pdr2***

Pi deficiency induced genes (A) and repressed genes (B) (adjusted p-value < 0.05;  $-1 > \log_2FC > 1$ ) were analyzed for GO enrichment. 20 select significantly enriched terms (p-value < 0.05) were included in the dot plot. Full datasets are available in Tab. S6-4 & 5. Count: number of DEGs concerning this GO term. Gene ratio: ratio between the number of DEGs in each GO term and all the genes that can be found involved in this GO term in GO database. Yellow dots mark the GO terms that shared with WT. Green dots mark the GO terms that are associated with protein synthesis and process.

GO analysis of the 14 upregulated genes in the insensitive *lpr1lpr2* line revealed 4 significantly enriched categories (Fig. 2-9). All those GO terms are related to Pi homeostasis, which indicates that the systemic Pi response was maintained in *lpr1lpr2* root tips.

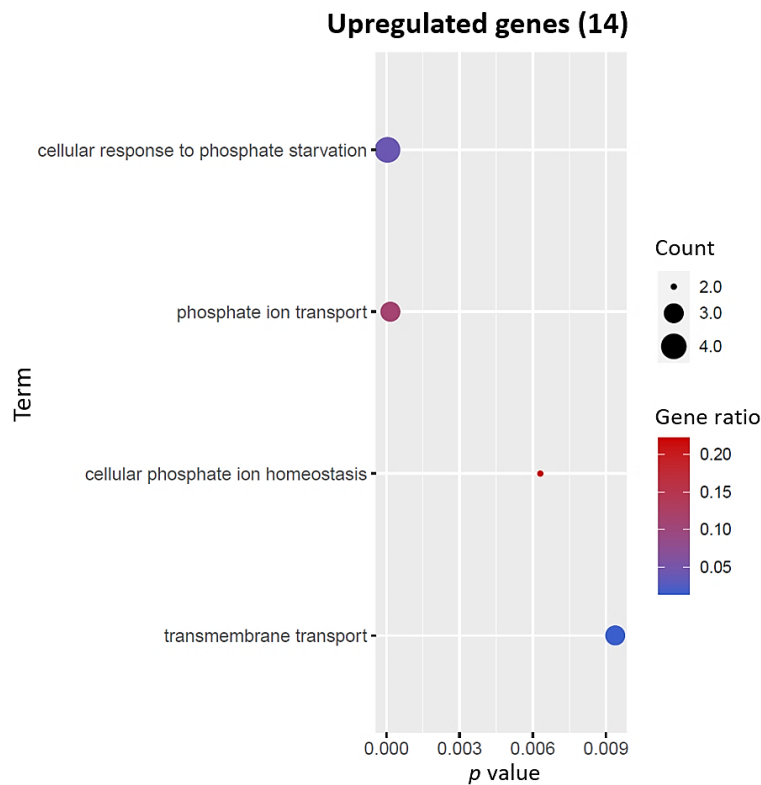


**Fig. 2-9: GO biological process term analysis of Pi-responsive genes in *lpr1lpr2***

Pi deficiency induced genes (adjusted p-value < 0.05;  $-1 > \log_2FC > 1$ ) were analyzed for GO enrichment. All significantly enriched terms (p-value < 0.05) were included in the dot plot. Full dataset is available in Tab. S6-6. Count: number of DEGs concerning this GO term. Gene ratio: ratio between the number of DEGs in each GO term and all the genes that can be found involved in this GO term in GO database.

### 2.1.6 Identification of local Pi-responsive genes

Analysis of the genes that were regulated in WT and the hypersensitive *pdr2* mutant but not in the insensitive *lpr1lpr2* line (a total of 2426 DEGs) will help to identify genes that are involved in the local Pi response. Among those genes, 267 DEGs are shared between WT and *pdr2* only (Fig. 2-5). Among these, 218 genes were upregulated, and 41 genes were downregulated in both WT and *pdr2* (Fig. S6-2A and B). Moreover, 146 genes were more highly induced, and 34 genes were more highly suppressed in Pi-starved *pdr2* compared to the WT (Fig. S6-2A). Only eight genes showed different expression pattern between WT and *pdr2* (Fig. S6-2A and B). GO analysis of the upregulated shared genes (218 genes) in Pi-starved WT and *pdr2* and the genes that were more highly induced in Pi-starved *pdr2* compared to the WT (146 genes) revealed similar GO categories (Tab. S6-16 and S6-17) that were illustrated in the GO analysis results of all upregulated genes in Pi-starved WT (Fig. 2-7).

Hierarchical clustering analysis can be used to group genes according to similar gene expression profiles and the genes clustered together may work in the same pathway. Hierarchical clustering analysis was performed with those 2426 DEGs using the TIGR-MEV software. Z-scores were calculated, and the scaled data were hierarchically clustered. Relative changes in gene expression in root tips between +Pi and -Pi treatment after transfer of WT and *pdr2* seedlings were visualized in a heatmap (Fig. 2-10). The 2426 DEGs

were grouped into 31 clusters. For further analysis, we focused on the genes that were highly induced in WT and *pdr2* root tips after low Pi treatment compared with Pi sufficient condition. Five distinct gene clusters which displayed slight differences in expression patterns meet this criterion. (Fig. 2-10, Tab. S6-8). The expression patterns of genes in cluster 3 reveal a striking difference compared to the other four clusters. Almost 30 percent of those low Pi-inducible genes showed significantly higher expression levels in *pdr2* under +Pi condition when compared to WT (Tab. S6-8).

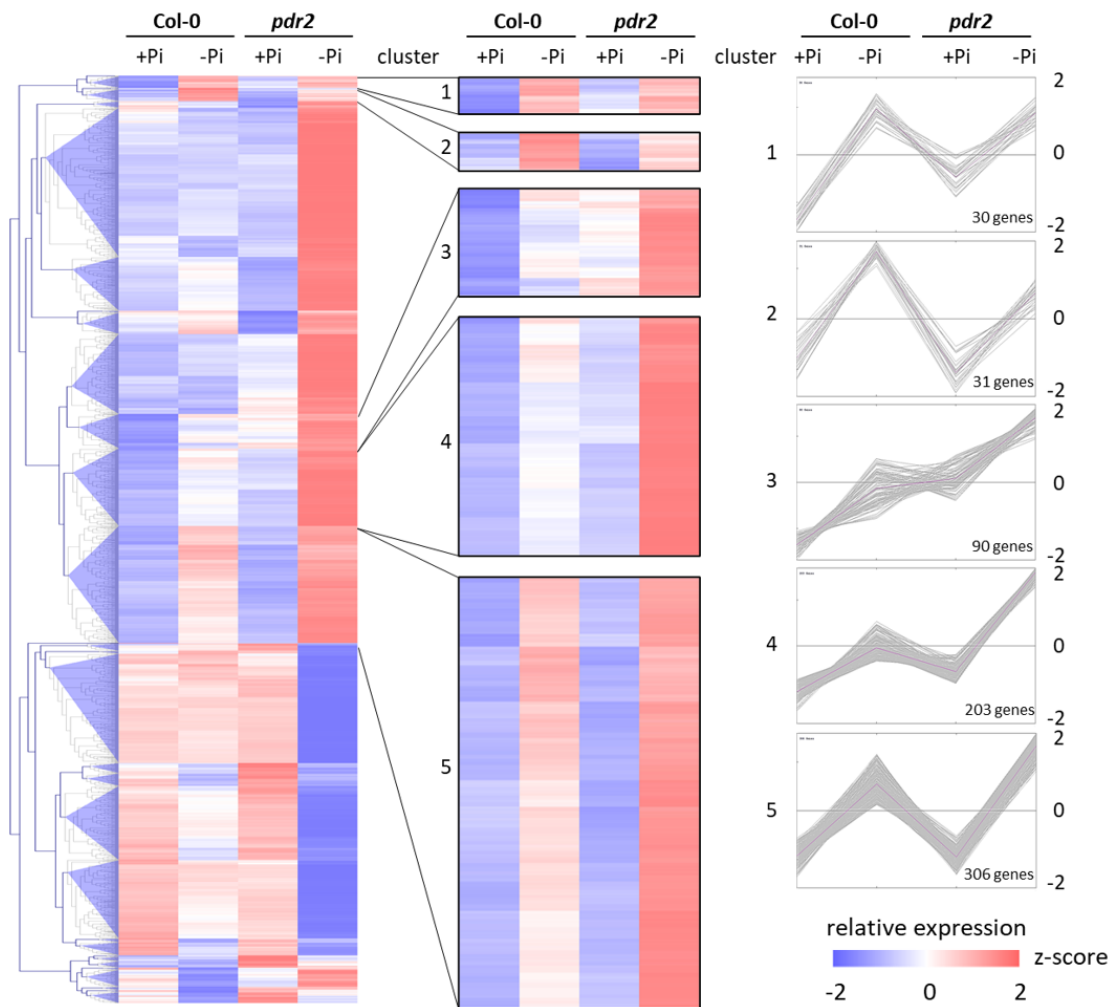


**Fig. 2-10: Hierarchical clustering analysis of Pi-responsive genes in WT and *pdr2***

Scaled expression data of 2426 genes that are differentially regulated in WT and *pdr2* in response to Pi deficiency (adjusted p-value < 0.05;  $-1 > \log_2FC > 1$ ). Each row represents a gene with z-score that represents relative expression level on a color scale. Blue = low expression (-2), red = high expression (2). Left panel: Hierarchical clustering was conducted using “Pearson correlation” and “average linkage clustering”. Distinct clusters are highlighted in purple. Middle panel: Gene expression heat maps of five identified clusters of interest (increased magnitude). Right panel: Gene expression profiles for select clusters. Full dataset is available in Tab. S6-8.

Considering that genes which clustered together may be functionally related or work in the same pathway, functional protein association networks were generated for each select cluster based on the STRING database (Szkarczyk *et al.*, 2019) (Fig. 2-11). No interactions were identified between the 30 DEGs in cluster 1.

In cluster 2 (31 DEGs), five genes group together, four of which are involved in protein degradation or folding (Fig. 2-11). ACHT5 (Atypical CYS HIS-rich thioredoxin 5) may participate in various redox reactions and regulate protein degradation through BT5 (Tab. 2-3).

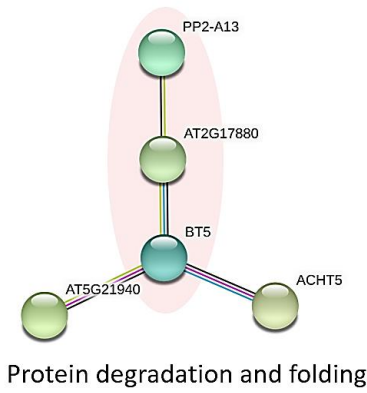
Analysis of cluster 3 (90 DEGs) revealed a group of genes that are associated with redox homeostasis (Fig. 2-11). Interestingly, *GLUTATHIONE S-TRANSFERASE 6 (GSTF6)* and *PHYTOALEXIN DEFICIENT 3 (PAD3)* are involved in camalexin biosynthesis (Tab. 2-3). Additionally, the hub gene *AT5G39670 (CALMODULIN-LIKE 46 (CML46))*, which is a potential calcium sensor, is connected to *GSTF6* (Tab. 2-3).

In cluster 4 (209 DEGs), 9 genes were grouped in a network containing genes associated with photosynthesis and light harvesting (Fig. 2-11). THIOREDOXIN F2 (TRXF2) and THIOREDOXIN M-TYPE 4 (TRX-M4) are thiol-disulfide oxidoreductases that involved in the redox regulation of enzymes of both reductive and oxidative pentose phosphate pathway. Notably, all genes mentioned above in cluster 4 were induced only in the hypersensitive *pdr2* mutant but not in WT (Tab. S6-8).

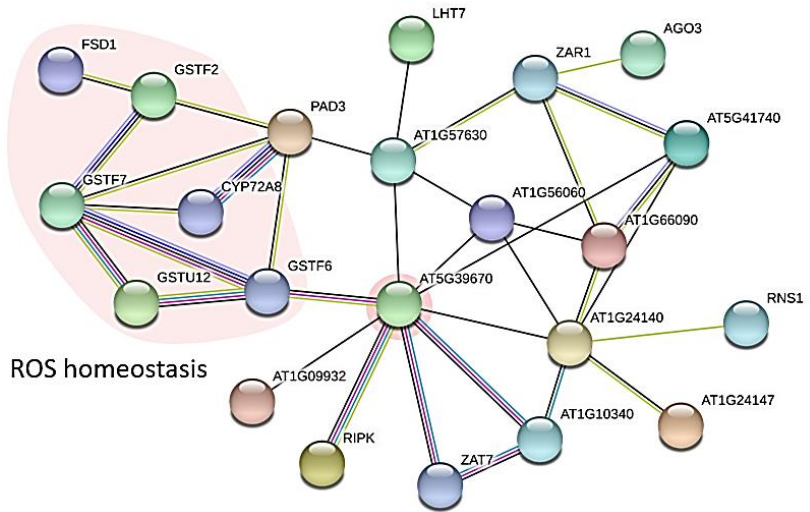
Cluster 5 contained 306 DEGs. Six of them encode enzymes related to trehalose metabolism, including Tre6P synthase (TPS)6, TPS8, TPS9, TPS11, Tre6P phosphatase (TPP)G and TREHALASE1 (TRE1). A screening for all *TPS* and *TPP* discovered more *TPP* genes that were upregulated in WT and *pdr2* upon Pi limitation (Tab. S6-13). Trehalose 6-phosphate (Tre6P), a phosphorylated intermediate of trehalose, is synthesized from UDP-Glc and Glc 6-phosphate by TPS (Cabib & Leloir, 1958). TPP then dephosphorylates Tre6P to trehalose (Cabib & Leloir, 1958). Trehalose can be hydrolyzed into two glucose monomers by trehalase. In Arabidopsis, *TRE1* is the single gene that encodes trehalase (Müller *et al.*, 2001; Lunn, 2007). It is noteworthy that all those trehalose-related genes that were differentially regulated were more highly induced by Pi deficiency in *pdr2* compared to WT root tips (Tab. 2-3, Tab. S6-13). Four hub genes connected to the trehalose group are *AT3G15450* (aluminum induced protein), *AT5G22920* (ROS production), *TLP1* (putative blue light receptor protein) and *AT2G20670* (sugar phosphate exchanger). They may reflect a role of trehalose in regulating Pi deficiency by coordinating with other pathways. Additionally, there are four genes grouped together that are associated with oxidative stress and cell wall biosynthesis. Five genes involved in photosystem constituted another distinct network and were mainly induced in *pdr2* but not in

WT root tips. These results are in line with the enrichment analysis in section 2.1.5 and illustrate the potential role of trehalose metabolism and ROS in root adaptation to limited phosphate availability. A selection of prominent genes that may regulate local Pi response are listed in Tab. 2-3.

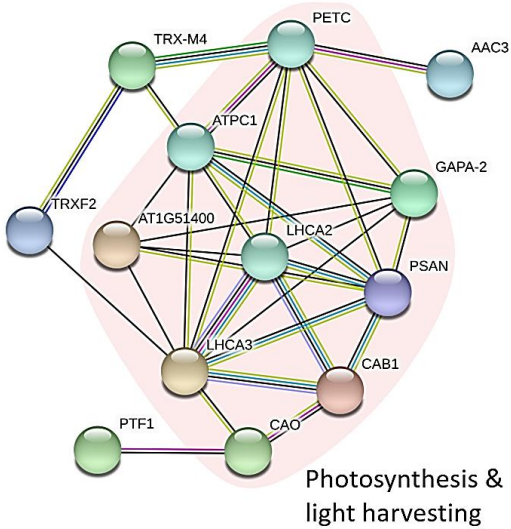
**Cluster 2 (31)**



**Cluster 3 (90)**



**Cluster 4 (203)**



**Protein-protein associations**

- from curated databases
- experimentally determined
- Textmining
- co-expression
- protein homology





**Tab. 2-3: Select genes that may regulate local Pi response.**

log<sub>2</sub>FC of the genes that were significantly induced (adjusted p-value < 0.05) are labeled in bold.

Gene ID	Gene name	log <sub>2</sub> FC <sub>-Pi/+Pi</sub>		Gene description	Cluster
		WT	<i>pdr2</i>		
AT5G61440	<i>ACHT5</i>	<b>1.54</b>	<b>1.02</b>	Atypical CYS HIS rich thioredoxin 5; may participate in various redox reactions	2
AT5G39670	<i>CML46</i>	<b>2.98</b>	<b>3.79</b>	Calcium-binding EF-hand family protein; Potential calcium sensor	3
AT3G26830	<i>PAD3</i>	0.78	<b>1.91</b>	Bifunctional dihydrocamalexate synthase/camalexin synthase	3
AT3G14620	<i>CYP72A8</i>	1.54	<b>2.54</b>	Cytochrome P450, family 72, subfamily A, polypeptide 8	3
AT4G25100	<i>FSD1</i>	1.74	<b>2.75</b>	Superoxide dismutase [Fe] 1, chloroplastic; Destroys superoxide anion radicals	3
AT4G02520	<i>GSTF2</i>	0.93	<b>2.08</b>	Glutathione S-transferase PHI 2; Binds auxin, endogenous flavonoids and the camalexin	3
AT1G02930	<i>GSTF6</i>	<b>2.45</b>	<b>2.80</b>	Glutathione S-transferase F6; Involved in camalexin biosynthesis	3
AT1G02920	<i>GSTF7</i>	2.02	<b>1.75</b>	Glutathione S-transferase F7; conjugation of reduced GSH to hydrophobic electrophiles	3
AT1G69920	<i>GSTU12</i>	2.35	<b>2.48</b>	Glutathione S-transferase TAU 12; conjugation of reduced GSH to hydrophobic electrophiles	3
AT3G14620	<i>CYP72A8</i>	1.54	<b>2.54</b>	Cytochrome P450, family 72, subfamily A, polypeptide 8	3
AT1G68020	<i>ATPS6</i>	<b>0.75</b>	<b>1.47</b>	UDP-Glycosyltransferase / trehalose-phosphatase family protein; trehalose biosynthesis	5
AT1G70290	<i>TPS8</i>	<b>1.66</b>	<b>3.03</b>	Probable alpha,alpha-trehalose-phosphate synthase [UDP-forming] 8; trehalose biosynthesis	5
AT1G23870	<i>TPS9</i>	<b>1.41</b>	<b>1.65</b>	Probable alpha,alpha-trehalose-phosphate synthase [UDP-forming] 9; trehalose biosynthesis	5
AT4G22590	<i>TPPG</i>	<b>1.10</b>	<b>1.47</b>	Haloacid dehalogenase-like hydrolase (HAD) superfamily protein; produce free trehalose	5
AT2G18700	<i>TPS11</i>	<b>1.56</b>	<b>2.53</b>	Probable alpha,alpha-trehalose-phosphate synthase [UDP-forming] 11; trehalose biosynthesis	5
AT4G24040	<i>TRE1</i>	<b>1.30</b>	<b>2.31</b>	Trehalase 1; regulate trehalose content	5
AT3G15450	<i>AT3G15450</i>	<b>3.06</b>	<b>3.82</b>	Aluminium induced protein with YGL and LRDR motifs	5
AT5G22920	<i>AT5G22920</i>	<b>2.62</b>	<b>2.21</b>	CHY-type/CTCHY-type/RING-type Zinc finger protein; ROS production	5
AT2G20670	<i>AT2G20670</i>	<b>2.80</b>	<b>2.52</b>	Sugar phosphate exchanger, putative (DUF506)	5
AT3G30775	<i>EDR5</i>	<b>2.32</b>	<b>2.41</b>	Methylenetetrahydrofolate reductase family protein; response to oxidative stress	5
AT4G39650	<i>GGT2</i>	1.31	<b>1.71</b>	Gamma-glutamyl transpeptidase 2; involved in the degradation of glutathione	5
AT2G19800	<i>MIOX2</i>	<b>2.50</b>	<b>3.06</b>	Myo-inositol oxygenase 2; cell wall; ascorbate biosynthesis	5
AT5G14470	<i>GLCAK2</i>	<b>2.43</b>	<b>2.71</b>	GHMP kinase family protein; cell wall	5

### 2.1.7 Pi depletion alters expression of redox signaling-related genes

The generation of ROS appears to be involved in Pi deficiency response in root tips (Müller *et al.*, 2015; Zheng *et al.*, 2019). However, it is not fully understood how ROS work as toxic or signaling molecules to regulate primary root inhibition in response to low Pi.

To identify genes that may participate in ROS signaling, DEGs of the GO category “response to oxidative stress”, which are responsive to Pi limitation in WT and *pdr2*, were analyzed further (Fig. 2-7, Fig. 2-8, Tab. S6-7). Notably, all 13 oxidative stress-responsive genes in WT were also induced in *pdr2* root tips (Fig. 2-12A). The gene set contains three genes that are presumably involved in ROS homeostasis (*GSTF6*, *PRX54*, *PRX21*), one gene that participates in detoxification of reactive carbonyls (*AER*), and two genes associated with galactose metabolism (*DIN10* and *SIP2*) (Fig. 2-12B, Tab. S6-7). *OZF1* encodes an oxidation-related Zinc Finger 1, which is a plasma membrane protein (Fig. 2-12B, Tab. S6-7). In addition, there are 31 oxidative stress-responsive genes, which were only upregulated in *pdr2*, not in WT root tips (Fig. 2-12A and C). Among those DEGs, 12 *PRX* genes encode Class III peroxidases and four genes are known to be



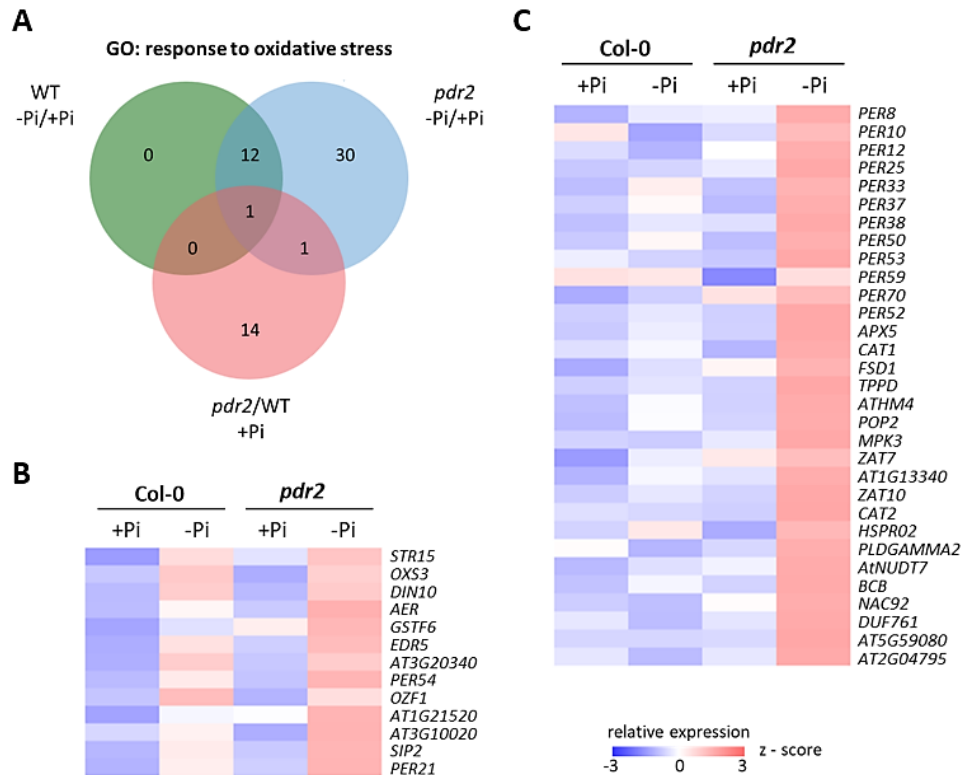


**Fig. 2-12: Pi deficiency induced the expression of oxidative stress-responsive genes in WT and *pdr2***

(A) VENN diagram of oxidative stress responsive genes that were induced by low Pi availability in WT and *pdr2* and those that were induced in *pdr2* compared to WT under +Pi condition (adjusted p-value < 0.05;  $-1 > \log_2(\text{fold change}) > 1$ ). Heat maps show the relative gene expression (z-score) of the oxidative stress responsive genes that were commonly regulated in both lines (B) or only regulated in *pdr2* (C). Full dataset is available in Tab. S6-7. Blue = low expression (-3); red = high expression (3); GO, gene ontology.

involved in ROS detoxification (*APX5*, *CAT1*, *CAT2*, *FSD1*) (Fig. 2-12C). A screen for all *PRX* genes revealed three (*PRX4*, *PRX27*, *PRX63*) that were downregulated in Pi-depleted *pdr2* (Tab. S6-7). Notably, a comparison with the proteomic analysis that was carried in our group (Hoehenwarter *et al.*, 2016) revealed that *PRX8*, *PRX37*, and *FSD1* were stabilized in WT or *pdr2* root during Pi deficiency response. Although expression of 16 oxidative stress-responsive genes was significantly higher in *pdr2* compared to WT under +Pi condition (Fig. 2-12A, Tab. S6-7), only two of those genes are shared with Pi-starved *pdr2* (*GSTF6* and *PRX70*, Fig. 2-12A). Besides, *GSTF6* is also induced in Pi-starved WT root tips.

We next focused on identifying transcription factors (TFs) that may be involved in ROS signaling. Using the integrated gene regulatory network, De Clercq *et al.* predicted 157 TFs with oxidative stress signaling and/or responsiveness functions (De Clercq *et al.*, 2021). Among them, 68 genes were differentially regulated in WT and/or *pdr2* during Pi deficiency response (adjusted p-value < 0.05;  $-0.7 > \log_2(\text{fold$

change) > 0.7) (Tab. S6-9). Table 2-4 lists 11 ROS-related TFs that were commonly regulated in WT and *pdr2*. The gene set consists of five *WRKYs* (*WRKY15*, *WRKY28*, *WRKY38*, *WRKY40*, *WRKY48*), three *ERFs* (*ERF013*, *ERF098*, *ERF114*, *ERF115*), *HHO3* and *BEH3*. *ERF114* was not predicted to be ROS regulator (De Clercq *et al.*, 2021), however, it has been reported to be H<sub>2</sub>O<sub>2</sub>-responsive (Kong *et al.*, 2018). Notably, all those TFs were more highly induced in *pdr2* compared to WT root tips (Tab. 2-4). Considering that the expression of 14 *PRXs* genes was induced by Pi deficiency as described above, it would be interesting to investigate how they are regulated. TFs predictions were therefore performed using Gene Group Analysis on the Plant Promoter Analysis Navigator (PlantPAN) v2.0 (<http://plantpan.itps.ncku.edu.tw/>). Of the 331 predicted TFs, 42 coding genes were differentially regulated in WT or *pdr2* root tips (adjusted p-value < 0.05;  $-1 > \log_2(\text{fold change}) > 1$ ) (Tab. S6-10). Surprisingly, five TF genes (*WRKYs*) were commonly induced in WT and *pdr2*, and these were those *WRKYs* predicted to be involved in ROS regulation (Tab. 2-4).

**Tab. 2-4: All ROS related transcription factors that were commonly regulated in WT and *pdr2*.**

Adjusted p-value < 0.05,  $-0.7 > \log_2(\text{fold change}) > 0.7$ . QC: quiescent center. FC: fold change.

Gene ID	Gene name	$\log_2\text{FC}_{-Pi/+Pi}$		Gene description
		WT	<i>pdr2</i>	
AT5G07310	<i>ERF115</i>	7.23	9.28	Ethylene-responsive TF; rate-limiting factor of QC cell division active
AT5G61890	<i>ERF114</i>	5.65	9.90	Ethylene-responsive TF; cell proliferation regulator
AT3G23230	<i>ERF098</i>	4.48	3.90	Ethylene-responsive TF; stress response
AT4G18170	<i>WRKY28</i>	3.65	4.33	WRKY TF
AT5G49520	<i>WRKY48</i>	3.30	4.75	Probable WRKY TF; stress- and pathogen-induced
AT1G80840	<i>WRKY40</i>	1.37	2.32	Probable WRKY TF; pathogen-induced
AT1G77640	<i>ERF013</i>	1.21	2.39	Ethylene-responsive TF; stress response
AT5G22570	<i>WRKY38</i>	1.20	2.68	Probable WRKY TF
AT1G25550	<i>HHO3</i>	0.84	1.06	TF HHO3; involved in phosphate signaling in roots
AT2G23320	<i>WRKY15</i>	0.75	1.91	Probable WRKY TF 15
AT4G18890	<i>BEH3</i>	0.70	1.01	BES1/BZR1 homolog protein 3

PLASMA MEMBRANE INTRINSIC PROTEINS (PIPs) have been proposed to translocate H<sub>2</sub>O<sub>2</sub> among different cell compartments to transduce ROS signaling. For example, it was reported that *PIP1;4* can effectively facilitate the transport of apoplastic H<sub>2</sub>O<sub>2</sub> into cytoplasm to trigger callose synthesis during plant bacterial defense response in leaves (Tian *et al.*, 2016). The expression level of *PIP2;4* has been reported to be downregulated in response to low Pi (Lin *et al.*, 2011). PIPs might be involved in Pi deficiency-triggered ROS signaling. We therefore screened all *PIP* genes in our data set. We observed that all *PIPs*, except *PIP1;5*, are expressed in the root tips (FPKM < 0.5) (Fig. 2-13). In addition, the expression level of *PIP1;1*, *PIP1;2*, *PIP1;3*, *PIP2;1*, *PIP2;2* and *PIP2;7* is higher than the rest of the *PIP* genes (Fig. 2-13). Upon Pi limitation, *PIP2;4* was downregulated in both WT and the hypersensitive *pdr2* mutant (Fig. 2-13, Tab. S6-11). *PIP2;6*

was upregulated only in WT during low Pi response (Fig. 2-13, Tab. S6-11). Moreover, more *PIP* genes (*PIP1;5*, *PIP2;3*, *PIP2;7* and *PIP2;8*) were downregulated in Pi-starved *pdr2* root tips (Fig. 2-13, Tab. S6-11). Interestingly, the expression level of all *PIPs* was not affected by Pi limitation in the insensitive line *lpr1lpr2*. Thus, *PIPs* seem to play, if at all, a role in the local Pi response.

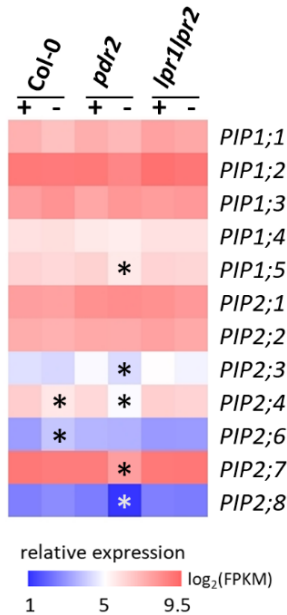


**Fig. 2-13: Transcript level heat map of *PIPs* in WT, *pdr2* and *lpr1lpr2* during Pi deficiency**

Log<sub>2</sub>(FPKM) which represents relative expression levels of *PIPs* were shown on a color scale, blue = low expression (1), red = high expression (9.5). "+" = +Pi, "-" = -Pi. Stars mark the DEGs (adjusted p-value < 0.05; -0.7 > log<sub>2</sub>FC > 0.7) in response to Pi deficiency. *PIP2;5* which is not included in the heat map didn't express in the root tips (FPKM < 0.5). Full dataset is available in Tab. S6-11.

ROS have long been associated with plasmodesmata permeability by regulating callose deposition during plant-pathogen interactions (Cheval & Faulkner, 2018). Callose accumulation is coordinated by the antagonistic activities of callose synthases (CalSs) (Ellinger & Voigt, 2014) and  $\beta$ -(1,3)-glucanases (BGs) (Tilsner *et al.*, 2016). Moreover, callose deposition is regulated by plasmodesmata-localized proteins (PDLs) and by plasmodesmata callose-binding proteins (PDCBs) (Tilsner *et al.*, 2016). To get a better understanding of callose accumulation mechanism upon Pi limitation, transcript changes of plasmodesmata callose associated genes were checked in our RNA-seq data set, including 12 *CalSs* (Cui & Lee, 2016), three *BGs* (*BG\_PPAP*, *BG1*, *BG2*) that encode plasmodesmata-localized BGs (Tilsner *et al.*, 2016), five *PDCBs* (Simpson *et al.*, 2009), and eight *PDLs* (Lee *et al.*, 2011) (Fig. 2-14, Tab. S6-12). The results show that *CalS* genes were not regulated in WT upon Pi limitation. Only *CalS6* and *CalS7* were slightly induced in *pdr2* by low Pi (around 1.6-fold for both genes) (Fig. 2-14, Tab. S6-12). *BG1* and *BG2* were not expressed in root tips (FPKM < 0.5). Pi deficiency did not influence the transcripts of *BG\_PPAP*. Besides, *PDCB2* and *PDL1* were highly induced in both WT and *pdr2* root tips upon Pi limitation. Whereas *PDCB5* and *PDL2* were slightly downregulated in Pi-starved *pdr2*. Additionally, *CALMODULINLIKE41* (*CML41*), which encodes a plasmodesmata-localized Ca<sup>2+</sup> binding protein and participates in callose deposition (Xu

*et al.*, 2017), was highly induced in *pdr2* root tips upon Pi limitation (around 130-fold) (Fig. 2-14, Tab. S6-12).

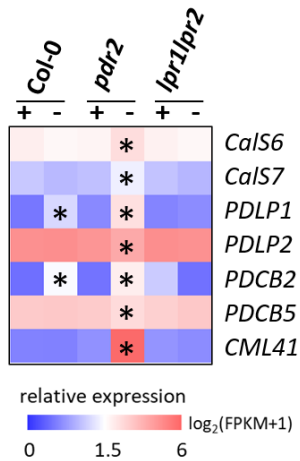


**Fig. 2-14: Transcript level heat map of callose-related genes in WT, *pdr2* and *lpr1lpr2* during Pi deficiency**

$\log_2(\text{FPKM}+1)$  which represents relative expression levels of genes were shown on a color scale, blue = low expression (0), red = high expression (6). "+" = +Pi, "-" = -Pi. Stars mark the DEGs (adjusted p-value < 0.05;  $-0.7 > \log_2\text{FC} > 0.7$ ) in response to Pi deficiency. Full dataset is available in Tab. S6-12.

## 2.2 Functional characterization of the *PIP* gene family during the local Pi deficiency response

### 2.2.1 Rationale

Members of the PIP family have been proposed to translocate  $\text{H}_2\text{O}_2$  among different cell compartments to transduce ROS signaling. We therefore analyzed the 13 members of the PIP family in *Arabidopsis thaliana* (PIP1;1 – PIP1;5 and PIP2;1 – PIP2;8) for a potential role in the local Pi deficiency response. We monitored (i) the expression patterns of *PIP* promoters in primary roots and (ii) the primary root growth response to Pi limitation. Because preliminary tests with the *pip2;4* and *pip2;6* loss-of-function mutants did not show an obvious root phenotype in response to low Pi, we added a low concentration of AI (2.5  $\mu\text{M}$ ) to the media, which stimulates the local Pi deficiency response (unpublished data by our group).

### 2.2.2 Expression analysis of *PIP* promoter reporter lines

To monitor the expression patterns of the *PIP* gene family in response to Pi deficiency, histochemical analysis of GUS reporter expression was performed with transgenic *Arabidopsis thaliana* lines transformed with either *pPIP::GFP-GUS* or *pPIP::GUS* constructs. GUS reporter activities driven by *PIP1;2*, *PIP1;3*, *PIP1;4*, *PIP2;3*, *PIP2;4*, *PIP2;5*, *PIP2;7* promoters were detected in root tips under Pi sufficiency (Fig. 2-15A). Stronger *PIP1;3* promoter activity was detected after Pi-starvation treatment, and induction of *PIP1;4* promoter activity was also observed in Pi-deficient root tips (Fig. 2-15A). *PIP2;3* promoter activity was not

induced after Pi-starvation treatment (Fig. 2-15A). However, *PIP2;3* promoter activity was detected only in the root meristem where *LPR1* is expressed (Fig. 2-15A). The expression domain of *PIP2;3* was also monitored using GFP as a reporter (Fig. 2-15B). GFP-fluorescence was mainly detected in the endodermis near the stem cell niche. There was no GUS expression driven by promoters of *PIP1;1*, *PIP1;5*, *PIP2;1*, *PIP2;2*, *PIP2;6*, *PIP2;8* in root tips (Fig. 2-15A). However, *PIP1;1*, *PIP1;5* and *PIP2;6* promoter activities were detected in upper part of the root (Fig. S6-4). *PIP2;1*, *PIP2;2* and *PIP2;8* were expressed in leaves (Fig. S6-4).

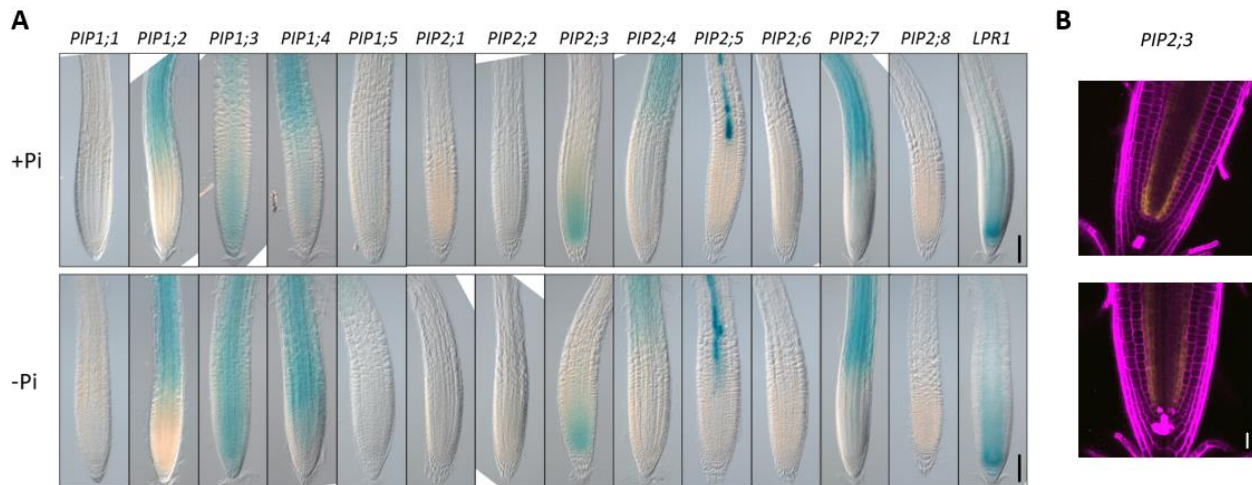


**Fig. 2-15: Tissue-specific expression analysis of PIPs**

GUS staining (A) and GFP fluorescence detection (B) of *pPIP::GFP-GUS* and *pPIP::GUS* reporter lines when grown under Pi-sufficient and Pi-deficient conditions in the primary root tip. Seeds were germinated on +Pi agar plates for 5 days and then transferred to +Pi (50  $\mu$ M Fe, 2.5  $\mu$ M Al) or -Pi (50  $\mu$ M Fe, 2.5  $\mu$ M Al) conditions. After 1 day of transfer, GUS staining or GFP fluorescence detection were performed. Shown are representative images (n=5-6). Scale bars = 100  $\mu$ m (A) & 20  $\mu$ m (B). For *pPIP1;3::GFP-GUS*, *pPIP1;4::GFP-GUS*, *pPIP2;3::GFP-GUS*, two independent lines were analyzed, one representative line for each construct is shown.

### 2.2.3 Primary root growth characterization of *pip* mutants

Gain of primary root length of all *pip* single mutants was recorded. *pip1;1*, *pip1;2*, *pip1;3*, *pip2;3* and *pip2;8* exhibited slightly shorter primary roots compared to WT after Pi-starvation; however, the shorting was not very striking (< 1.6-fold) (Fig. 2-16). The *pip2;7* mutant (*Ler* background) responds like the respective WT to Pi deficiency (Fig. 2-16). Since *PIP1;3* and *PIP1;4* promoter activities are induced by Pi deficiency and both genes may function redundantly, the *pip1;3 pip1;4* double mutant was generated. Although primary root extension of Pi-deficient *pip1;3 pip1;4* was statistically shorter than that of WT, the shorting was only 1.2-fold (Fig. 2-17). In addition, we obtained the *quintuple mutant* (*pip2;1 pip2;2 pip2;4 pip2;6 pip2;7*)

from our collaborator (Anton R Schäffner, LMU München, Germany). Gain of primary root length of the *quintuple mutant* was recorded. However, upon transfer to low Pi medium, the *quintuple mutant* developed a significantly longer primary root than the WT (Fig. 2-17).

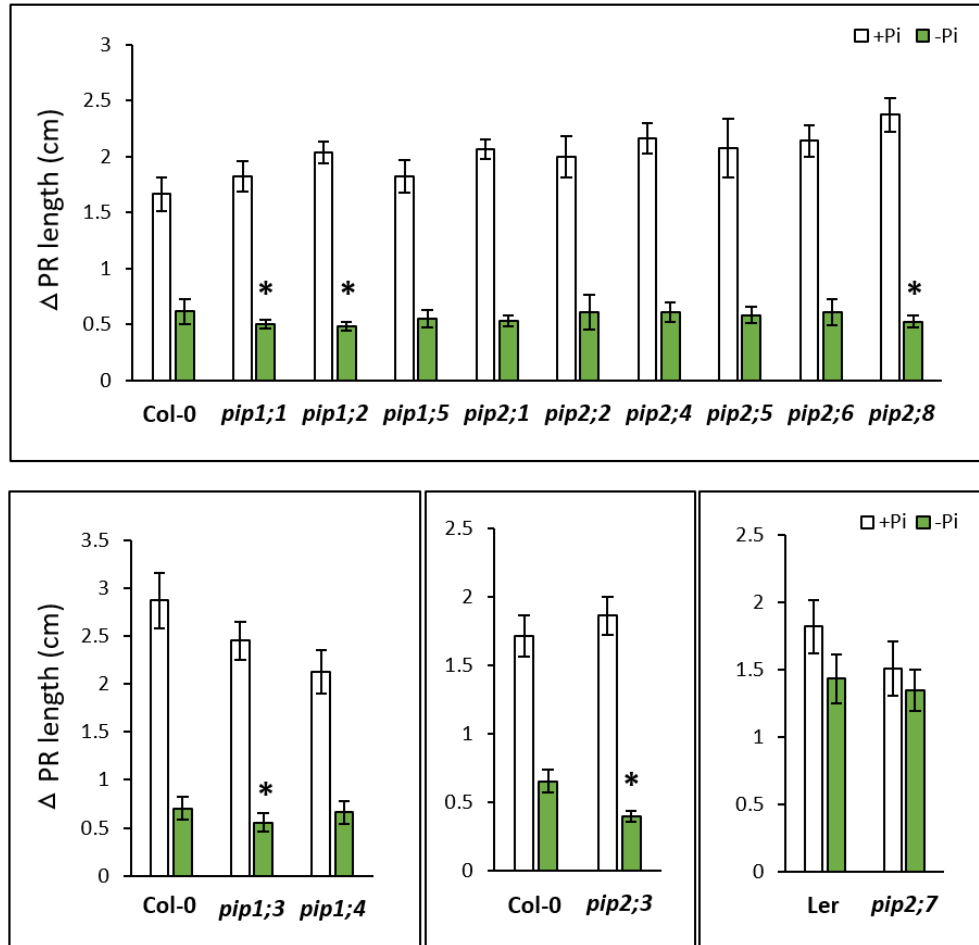


**Fig. 2-16: Comparison of primary root inhibition among all *pip* single mutants and WT seedlings**

Seeds were germinated on +Pi agar plates for 5 days, transferred to +Pi (50  $\mu$ M Fe, 2.5  $\mu$ M Al) or -Pi (50  $\mu$ M Fe, 2.5  $\mu$ M Al) conditions. After 3 days of transfer,  $\Delta$  primary root length was measured ( $\pm$ SD; n=10-20). *pip2;7* is in Ler background. Asterisks indicate significant differences as determined by Student's t-test (two-tailed, equal variances,  $p < 0.05$ ) compared to Col-0 -Pi condition.

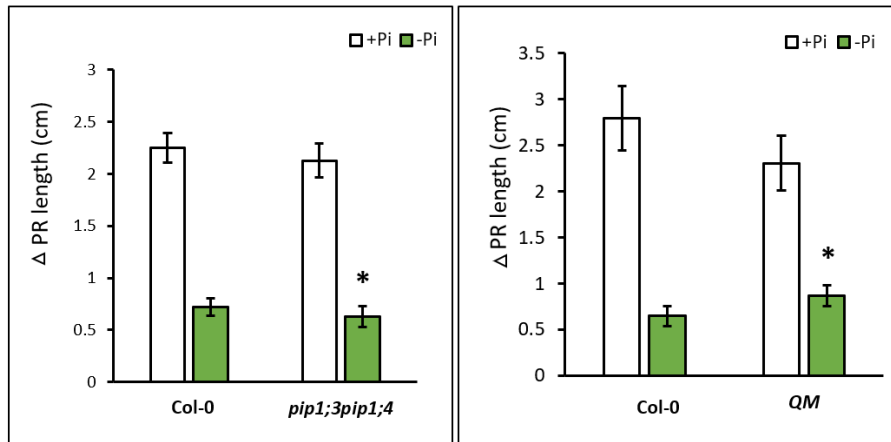


**Fig. 2-17: Comparison of primary root inhibition among *pip* higher order mutants and WT seedlings**

Seeds were germinated on +Pi agar plates for 5 days, transferred to +Pi (50  $\mu$ M Fe, 2.5  $\mu$ M Al) or -Pi (50  $\mu$ M Fe, 2.5  $\mu$ M Al) conditions. After 3 days of transfer,  $\Delta$  primary root length was measured ( $\pm$ SD; n=20). Data is representative of two independent experiments. Asterisks indicate significant differences as determined by Student's t-test (two-tailed, equal variances,  $p < 0.05$ ) compared to Col-0 -Pi condition.

## 2.3 Analysis of ROS signaling in root tips during the local Pi deficiency response

### 2.3.1 Rationale

Previous study showed that Pi deficiency triggers the generation of ROS in root meristems (particularly in the SCN) of WT and *pdr2* seedlings, but not in insensitive *lpr1/lpr2* plants (Müller *et al.*, 2015). Our transcriptome analysis revealed an overrepresentation of genes related to oxidative stress (Fig. 2-7 and Fig. 2-8). We also identified a group of TFs that may participate in ROS signaling (Tab. 2-4). To gain insight into the mechanism of how ROS are involved in the local Pi deficiency response, ROS-related mutants were investigated. Moreover, using different dyes and genetically encoded probes for ROS detection, we studied in more detail about ROS formation and accumulation in root tips upon Pi deprivation.

### 2.3.2 Analysis of select ROS-related mutants

ROS have been shown to act as signal in regulating root growth (Eljebbawi *et al.*, 2021; Mase & Tsukagoshi, 2021). If this is also the case during the local Pi response, one would expect that disturbing the expression of the oxidative stress responsive genes which are involved in ROS signaling may influence the root response to low Pi. On the other hand, if ROS only functions as toxic chemical to the cell, disturbing the ROS detoxifying system might lead to a hypersensitive response to Pi deficiency. To test this hypothesis, several genes that may participate in ROS signaling and detoxification were selected from our RNA-seq

dataset for further investigation (Tab. 2-5). The respective mutants were ordered and the mutations were verified by PCR. To study how those mutants respond to Pi deficiency, primary root extension was compared to WT upon transfer from Pi-sufficient conditions (5 days) to +Pi or –Pi condition for 4 days. However, no obvious primary root growth difference was observed among those of mutants when compared the WT (Fig. 2-18).

**Tab. 2-5: Select oxidative stress responsive genes that were studied further.**

$\log_2$ FC of the genes that were significantly induced (adjusted p-value < 0.05) are labeled in bold. FC: fold change.

Gene ID	Gene name	$\log_2$ FC <sub>-Pi/+Pi</sub>		Gene description
		WT	<i>pdr2</i>	
AT5G20250	<i>DIN10</i>	<b>3.13</b>	<b>3.03</b>	Probable galactinol--sucrose galactosyltransferase 6; expression is responding to sugar level
AT5G16970	<i>AER</i>	<b>3.05</b>	<b>5.96</b>	NADPH-dependent oxidoreductase 2-alkenal reductase; detoxification of reactive carbonyls
AT1G02930	<i>GSTF6</i>	<b>2.45</b>	<b>2.80</b>	Glutathione S-transferase F6; camalexin biosynthesis
AT3G30775	<i>EDR5</i>	<b>2.32</b>	<b>2.41</b>	Methylenetetrahydrofolate reductase family protein; Encodes a proline oxidase
AT2G19810	<i>OZF1</i>	<b>1.91</b>	<b>1.38</b>	Encodes Oxidation-related Zinc Finger 1 (OZF1), a plasma membrane protein
AT3G57520	<i>SIP2</i>	<b>1.40</b>	<b>1.97</b>	Probable galactinol--sucrose galactosyltransferase 2; unloading raffinose from the phloem
AT4G25100	<i>FSD1</i>	1.74	<b>2.75</b>	Superoxide dismutase [Fe] 1; Destroys superoxide anion radicals
AT1G35910	<i>TPPD</i>	0.77	<b>5.27</b>	Haloacid dehalogenase-like hydrolase (HAD) superfamily prote

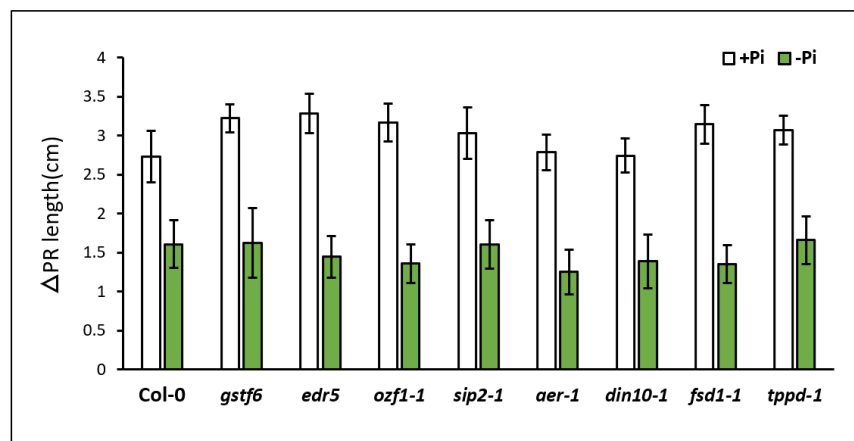


**Fig. 2-18: Comparison of primary root inhibition among oxidative stress-related mutants and WT seedlings**

Seeds were germinated on +Pi agar plates for 5 days, transferred to +Pi (25  $\mu$ M Fe) or -Pi (25  $\mu$ M Fe) conditions. After 4 days of transfer,  $\Delta$  primary root length was measured ( $\pm$ SD; n=11-30). Shown data is from one representative out of two independent experiments.

### 2.3.3 Monitoring of ROS accumulation in root tips

ROS exist in various forms and each type of ROS species has distinct chemical properties. Investigation of which ROS species are formed and where do ROS accumulate in Pi-starved root tips will help to understand



the mechanisms by which ROS participate in local Pi deficiency responses. We therefore used different dyes to specifically monitor the formation of  $O_2^{\cdot-}$ ,  $H_2O_2$  and  $\cdot OH$  in Pi-starved root tips.

Firstly, root cell integrity of SCN was monitored by propidium iodide (PI) staining. Frequent cell death was observed in the QC of WT within 20 h after transfer to -Pi (Fig. 2-19A and B). To gain an overview of where ROS accumulate, Carboxy-H2DCFDA staining that stains a wide variety of ROS was performed. The fluorescent signal was not detectable in Pi-replete RAM of WT, *pdr2* and *lpr1lpr2* (Fig. 2-19C). Strong signals were observed in the SCN and columella cells of WT and *pdr2* after transfer to -Pi for 1 day, which did not appear in the Pi-starved *lpr1lpr2* root tips (Fig. 2-19C).

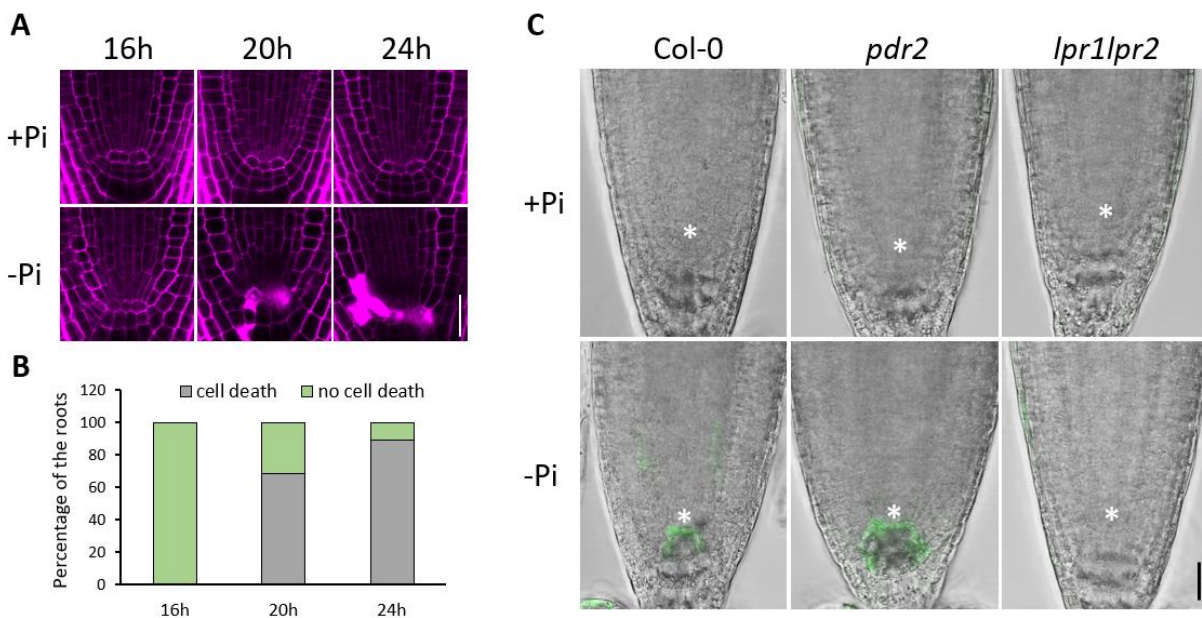


**Fig. 2-19: ROS accumulation in Pi-sufficient and Pi-deprived root tips**

(A) Propidium iodide-stained root tips of WT upon transfer of 5-day-old seedlings from +Pi (25  $\mu M$  Fe) agar plates to +Pi (25  $\mu M$  Fe) or -Pi (25  $\mu M$  Fe) medium for up to 24 h. (B) Percentage of the Pi-starved WT primary roots that have cell death within QC (n=8 for 16h, n=48 for 20h, n= 36 for 24h). (C) Representative images of ROS accumulation in the RAM of WT, *pdr2* and *lpr1lpr2* revealed by Carboxy-H2DCFDA staining (n=10). Staining was performed after 1 day of transfer from +Pi (25  $\mu M$  Fe) agar plates to +Pi (25  $\mu M$  Fe) or -Pi (25  $\mu M$  Fe) medium. Asterisks mark the QC. Scale bars (A and C) = 25  $\mu m$ .

By performing nitro blue tetrazolium (NBT) staining we could observe the presence of  $O_2^{\cdot-}$  mainly in the inner tissues of the transition zone, and which extended to the meristematic zone and elongation zone in all genotypes on Pi-replete condition (Fig. 2-20). In Pi-deprived WT, the staining in the RAM appeared more intense after 20 h of transfer compared to Pi-replete root tips (Fig. 2-20). Moreover, the difference became more obvious after 24 h of transfer to low Pi (Fig. 2-20). Higher level of  $O_2^{\cdot-}$  in the RAM of Pi-starved *pdr2*

was observed within 10 h on -Pi and the level increased 20 h after transfer (Fig. 2-20). The enhanced  $O_2^{\bullet-}$  level was suppressed in the insensitive *lpr1lpr2* line during low Pi response (Fig. 2-20).

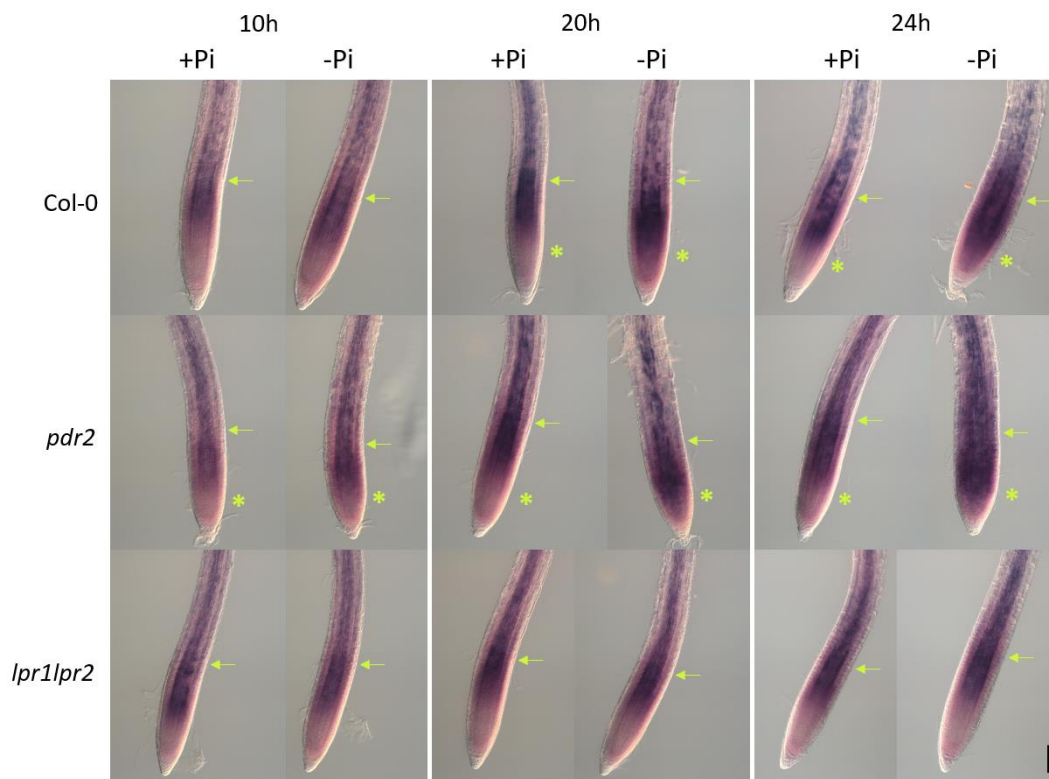


**Fig. 2-20: Distribution of superoxide in root tips visualized by NBT staining during low Pi response**

Representative images of  $O_2^{\bullet-}$  distribution in the root tips of WT, *pdr2* and *lpr1lpr2* ( $n=10$ ). Seeds were germinated on +Pi (25  $\mu$ M Fe) agar plates for 5 days and then transferred to +Pi (25  $\mu$ M Fe) or -Pi (25  $\mu$ M Fe) conditions. After 10h, 20h, 24h of transfer, NBT staining was performed. Transition zones are indicated by arrows. Asterisks mark the site where the difference of staining triggered by -Pi was observed. Scale bar = 100  $\mu$ m.

We used a second dye, dihydroethidium (DHE), to detect  $O_2^{\bullet-}$ . There was fluorescent signal in the root tips, especially in the meristematic zone (Fig. 2-21A). In response to Pi deficiency, no obvious difference of the fluorescence level was observed in WT, *pdr2* and *lpr1lpr2* root tips (Fig. 2-21A). However, the signal was significantly increased in the QC of WT after 17 h of Pi starvation treatment (Fig. 2-21B and C). Overaccumulation of  $O_2^{\bullet-}$  in QC was not evident in the insensitive *lpr1lpr2* mutant (Fig. 2-21B and C).

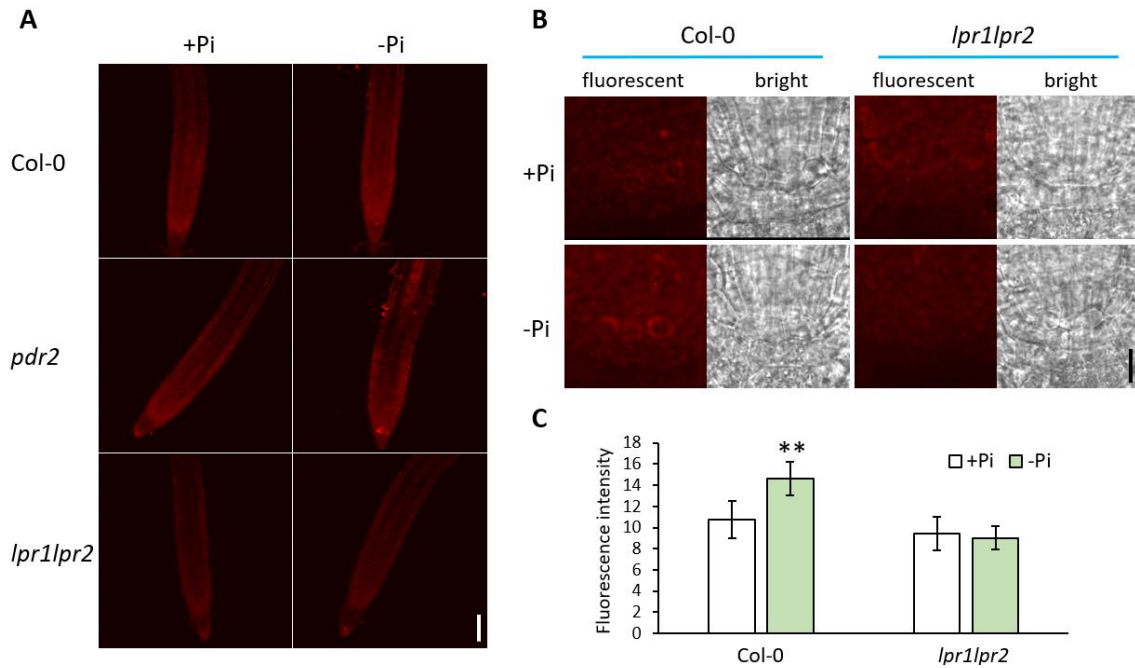


**Fig. 2-21: Distribution of superoxide in root tips visualized by DHE staining during low Pi response**

Seeds were germinated on +Pi (50  $\mu$ M Fe, 2.5  $\mu$ M Al) agar plates for 5 days and then transferred to +Pi (50  $\mu$ M Fe, 2.5  $\mu$ M Al) or -Pi (50  $\mu$ M Fe, 2.5  $\mu$ M Al) conditions. (A) Representative images of  $O_2^{\cdot-}$  distribution in the root tips of WT, *pdr2* and *lpr1lpr2* after 1 day of transfer (n=5). (B) Representative images of  $O_2^{\cdot-}$  distribution in the QC of WT and *lpr1lpr2* after 17h of transfer (n=15-21). (C) Quantification of  $O_2^{\cdot-}$  levels in the QC from (B). Asterisks indicate significant differences as determined by Student's t-test (two-tailed, equal variances, \*p < 0.001) compared to +Pi condition. Error bars represent  $\pm$  SD. Scale bars = 100  $\mu$ m (A); 10  $\mu$ m (B).

To determine the distribution of  $H_2O_2$ , we stained the roots with BES-  $H_2O_2$ -Ac, which responds specifically to hydrogen peroxide (Maeda *et al.*, 2004). Fluorescence was detected in the whole root tip and was brighter in the transition zone and elongation zone (Fig. 2-22). Results of the Pi deficiency treatment showed that it did not alter the  $H_2O_2$  level in WT, *pdr2* and *lpr1lpr2* (Fig. 2-22).

In addition,  $\cdot$ OH levels were assessed using 3'-(p-hydroxyphenyl) fluorescein (HPF) staining in WT. Strong fluorescence signal was observed in root cap and epidermis of the elongation zone under Pi-sufficient condition (Fig. 2-23). After Pi starvation, the signal was not affected (Fig. 2-23).

Taken together, after Pi starvation, a burst of ROS was detected in the SCN where cell death eventually occurred. Moreover, Pi deficiency triggered the overaccumulation of  $O_2^{\cdot-}$  in the cytosol of the QC and the meristematic zone.

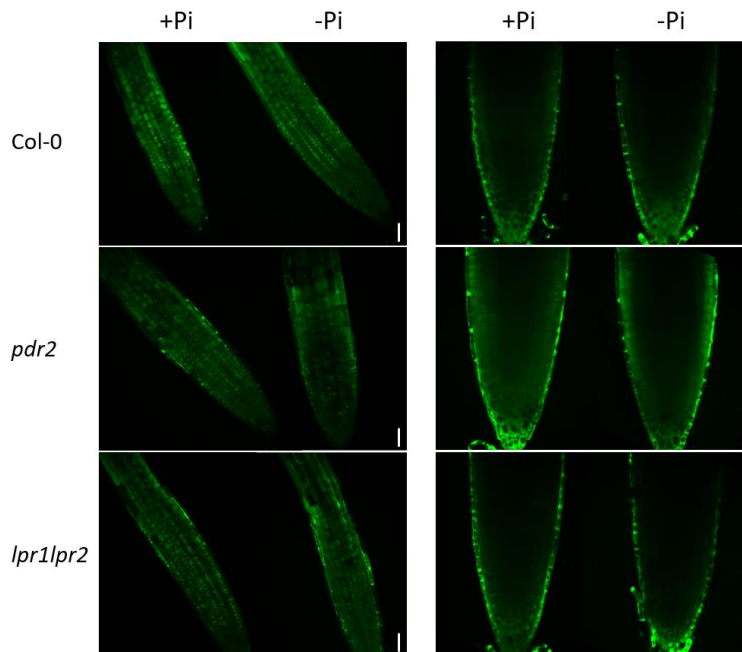


**Fig. 2-22: H<sub>2</sub>O<sub>2</sub> levels in root tips during low Pi response**

Representative images of H<sub>2</sub>O<sub>2</sub>-BES-Ac-stained RAM (top images) and root tips (bottom images) of WT, *pdr2* and *lpr1lpr2* (n=5). Seeds were germinated on +Pi (50  $\mu$ M Fe, 2.5  $\mu$ M Al) agar plates for 5 days and then transferred to +Pi (50  $\mu$ M Fe, 2.5  $\mu$ M Al) or -Pi (50  $\mu$ M Fe, 2.5  $\mu$ M Al) conditions. After 1 day of transfer, staining was performed. Scale bars = 25  $\mu$ m (top images); 50  $\mu$ m (bottom images).

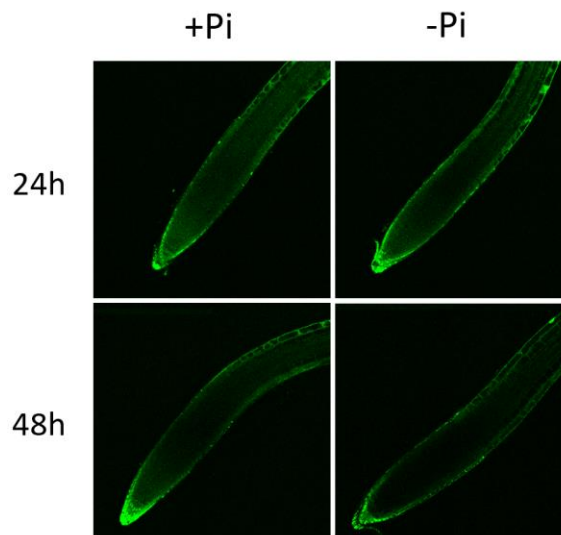


**Fig. 2-23: Distribution of  $\cdot$ OH in root tips during low Pi response**

Five-day-old +Pi (10  $\mu$ M Fe) seedlings of WT were transferred to +Pi (10  $\mu$ M Fe) or -Pi (10  $\mu$ M Fe) medium for 1 day or 2 days. Then the levels of  $\cdot$ OH were analyzed by HPF staining (n=5). Scale bars = 100  $\mu$ m.

### 2.3.4 Effect of diphenylene iodonium on primary root length in low Pi

To investigate the role of  $O_2^{\cdot-}$  in low Pi regulated primary root growth inhibition, we treated seedlings with diphenylene iodonium (DPI). DPI primarily inhibits the activities of RBOHs which are known as  $O_2^{\cdot-}$  generators. DPI treatment decreased the primary root length in WT, *pdr2* and *lpr1lpr2* in a concentration dependent manner under +Pi condition (Fig. 2-24). An inhibition of primary root growth was also observed in DPI-treated *lpr1lpr2* on -Pi medium (Fig. 2-24). In contrast, no obvious difference of the primary root growth was observed between DPI treated and no DPI treated WT and *pdr2* under - Pi condition (Fig. 2-24).

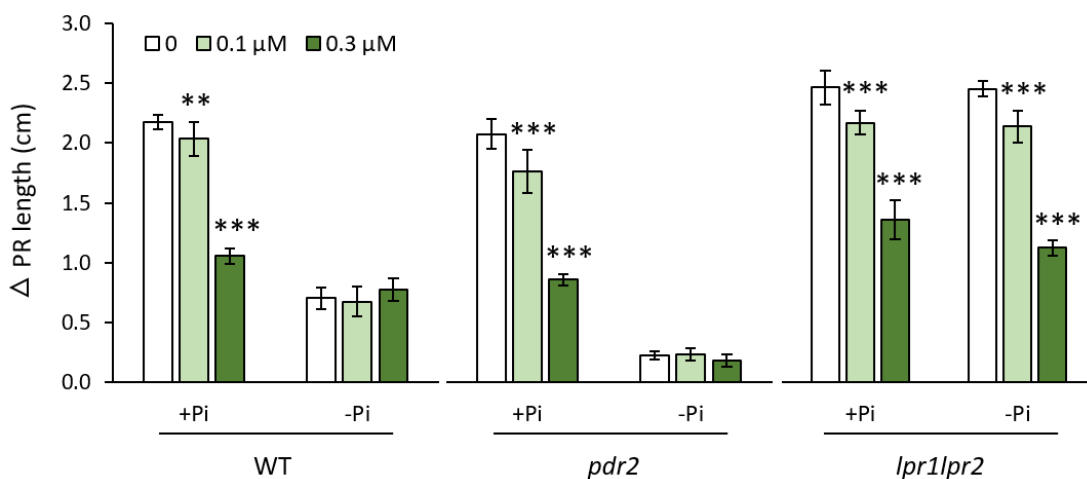


**Fig. 2-24: Effect of a superoxide scavenger on the primary root growth during low Pi response**

Primary root growth analysis of DPI (a  $O_2^{\cdot-}$  scavenger) treated seedlings of WT, *pdr2* and *lpr1lpr2*. Seeds were germinated on +Pi (25  $\mu$ M Fe) agar plates for 5 days, transferred to +Pi (25  $\mu$ M Fe) or -Pi (25  $\mu$ M Fe) conditions. After 3 days of transfer,  $\Delta$  primary root length was measured (n=10). Asterisks indicate significant differences as determined by Student's t-test (two-tailed, equal variances, \*\*p < 0.01, \*\*\*p < 0.001) compared to control condition. Error bars represent  $\pm$  SD.

### 2.3.5 Monitoring of cellular redox potential in root tips

ROS can be partly detoxified by the glutathione-ascorbate pathway, which may transiently alter the glutathione redox potential ( $E_{GSH}$ ). It has been shown that the genetically encoded redox probe Grx1-roGFP2 can dynamically measure the  $E_{GSH}$  *in vivo* (Meyer *et al.*, 2007; Ugalde *et al.*, 2020). Reduced and oxidized roGFP2 can be excited at 488nm and 405nm respectively. The emission peaks of both roGFP2 forms are same. By measuring the fluorescence ratio of 405/488nm, cytosolic  $E_{GSH}$  and ROS level can therefore be estimated.

A transgenic line expressing Grx1-roGFP2 under the control of the *UBQ10* promoter (*pUBQ10:Grx1-roGFP2*) in the Col-0 background was obtained from our collaborator (Rainer Waadt, Centre for Organismal Studies Heidelberg, Germany) and crossed into *pdr2* and *lpr1lpr2*. Genotyping and Basta selection were performed to obtain homogenous lines of *pUBQ10:Grx1-roGFP2* in the *pdr2* and *lpr1lpr2* background. To establish the method in our working condition, some tests were performed first.

Excitation at 405 nm triggered autofluorescence in WT seedlings containing no roGFP2 (Fig. S6-5), but not at 488 nm. To elucidate if the low Pi treatment affects the autofluorescence, root tips of WT, *pdr2* and *lpr1lpr2* were checked after 20 h of -Pi treatment. Pi deficiency did not alter the autofluorescence level in WT and *lpr1lpr2* root tips (Fig. 2-25A and B). However, the level was reduced in Pi-deficient root tips of *pdr2*. In addition, ratio measurement of 405/488nm should avoid dead cell. Because on one hand, the construct is designed for cytosolic  $E_{GSH}$  measurement, and on the other hand, cell death enhanced the autofluorescence triggered by 405nm.

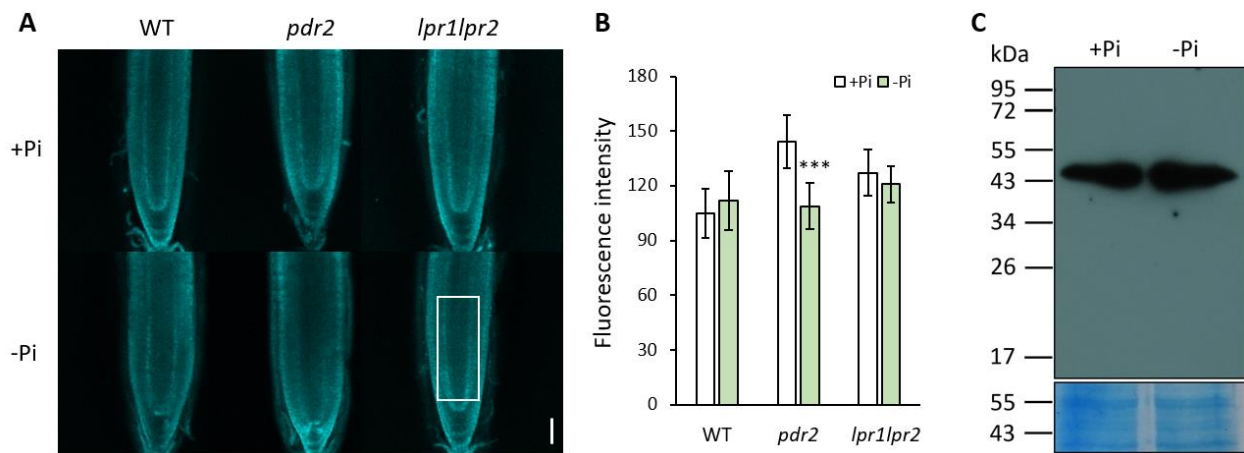


**Fig. 2-25: 405 nm triggered autofluorescence and detection of Grx1-roGFP2 in response to Pi deficiency**

(A) Representative confocal images of WT, *pdr2* and *lpr1lpr2* excited by 405 nm (n=9-12). Seeds were germinated on +Pi (25  $\mu$ M Fe) agar plates for 5 days and then transferred to +Pi (25  $\mu$ M Fe) or -Pi (25  $\mu$ M Fe) conditions. After 20h of transfer, root tips were scanned. Scale bars = 50  $\mu$ m. (B) Quantification of autofluorescence in root tips marked with white rectangle from (A). Asterisks indicate significant difference as determined by Student's t-test (two-tailed, equal variances, \*\*\* $p < 0.001$ ) compared to +Pi condition. Error bars represent  $\pm$  SD. (C) Total protein was extracted from whole roots of in stably transformed WT Arabidopsis seedlings after transfer from +Pi (25  $\mu$ M Fe) to +Pi (25  $\mu$ M Fe) or -Pi (25  $\mu$ M Fe) medium (1 day). Protein extracts were separated by SDS-PAGE (bottom image, Coomassie-stained gel) and transferred to membranes for immunoblot analysis using anti-GFP antibody (top image).

Western blot analysis was performed using an anti-GFP antibody to detect if free GFP is formed during Pi deficiency in WT. A band of around 43 kDa was expected for Grx1-roGFP2 (MW of Grx1, linker and roGFP2

is 11.8 kDa, 1.9 kDa and 28.9 kDa, respectively). In both +Pi sample and -Pi sample, only a band around 43 kDa was detected, which indicated that no free GFP was formed (Fig. 2-25C).

To investigate the influence of Pi starvation on the cytosolic  $E_{GSH}$  at root tip, a time series was performed first in WT to find out the most promising time point. We noticed that the ratio of 405/488nm in Pi-deficient RAM was higher than Pi-replete RAM (around 1.3-fold) after 6 h of transfer, which indicates the oxidation of the roGFP2 during low Pi (Fig. 2-26). Treatment with 10 mM  $H_2O_2$  resulted in a stronger increase of the ratio (around 2-fold). However, we could not obtain consistent results in repeated experiments. The result from the second replicate showed that low Pi led to the decrease of the 405/488nm ratio (around 1.2-fold), whereas the last two replicates revealed no influence of -Pi on the ratio. Therefore, no conclusion can be drawn based on those results. The redox sensor was investigated in *pdr2* and *lpr1lpr2* one time after low Pi treatment for 6 h. No ratio difference was observed in Pi-replete and Pi-deficient RAM of both lines (Fig. 2-27).



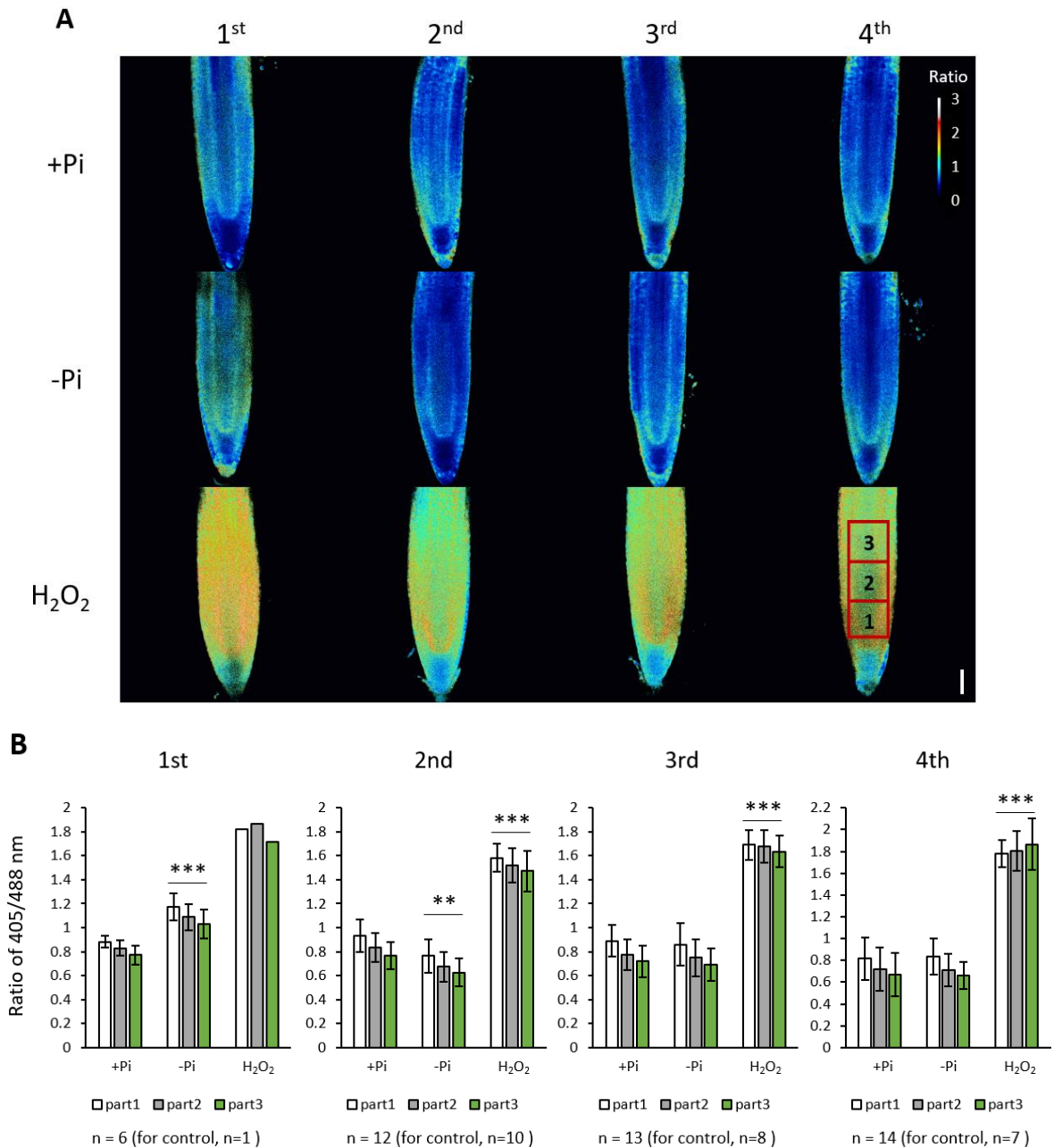


**Fig. 2-26: Response of cytosolic Grx1-roGFP2 to Pi deficiency in the RAM of WT**

(A) Representative 405/488 nm ratio images of WT from four independent biological replicates (1<sup>st</sup>, 2<sup>nd</sup>, 3<sup>rd</sup>, 4<sup>th</sup>). Seeds were germinated on +Pi (25  $\mu$ M Fe) agar plates for 5 days and then transferred to +Pi (25  $\mu$ M Fe) or -Pi (25  $\mu$ M Fe) conditions. After 6h of transfer, stacks of images were taken with excitation at 405 and 488 nm, respectively, and then used to calculate ratio images. To oxidize roGFP2, root tips were treated with 10 mM H<sub>2</sub>O<sub>2</sub> for 5 min before the images were taken. The color scale indicates reduced roGFP2 in blue and oxidized roGFP2 in red. Scale bars = 50  $\mu$ m. (B) Quantification of ratio in the RAM marked with red rectangle from (A). Asterisks indicate significant difference as determined by Student's t-test (two-tailed, equal variances, \*\*p < 0.01, \*\*\*p < 0.001) compared to +Pi condition. Error bars represent  $\pm$  SD.



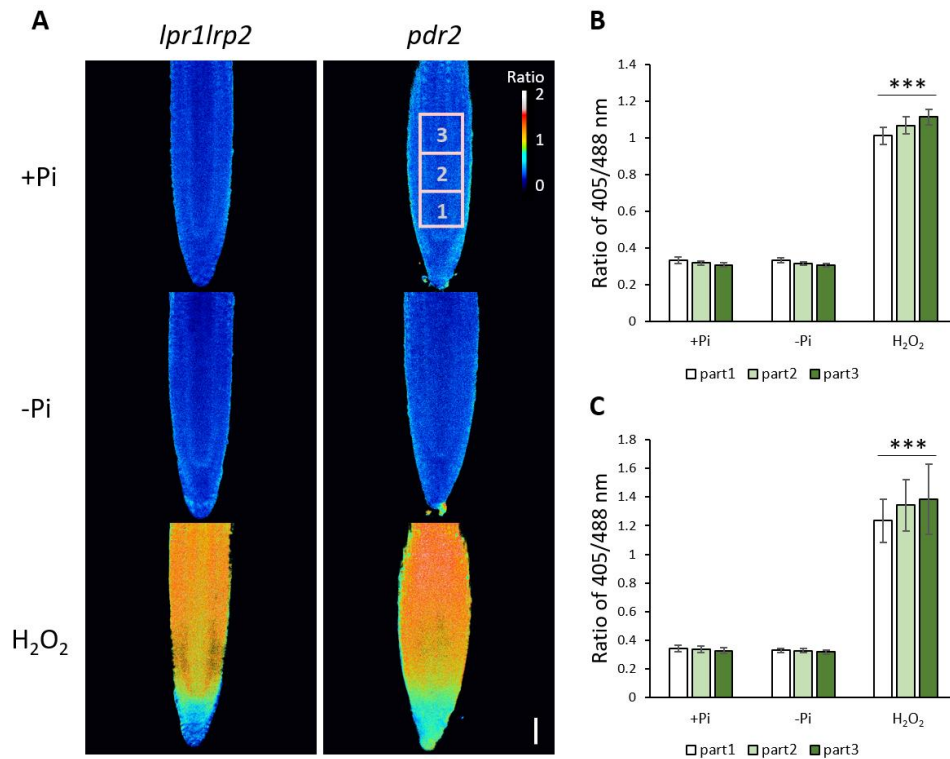


**Fig. 2-27: Response of cytosolic Grx1-roGFP2 to Pi deficiency in the RAM of *lpr1lpr2* and *pdr2***

(A) Representative 405/488 nm ratio images of *lpr1lpr2* (n=11-15) and *pdr2* (n=10-14). Seeds were germinated on +Pi (25  $\mu$ M Fe) agar plates for 5 days and then transferred to +Pi (25  $\mu$ M Fe) or -Pi (25  $\mu$ M Fe) conditions. After 6h of transfer, stacks of images were taken with excitation at 405 and 488 nm, respectively, and then used to calculate ratio images. To oxidize roGFP2, root tips were treated with 10 mM H<sub>2</sub>O<sub>2</sub> for 5 min before the images were taken. The color scale indicates reduced roGFP2 in blue and oxidized roGFP2 in red. Scale bars = 50  $\mu$ m. Quantification of ratio in the RAM of *lpr1lpr2* (B) and *pdr2* (C) marked with pink rectangle from (A). Asterisks indicate significant difference as determined by Student's t-test (two-tailed, equal variances, \*\*\*p < 0.001) compared to +Pi condition. Error bars represent  $\pm$  SD.

To specifically monitor the  $E_{GSH}$  in the QC, transgenic line transformed with *pWOX5:Grx1-roGFP2* was generated. The expression site of Grx1-roGFP2 was checked first. Main signals were observed in the QC while weaker signals were also visible in QC-surrounding cells, which could be caused by the diffusion of RNA or protein through plasmodesmata (Fig. 2-28A). Furthermore, the ratio of 405/488nm was measured for the QC. Treatment with 10 mM H<sub>2</sub>O<sub>2</sub> resulted in an increase of the 405/488nm ratio in QC compared to +Pi condition (around 3-fold). Pi starvation did not alter the ratio values in QC after 18 h of transfer (Fig. 2-28B). For other time points (2h, 4h, 6h) studied, no ratio difference was observed between Pi-replete and Pi-deficient QC as well (Fig. S6-6).

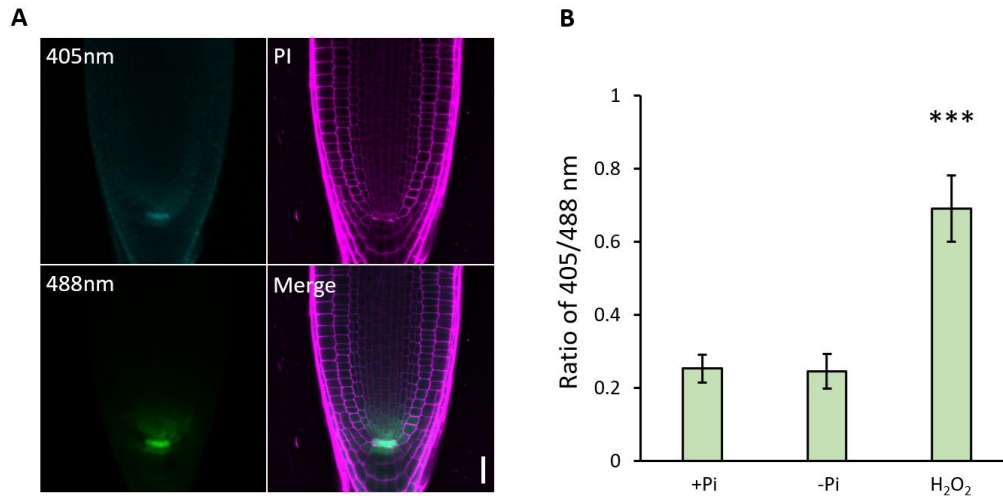


**Fig. 2-28: Response of cytosolic Grx1-roGFP2 to Pi deficiency in the QC of WT**

(A) Expression of pWOX5:Grx1-roGFP2 in 6-day-old WT counterstained with propidium iodide. Scale bars = 25  $\mu$ m. (B) Quantification of 405/488 nm ratio in the QC of WT after transfer from +Pi (25  $\mu$ M Fe) agar plates to +Pi (25  $\mu$ M Fe) or -Pi (25  $\mu$ M Fe) conditions (18h) (n=9-12 for +Pi and -Pi samples; n=5 for H<sub>2</sub>O<sub>2</sub> samples). To oxidize roGFP2, root tips were treated with 10 mM H<sub>2</sub>O<sub>2</sub> for 2 min before the images were taken. Asterisks indicate significant difference as determined by Student's t-test (two-tailed, equal variances, \*\*\*p < 0.001) compared to +Pi condition. Error bars represent  $\pm$  SD.

### 3. DISCUSSION AND FUTURE PERSPECTIVES

#### 3.1 Transcriptome analysis of Pi-deficient root tips

Our previous study and work from other groups have shown that Pi limitation triggers prominent changes in the transcriptional profile of whole roots (Thibaud *et al.*, 2010; Lan *et al.*, 2015; Hoehenwarter *et al.*, 2016). Root tips are proposed to play an essential role in sensing Pi limitation in the rhizosphere and locally inform root development (Ticconi *et al.*, 2004; Svistoonoff *et al.*, 2007). In this study, our transcriptomic analysis of WT, *pdr2*, and *lpr1lpr2*, which show contrasting Pi-dependent root phenotypes upon Pi limitation, gives insight into Pi-dependent acclimation processes specifically in root tips. In line with the hypersensitive primary root response phenotype, we observed many genes that were differentially expressed in *pdr2* (2343) compared to WT (373), while only 15 genes were regulated in insensitive *lpr1lpr2* upon Pi deficiency (Fig. 2-2). Four systemic PSI genes (*SPX1*, *AT4*, *PAP17*, *GDPD1*) were upregulated in all lines (Fig. 2-5 and 2-6, Tab. 2-2), demonstrating the validity of our survey. It also revealed that the systemic response to Pi limitation was already initiated and was likely kept in *pdr2* and *lpr1lpr2* mutants. Our transcriptomic analysis also confirms the observations that the key regulators of local response, *PDR2*, *LPR1*, and *STOP1*, are not regulated transcriptionally by low Pi (Fig. 2-6) (Balzergue *et al.*, 2017; Mora-Macias *et al.*, 2017; Naumann *et al.*, 2022). Induction of *ALMT1* expression by Pi limitation was only observed in *pdr2* and *lpr1lpr2*, not in WT, which contradicts some studies that showed the upregulation of *ALMT1* in Pi-starved WT (Fig. 2-6) (Balzergue *et al.*, 2017; Mora-Macias *et al.*, 2017; Chutia, 2019). This could be due to the difference in treatment time. In those studies, increased mRNA abundance of *ALMT1* was all observed at least two days after low Pi treatment. In this study, RNA-seq was performed one day after exposure to Pi limitation, at a time when the transcriptional response of *ALMT1* was probably not started. In addition, our observation of upregulation of *ALMT1* in Pi-starved *lpr1lpr2* root tips is consistent with the study, which reported that stronger GUS reporter activity driven by the *ALMT1* promoter was detected in *lpr1* after Pi-starvation (Balzergue *et al.*, 2017).

Genes related to oxidative stress, ethylene and auxin response, regulation of transcription as well as cell wall biogenesis were upregulated in Pi-starved root tips of WT and *pdr2* upon Pi limitation (Fig. 2-7, Fig. 2-8), suggesting that these processes are involved in the local Pi response. This analysis confirms the previous observations in whole root (Thibaud *et al.*, 2010; Lan *et al.*, 2015; Hoehenwarter *et al.*, 2016) and shows more accurate information about how root tips of young seedlings respond to Pi deficiency. In addition, we observed overrepresented categories contain genes involved in metal ion homeostasis only in *pdr2*

upon Pi limitation (Fig. 2-8), reflecting the function of PDR2 in regulating metal ion homeostasis. This is in agreement with the findings that the root tips of Pi-starved *pdr2* accumulate more Fe compared to WT (Müller *et al.*, 2015; Naumann *et al.*, 2022). Interestingly, we found several genes which participate in protein degradation and chaperone-mediated protein folding were upregulated in root tips of Pi-starved *pdr2* (Fig. 2-8, Tab. S6-4), while many genes involved in protein synthesis were suppressed in *pdr2* upon Pi limitation (Fig. 2-8). This likely points to the ER stress response. When facing ER stress, a situation of accumulating misfolded proteins in ER, plant activates the unfolded protein response (UPR) to restore proteostasis (Angelos *et al.*, 2017; De Clercq *et al.*, 2021). The UPR moderates the development of ER stress through stimulating ER-associated degradation, up-regulating molecular chaperones to aid protein folding, and attenuating synthesis of secretory proteins to reduce ER protein load (Pastor-Cantizano *et al.*, 2020; Singh *et al.*, 2021). We previously reported the augmented ER stress in *pdr2* upon Pi limitation (Naumann *et al.*, 2019). Thus, the regulation of the genes associated with protein synthesis, degradation and folding in Pi-starved root tips supports this notion.

### 3.1.1 Trehalose metabolism may involve in local Pi response

We observed upregulation of many trehalose metabolism-related genes in WT and *pdr2* upon Pi limitation, including *TRE1*, several *TPS* and *TPP* genes (Fig. 2-7 and 2-8, Fig. 2-11, Tab. 2-3, Tab. 13). Interestingly, all those genes were more upregulated in *pdr2* compared to WT upon Pi limitation. TPS catalyzes the formation of Tre6P from UDP-Glc and Glc 6-phosphate (Cabib & Leloir, 1958). Tre6P can be then dephosphorylated to trehalose by TPP (Cabib & Leloir, 1958). TRE1 hydrolyzes trehalose into glucose (Müller *et al.*, 2001; Lunn, 2007). Our data indicate that trehalose metabolism is likely altered during Pi deficiency response. The functions of Tre6P have been proposed in the sucrose-Tre6P nexus model, which postulates that Tre6P can act as a signal and a negative feedback regulator of sucrose levels (Yadav *et al.*, 2014). Shoot-to-root transport of sucrose appears to be a systemic regulator of Pi starvation responses in roots (Chiou & Lin, 2011). It could also be a source of malate production in roots (Abel, 2017). Moreover, Shane *et al.* reported that elevated intracellular levels of sucrose, Tre6P and organic acids (e.g., malate, citrate, fumarate) were correlated with phosphorylation of PPC in cluster roots of Pi-starved white lupin (*Lupinus albus*) (Shane *et al.*, 2016). High Tre6P levels was also shown to lead to phosphorylation of PPC and increased levels of organic acids in leaves (Figueroa *et al.*, 2016). Hence, Tre6P may constitute a potential link between sucrose availability and malate synthesis by phosphorylation of PPC which may lead to malate exudation and primary root shorting during Pi deficiency response.

To figure out if trehalose metabolism is involved in local Pi response, influence of Pi deficiency on various metabolites levels, such as sucrose, malate, Tre6P, and trehalose, needs to be analyzed in root tips first. Phosphorylation of PPCs is conducted by PPCKs upon Pi limitation (Gregory *et al.*, 2009). It would be interesting to ascertain if the levels of Tre6P and trehalose influence PPCK enzyme activity. TRE1 is the only trehalase in Arabidopsis (Müller *et al.*, 2001; Lunn, 2007). Manipulation of Tre6P and trehalose levels might be achieved through knock out (down) of *TRE1* or overexpression of *TRE1* in Arabidopsis. Phenotypic comparisons regarding primary root growth, PPCK enzyme activity and metabolites levels between Pi-starved WT and the generated lines could reveal if disturbing trehalose metabolism will influence primary root responses to Pi limitation.

### 3.1.2 ROS may involve in local Pi response as signaling molecules

Our results and previous studies from other groups point to the essential role of ROS in regulating primary root response to Pi deficiency. However, the principles of how ROS are involved in this process are not fully understood. Our transcriptome analysis identifies some pathways in which ROS may work as signaling to modulate primary root responses to Pi limitation.

#### ROS may regulate callose deposition

Fe accumulation and callose deposition were reported in Pi-starved SCN of WT and *pdr2* (Müller *et al.*, 2015; Naumann *et al.*, 2022), the same site where a burst of ROS was observed in this study. Our recent study supports the speculation that ROS could be generated during Fe redox cycling and lead to callose deposition in SCN (Naumann *et al.*, 2022). After treating the seedlings with dimethylthiourea (DMTU), a scavenger of OH $\cdot$  generated in Fe redox cycling, ROS generation and callose deposition in SCN were reduced. However, the molecular mechanisms by which ROS trigger callose deposition is unclear.

It is known that CalSs are responsible for callose synthesis (Ellinger & Voigt, 2014). As revealed in RNA-seq analysis, none of the *CalS* genes was regulated in WT upon Pi limitation (Fig. 2-14, Tab. S6-12). Only two *CalS* genes (*CalS6* and *CalS7*) were slightly induced (around 1.6-fold) in *pdr2* (Fig. 2-14, Tab. S6-12), indicating that transcriptional regulation of those *CalSs* is likely not essential during Pi deficiency response. However, RNA-seq experiment was performed 1 day after seedlings were exposed to -Pi, when QC already started dying (Fig. 2-19A). We cannot exclude the possibility that there may be transcriptional regulation of those *CalSs* in QC at earlier time point. Besides, whether CalSs are responsible for low Pi-triggered callose synthesis still need to be investigated regarding the protein levels and activities of CalSs.

Interestingly, we observed the expression changes of *PDLPs* and *PDCBs*, which encode two regulatory protein families that regulate callose accumulation (Fig. 2-14, Tab. S6-12). Pi limitation led to the upregulation of *PDLP1* in both WT and *pdr2*. Whereas *PDLP2* was slightly reduced by low Pi only in *pdr2*. *PDLPs* have been reported to have multiple functions in regulating ROS signal and callose deposition in response to biotic and abiotic stress. Several studies showed that *PDLP1* and *PDLP5* promote plasmodesmata callose deposition, probably by recruiting or regulating the activity of *CalSs* in response to ROS (Thomas *et al.*, 2008; Lee *et al.*, 2011; Caillaud *et al.*, 2014; Cui & Lee, 2016). One recent study reported that high light stress-induced local ROS generation increased pore size of plasmodesmata and cell-to-cell transport in a manner dependent on *PDLP1* and *PDLP5* (Fichman *et al.*, 2021). This process was further shown to be important for the generation of systemic ROS signals (Fichman *et al.*, 2021). The *PDLP* family encompasses two extracellular Domain of Unknown Function 26 (*DUF26*) domains (Thomas *et al.*, 2008), which contains three cysteine residues and have been proposed to function in sensing and/or signaling of ROS (Bourdais *et al.*, 2015). It is possible that low Pi-induced ROS are sensed by *PDLPs* and subsequently regulate callose deposition. Opposite expression pattern of *PDLP1* and *PDLP2* in *pdr2* suggests that they may play different roles in regulating callose deposition. *PDCBs* have also been shown to regulate callose deposition at the neck of plasmodesmata (Simpson *et al.*, 2009). *PDCB2* was highly induced in WT and *pdr2* upon Pi limitation. It was reported that *PDCB1* and *PDCB2* can bind callose *in vitro* (Simpson *et al.*, 2009). Overexpression of *PDCB1* led to an increase in callose deposition and thus reduced plasmodesmata permeability (Simpson *et al.*, 2009). However, it is not known if *PDCB2* has a similar function like *PDCB1*. Moreover, we observed extreme upregulation of *CML41*, which encodes a plasmodesmata-localized  $\text{Ca}^{2+}$  binding protein, in Pi-starved *pdr2* (around 130-fold) (Fig. 2-14, Tab. S6-12). *CML41* was reported to be upregulated by *flg22* and facilitated rapid callose deposition at plasmodesmata (Xu *et al.*, 2017). Putative links between  $\text{Ca}^{2+}$  signaling and callose deposition have also been described in other studies (Tucker & Boss, 1996; Holdaway-Clarke *et al.*, 2000; Sager & Lee, 2014). In addition,  $\text{Ca}^{2+}$  influx has long been thought to play a role in  $\text{H}_2\text{O}_2$  perception and signaling (Pei *et al.*, 2000; Foreman *et al.*, 2003; Demidchik & Shabala, 2018; Waszczak *et al.*, 2018; Matthus *et al.*, 2019).

Collectively, callose deposition could be regulated by ROS,  $\text{Ca}^{2+}$ , and regulatory proteins during Pi deficiency response. To determine if transcriptional regulation of *CalSs* exists in QC, real-time quantitative reverse transcription PCR (qRT-PCR) needs to be performed at earlier time point. Analysis of the levels and activities of *CalSs* upon Pi limitation could reveal how and which *CalSs* are involved in callose deposition. Furthermore, analyzing the primary root growth response and callose deposition in knock out mutants of

*PDLP1*, *PDCB2* and *CML41* will provide important hints on how callose deposition is regulated. To further study if ROS signaling is dependent on *PDLP1*, *PDCB2* and *CML41*, how ROS scavenging chemicals (eg., DPI, KI, DMTU)(Chung *et al.*, 2008; Zheng *et al.*, 2019) influence the expression levels of these genes could be investigated. Additionally, it would be desirable to study if disturbance of the extracellular Cys-rich of PDLP1 in WT will abolish primary root growth inhibition and callose accumulation in response to Pi deficiency, which will help to reveal if ROS signaling is sensed by PDLP1.

### **Peroxidases may regulate ROS formation and cell wall dynamics**

We identified in total 17 *PRXs* that were differentially expressed in WT and/or *pdr2* upon Pi limitation (Fig. 2-12, Tab. S6-7). Our analysis confirmed 7 *PRXs* (*PRX8*, *PRX12*, *PRX25*, *PRX37*, *PRX38*, *PRX52*, *PRX54*) that were previously reported to be upregulated and 2 *PRXs* (*PRX4*, *PRX27*) to be downregulated in whole root of WT and/or *pdr2* upon Pi limitation (Hoehenwarter *et al.*, 2016). *PRXs* are mainly considered as cell wall targeted proteins (Francoz *et al.*, 2015). They are involved in superoxide generation (Shigeto & Tsutsumi, 2016) as well as H<sub>2</sub>O<sub>2</sub> scavenging, which lead to the formation of OH· (Chen & Schopfer, 1999; Francoz *et al.*, 2015). Hydroxyl radicals are able to break covalent bonds in cell wall polymers and loosen cell walls (Schopfer *et al.*, 2001). In contrast, *PRXs* can also oxidize cell wall aromatic compounds within proteins and phenolics, using H<sub>2</sub>O<sub>2</sub> for oxidative power, and thus build a rigid cell wall (Marjamaa *et al.*, 2009). Therefore, *PRXs* are tightly connected to cell wall loosening and stiffening.

Balergue *et al.* reported that Pi deficiency induced *PRX* activity in root tips of WT but not in *lpr1lpr2* (Balergue *et al.*, 2017). Cell wall stiffness, probably caused by the upregulated *PRXs* activity, inhibit the cell elongation in the transition zone (Balergue *et al.*, 2017). Although *PRXs* consist of 73 members in Arabidopsis, several studies have demonstrated that each isoform could have specific functions (Francoz *et al.*, 2015; Marzol *et al.*, 2022; Pacheco *et al.*, 2022). Among 17 class *PRXs* that were identified in our data set, of particular interest are seven *PRXs* (*PRX4*, *PRX10*, *PRX21*, *PRX25*, *PRX37*, *PRX53*, *PRX54*), which all expressed in RAM and/or elongation zone, based on the published data (Brady *et al.*, 2007; Wendrich *et al.*, 2020). Disruption of *AtPRX4* did not influence plant growth but reduced lignin content (Fernandez-Perez *et al.*, 2015). *PRX25* and *PRX37* have also been proposed to be involved in cell wall stiffening mostly through lignin polymerization (Pedreira *et al.*, 2011; Shigeto *et al.*, 2013). Decrease in the total lignin content and altered lignin structures were observed in *AtPRX25* deficient mutants (Shigeto *et al.*, 2013). Overexpression of *AtPRX37* caused a dwarf phenotype with smaller plants compared to WT (Pedreira *et al.*, 2011). We previously reported the increased lignification in the root tips of Pi-starved WT and *pdr2* (Ziegler *et al.*, 2016). Therefore, those *PRXs* may contribute to Pi deficiency-triggered lignin deposition in

root tips and may thus be implicated in primary root growth inhibition. Upregulation of *PRX10* led to a restriction of the leaf expansion probably through increasing  $H_2O_2$  level (Schmidt *et al.*, 2016). Moreover, *AtPRX53* has been shown to play a strong negative effect on cell elongation of hypocotyl, possibly through catalyzing the cross linking of cell wall compounds (Jin *et al.*, 2011). It is noteworthy that only two *PRXs* (*PRX21* and *PRX54*) without well-defined function were unregulated in Pi-starved WT (Fig. 2-12B). Because one day after transfer, the elongation zone is already shorter in WT-deficient root tips, *PRX21* and *PRX54* could be the very early responded *PRXs* that regulate cell elongation upon Pi limitation. Together, those *PRXs* discussed above may play specific role in modulating ROS levels, lignin formation and CW dynamics, which lead to inhibition of cell elongation upon Pi deficiency.

*UPB1* has been reported to be a key TF that regulate the expression of a group of *PRXs* during root growth (Tsukagoshi *et al.*, 2010). However, Balzergue *et al.*, showed that *UPB1* is not essential for primary root response to low Pi (Balzergue *et al.*, 2017), which is also confirmed in this study (Fig. S6-3). In line with this, expression levels of *PRXs* that are regulated by *UPB1* were not influenced by Pi limitation in our data set. Based on the prediction on PlantPAN, we identified five *WRKYs* (*WRKY15*, *WRKY28*, *WRKY38*, *WRKY40* and *WRKY48*) that may regulate the *PRXs* that were differentially expressed in WT and/or *pdr2* during low Pi response (Tab. 2-4). All five *WRKYs* were upregulated in WT and *pdr2* upon Pi limitation (Tab. 2-4). *WRKY15* is  $H_2O_2$ -responsive and expresses in root tips as shown with GUS reporter assay (Vanderauwera *et al.*, 2005; Vanderauwera *et al.*, 2012). Overexpression of *WRKY15* promoted leaf growth by increasing cell expansion, whereas *WRKY15*-amiR plants that had reduced *WRKY15* expression level showed a decreased leaf cell area, which support its involvement in plant growth (Vanderauwera *et al.*, 2012). It has been shown that *WRKY28* were upregulated exclusively in leaves by methyl viologen (MV) treatment, which induce the generation of superoxide (Scarpeci *et al.*, 2008). Co-expression of *AtWRKY28* and *AtbHLH17* improved the resistance to MV-induced oxidative stress in Arabidopsis leaves (Babitha *et al.*, 2013).

Since only *PRX21* and *PRX54* were upregulated in both WT and *pdr2* upon Pi limitation, they could be the key *PRXs* that regulate cell elongation upon Pi limitation. Whether the length of elongation zone and ROS formation can be influenced by knockout (down) or overexpression of *PRX21* and *PRX54* upon Pi limitation need to be studied. To figure out if identified *WRKYs* are responsible for the upregulation of *PRXs* during Pi deficiency, chromatin immunoprecipitation (ChIP) assays could be performed. As discussed above, ROS may induce the expression of *WRKY15* and *WRKY28* and modulates primary root response to low. To test this hypothesis, ROS scavengers could be applied to determine if the upregulation of *WRKY15* and *WRKY28* could be dismissed. Moreover, phenotypic comparisons regarding primary root growth and ROS formation



between WT and knockout mutants of *WRKY15* and *WRKY28* could reveal if these two genes are involved in ROS signaling and local Pi response.

### **ROS may involve in SCN regeneration**

We identified eleven ROS signaling regulators (Kong *et al.*, 2018; De Clercq *et al.*, 2021) that were induced in both WT and *pdr2* upon Pi limitation. Those regulators consist of five WRKYs that have been discussed above, four ethylene-responsive transcription factors (*ERF013*, *ERF098*, *ERF114*, *ERF115*), BES1/BZR1 homolog protein 3 (*BEH3*) (Tab. 2-4).

It has been reported that *ERF115*, *114*, and *109* are ROS-responsive factors that mediate PHB3-modulated ROS signaling and control QC cell division as well as stem cell differentiation (Kong *et al.*, 2018). PHB3 was shown to be essential in maintaining the SCN identity by restricting ROS (superoxide and H<sub>2</sub>O<sub>2</sub>) levels and spatial expression of the ROS-responsive factors *ERF115*, *114*, and *109* in root tips (Kong *et al.*, 2018). Besides, those ERFs regulate SCN maintenance by directly activating the expression of *phytosulfokine 5* (*PSK5*) and *PSK2* peptide hormones in response to PHB3-modulated ROS signaling. Interestingly, upregulation of *PSK5* was also observed in Pi-starved WT and *pdr2* (Tab. S6-9). It is likely that the increased transcript of *ERF115* and *ERF114* are triggered by ROS signaling upon Pi starvation and further led to the activation of *PSK5*. It is noteworthy that cell death in SCN was already observed in WT after 20 hours of low Pi treatment (Fig. 2-19A). However, *WOX5* expression was highly induced in WT and *pdr2* after 1 day of transfer to low Pi (Tab. S6-9), indicating the regeneration of QC cells. This is reminiscent to the role of *ERFs* in promoting SCN regeneration after cell death (Heyman *et al.*, 2013; Heyman *et al.*, 2016; Zhou *et al.*, 2019). Upon Pi limitation, ROS accumulation likely activate *ERF115/ERF114-PSK5* signaling pathway and contribute to the SCN regeneration, which will allow roots to resume growth after release from the low Pi stress.

Brassinosteroids (BRs) also play a key role in maintaining QC identity (Gonzalez-Garcia *et al.*, 2011; Heyman *et al.*, 2013; Planas-Riverola *et al.*, 2019). In addition, BRs-induced QC divisions are partially dependent on *ERF115/PSK5* signaling pathway (Heyman *et al.*, 2013). Among the six *BZR/BEH* family members that are involved in BRs signaling (Wang *et al.*, 2002), only *BEH3* was upregulated in both WT and *pdr2* in response to Pi deficiency. Apart from the prediction of *BEH3* being ROS signaling regulators (De Clercq *et al.*, 2021), it has been reported that H<sub>2</sub>O<sub>2</sub> level was lower in *beh3* mutant compared to WT upon osmotic stress (Van Nguyen *et al.*, 2021). *BEH3* seems involve in ROS accumulation and SCN regeneration upon Pi limitation.

To determine if ROS is responsible for the upregulation of *ERF115* and *ERF114* as well as QC regeneration, influence of ROS scavenging chemicals on the gene expression levels of *ERFs* and *WOX5* should be evaluated in WT upon Pi limitation. Comparison of the root recovering length between WT, *erf115* knockout mutant and *ERF115-SRDX*, a dominant-negative form of ERF115 by fusing it with the SUPERMAN repression domain (SRDX) (Ikeda & Ohme-Takagi, 2009), after releasing from the low Pi stress will help to find out if ERF115 is necessary for QC regeneration. The same study strategy also applies for *ERF114* and *BEH3*. In addition, it would be interesting to monitor ROS levels in *beh3* knockout mutant in order to find out if *BEH3* regulate ROS formation upon Pi limitation.

Taken together, our analysis show that the ROS generated during Pi deficiency may work as signaling molecules and play multiple roles in regulating Pi deficiency responses. ROS likely induce callose deposition by regulating *CalSs*, *PDLPs*, and *PDCBs*, which probably involve  $Ca^{2+}$  signals, and thus contribute for the primary root inhibition upon Pi limitation. Several PRXs may modulate ROS generation and cell wall dynamics to restrain cell elongation in response to Pi deficiency. Moreover, ROS may be implicated in SCN regeneration through *ERFs-PSK5* signaling pathway and *BEH3*. Further investigations on each direction will extend our understanding on the mechanism by which ROS work as signaling molecules.

### 3.2 Influence of Pi deficiency on ROS generation

Different ROS staining results showed that  $O_2^{\bullet-}$  mainly accumulates in the apical meristem, whereas  $H_2O_2$  and  $OH\cdot$  are mainly distributed in the elongation zone (Fig. 2-20-23). This is in agreement with the published data (Dunand *et al.*, 2007; Tsukagoshi *et al.*, 2010; Reyt *et al.*, 2015; Zheng *et al.*, 2019; Yamada *et al.*, 2020). Overaccumulation of  $O_2^{\bullet-}$  (DHE) was observed in Pi-starved QC of WT (Fig. 2-21B and C). Since  $O_2^{\bullet-}$  has a potential role in damaging Fe- and FeS-containing proteins and reacts with various cellular constituents to form reactive radicals, it might ultimately cause cell death (Choudhary *et al.*, 2020). Frequent QC death was indeed observed in WT after being exposed to low Pi for 20h (Fig. 2-19 A and B). However, the mechanisms by which  $O_2^{\bullet-}$  triggers cell death need to be further studied. A burst of ROS (Carboxy-H2DCFDA) was detected in the SCN of Pi-starved WT and *pdr2* after the QC started dying (Fig. 2-19C). In the pathogen field, several studies have reported the presence of rapid and long-distance ROS signals in leaves (Fichman & Mittler, 2020; Castro *et al.*, 2021), the ROS generated in SCN during low Pi response could also be a signal for neighbor cells and lead to transcriptional changes of ROS-related genes. The potential role of ROS work as signaling molecules has been discussed in section 3.1.2.

In addition, Pi deficiency increased  $O_2^{\bullet-}$  (NBT) level in the RAM of WT and the hypersensitive *pdr2* mutant (Fig. 2-20). This is consistent with some published data (Müller *et al.*, 2015; Gao *et al.*, 2021). However, Suen *et al.* observed weaker NBT staining in the RAM of Pi-deplete WT (Suen *et al.*, 2018). One reason for such discrepancy is probably due to the differences in the age of the seedlings used for analysis. Suen *et al.* let the seedlings grow for 7 days and then transferred to the +Pi or -Pi conditions for another 7 days before performing the NBT staining. Whereas in this study, staining was performed within 2 days after transferring 5-day-old seedlings to +Pi or -Pi medium.  $O_2^{\bullet-}$  may play different roles in regulating primary root adjusting to low Pi at different response stages. In addition, DPI treatment, which inhibits the activities of RBOHs, supports the view that  $O_2^{\bullet-}$  is required for the low Pi response (Fig. 2-24). It has been shown that  $O_2^{\bullet-}$  is necessary for proper root growth and decreasing the  $O_2^{\bullet-}$  levels by DPI can lead to root shorting (Dunand *et al.*, 2007; Tsukagoshi *et al.*, 2010; Yamada *et al.*, 2020). In line with this, inhibition of primary root growth in DPI-treated WT, *pdr2*, and *lpr1lpr2* was observed under +Pi condition (Fig. 2-24). DPI treatment did not further inhibit root growth of WT and *pdr2* upon Pi limitation (Fig. 24), indicating that decreasing  $O_2^{\bullet-}$  level by DPI can partly rescue the low Pi response. However, DPI treatment did not block the root shorting response completely. This could be because that  $O_2^{\bullet-}$  may be generated via other ways as well, such as mitochondrial respiration, not only via RBOHs, to regulate primary root response to low Pi.

$H_2O_2$  and  $OH\cdot$  levels in root tips were not altered by low Pi in WT (Fig. 2-22 and 23). However, Zhang showed a decrease in  $H_2O_2$  and an increase in  $OH\cdot$  upon Pi deficiency response (Zheng *et al.*, 2019). This contradiction could again be due to the differences in growth conditions. Fe availability in the medium has been shown to influence the primary root responses to Pi deficiency (Naumann *et al.*, 2022). For instance, the inhibition of primary root growth of seedlings grown on -Pi medium supplied with 50  $\mu$ M Fe is weaker than on 25  $\mu$ M Fe (Naumann *et al.*, 2022). Accordingly, it is possible that ROS generation is not constant and may happen at different response stages. Since the Fe concentration of the medium used in Zhang's study was not claimed, although the time point at which we performed the experiment was same, the ROS staining results we got might be different. Another group reported opposite results in which they showed less accumulation of  $OH\cdot$  in the RAM and the elongation zone (Suen *et al.*, 2018). As discussed above, the contradicting results could be caused by differences in the age of the seedlings we used. Nevertheless, Zhang *et al.* showed that  $H_2O_2$  scavenger (KI) and  $OH\cdot$  scavengers (thiourea and glutathione) can rescue the primary root inhibition phenotype upon Pi limitation, indicating that  $H_2O_2$  and  $OH\cdot$  are necessary for primary root response to low Pi (Zheng *et al.*, 2019). It was proposed that the toxicity of  $OH\cdot$  leads to root

shorting. However, the over-accumulated  $\text{OH}\cdot$  was only observed in the epidermis (Zheng *et al.*, 2019). How  $\text{OH}\cdot$  influences the inner cell layers remains unclear.

Genetically encoded sensor Grx1-roGFP2 has been developed to monitor cytosolic glutathione redox potential ( $E_{\text{GSH}}$ ) *in vivo*, which may reflect ROS level as well (Meyer & Dick, 2010; Ugalde *et al.*, 2022). How Pi limitation influences  $E_{\text{GSH}}$  in the RAM of WT was investigated with the transgenic line *pUBQ10:Grx1-roGFP2*. However, no consistent results were obtained (Fig. 2-26). One possible reason for the inconsistency could be that the changes of the  $E_{\text{GSH}}$  are transient. There might be a short peak of  $E_{\text{GSH}}$  that could not be captured in every single replicate. To figure out if the short peak exists or not, light-sheet microscope can be used to constantly monitor roGFP2. In addition, no obvious difference in  $E_{\text{GSH}}$  was observed in the QC where  $\text{O}_2^{\cdot-}$  accumulated in response to low Pi (Fig. 2-28). Although superoxide reacts with GSH and thus influences  $E_{\text{GSH}}$ , the reaction is relatively slow (Winterbourn & Metodiewa, 1994; Winterbourn, 2016). Besides,  $\text{O}_2^{\cdot-}$  can also be detoxified by SOD. Therefore, the over-accumulated  $\text{O}_2^{\cdot-}$  may not translate into an increase in  $E_{\text{GSH}}$ .

Collectively,  $\text{O}_2^{\cdot-}$  generation was observed in the QC of Pi-starved WT, which may lead to cell death. In response to Pi deficiency, a burst of ROS was detected in the SCN of WT and *pdr2* where QC identity has been disturbed. In addition, Pi limitation triggered the overaccumulation of  $\text{O}_2^{\cdot-}$  in the RAM of WT and *pdr2*. These are consistent with our RNA-seq analysis which revealed that several genes associated with ROS generation and scavenging (*PRXs*, *FSD1*, *GSTFs*, *CATs*), as well as response to oxidative stress (*AER*, *DIN10*, *SIP2*), were upregulated in WT and *pdr2* during Pi deficiency response (Fig. 2-12, Tab. 2-3). In line with higher levels of ROS in Pi-starved *pdr2* compared to WT (Fig. 2-19 and 20), more ROS-related genes were upregulated in *pdr2* upon Pi limitation (Fig. 2-12). Besides, no ROS related gene was upregulated in Pi-starved insensitive *lpr1lpr2* line, consistent with the observations that level of ROS was not altered in *lpr1lpr2* upon Pi limitation (Fig. 2-19 and 20). Apart from the possibilities that mitochondrial respiration, RBOHs, PRXs, and FSD1 may contribute to the ROS generation in response to Pi deficiency, LPR1 and Fe redox cycling play an essential role in ROS generation. Upon Pi limitation, LPR1 activity was proposed to be related to  $\text{Fe}^{2+}$  acquisition processes and LPR1 mediated  $\text{Fe}^{2+}$  oxidation promote the Fe redox cycling (Naumann *et al.*, 2022).  $\text{Fe}^{3+}$  could be reduced by ascorbate and via Photo-Fenton reaction and further support the Fenton reaction which generate  $\text{OH}\cdot$  (Naumann *et al.*, 2022) (Zheng *et al.*, 2019).

### 3.3 Role of PIPs in Pi deficiency response

The tissue-specific expression analysis by GUS staining revealed that out of 13 *PIPs*, only *PIP1;2*, *PIP1;3*, *PIP1;4*, *PIP2;3*, *PIP2;4*, *PIP2;5*, *PIP2;7* were expressed in root tips (Fig. 2-15). This is partly in agreement with our RNA-seq results which showed that all *PIPs* were expressed in root tips except *PIP2;5* (Fig. 2-13). The reason for such contradiction could be that the growth conditions used in the two experiments were different. For GUS staining, seedlings were grown on the medium supplemented with 50  $\mu\text{M}$  Fe and 2.5  $\mu\text{M}$  Al. Whereas the seedlings used for the RNA-seq experiment were cultured on medium containing 25  $\mu\text{M}$  Fe and no Al. Cavalheiro et al. reported downregulation of *CIP1;1* and *CIP2* and upregulation of *CIP1;2* in 'Rangpur' lime plants (*Citrus limonia* L.) when exposed to Al (Cavalheiro *et al.*, 2020). Expression of *PIPs* in root tips seems to be regulated by the presence of Al.

Low Pi treatment induced the promoter activities of *PIP1;3* and *PIP1;4* in root tips based on GUS staining (Fig. 2-15). However, the transcript levels of *PIP1;3* and *PIP1;4* were not influenced by low Pi as revealed in RNA-seq results (Fig. 2-13). This again could be caused by the presence of Al as discussed above. *Arabidopsis* nodulin 26-like intrinsic protein (NIP) 1;2 has been shown to facilitate the transport of Al-malate from the root cell wall into the symplasm and thus play a key role in Al detoxification (Wang *et al.*, 2017). Upregulation of *PIP1;3* and *PIP1;4* as revealed by GUS staining could be caused by Al, not Pi deficiency. Besides, RNA-seq analysis showed that *PIP2;4* was downregulated in Pi-starved root tips of WT and hypersensitive *pdr2* mutant (Fig. 2-13). In line with this, Wen-Dar Lin showed with microarray experiment that expression of *PIP2;4* was inhibited in response to low Pi (Lin *et al.*, 2011). Moreover, longer root hairs were observed in *pip2;4* compared to WT under +Pi condition and -Pi condition, respectively. However, the researchers didn't perform a two-way ANOVA analysis, it's not clear if the root hairs of *pip2;4* were longer than WT during low Pi response. What role *PIP2;4* may play in response to Pi deficiency need to be studied further. In addition, apart from *PIP2;4*, more *PIPs* (*PIP1;5*, *PIP2;3*, *PIP2;7* and *PIP2;8*) were downregulated in Pi-starved *pdr2*. Based on our initial hypothesis, upon Pi deficiency, if *PIPs* work not only as water channels but can transfer  $\text{H}_2\text{O}_2$  from apoplast into cytosol and trigger the callose deposition, we will expect upregulation of *PIPs*. Therefore, those *PIPs* likely only function as water channels in response to Pi deficiency. It has been shown that water transport in the root of 15-day-old *Arabidopsis* seedlings was inhibited after 6 days of low Pi treatment (di Pietro *et al.*, 2013). The low Pi-triggered inhibition of root water permeability may also happen to younger seedlings (in our case, 6 days old) by regulating those *PIPs*. Moreover, since continuous uptake of water into cells is required for cell expansion (Fricke & Chaumont, 2007; Liu *et al.*, 2008), downregulation of those *PIPs* could contribute to the inhibition

of root cell elongation upon Pi limitation. How the roots of *pip* mutants respond to Pi deficiency was further studied. Although statistically, slightly primary root inhibition of *pip1;1*, *pip1;2*, *pip1;3*, *pip1;3pip1;4*, *pip2;3* and *pip2;8* was observed compared to Pi-starved WT (Fig. 2-16 and 17), it may not help to explain any biological question. After low Pi treatment, the *quintuple mutant* was significantly longer than WT (Fig. 2-17). However, since the mutant was generated by crossing, it contains Ler background. The insensitive phenotype of the *quintuple mutant* might be caused by Ler. In summary, single *PIPs* were not essential in regulating low Pi-induced primary root growth inhibition. ROS generated during Pi deficiency did not likely play a role through *PIPs*.

## 4. MATERIALS AND METHODS

### 4.1 Materials

#### 4.1.1 Chemicals

Unless otherwise indicated, all chemicals were obtained from Carl Roth (Karlsruhe, Germany), Duchefa Biochemie, Merck (Darmstadt, Germany), Sigma-Aldrich (St Louis, MO, USA), AppliChem GmbH (Darmstadt, Germany), Serva (Heidelberg, Germany), and BioRad (Hercules, USA). Molecular biology supplies and kits were ordered from Thermo Fischer Scientific and Life Technologies (California, USA). Primer syntheses were carried out by Eurofins Genomics (Ebersberg, Germany).

#### 4.1.2 Media

Media used for growing Arabidopsis and for culturing *E. coli* and Agrobacterium are listed with their composition in Table 4-1. To remove residual phosphate in the agar (Duchefa) that was used to prepare the ATS medium, the agar was routinely purified by repeated washings in deionized water and subsequent dialysis using Dowex 1X8, 200-400 mesh, ion-exchange (ThermoFisher). The agar was then dried at 60° C in the oven (100% ventilation) for 1 day. All media were sterilized at 121° C for 20 min. Al, Basta, and antibiotics were filter sterilized and added to autoclaved growth media.

**Tab. 4-1: Media composition**

Medium	Composition
Modified ATS medium ( <i>A. thaliana</i> )	2.5 mM (+Pi) or 0 mM (-Pi) KH <sub>2</sub> PO <sub>4</sub> , 0.5% D-Sucrose, 5mM KNO <sub>3</sub> , 0.01 mM/0.025 mM /0.05 mM Fe <sup>3+</sup> -EDTA, 2 mM Ca(NO <sub>3</sub> ) <sub>2</sub> , 2 mM MgSO <sub>4</sub> , 2.5 mM MES-KOH, 0.005 mM CuSO <sub>4</sub> , 0.001 mM ZnSO <sub>4</sub> , 0.07 mM H <sub>3</sub> BO <sub>3</sub> , 0.014 mM MnCl <sub>2</sub> , 0.0002 mM Na <sub>2</sub> MoO <sub>4</sub> , 0.010 mM CoCl <sub>2</sub> , 0.0025 mM Al (if state in the legend) pH 5.6. 1% Washed Agar were added for solid medium.
Lysogeny broth (LB) medium ( <i>E. coli</i> , <i>A. tumefaciens</i> ; bacterial transformation)	10 g/l tryptone; 5 g/l NaCl; 10 g/l yeast extract. 15 g/l Agar-agar were added for the preparation of solid medium.

### 4.1.3 Plant materials and cultivation

#### 4.1.3.1 Plant lines

For all experiments, *Arabidopsis thaliana* ecotype Columbia-0 (Col-0) or mutants in Col-0 background were used if not specified otherwise. *pip2;7* is in Landsberg *erecta* (*Ler*) background. Seeds of *pip* single mutants except for *pip2;4*, *Ler*, *pPIP::GFP-GUS* lines and *pPIP::GUS* lines were obtained from Anton R Schöffner's lab. *pip2;4* was obtained from Wolfgang Schmidt's lab. Seeds of *pUBQ10:Grx1-roGFP2* in WT background were obtained from Rainer Waadt (Institute of Biochemical Plant Pathology, Helmholtz Zentrum München, Germany). All other T-DNA insertion lines were purchased from the Nottingham Arabidopsis Stock Centre (NASC).

**Tab. 4-2: Mutants analyzed in this study**

Mutant name	Locus	T-DNA insertion line	Additional information	Molecular Characterization
<i>pip1;1</i>	AT3G61430	GABI_437B11	(Ines, 2008)	Knockdown
<i>pip1;2</i>	AT2G45960	SALK_019794	(Postaire <i>et al.</i> , 2010)	Knockout
<i>pip1;3</i>	AT1G01620	SALK_051107	(Liu, 2015)	Knockout
<i>pip1;4</i>	AT4G00430	SAIL_808_A10	(Liu, 2015)	Knockout
<i>pip1;5</i>	AT4G23400	SALK_056898	This work	N/A
<i>pip2;1</i>	AT3G53420	SM_3_35928	(Ines, 2008)	Knockout
<i>pip2;2</i>	AT2G37170	SAIL_169_A03	(Ines, 2008)	Knockout
<i>pip2;3</i>	AT2G37180	SAIL_1215_D03	(Ines, 2008)	Knockout
<i>pip2;4</i>	AT5G60660	SAIL_535_D05	(Lin <i>et al.</i> , 2011)	Knock down
<i>pip2;5</i>	AT3G54820	SAIL_452H09	(Ines, 2008)	Knockout
<i>pip2;6</i>	AT2G39010	SALK_092140	(Prado <i>et al.</i> , 2013)	Knockout
<i>pip2;7</i>	AT4G35100	CSHL_GT19652	(Prado <i>et al.</i> , 2013)	Knockout
<i>pip2;8</i>	AT2G16850	SALK_099098	(Ines, 2008)	Knockout
<i>pip1;3 pip1;4</i>	AT1G01620, AT4G00430	SALK_051107, SAIL_808_A10	This work	Knockout
<i>pip2;1-2;2-2;4-2;6-2;7</i>		SM_3_35928, SAIL_169_A03, SM_3_20853, SALK_092140, CSHL_GT19652	Anton R Schöffner	Knockout
<i>din10-1</i>	AT5G20250	SALK_066490C	(Christ, 2013)	NA



Tab. 4-2 (continued)

Mutant name	Locus	T-DNA insertion line	Additional information	Molecular Characterization
<i>aer-1</i>	AT5G16970	SALK_005324C	(Mata-Perez <i>et al.</i> , 2020)	Knockdown
<i>gstf6</i>	AT1G02930	SALK_026398	(Su <i>et al.</i> , 2011)	Knockout
<i>edr5-1</i>	AT3G30775	SALK_119334C	(Cabassa-Hourton <i>et al.</i> , 2016)	Knockout
<i>ozf1-1</i>	AT2G19810	SALK_151571C	(Huang <i>et al.</i> , 2011)	NA
<i>sip2-1</i>	AT3G57520	SALK_038166C	(Egert, 2011)	NA
<i>fsd1-1</i>	AT4G25100	SALK_029455	(Dvorak <i>et al.</i> , 2021)	Knockout
<i>tppd-1</i>	AT1G35910	SALK_120962C	This work	NA
<i>lpr1lpr2</i>	AT1G23010, AT1G71040	SALK_016297, SALK_091930	(Svistoonoff <i>et al.</i> , 2007)	Knockout
Mutant name	Locus	Point mutation line	Additional information	Molecular Characterization
<i>pdr2</i>	At5G23630	T699I	(Ticconi <i>et al.</i> , 2009)	

Tab. 4-3: Transgenic lines analyzed in this study

Transgenic lines	Background	Purpose
<i>PIP1;1::GUS</i>	C24	Tissue-specific localization
<i>PIP1;2::GFP-GUS</i>	C24	Tissue-specific localization
<i>PIP1;3::GFP-GUS</i>	Col-0	Tissue-specific localization
<i>PIP1;4::GFP-GUS</i>	Col-0	Tissue-specific localization
<i>PIP1;5::GFP-GUS</i>	Col-0	Tissue-specific localization
<i>PIP2;1::GUS</i>	C24	Tissue-specific localization
<i>PIP2;2::GUS</i>	C24	Tissue-specific localization
<i>PIP2;3::GUS</i>	C24	Tissue-specific localization
<i>PIP2;3-GFP-GUS</i>	Col-0	Tissue-specific localization
<i>PIP2;4::GFP-GUS</i>	Col-0	Tissue-specific localization
<i>PIP2;5::GFP-GUS</i>	Col-0	Tissue-specific localization
<i>PIP2;6::GFP-GUS</i>	Col-0	Tissue-specific localization
<i>PIP2;7::GFP-GUS</i>	Col-0	Tissue-specific localization
<i>PIP2;8::GFP-GUS</i>	C24	Tissue-specific localization
<i>pUBQ10:Grx1-roGFP2</i>	Col-0	$E_{GSH}$ measurement

Tab. 4-3 continued

Transgenic lines	Background	Purpose	Additional information
<i>pUBQ10:Grx1-roGFP2</i>	<i>pdr2</i>	<i>E<sub>GSH</sub></i> measurement	This study
<i>pUBQ10:Grx1-roGFP2</i>	<i>lpr1lpr2</i>	<i>E<sub>GSH</sub></i> measurement	This study
<i>pWOX5:Grx1-roGFP2</i>	Col-0		This study; plasmid was obtained from Rainer Waadt

#### 4.1.3.2 Plant cultivation

Plants for transformation, selection, and propagation purposes were grown on soil in the greenhouse at 18-20° C and 55-65% relative humidity under long-day conditions (16 h light/8 h dark). The substrate used was "Einheitserde Classic Kokos" (45% (w/w) white peat, 20% (w/w) clay, 20% (w/w) coco fibers, 15% (w/w) block peat; Balster Einheitserdewerk, Germany) mixed with vermiculite (1-2 mm) in a 4:3 ratio.

For experiments on solid agar media, seeds were surface sterilized, placed on modified ATS medium, and then stratified at 4 ° C in the dark for 2 days. Thereafter, the plates were placed vertically in a growth chamber at 22° C under around 160  $\mu\text{mol s}^{-1} \text{m}^{-2}$  light (Protec. class, Leuchtstofflampe 36W/840, PLSL 36WT8, Germany), with a 16 h light/8 h dark photoperiod.

#### 4.1.4 Bacteria

The *Escherichia coli* strain TOP10 (Thermo) was used for the propagation of plasmids. *Agrobacterium tumefaciens* strain GV3101 was used for *A. thaliana* transformation via the floral dip method.

Antibiotics were used in the following concentrations: Spectinomycin (50  $\mu\text{g/ml}$ ), Gentamycin (25  $\mu\text{g/ml}$ ), Rifampicin (100  $\mu\text{g/ml}$ ).

## 4.2 Methods

### 4.2.1 Molecular biology methods

#### 4.2.1.1 Isolation of genomic DNA for genotyping

Plant leaves were collected in 2 ml Eppendorf tubes and 5 mm steel beads were added for grinding the sample. After being frozen in liquid nitrogen, samples were ground using a Tissue Lyser II (QIAGEN) bead mill at 30 s<sup>-1</sup> for 60 s. 400  $\mu\text{l}$  of DNA extraction buffer (consisting of 200 mM Tris-HCl (pH-7.5), 25 mM EDTA (pH-8), 250 mM NaCl, 0.5% w/v SDS) was added to the tube, followed by mixing properly. After centrifuging

at 13000 rpm for 5 min, 300  $\mu$ l of supernatant was transferred to a 1.5 ml Eppendorf tube containing 300  $\mu$ l of isopropanol. After being inverted 6-7 times, the tubes were centrifuged at 13000 rpm for 5 min. The supernatant was then discarded, and the DNA pellet was washed with 300  $\mu$ l of 70% ethanol. After centrifuging at 13000 rpm for 5 min, ethanol was discarded, and the pellet was air-dried followed by resuspending in 30-50  $\mu$ l of sterile Millipore water. The extracted DNA was stored at -20° C or 4° C till further use.

#### 4.2.1.2 Isolation of genomic DNA from *E. coli*

Plasmid DNA was extracted with the GeneJET Plasmid Mini Prep Kit (Thermo Fisher Scientific) following the supplier's protocol. The concentration of isolated plasmid was measured using Infinite® 200 NanoQuant (Tecan) device.

#### 4.2.1.3 Genotyping

Genotyping of T-DNA insertion lines, single point mutation line (*pdv2*), and GFP lines was conducted using homemade polymerase. Genotyping of GUS lines was performed using DreamTaq polymerase (Thermo Fischer Scientific). A reaction volume of 20  $\mu$ l was used and all the components are listed in Tab. 4-4. The thermal profile is shown in Tab. 4-5. Primers used for genotyping are listed in Tab. S6-18. PCR products >300 bp were analyzed through electrophoretic separation on 1% agarose gels and <300bp products were separated on 2% agarose gels.

**Tab. 4-4: Components of PCR reaction**

Components	Volume
Dream Taq Polymerase Green buffer (10 x)	2 $\mu$ l
dNTPs (10 mM)	0.5 $\mu$ l
Forward primer (10 $\mu$ M)	0.5 $\mu$ l
Reverse primer (10 $\mu$ M)	0.5 $\mu$ l
Template	1 $\mu$ l
DNA polymerase	0.5 $\mu$ l <sup>1</sup> or 0.1 $\mu$ l <sup>2</sup>
Millipore water	15 $\mu$ l <sup>1</sup> or 15.4 $\mu$ l <sup>2</sup>

1. homemade polymerase; 2. DreamTaq polymerase

Tab. 4-5: PCR program

Phase	Homemade polymerase		DreamTaq polymerase		No. of cycles
	Temperature	Duration	Temperature	Duration	
Initial denaturation	95 °C	2 min	95 °C	1 min	1
Denaturation	95 °C	30 s	95 °C	30 s	35
Annealing	~T <sub>m</sub> -5° C	30 s	~T <sub>m</sub> -5° C	30 s	35
Extension	72 °C	1kb/min	72 °C	1kb/min	35
Final extension	72 °C	7 min	72 °C	5 min	1

## 4.2.2 Transformation

### 4.2.2.1 *E.coli* heat-shock transformation

*Escherichia coli* (*E. coli*) strains were transformed through heat shock method. Competent cells (50 µl) were thawed on ice and the plasmid (10 pg to 100 ng) were added. Cells with plasmids were incubated on ice for 30 min before applying a heat shock (37°C, 2 min). Subsequently, cells were incubated on ice for 2 min and 700 µl of LB Medium were added. After incubating cells at 37°C for 1h, they were plated on solid LB media containing respective antibiotics and cultivated overnight at 37°C.

### 4.2.2.2 *Agrobacterium tumefaciens* cold-shock transformation

For transformation of *Agrobacterium* strain GV3101, 150 ng to 500 ng plasmids were mixed with 50µl competent cells followed by incubation on ice for 30 min. Cells were then shock-frozen in liquid nitrogen for 5 min and subsequently incubated at 37°C for 5 min and stayed in ice for 5 min. After adding 1 ml LB medium, cells were incubated at 28°C for 3-4 h before being plated on solid LB medium supplemented with respective antibiotics. Cells were then cultured for 48 at 28°C

### 4.2.2.3 *Agrobacterium-mediated* plant stable transformation

Transgenic *A. thaliana* lines were generated by *A. tumefaciens* mediated transfection with the floral dip method as described in (Clough & Bent, 1998). *Agrobacteria* harboring the gene were incubated on LB plates with respective antibiotics for 2 days at 28° C. The cells were resuspended in 60 ml liquid LB medium till the OD600 reached 2.0. A 5 % (w/v) sucrose solution of 4x volume was subsequently added to the bacterial suspension. Before dipping, Silwet-L77 in a final concentration of 0.03% (v/v) was added to the suspension. Arabidopsis plants that had more closed buds were dipped into the suspension solution for

10-15 s under gently agitating. The plants were then placed horizontally on a tray and covered with plastic foil to keep them moist. After 2 days, the plastic foil was removed. The plants were kept vertically and cultivated in the greenhouse for setting seeds.

#### **4.2.2.4 Selection of transformed Arabidopsis plants**

Transformed seeds expressing Grx1-roGFP2 in T1 were sowed densely on soil and selected by Basta (80 mg/l) spraying. T2 and T3 generations were selected on Basta (10 µg/ml) plates. Segregation analysis in a 3:1 ratio was performed in 15 independent T2 lines. T3 seeds were then selected for homozygous lines based on the survival rate (100%).

### **4.2.3 Histochemical analysis**

#### **4.2.3.1 GUS ( $\beta$ -glucuronidase) staining**

Seedlings were vacuum infiltrated with GUS staining solution [50 mM Na-phosphate (pH 7.2), 10 mM EDTA (pH 8), 0.5 mM  $K_3Fe(CN)_6$ , 0.5 mM  $K_4Fe(CN)_6$ , 0,1% (v/v) Triton X-100 and 2 mM X-Gluc] for few minutes and incubated in this staining solution for 15 min up to 24 h at 37° C, depending on the intensity of staining. Stop the staining reaction with pure ethanol. Seedlings were thereafter mounted in chloral hydrate and photographed immediately using a Zeiss Apotome 2 microscope with a 10x DIC objective. The scheme of experiment procedure is shown in Fig. 4-1.

#### **4.2.3.2 NBT staining**

The presence of superoxide was determined by NBT (Abcam) staining as described (Dunand *et al.*, 2007) with some changes. Seedlings were submerged in staining solution (0.05% NBT in 20 mM phosphate buffer (pH 6.1)) in the dark for 10 min and rinsed twice with phosphate buffer. After rinsing, wait for 10 min to let the reaction finish. Chloral hydrate-mounted seedlings were then photographed using a Zeiss Apotome 2 microscope with a 10x DIC objective within 30 min. The scheme of experiment procedure is shown in Fig. 4-1.

#### **4.2.4 Fluorescence ROS probes staining**

All the staining procedures were performed under darkness. To avoid autofluorescence of the dyes and toxicity may triggered by the dyes which will lead to ROS formation, photographing was finished within 30 min in the dark right after the staining finished. The scheme of experiment procedure is shown in Fig. 4-1.

#### 4.2.4.1 Carboxy-H2DCFDA staining

The presence of ROS was monitored in root tips as described (Freeman *et al.*, 2004). Seedlings were stained with 10  $\mu$ M Carboxy-H2DCFDA (Invitrogen) in 1x Phosphate Buffered Saline (PBS) buffer for 10 min. Root tips were subsequently mounted with 1x PBS and imaged with LSM 780. Excitation/emission range: 488/530-560 nm.

#### 4.2.4.2 DHE staining

Superoxide was determined using DHE (Sigma-Aldrich) as described (Reyt *et al.*, 2015). Seedlings were incubated in liquid +Pi or -Pi medium containing 10  $\mu$ M DHE (Sigma-Aldrich) for 25 min. Thereafter, the roots were mounted with liquid medium and imaged with LSM 780. Excitation/emission range: 535/550-650 nm.

#### 4.2.4.3 BES- H<sub>2</sub>O<sub>2</sub>-Ac

BES- H<sub>2</sub>O<sub>2</sub>-Ac (WAKO, Japan) was used for H<sub>2</sub>O<sub>2</sub> staining as described (Maeda *et al.*, 2004; Yamada *et al.*, 2020). Seedlings were incubated in 50 $\mu$ M of BES-H<sub>2</sub>O<sub>2</sub>-Ac for 30 min. Roots were mounted with water and observed using LSM 700. Excitation/emission range: 488/500-550 nm.

#### 4.2.4.4 HPF

Detection of  $\cdot$ OH was performed with HPF (Goryo Chemical) as described (Zheng *et al.*, 2019) with some changes. Seedlings were incubated in staining solution (10  $\mu$ M HPF in 100 mM phosphate buffer (pH 7.4)) for 30 min. Roots were then mounted with phosphate buffer and observed using LSM 780. Excitation/emission range: 488/490-520 nm.

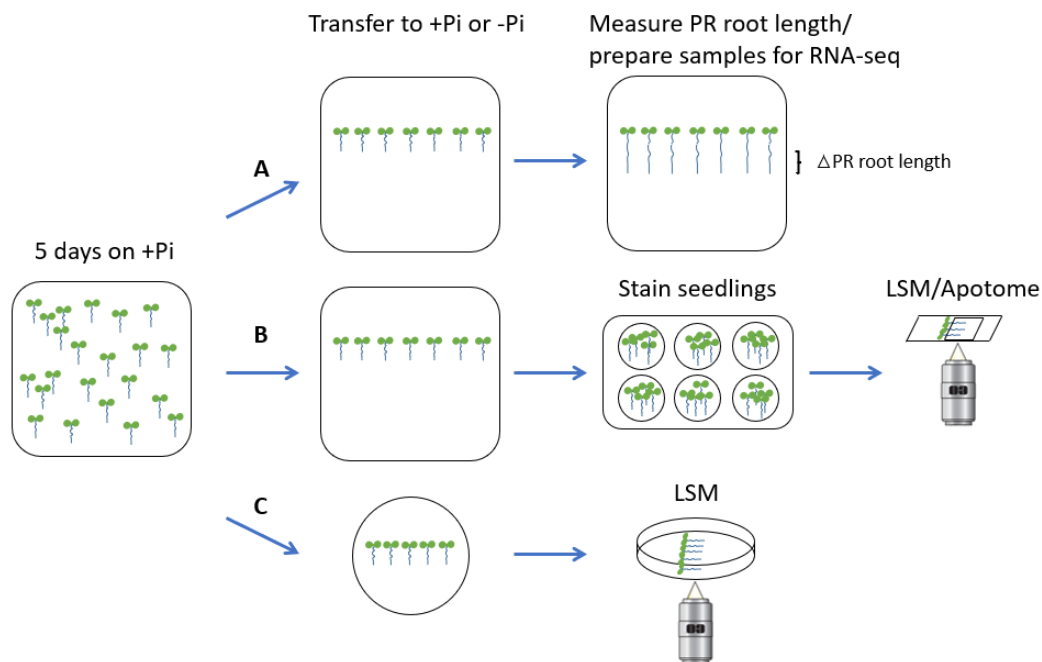


**Fig. 4-1: Scheme of the experiment procedure**

(A)  $\Delta$  primary root measurement and sample preparation for RNA-seq. (B) ROS probs staining and (C) Grx1-roGFP2 analysis of seedlings transferred from +Pi plates to +Pi or -Pi plates. PR, primary root

#### 4.2.5 Confocal laser scanning microscopy (CLSM)

Images were acquired with Zeiss LSM700, LSM780 and LSM880 confocal microscopes. 20x or 40x Water immersion objectives were used, if not stated otherwise. To operate the microscope, Zen Software (Zeiss) was used. Images were processed with Zen or Fiji software.

For staining with PI (propidium iodide, Sigma-Aldrich), seedlings were directly mounted in 10  $\mu$ g/ml PI and observed by confocal microscope. Excitation/emission range within different experiments were set as follows: GFP: 488/492-550 nm; PI: 561/570-650 nm.

For Grx1-roGFP2, 5-day-old seedlings were transferred to +Pi or -Pi chamber plates with thin membrane bottom (lumox<sup>®</sup> dish 50, Sarstedt, diameter: 5cm). 2 ml medium was used to prepare one chamber plate. Seedlings were directly imaged on the plate as shown in Fig. 4-1C. To rule out of the position influence on the results, five seedlings were transferred to one chamber plate but only the three seedlings in the middle were imaged. Two tracks were set up for imaging roGFP2 with excitation at 405nm and 488 nm, respectively. The fluorescence was collected between 508 nm and 530 nm for both tracks. Imaging of seedlings expressing *pUBQ10:Grx1-roGFP2* and *pWOX5:Grx1-roGFP2* was performed using LSM780 and LSM880, respectively. For *pUBQ10:Grx1-roGFP2*, 405nm and 488 nm laser power were set as 3. For

*pWOX5:Grx1-roGFP2*, 405nm and 488 nm laser power was set as 4 and 3, respectively. Rest of the settings remain the same for both channels. One drop of 10 mM H<sub>2</sub>O<sub>2</sub> was applied to the root tip directly on the plate. After 2 min or 5 min, the drop was removed, and seedling was imaged.

#### 4.2.6 Ratiometric analysis of roGFP2

Ratio images were calculated as previously described (Meyer *et al.*, 2007) with Fiji. Set threshold for both 405nm and 488 nm images after converting the original images to 32-bit to lower the background using the 'Threshold' function under 'Image'. Images were then saved as 'Tiff' form. Ratio image was generated through dividing 405 nm image by 488 nm image (32-bit float result). The grayscale was then converted to color using the Fiji look-up table 'royal' to illustrate the evaluated 405 nm/488 nm intensity ratio images. To measure the ratio, regions of interest was cropped directly after the ratio images were generated and average ratio measured using 'Measure' under 'Analyze'. To speed up the image process from original images to ratio images, a Macro script was applied. Script is available in the Supplementary method.

#### 4.2.7 Root length measurement assay

After growing on vertically placed medium for 5 days, seedlings were transferred to +Pi or -Pi medium (Fig. 4-1). Images of seedlings growing on the plates for additional 3 to 4 days were taken with a Nikon camera.  $\Delta$  primary root length measurement was performed using Fiji software (<https://fiji.sc/>) (Schindelin *et al.*, 2012) with NeuronJ plugin (Meijering *et al.*, 2004). Original images were converted to 8-bit images first. To make the processing faster, a Macro script was applied. Script is available in the supplementary method.

#### 4.2.8 Analysis of protein from plant tissues

##### 4.2.8.1 Protein extraction from seedlings

Around 50 roots of Arabidopsis seedlings were collected for one sample and frozen in liquid nitrogen. Samples were ground in a Tissue Lyser II (QIAGEN) at 25 s<sup>-1</sup> for 30s. Total protein was extracted by adding 100  $\mu$ l RIPA buffer (50 mM Tris-Cl pH 7.5; 150 mM NaCl; 20 mM NaF; 0.1% (v/v) Nonidet P40; 0.05% (w/v) Deoxycholate; 10 mM Na<sub>4</sub>P<sub>2</sub>O<sub>7</sub>; 1 mM EDTA; 0.5 mM EGTA). The samples were briefly vortexed and kept on a rotator at 4° C for 30 min. After extraction, the samples were centrifuged at 10000 rpm for 10 min at 4° C and 40  $\mu$ l supernatant was collected in an Eppendorf tube.



#### 4.2.8.2 Sodium dodecyl sulfate polyacrylamide gel electrophoresis (SDS-PAGE) and immunoblotting

Protein samples were mixed with 5x loading buffer (350 mM Tris-HCl, pH 6.8, 10% SDS, 30% glycerol, and 600mM DTT), incubated for 5 min at 96° C and electrophoretically separated on an SDS-PAGE gel with 10% separating gel and 4% stacking gel. SDS-PAGE was performed at 85 V in 1x running buffer (25 mM Tris, 192 mM glycine, and 0.1% SDS) for 15 min and then at 135 V until the dye front reaches the lower rim of the gel. The composition of separating and stacking gel is mentioned in Tab. 4-6. Proteins separated on the SDS-PAGE gel were subsequently transferred semi-dry to a nitrocellulose membrane (Amersham Protran 0.45 µm) in towbin transfer buffer (25 mM Tris-HCl, 20% methanol, 192 mM Glycine, 1.3 mM SDS, pH 8.3 (without adjustment)) for 1 h at 20 V. After blocking the membrane with 5% milk powder in 1x TBST for 1 h, primary antibody (3H9 anti-GFP, rat mAb, Chromotek) was applied over the membrane at a dilution of 1:2000 with 3% milk powder in 1x TBST and incubated overnight at 4° C with gentle shaking. After washing the membrane three times for 10 min with TBST, the secondary antibody (Anti-rat IgG-HRP, Thermo) was added at a dilution of 1: 5000 with 3 % milk powder in 1x TBST buffer and incubated for 1 h with gentle shaking. Then the membrane was washed three times for 10 min with TBST. Detection of signals was preformed using ECL Prime Kit (Amersham) according to manufacturer's instructions.

**Tab. 4-6: Composition of SDS-PAGE Gel**

Components	Stacking gel (4%)	Separating gel (12%)
Millipore water	1.4	4
1 M Tris pH 6.8	0.25	-
1.5 M Tris pH 8.8	-	2.5
10% SDS	0.02	0.1
30% Acrylamide	0.33	3.3
10% APS	0.02	0.1
TEMED	0.002	0.004
Total Volume	2 ml	10 ml

#### 4.2.9 Diphenylene iodonium (DPI) treatment

To decrease  $O_2^{\cdot-}$  levels, filter sterilized DPI (Tocris) which was dissolved in DMSO was added into the autoclaved medium. Seedlings were grown on +Pi medium for 5 days, then transferred to +Pi or -Pi medium containing 0.1 µM or 0.3 µM DPI. For control, same amount of DMSO was added.

#### 4.2.10 RNA preparation and RNA-seq analysis

Seedlings (5-days-old) were transferred from +Pi (25  $\mu$ M Fe) to either +Pi (25  $\mu$ M Fe) or -Pi (25  $\mu$ M Fe) medium. After 1 day of transfer, root tips were cut off between 10<sup>th</sup> to 20<sup>th</sup> root hair on the plate and frozen in liquid nitrogen. Each sample consisted of 150 root tips except the -Pi sample of *pdr2* which contained 300 root tips. Total RNA was extracted using the peqGOLD Plant Kit from VWR and meanwhile, the on-column DNA digestion was performed using Qiagen RNase-free DNase Set following the manufacturer's protocol. The quality of RNA was verified with Agilent 2100 Bioanalyzer (Agilent). RNA samples (2.2  $\mu$ g for each) with an RNA integrity number (RIN)  $\geq$  6.5 were sent to Novogene. Three biological replicates were sequenced per genotype and treatment. Sequencing libraries (strand specific) were prepared using NEBNext<sup>®</sup> Ultra TM RNA Library Prep Kit for Illumina<sup>®</sup> (NEB, USA). Samples were sequenced on an Illumina NovaSeq platform with 150bp paired end (PE) read. Reads were quality filtered through fastp (v. 0.20.0) (Chen *et al.*, 2018) and mapped to the *A. thaliana* genome (TAIR10) using HISAT2 (v. 2.2.0) (Kim *et al.*, 2019). Differential gene expression analysis was conducted using the DESeq2 R package (Love *et al.*, 2014). Benjamini and Hochberg's approach for controlling the False Discovery Rate (FDR) was used to adjust *p* values (Benjamini & Hochberg, 1995).

#### 4.2.11 *In silico* data analysis

Principal component analysis (PCA) was performed in R software (v. 4.0.4). FPKM of all the expressed genes in WT, *pdr2* and *lpr1lpr2* were normalized by log<sub>2</sub> transformation and then conducted for further analysis. R script is available in the supplementary method. 3D plot with respect to the first three principal components was performed using Data Visualization (Cubemark) on Altius Institute-Tools website (<https://tools.altiusinstitute.org/overview/>).

Gene ontology (GO) enrichment analysis and Kyoto Encyclopedia of Genes and Genomes (KEGG) pathway analysis were performed using the Functional Annotation Tool on DAVID server (<https://david.ncifcrf.gov/>) (Huang *et al.*, 2009b; Huang *et al.*, 2009a). Enrichment of GO terms KEGG pathways were tested by modified Fisher exact test. Results were visualized with dot plots generated in R. R script was provided by colleague Pinelopi Moutesidi.

For Hierarchical clustering analysis, z-scores were calculated from FPKM values, and the scaled data was clustered in TIGR-MEV (v. 4.9.0) (<http://mev.tm4.org>) using Pearson correlation and average linkage clustering (Saeed *et al.*, 2003). All heatmaps were generated in TIGR-MEV as well.

Groups of DEGs identified by Hierarchical clustering were analyzed for functional protein association networks with the STRING tool (v. 11.5) (<https://string-db.org/>) (Szklarczyk *et al.*, 2019). Networks for the genes from cluster 1, 2 and 3 were created with medium confidence interaction score of 0.4 due to relatively low number of genes in the lists. High confidence interaction score of 0.7 was applied for genes from cluster 4 and 5.

Venn diagrams that visualize the overlaps in gene lists were generated using jvenn (<http://jvenn.toulouse.inra.fr/app/index.html>) (Bardou *et al.*, 2014).

Transcription factors that may regulate a given list of genes were predicted using Gene Group Analysis on the Plant Promoter Analysis Navigator (PlantPAN) v2.0 (<http://plantpan2.itps.ncku.edu.tw/>) (Chow *et al.*, 2016).

## 5. REFERENCES

- Abel S. 2017.** Phosphate scouting by root tips. *Curr Opin Plant Biol* **39**: 168-177.
- Ahmed R. 2015.** *Molecular identification and characterization of the phosphate deficiency response related genes, PRT1 (ATP-Phosphoribosyl Transferase 1) and ALMT1 (Aluminium-activated Malate Transporter 1).*
- Amsbury S, Kirk P, Benitez-Alfonso Y. 2017.** Emerging models on the regulation of intercellular transport by plasmodesmata-associated callose. *J Exp Bot* **69**(1): 105-115.
- Angelos E, Ruberti C, Kim SJ, Brandizzi F. 2017.** Maintaining the factory: the roles of the unfolded protein response in cellular homeostasis in plants. *Plant J* **90**(4): 671-682.
- Apel K, Hirt H. 2004.** Reactive oxygen species: metabolism, oxidative stress, and signal transduction. *Annu Rev Plant Biol* **55**: 373-399.
- Asada K. 1999.** THE WATER-WATER CYCLE IN CHLOROPLASTS: Scavenging of Active Oxygens and Dissipation of Excess Photons. *Annu Rev Plant Physiol Plant Mol Biol* **50**: 601-639.
- Babitha KC, Ramu SV, Pruthvi V, Mahesh P, Nataraja KN, Udayakumar M. 2013.** Co-expression of AtbHLH17 and AtWRKY28 confers resistance to abiotic stress in Arabidopsis. *Transgenic Res* **22**(2): 327-341.
- Baluska F, Volkmann D, Barlow PW. 1996.** Specialized zones of development in roots: view from the cellular level. *Plant Physiol* **112**(1): 3-4.
- Balergue C, Darteville T, Godon C, Laugier E, Meisrimler C, Teulon JM, Creff A, Bissler M, Bouchoud C, Hagege A, et al. 2017.** Low phosphate activates STOP1-ALMT1 to rapidly inhibit root cell elongation. *Nat Commun* **8**: 15300.
- Band LR, Ubeda-Tomas S, Dyson RJ, Middleton AM, Hodgman TC, Owen MR, Jensen OE, Bennett MJ, King JR. 2012.** Growth-induced hormone dilution can explain the dynamics of plant root cell elongation. *Proc Natl Acad Sci U S A* **109**(19): 7577-7582.
- Bardou P, Mariette J, Escudie F, Djemiel C, Klopp C. 2014.** jvenn: an interactive Venn diagram viewer. *BMC Bioinformatics* **15**: 293.
- Bashandy T, Guilleminot J, Vernoux T, Caparros-Ruiz D, Ljung K, Meyer Y, Reichheld JP. 2010.** Interplay between the NADP-linked thioredoxin and glutathione systems in Arabidopsis auxin signaling. *Plant Cell* **22**(2): 376-391.
- Belousov VV, Fradkov AF, Lukyanov KA, Staroverov DB, Shakhbazov KS, Terskikh AV, Lukyanov S. 2006.** Genetically encoded fluorescent indicator for intracellular hydrogen peroxide. *Nat Methods* **3**(4): 281-286.
- Benitez-Alfonso Y, Jackson D, Maule A. 2011.** Redox regulation of intercellular transport. *Protoplasma* **248**(1): 131-140.
- Benjamini Y, Hochberg Y. 1995.** Controlling the false discovery rate: a practical and powerful approach to multiple testing. *Journal of the royal statistical society series b-methodological* **57**: 289-300.

- Bhatt I, Tripathi BN. 2011.** Plant peroxiredoxins: Catalytic mechanisms, functional significance and future perspectives. *Biotechnology Advances* **29**(6): 850-859.
- Bielski BHJ, Shiue GG, Bajuk S. 1980.** Reduction of nitro blue tetrazolium by CO<sub>2</sub>- and O<sub>2</sub>- radicals. *The Journal of Physical Chemistry* **84**(8): 830-833.
- Bindraban PS, Dimkpa CO, Pandey R. 2020.** Exploring phosphorus fertilizers and fertilization strategies for improved human and environmental health. *Biology and Fertility of Soils* **56**(3): 299-317.
- Bindschedler LV, Dewdney J, Blee KA, Stone JM, Asai T, Plotnikov J, Denoux C, Hayes T, Gerrish C, Davies DR, et al. 2006.** Peroxidase-dependent apoplastic oxidative burst in Arabidopsis required for pathogen resistance. *Plant J* **47**(6): 851-863.
- Bonser AM, Lynch J, Snapp S. 1996.** Effect of phosphorus deficiency on growth angle of basal roots in *Phaseolus vulgaris*. *New Phytol* **132**(2): 281-288.
- Borisova MM, Kozuleva MA, Rudenko NN, Naydov IA, Klenina IB, Ivanov BN. 2012.** Photosynthetic electron flow to oxygen and diffusion of hydrogen peroxide through the chloroplast envelope via aquaporins. *Biochimica et Biophysica Acta (BBA) - Bioenergetics* **1817**(8): 1314-1321.
- Bourdais G, Burdiak P, Gauthier A, Nitsch L, Salojarvi J, Rayapuram C, Idanheimo N, Hunter K, Kimura S, Merilo E, et al. 2015.** Large-Scale Phenomics Identifies Primary and Fine-Tuning Roles for CRKs in Responses Related to Oxidative Stress. *Plos Genetics* **11**(7).
- Brady SM, Orlando DA, Lee JY, Wang JY, Koch J, Dinneny JR, Mace D, Ohler U, Benfey PN. 2007.** A high-resolution root spatiotemporal map reveals dominant expression patterns. *Science* **318**(5851): 801-806.
- Burstenbinder K, Moller B, Plotner R, Stamm G, Hause G, Mitra D, Abel S. 2017.** The IQD Family of Calmodulin-Binding Proteins Links Calcium Signaling to Microtubules, Membrane Subdomains, and the Nucleus. *Plant Physiol* **173**(3): 1692-1708.
- Bustos R, Castrillo G, Linhares F, Puga MI, Rubio V, Perez-Perez J, Solano R, Leyva A, Paz-Ares J. 2010.** A central regulatory system largely controls transcriptional activation and repression responses to phosphate starvation in Arabidopsis. *PLoS Genet* **6**(9): e1001102.
- Cabassa-Hourton C, Schertl P, Bordenave-Jacquemin M, Saadallah K, Guivarc'h A, Lebreton S, Planchais S, Klodmann J, Eubel H, Crilat E, et al. 2016.** Proteomic and functional analysis of proline dehydrogenase 1 link proline catabolism to mitochondrial electron transport in Arabidopsis thaliana. *Biochemical Journal* **473**: 2623-2634.
- Cabib E, Leloir LF. 1958.** The biosynthesis of trehalose phosphate. *J Biol Chem* **231**(1): 259-275.
- Caillaud MC, Wirthmueller L, Sklenar J, Findlay K, Piquerez SJM, Jones AME, Robatzek S, Jones JDG, Faulkner C. 2014.** The Plasmodesmal Protein PDL1 Localises to Haustoria-Associated Membranes during Downy Mildew Infection and Regulates Callose Deposition. *Plos Pathogens* **10**(11).
- Castro B, Citterico M, Kimura S, Stevens DM, Wrzaczek M, Coaker G. 2021.** Stress-induced reactive oxygen species compartmentalization, perception and signalling. *Nat Plants* **7**(4): 403-412.
- Cavalheiro MF, Gavassi MA, Silva GS, Nogueira MA, Silva CMS, Domingues DS, Habermann G. 2020.** Low root PIP1-1 and PIP2 aquaporins expression could be related to reduced hydration in 'Rangpur' lime plants exposed to aluminium. *Funct Plant Biol* **47**(2): 112-121.

- Chapman JM, Muhlemann JK, Gayomba SR, Muday GK. 2019.** RBOH-Dependent ROS Synthesis and ROS Scavenging by Plant Specialized Metabolites To Modulate Plant Development and Stress Responses. *Chem Res Toxicol* **32**(3): 370-396.
- Chen SF, Zhou YQ, Chen YR, Gu J. 2018.** fastp: an ultra-fast all-in-one FASTQ preprocessor. *Bioinformatics* **34**(17): 884-890.
- Chen SX, Schopfer P. 1999.** Hydroxyl-radical production in physiological reactions. A novel function of peroxidase. *European Journal of Biochemistry* **260**(3): 726-735.
- Cheval C, Faulkner C. 2018.** Plasmodesmal regulation during plant-pathogen interactions. *New Phytol* **217**(1): 62-67.
- Chevalier F, Rossignol M. 2011.** Proteomic analysis of Arabidopsis thaliana ecotypes with contrasted root architecture in response to phosphate deficiency. *J Plant Physiol* **168**(16): 1885-1890.
- Chiou TJ, Lin SI. 2011.** Signaling network in sensing phosphate availability in plants. *Annu Rev Plant Biol* **62**: 185-206.
- Choudhary A, Kumar A, Kaur N. 2020.** ROS and oxidative burst: Roots in plant development. *Plant Divers* **42**(1): 33-43.
- Chow CN, Zheng HQ, Wu NY, Chien CH, Huang HD, Lee TY, Chiang-Hsieh YF, Hou PF, Yang TY, Chang WC. 2016.** PlantPAN 2.0: an update of plant promoter analysis navigator for reconstructing transcriptional regulatory networks in plants. *Nucleic Acids Res* **44**(D1): D1154-1160.
- Christ B. 2013.** *Chlorophyll Breakdown: Modifications of Colorless Chlorophyll Catabolites.*
- Chung JS, Zhu JK, Bressan RA, Hasegawa PM, Shi H. 2008.** Reactive oxygen species mediate Na<sup>+</sup>-induced SOS1 mRNA stability in Arabidopsis. *Plant J* **53**(3): 554-565.
- Chutia R. 2019.** *Manipulation of malate biosynthesis and exudation in Arabidopsis thaliana.*
- Clark G, Konopka-Postupolska D, Hennig J, Roux S. 2010.** Is annexin 1 a multifunctional protein during stress responses? *Plant signaling & behavior* **5**(3): 303-307.
- Clough SJ, Bent AF. 1998.** Floral dip: a simplified method for Agrobacterium-mediated transformation of Arabidopsis thaliana. *Plant J* **16**(6): 735-743.
- Cordell D, Drangert JO, White S. 2009.** The story of phosphorus: Global food security and food for thought. *Global Environmental Change-Human and Policy Dimensions* **19**(2): 292-305.
- Cui W, Lee JY. 2016.** Arabidopsis callose synthases CalS1/8 regulate plasmodesmal permeability during stress. *Nature Plants* **2**(5).
- De Clercq I, Van de Velde J, Luo X, Liu L, Storme V, Van Bel M, Pottier R, Vanechoutte D, Van Breusegem F, Vandepoele K. 2021.** Integrative inference of transcriptional networks in Arabidopsis yields novel ROS signalling regulators. *Nat Plants* **7**(4): 500-513.
- De Veylder L, Beeckman T, Inze D. 2007.** The ins and outs of the plant cell cycle. *Nat Rev Mol Cell Biol* **8**(8): 655-665.

- Demidchik V, Shabala S. 2018.** Mechanisms of cytosolic calcium elevation in plants: the role of ion channels, calcium extrusion systems and NADPH oxidase-mediated 'ROS-Ca(2+) Hub'. *Funct Plant Biol* **45**(2): 9-27.
- di Pietro M, Vialaret J, Li GW, Hem S, Prado K, Rossignol M, Maurel C, Santoni V. 2013.** Coordinated post-translational responses of aquaporins to abiotic and nutritional stimuli in Arabidopsis roots. *Mol Cell Proteomics* **12**(12): 3886-3897.
- Dietz KJ. 2003.** Plant peroxiredoxins. *Annu Rev Plant Biol* **54**: 93-107.
- Dissanayaka D, Ghahremani M, Siebers M, Wasaki J, Plaxton WC. 2021.** Recent insights into the metabolic adaptations of phosphorus-deprived plants. *J Exp Bot* **72**(2): 199-223.
- Dixon DP, Edwards R. 2010.** *Glutathione Transferases*.
- Dong J, Ma G, Sui L, Wei M, Satheesh V, Zhang R, Ge S, Li J, Zhang T-E, Wittwer C, et al. 2019.** Inositol Pyrophosphate InsP8 Acts as an Intracellular Phosphate Signal in Arabidopsis. *Molecular Plant* **12**(11): 1463-1473.
- Dunand C, Crevecoeur M, Penel C. 2007.** Distribution of superoxide and hydrogen peroxide in Arabidopsis root and their influence on root development: possible interaction with peroxidases. *New Phytol* **174**(2): 332-341.
- Dvorak P, Krasnylenko Y, Ovecka M, Basheer J, Zapletalova V, Samaj J, Takac T. 2021.** In vivo light-sheet microscopy resolves localisation patterns of FSD1, a superoxide dismutase with function in root development and osmoprotection. *Plant Cell Environ* **44**(1): 68-87.
- Egert A. 2011.** *Raffinose Oligosaccharide Catabolism in Arabidopsis thaliana*.
- Eljebbawi A, Guerrero Y, Dunand C, Estevez JM. 2021.** Highlighting reactive oxygen species as multitaskers in root development. *iScience* **24**(1): 101978.
- Ellinger D, Voigt CA. 2014.** Callose biosynthesis in Arabidopsis with a focus on pathogen response: what we have learned within the last decade. *Ann Bot* **114**(6): 1349-1358.
- Eltayeb AE, Kawano N, Badawi GH, Kaminaka H, Sanekata T, Shibahara T, Inanaga S, Tanaka K. 2007.** Overexpression of monodehydroascorbate reductase in transgenic tobacco confers enhanced tolerance to ozone, salt and polyethylene glycol stresses. *Planta* **225**(5): 1255-1264.
- Fernandez-Perez F, Vivar T, Pomar F, Pedreno MA, Novo-Uzal E. 2015.** Peroxidase 4 is involved in syringyl lignin formation in Arabidopsis thaliana. *J Plant Physiol* **175**: 86-94.
- Fichman Y, Mittler R. 2020.** Rapid systemic signaling during abiotic and biotic stresses: is the ROS wave master of all trades? *Plant Journal* **102**(5): 887-896.
- Fichman Y, Myers RJ, Grant DG, Mittler R. 2021.** Plasmodesmata-localized proteins and ROS orchestrate light-induced rapid systemic signaling in Arabidopsis. *Science Signaling* **14**(671).
- Figueroa CM, Feil R, Ishihara H, Watanabe M, Kolling K, Krause U, Hohne M, Encke B, Plaxton WC, Zeeman SC, et al. 2016.** Trehalose 6-phosphate coordinates organic and amino acid metabolism with carbon availability. *Plant J* **85**(3): 410-423.

- Foreman J, Demidchik V, Bothwell JH, Mylona P, Miedema H, Torres MA, Linstead P, Costa S, Brownlee C, Jones JD, et al. 2003. Reactive oxygen species produced by NADPH oxidase regulate plant cell growth. *Nature* **422**(6930): 442-446.
- Foyer CH, Noctor G. 2009. Redox regulation in photosynthetic organisms: signaling, acclimation, and practical implications. *Antioxid Redox Signal* **11**(4): 861-905.
- Foyer CH, Noctor G. 2011. Ascorbate and glutathione: the heart of the redox hub. *Plant Physiol* **155**(1): 2-18.
- Francoz E, Ranocha P, Nguyen-Kim H, Jamet E, Burlat V, Dunand C. 2015. Roles of cell wall peroxidases in plant development. *Phytochemistry* **112**: 15-21.
- Freeman JL, Persans MW, Nieman K, Albrecht C, Peer W, Pickering IJ, Salt DE. 2004. Increased glutathione biosynthesis plays a role in nickel tolerance in thlaspi nickel hyperaccumulators. *Plant Cell* **16**(8): 2176-2191.
- Fricke W, Chaumont F. 2007. Solute and Water Relations of Growing Plant Cells. In: Verbelen J-P, Vissenberg K eds. *The Expanding Cell*. Berlin, Heidelberg: Springer Berlin Heidelberg, 7-31.
- Fridovich I. 1997. Superoxide anion radical (O<sub>2</sub><sup>-</sup>), superoxide dismutases, and related matters. *J Biol Chem* **272**(30): 18515-18517.
- Gao YQ, Bu LH, Han ML, Wang YL, Li ZY, Liu HT, Chao DY. 2021. Long-distance blue light signalling regulates phosphate deficiency-induced primary root growth inhibition. *Mol Plant* **14**(9): 1539-1553.
- Gonzalez-Garcia MP, Vilarrasa-Blasi J, Zhiponova M, Divol F, Mora-Garcia S, Russinova E, Cano-Delgado AI. 2011. Brassinosteroids control meristem size by promoting cell cycle progression in Arabidopsis roots. *Development* **138**(5): 849-859.
- Gregory AL, Hurley BA, Tran HT, Valentine AJ, She YM, Knowles VL, Plaxton WC. 2009. In vivo regulatory phosphorylation of the phosphoenolpyruvate carboxylase AtPPC1 in phosphate-starved Arabidopsis thaliana. *Biochem J* **420**(1): 57-65.
- Grillet L, Ouerdane L, Flis P, Hoang MT, Isaure MP, Lobinski R, Curie C, Mari S. 2014. Ascorbate efflux as a new strategy for iron reduction and transport in plants. *J Biol Chem* **289**(5): 2515-2525.
- Gutscher M, Pauleau AL, Marty L, Brach T, Wabnitz GH, Samstag Y, Meyer AJ, Dick TP. 2008. Real-time imaging of the intracellular glutathione redox potential. *Nat Methods* **5**(6): 553-559.
- Helariutta Y, Fukaki H, Wysocka-Diller J, Nakajima K, Jung J, Sena G, Hauser MT, Benfey PN. 2000. The SHORT-ROOT gene controls radial patterning of the Arabidopsis root through radial signaling. *Cell* **101**(5): 555-567.
- Heyman J, Cools T, Canher B, Shavialenka S, Traas J, Vercauteren I, Van den Daele H, Persiau G, De Jaeger G, Sugimoto K, et al. 2016. The heterodimeric transcription factor complex ERF115-PAT1 grants regeneration competence. *Nat Plants* **2**(11): 16165.
- Heyman J, Cools T, Vandenbussche F, Heyndrickx KS, Van Leene J, Vercauteren I, Vanderauwera S, Vandepoele K, De Jaeger G, Van Der Straeten D, et al. 2013. ERF115 controls root quiescent center cell division and stem cell replenishment. *Science* **342**(6160): 860-863.



- Hinsinger P, Herrmann L, Lesueur D, Robin A, Trap J, Waithaisong K, Plassard C 2015. Impact of roots, microorganisms and microfauna on the fate of soil phosphorus in the rhizosphere. *Annual Plant Reviews Volume 48*, 375-407.
- Hoehenwarter W, Monchgesang S, Neumann S, Majovsky P, Abel S, Muller J. 2016. Comparative expression profiling reveals a role of the root apoplast in local phosphate response. *BMC Plant Biol* 16: 106.
- Hoekenga OA, Maron LG, Pineros MA, Cancado GMA, Shaff J, Kobayashi Y, Ryan PR, Dong B, Delhaize E, Sasaki T, et al. 2006. AtALMT1, which encodes a malate transporter, is identified as one of several genes critical for aluminum tolerance in Arabidopsis. *Proceedings of the National Academy of Sciences of the United States of America* 103(25): 9738-9743.
- Holdaway-Clarke TL, Walker NA, Hepler PK, Overall RL. 2000. Physiological elevations in cytoplasmic free calcium by cold or ion injection result in transient closure of higher plant plasmodesmata. *Planta* 210(2): 329-335.
- Huang DW, Sherman BT, Lempicki RA. 2009a. Bioinformatics enrichment tools: paths toward the comprehensive functional analysis of large gene lists. *Nucleic Acids Research* 37(1): 1-13.
- Huang DW, Sherman BT, Lempicki RA. 2009b. Systematic and integrative analysis of large gene lists using DAVID bioinformatics resources. *Nature Protocols* 4(1): 44-57.
- Huang P, Chung MS, Ju HW, Na HS, Lee DJ, Cheong HS, Kim CS. 2011. Physiological characterization of the Arabidopsis thaliana Oxidation-related Zinc Finger 1, a plasma membrane protein involved in oxidative stress. *Journal of Plant Research* 124(6): 699-705.
- Ikeda M, Ohme-Takagi M. 2009. A Novel Group of Transcriptional Repressors in Arabidopsis. *Plant and Cell Physiology* 50(5): 970-975.
- Ines OD. 2008. *Functional analysis of PIP2 aquaporins in Arabidopsis thaliana*.
- Jaenen V, Fraguas S, Bijmens K, Heleven M, Artois T, Romero R, Smeets K, Cebria F. 2021. Reactive oxygen species rescue regeneration after silencing the MAPK-ERK signaling pathway in *Schmidtea mediterranea*. *Sci Rep* 11(1): 881.
- Jin J, Hewezi T, Baum TJ. 2011. Arabidopsis peroxidase AtPRX53 influences cell elongation and susceptibility to *Heterodera schachtii*. *Plant Signal Behav* 6(11): 1778-1786.
- Johanson U, Karlsson M, Johansson I, Gustavsson S, Sjovalld S, Fraysse L, Weig AR, Kjellbom P. 2001. The complete set of genes encoding major intrinsic proteins in Arabidopsis provides a framework for a new nomenclature for major intrinsic proteins in plants. *Plant Physiol* 126(4): 1358-1369.
- Kiernan JA. 2003. Stability and solubility of 3,3'-diaminobenzidine (DAB). *Biotech Histochem* 78(2): 135.
- Kim D, Paggi JM, Park C, Bennett C, Salzberg SL. 2019. Graph-based genome alignment and genotyping with HISAT2 and HISAT-genotype. *Nat Biotechnol* 37(8): 907-915.
- Kochian LV, Pineros MA, Liu JP, Magalhaes JV. 2015. Plant Adaptation to Acid Soils: The Molecular Basis for Crop Aluminum Resistance. *Annual Review of Plant Biology, Vol 66* 66: 571-598.
- Kong X, Tian H, Yu Q, Zhang F, Wang R, Gao S, Xu W, Liu J, Shani E, Fu C, et al. 2018. PHB3 Maintains Root Stem Cell Niche Identity through ROS-Responsive AP2/ERF Transcription Factors in Arabidopsis. *Cell Rep* 22(5): 1350-1363.

- Laloi C, Havaux M. 2015.** Key players of singlet oxygen-induced cell death in plants. *Front Plant Sci* **6**: 39.
- Lan P, Li W, Schmidt W. 2012.** Complementary proteome and transcriptome profiling in phosphate-deficient Arabidopsis roots reveals multiple levels of gene regulation. *Mol Cell Proteomics* **11**(11): 1156-1166.
- Lan P, Li W, Schmidt W 2015.** 'Omics' Approaches Towards Understanding Plant Phosphorus Acquisition and Use. *Annual Plant Reviews Volume 48*, 65-97.
- Lazaro JJ, Jimenez A, Camejo D, Iglesias-Baena I, Marti Mdel C, Lazaro-Payo A, Barranco-Medina S, Sevilla F. 2013.** Dissecting the integrative antioxidant and redox systems in plant mitochondria. Effect of stress and S-nitrosylation. *Front Plant Sci* **4**: 460.
- Le J, Vandenbussche F, Van Der Straeten D, Verbelen JP. 2004.** Position and cell type-dependent microtubule reorientation characterizes the early response of the Arabidopsis root epidermis to ethylene. *Physiologia Plantarum* **121**(3): 513-519.
- Lee JY, Wang X, Cui W, Sager R, Modla S, Czymmek K, Zybaliow B, van Wijk K, Zhang C, Lu H, et al. 2011.** A Plasmodesmata-Localized Protein Mediates Crosstalk between Cell-to-Cell Communication and Innate Immunity in Arabidopsis. *Plant Cell* **23**(9): 3353-3373.
- Lin WD, Liao YY, Yang TJ, Pan CY, Buckhout TJ, Schmidt W. 2011.** Coexpression-based clustering of Arabidopsis root genes predicts functional modules in early phosphate deficiency signaling. *Plant Physiol* **155**(3): 1383-1402.
- Liu C. 2015.** The PIP1 protein expression is positively regulated by PIP2;1 and PIP2;2 in Arabidopsis thaliana.
- Liu D, Tu L, Wang L, Li Y, Zhu L, Zhang X. 2008.** Characterization and expression of plasma and tonoplast membrane aquaporins in elongating cotton fibers. *Plant Cell Rep* **27**(8): 1385-1394.
- Liu Y, Donner E, Lombi E, Li RY, Wu ZC, Zhao FJ, Wu P. 2013.** Assessing the contributions of lateral roots to element uptake in rice using an auxin-related lateral root mutant. *Plant and Soil* **372**(1-2): 125-136.
- Lopez-Arredondo DL, Leyva-Gonzalez MA, Gonzalez-Morales SI, Lopez-Bucio J, Herrera-Estrella L. 2014.** Phosphate nutrition: improving low-phosphate tolerance in crops. *Annu Rev Plant Biol* **65**: 95-123.
- Love MI, Huber W, Anders S. 2014.** Moderated estimation of fold change and dispersion for RNA-seq data with DESeq2. *Genome Biol* **15**(12): 550.
- Lunn JE. 2007.** Gene families and evolution of trehalose metabolism in plants. *Funct Plant Biol* **34**(6): 550-563.
- Lv Q, Zhong Y, Wang Y, Wang Z, Zhang L, Shi J, Wu Z, Liu Y, Mao C, Yi K, et al. 2014.** SPX4 Negatively Regulates Phosphate Signaling and Homeostasis through Its Interaction with PHR2 in Rice. *Plant Cell* **26**(4): 1586-1597.
- Lynch JP, Brown KM. 2001.** Topsoil foraging - an architectural adaptation of plants to low phosphorus availability. *Plant and Soil* **237**(2): 225-237.
- Mabuchi K, Maki H, Itaya T, Suzuki T, Nomoto M, Sakaoka S, Morikami A, Higashiyama T, Tada Y, Busch W, et al. 2018.** MYB30 links ROS signaling, root cell elongation, and plant immune responses. *Proc Natl Acad Sci U S A* **115**(20): E4710-E4719.

- Maeda H, Fukuyasu Y, Yoshida S, Fukuda M, Saeki K, Matsuno H, Yamauchi Y, Yoshida K, Hirata K, Miyamoto K. 2004. Fluorescent probes for hydrogen peroxide based on a non-oxidative mechanism. *Angew Chem Int Ed Engl* **43**(18): 2389-2391.
- Marjamaa K, Kukkola EM, Fagerstedt KV. 2009. The role of xylem class III peroxidases in lignification. *Journal of Experimental Botany* **60**(2): 367-376.
- Marty L, Siala W, Schwarzlander M, Fricker MD, Wirtz M, Sweetlove LJ, Meyer Y, Meyer AJ, Reichheld JP, Hell R. 2009. The NADPH-dependent thioredoxin system constitutes a functional backup for cytosolic glutathione reductase in Arabidopsis. *Proc Natl Acad Sci U S A* **106**(22): 9109-9114.
- Marzol E, Borassi C, Carignani Sardoy M, Ranocha P, Aptekmann AA, Bringas M, Pennington J, Paez-Valencia J, Martinez Pacheco J, Rodriguez-Garcia DR, et al. 2022. Class III Peroxidases PRX01, PRX44, and PRX73 Control Root Hair Growth in Arabidopsis thaliana. *Int J Mol Sci* **23**(10).
- Mase K, Tsukagoshi H. 2021. Reactive Oxygen Species Link Gene Regulatory Networks During Arabidopsis Root Development. *Front Plant Sci* **12**: 660274.
- Mata-Perez C, Padilla MN, Sanchez-Calvo B, Begara-Morales JC, Valderrama R, Chaki M, Aranda-Cano L, Moreno-Gonzalez D, Molina-Diaz A, Barroso JB. 2020. Endogenous Biosynthesis of S-Nitrosoglutathione From Nitro-Fatty Acids in Plants. *Frontiers in Plant Science* **11**.
- Matthus E, Wilkins KA, Swarbreck SM, Doddrell NH, Doccua FG, Costa A, Davies JM. 2019. Phosphate Starvation Alters Abiotic-Stress-Induced Cytosolic Free Calcium Increases in Roots. *Plant Physiol* **179**(4): 1754-1767.
- Maurel C, Verdoucq L, Luu DT, Santoni V. 2008. Plant aquaporins: membrane channels with multiple integrated functions. *Annu Rev Plant Biol* **59**: 595-624.
- Meijering E, Jacob M, Sarria JC, Steiner P, Hirling H, Unser M. 2004. Design and validation of a tool for neurite tracing and analysis in fluorescence microscopy images. *Cytometry A* **58**(2): 167-176.
- Meyer AJ, Brach T, Marty L, Kreye S, Rouhier N, Jacquot JP, Hell R. 2007. Redox-sensitive GFP in Arabidopsis thaliana is a quantitative biosensor for the redox potential of the cellular glutathione redox buffer. *Plant J* **52**(5): 973-986.
- Meyer AJ, Dick TP. 2010. Fluorescent protein-based redox probes. *Antioxid Redox Signal* **13**(5): 621-650.
- Meyer S, De Angeli A, Fernie AR, Martinoia E. 2010. Intra- and extra-cellular excretion of carboxylates. *Trends Plant Sci* **15**(1): 40-47.
- Mhamdi A, Van Breusegem F. 2018. Reactive oxygen species in plant development. *Development* **145**(15).
- Mittler R. 2017. ROS Are Good. *Trends Plant Sci* **22**(1): 11-19.
- Mittler R, Vanderauwera S, Gollery M, Van Breusegem F. 2004. Reactive oxygen gene network of plants. *Trends Plant Sci* **9**(10): 490-498.
- Mora-Macias J, Ojeda-Rivera JO, Gutierrez-Alanis D, Yong-Villalobos L, Oropeza-Aburto A, Raya-Gonzalez J, Jimenez-Dominguez G, Chavez-Calvillo G, Rellan-Alvarez R, Herrera-Estrella L. 2017. Malate-dependent Fe accumulation is a critical checkpoint in the root developmental response to low phosphate. *Proc Natl Acad Sci U S A* **114**(17): E3563-E3572.

- Müller J, Aeschbacher RA, Wingler A, Boller T, Wiemken A. 2001. Trehalose and trehalase in Arabidopsis. *Plant Physiol* **125**(2): 1086-1093.
- Müller J, Toev T, Heisters M, Teller J, Moore KL, Hause G, Dinesh DC, Burstenbinder K, Abel S. 2015. Iron-dependent callose deposition adjusts root meristem maintenance to phosphate availability. *Dev Cell* **33**(2): 216-230.
- Narang RA, Bruene A, Altmann T. 2000. Analysis of phosphate acquisition efficiency in different arabidopsis accessions. *Plant Physiology* **124**(4): 1786-1799.
- Naumann C, Heisters M, Brandt W, Janitza P, Alfs C, Tang N, Toto Nienguesso A, Ziegler J, Imre R, Mechtler K, et al. 2022. Bacterial-type ferroxidase tunes iron-dependent phosphate sensing during Arabidopsis root development. *Curr Biol* **32**(10): 2189-2205 e2186.
- Naumann C, Muller J, Sakhonwasee S, Wieghaus A, Hause G, Heisters M, Burstenbinder K, Abel S. 2019. The Local Phosphate Deficiency Response Activates Endoplasmic Reticulum Stress-Dependent Autophagy. *Plant Physiol* **179**(2): 460-476.
- Nietzel T, Elsasser M, Ruberti C, Steinbeck J, Ugalde JM, Fuchs P, Wagner S, Ostermann L, Moseler A, Lemke P, et al. 2019. The fluorescent protein sensor roGFP2-Orp1 monitors in vivo H<sub>2</sub>O<sub>2</sub> and thiol redox integration and elucidates intracellular H<sub>2</sub>O<sub>2</sub> dynamics during elicitor-induced oxidative burst in Arabidopsis. *New Phytol* **221**(3): 1649-1664.
- Noctor G, Mhamdi A, Chaouch S, Han Y, Neukermans J, Marquez-Garcia B, Queval G, Foyer CH. 2012. Glutathione in plants: an integrated overview. *Plant Cell Environ* **35**(2): 454-484.
- Orman-Ligeza B, Parizot B, de Rycke R, Fernandez A, Himschoot E, Van Breusegem F, Bennett MJ, Perilleux C, Beeckman T, Draye X. 2016. RBOH-mediated ROS production facilitates lateral root emergence in Arabidopsis. *Development* **143**(18): 3328-3339.
- Pacheco JM, Ranocha P, Kasulin L, Fusari CM, Servi L, Aptekmann AA, Gabarain VB, Peralta JM, Borassi C, Marzol E, et al. 2022. Apoplastic class III peroxidases PRX62 and PRX69 promote Arabidopsis root hair growth at low temperature. *Nat Commun* **13**(1): 1310.
- Pastor-Cantizano N, Ko DK, Angelos E, Pu Y, Brandizzi F. 2020. Functional Diversification of ER Stress Responses in Arabidopsis. *Trends Biochem Sci* **45**(2): 123-136.
- Pedreira J, Herrera MT, Zarra I, Revilla G. 2011. The overexpression of AtPrx37, an apoplastic peroxidase, reduces growth in Arabidopsis. *Physiologia Plantarum* **141**(2): 177-187.
- Pei ZM, Murata Y, Benning G, Thomine S, Klusener B, Allen GJ, Grill E, Schroeder JI. 2000. Calcium channels activated by hydrogen peroxide mediate abscisic acid signalling in guard cells. *Nature* **406**(6797): 731-734.
- Peret B, Clement M, Nussaume L, Desnos T. 2011. Root developmental adaptation to phosphate starvation: better safe than sorry. *Trends in Plant Science* **16**(8): 442-450.
- Petrov V, Hille J, Mueller-Roeber B, Gechev TS. 2015. ROS-mediated abiotic stress-induced programmed cell death in plants. *Front Plant Sci* **6**: 69.
- Planas-Riverola A, Gupta A, Betegon-Putze I, Bosch N, Ibanes M, Cano-Delgado AI. 2019. Brassinosteroid signaling in plant development and adaptation to stress. *Development* **146**(5).

- Plaxton WC, Tran HT. 2011.** Metabolic Adaptations of Phosphate-Starved Plants. *Plant Physiology* **156**(3): 1006-1015.
- Poirier Y, Bucher M. 2002.** Phosphate transport and homeostasis in Arabidopsis. *Arabidopsis Book* **1**: e0024.
- Postaire O, Tournaire-Roux C, Grondin A, Boursiac Y, Morillon R, Schaffner AR, Maurel C. 2010.** A PIP1 Aquaporin Contributes to Hydrostatic Pressure-Induced Water Transport in Both the Root and Rosette of Arabidopsis. *Plant Physiology* **152**(3): 1418-1430.
- Prado K, Boursiac Y, Tournaire-Roux C, Monneuse JM, Postaire O, Da Ines O, Schaffner AR, Hem S, Santoni V, Maurel C. 2013.** Regulation of Arabidopsis Leaf Hydraulics Involves Light-Dependent Phosphorylation of Aquaporins in Veins. *Plant Cell* **25**(3): 1029-1039.
- Price M, Reiners JJ, Santiago AM, Kessel D. 2009.** Monitoring singlet oxygen and hydroxyl radical formation with fluorescent probes during photodynamic therapy. *Photochem Photobiol* **85**(5): 1177-1181.
- Puga MI, Mateos I, Charukesi R, Wang Z, Franco-Zorrilla JM, de Lorenzo L, Irigoye ML, Masiero S, Bustos R, Rodriguez J, et al. 2014.** SPX1 is a phosphate-dependent inhibitor of PHOSPHATE STARVATION RESPONSE 1 in Arabidopsis. *Proceedings of the National Academy of Sciences of the United States of America* **111**(41): 14947-14952.
- Raghothama KG. 1999.** Phosphate acquisition. *Annual Review of Plant Physiology and Plant Molecular Biology* **50**: 665-693.
- Ramaiah M, Jain A, Raghothama KG. 2014.** Ethylene Response Factor070 regulates root development and phosphate starvation-mediated responses. *Plant Physiol* **164**(3): 1484-1498.
- Ravanat JL, Dumont E. 2022.** Reactivity of Singlet Oxygen with DNA, an Update. *Photochem Photobiol* **98**(3): 564-571.
- Reichheld JP, Khafif M, Riondet C, Droux M, Bonnard G, Meyer Y. 2007.** Inactivation of thioredoxin reductases reveals a complex interplay between thioredoxin and glutathione pathways in Arabidopsis development. *Plant Cell* **19**(6): 1851-1865.
- Remy E, Cabrito TR, Batista RA, Teixeira MC, Sa-Correia I, Duque P. 2012.** The Pht1;9 and Pht1;8 transporters mediate inorganic phosphate acquisition by the Arabidopsis thaliana root during phosphorus starvation. *New Phytol* **195**(2): 356-371.
- Reymond M, Svistonoff S, Loudet O, Nussaume L, Desnos T. 2006.** Identification of QTL controlling root growth response to phosphate starvation in Arabidopsis thaliana. *Plant Cell and Environment* **29**(1): 115-125.
- Reyt G, Boudouf S, Boucherez J, Gaymard F, Briat JF. 2015.** Iron- and ferritin-dependent reactive oxygen species distribution: impact on Arabidopsis root system architecture. *Mol Plant* **8**(3): 439-453.
- Ried MK, Wild R, Zhu J, Pipercevic J, Sturm K, Broger L, Harmel RK, Abriata LA, Hothorn LA, Fiedler D, et al. 2021.** Inositol pyrophosphates promote the interaction of SPX domains with the coiled-coil motif of PHR transcription factors to regulate plant phosphate homeostasis. *Nat Commun* **12**(1): 384.

- Robinson WD, Park J, Tran HT, Del Vecchio HA, Ying S, Zins JL, Patel K, McKnight TD, Plaxton WC. 2012.** The secreted purple acid phosphatase isozymes AtPAP12 and AtPAP26 play a pivotal role in extracellular phosphate-scavenging by *Arabidopsis thaliana*. *J Exp Bot* **63**(18): 6531-6542.
- Rubio V, Linhares F, Solano R, Martin AC, Iglesias J, Leyva A, Paz-Ares J. 2001.** A conserved MYB transcription factor involved in phosphate starvation signaling both in vascular plants and in unicellular algae. *Genes & Development* **15**(16): 2122-2133.
- Saeed AI, Sharov V, White J, Li J, Liang W, Bhagabati N, Braisted J, Klapa M, Currier T, Thiagarajan M, et al. 2003.** TM4: a free, open-source system for microarray data management and analysis. *Biotechniques* **34**(2): 374-378.
- Sager R, Lee JY. 2014.** Plasmodesmata in integrated cell signalling: insights from development and environmental signals and stresses. *J Exp Bot* **65**(22): 6337-6358.
- Sagi M, Fluhr R. 2006.** Production of reactive oxygen species by plant NADPH oxidases. *Plant Physiol* **141**(2): 336-340.
- Sanchez-Calderon L, Lopez-Bucio J, Chacon-Lopez A, Cruz-Ramirez A, Nieto-Jacobo F, Dubrovsky JG, Herrera-Estrella L. 2005.** Phosphate starvation induces a determinate developmental program in the roots of *Arabidopsis thaliana*. *Plant and Cell Physiology* **46**(1): 174-184.
- Scarpeci TE, Zanon MI, Carrillo N, Mueller-Roeber B, Valle EM. 2008.** Generation of superoxide anion in chloroplasts of *Arabidopsis thaliana* during active photosynthesis: a focus on rapidly induced genes. *Plant Mol Biol* **66**(4): 361-378.
- Schachtman DP, Reid RJ, Ayling SM. 1998.** Phosphorus uptake by plants: From soil to cell. *Plant Physiology* **116**(2): 447-453.
- Schindelin J, Arganda-Carreras I, Frise E, Kaynig V, Longair M, Pietzsch T, Preibisch S, Rueden C, Saalfeld S, Schmid B, et al. 2012.** Fiji: an open-source platform for biological-image analysis. *Nat Methods* **9**(7): 676-682.
- Schmidt R, Kunkowska AB, Schippers JH. 2016.** Role of Reactive Oxygen Species during Cell Expansion in Leaves. *Plant Physiol* **172**(4): 2098-2106.
- Schnaubelt D, Queval G, Dong Y, Diaz-Vivancos P, Makgopa ME, Howell G, De Simone A, Bai J, Hannah MA, Foyer CH. 2015.** Low glutathione regulates gene expression and the redox potentials of the nucleus and cytosol in *Arabidopsis thaliana*. *Plant Cell Environ* **38**(2): 266-279.
- Schopfer P, Plachy C, Frahy G. 2001.** Release of reactive oxygen intermediates (superoxide radicals, hydrogen peroxide, and hydroxyl radicals) and peroxidase in germinating radish seeds controlled by light, gibberellin, and abscisic acid. *Plant Physiology* **125**(4): 1591-1602.
- Schwarzlander M, Fricker MD, Muller C, Marty L, Brach T, Novak J, Sweetlove LJ, Hell R, Meyer AJ. 2008.** Confocal imaging of glutathione redox potential in living plant cells. *J Microsc* **231**(2): 299-316.
- Setsukinai K, Urano Y, Kakinuma K, Majima HJ, Nagano T. 2003.** Development of novel fluorescence probes that can reliably detect reactive oxygen species and distinguish specific species. *J Biol Chem* **278**(5): 3170-3175.

- Shane MW, Fedosejevs ET, Plaxton WC. 2013.** Reciprocal control of anaplerotic phosphoenolpyruvate carboxylase by in vivo monoubiquitination and phosphorylation in developing proteoid roots of phosphate-deficient harsh hakea. *Plant Physiol* **161**(4): 1634-1644.
- Shane MW, Feil R, Lunn JE, Plaxton WC. 2016.** Light-dependent activation of phosphoenolpyruvate carboxylase by reversible phosphorylation in cluster roots of white lupin plants: diurnal control in response to photosynthate supply. *Ann Bot* **118**(4): 637-643.
- Sharma P, Dubey RS. 2004.** Ascorbate peroxidase from rice seedlings: properties of enzyme isoforms, effects of stresses and protective roles of osmolytes. *Plant Science* **167**(3): 541-550.
- Shigeto J, Kiyonaga Y, Fujita K, Kondo R, Tsutsumi Y. 2013.** Putative Cationic Cell-Wall-Bound Peroxidase Homologues in Arabidopsis, AtPrx2, AtPrx25, and AtPrx71, Are Involved in Lignification. *Journal of Agricultural and Food Chemistry* **61**(16): 3781-3788.
- Shigeto J, Tsutsumi Y. 2016.** Diverse functions and reactions of class III peroxidases. *New Phytol* **209**(4): 1395-1402.
- Simpson C, Thomas C, Findlay K, Bayer E, Maule AJ. 2009.** An Arabidopsis GPI-Anchor Plasmodesmal Neck Protein with Callose Binding Activity and Potential to Regulate Cell-to-Cell Trafficking. *Plant Cell* **21**(2): 581-594.
- Singh MB, Lohani N, Bhalla PL. 2021.** The Role of Endoplasmic Reticulum Stress Response in Pollen Development and Heat Stress Tolerance. *Front Plant Sci* **12**: 661062.
- Smirnoff N, Arnaud D. 2019.** Hydrogen peroxide metabolism and functions in plants. *New Phytol* **221**(3): 1197-1214.
- Steen I. 1998.** Management of a nonrenewable resource. *Phosphorus & Potassium* **13**(217): 1-13.
- Su TB, Xu JA, Li YA, Lei L, Zhao L, Yang HL, Feng JD, Liu GQ, Ren DT. 2011.** Glutathione-Indole-3-Acetonitrile Is Required for Camalexin Biosynthesis in Arabidopsis thaliana. *Plant Cell* **23**(1): 364-380.
- Suen DF, Tsai YH, Cheng YT, Radjacomare R, Ahirwar RN, Fu H, Schmidt W. 2018.** The Deubiquitinase OTU5 Regulates Root Responses to Phosphate Starvation. *Plant Physiol* **176**(3): 2441-2455.
- Suzuki N, Miller G, Morales J, Shulaev V, Torres MA, Mittler R. 2011.** Respiratory burst oxidases: the engines of ROS signaling. *Curr Opin Plant Biol* **14**(6): 691-699.
- Svistonoff S, Creff A, Reymond M, Sigollot-Claude C, Ricaud L, Blanchet A, Nussaume L, Desnos T. 2007.** Root tip contact with low-phosphate media reprograms plant root architecture. *Nat Genet* **39**(6): 792-796.
- Szklarczyk D, Gable AL, Lyon D, Junge A, Wyder S, Huerta-Cepas J, Simonovic M, Doncheva NT, Morris JH, Bork P, et al. 2019.** STRING v11: protein-protein association networks with increased coverage, supporting functional discovery in genome-wide experimental datasets. *Nucleic Acids Res* **47**(D1): D607-D613.
- Takatsuka H, Umeda M. 2015.** Epigenetic Control of Cell Division and Cell Differentiation in the Root Apex. *Front Plant Sci* **6**: 1178.
- Thibaud MC, Arrighi JF, Bayle V, Chiarenza S, Creff A, Bustos R, Paz-Ares J, Poirier Y, Nussaume L. 2010.** Dissection of local and systemic transcriptional responses to phosphate starvation in Arabidopsis. *Plant Journal* **64**(5): 775-789.

- Thomas CL, Bayer EM, Ritzenthaler C, Fernandez-Calvino L, Maule AJ. 2008.** Specific targeting of a plasmodesmal protein affecting cell-to-cell communication. *Plos Biology* **6**(1): 180-190.
- Tian S, Wang X, Li P, Wang H, Ji H, Xie J, Qiu Q, Shen D, Dong H. 2016.** Plant Aquaporin AtPIP1;4 Links Apoplastic H<sub>2</sub>O<sub>2</sub> Induction to Disease Immunity Pathways. *Plant Physiol* **171**(3): 1635-1650.
- Ticconi CA, Delatorre CA, Lahner B, Salt DE, Abel S. 2004.** Arabidopsis pdr2 reveals a phosphate-sensitive checkpoint in root development. *Plant Journal* **37**(6): 801-814.
- Ticconi CA, Lucero RD, Sakhonwasee S, Adamson AW, Creff A, Nussaume L, Desnos T, Abel S. 2009.** ER-resident proteins PDR2 and LPR1 mediate the developmental response of root meristems to phosphate availability. *Proceedings of the National Academy of Sciences of the United States of America* **106**(33): 14174-14179.
- Tilsner J, Nicolas W, Rosado A, Bayer EM. 2016.** Staying Tight: Plasmodesmal Membrane Contact Sites and the Control of Cell-to-Cell Connectivity in Plants. *Annu Rev Plant Biol* **67**: 337-364.
- Tokizawa M, Kobayashi Y, Saito T, Kobayashi M, Iuchi S, Nomoto M, Tada Y, Yamamoto YY, Koyama H. 2015.** SENSITIVE TO PROTON RHIZOTOXICITY1, CALMODULIN BINDING TRANSCRIPTION ACTIVATOR2, and Other Transcription Factors Are Involved in ALUMINUM-ACTIVATED MALATE TRANSPORTER1 Expression. *Plant Physiology* **167**(3): 991-1003.
- Torres MA, Dangl JL, Jones JD. 2002.** Arabidopsis gp91phox homologues AtrbohD and AtrbohF are required for accumulation of reactive oxygen intermediates in the plant defense response. *Proc Natl Acad Sci U S A* **99**(1): 517-522.
- Tran HT, Plaxton WC. 2008.** Proteomic analysis of alterations in the secretome of Arabidopsis thaliana suspension cells subjected to nutritional phosphate deficiency. *Proteomics* **8**(20): 4317-4326.
- Triantaphylides C, Havaux M. 2009.** Singlet oxygen in plants: production, detoxification and signaling. *Trends Plant Sci* **14**(4): 219-228.
- Tsukagoshi H. 2016.** Control of root growth and development by reactive oxygen species. *Curr Opin Plant Biol* **29**: 57-63.
- Tsukagoshi H, Busch W, Benfey PN. 2010.** Transcriptional regulation of ROS controls transition from proliferation to differentiation in the root. *Cell* **143**(4): 606-616.
- Tucker EB, Boss WF. 1996.** Mastoparan-Induced Intracellular Ca<sup>2+</sup> Fluxes May Regulate Cell-to-Cell Communication in Plants. *Plant Physiol* **111**(2): 459-467.
- Tzafrir I, Pena-Muralla R, Dickerman A, Berg M, Rogers R, Hutchens S, Sweeney TC, McElver J, Aux G, Patton D, et al. 2004.** Identification of genes required for embryo development in Arabidopsis. *Plant Physiol* **135**(3): 1206-1220.
- Ugalde JM, Fecker L, Schwarzlander M, Muller-Schussele SJ, Meyer AJ. 2022.** Live Monitoring of ROS-Induced Cytosolic Redox Changes with roGFP2-Based Sensors in Plants. *Methods Mol Biol* **2526**: 65-85.
- Ugalde JM, Fecker L, Schwarzländer M, Müller-Schüssele SJ, Meyer AJ. 2020.**
- Ullricheberius CI, Novacky A, Vanbel AJE. 1984.** Phosphate-Uptake in Lemna-Gibba-G1 - Energetics and Kinetics. *Planta* **161**(1): 46-52.



- van den Berg C, Willemsen V, Hendriks G, Weisbeek P, Scheres B. 1997. Short-range control of cell differentiation in the Arabidopsis root meristem. *Nature* **390**(6657): 287-289.
- Van Nguyen T, Park CR, Lee KH, Lee S, Kim CS. 2021. BES1/BZR1 Homolog 3 cooperates with E3 ligase AtRZF1 to regulate osmotic stress and brassinosteroid responses in Arabidopsis. *J Exp Bot* **72**(2): 636-653.
- Vanderauwera S, Vandenbroucke K, Inze A, van de Cotte B, Muhlenbock P, De Rycke R, Naouar N, Van Gaever T, Van Montagu MCE, Van Breusegem F. 2012. AtWRKY15 perturbation abolishes the mitochondrial stress response that steers osmotic stress tolerance in Arabidopsis. *Proceedings of the National Academy of Sciences of the United States of America* **109**(49): 20113-20118.
- Vanderauwera S, Zimmermann P, Rombauts S, Vandenabeele S, Langebartels C, Grissem W, Inze D, Van Breusegem F. 2005. Genome-wide analysis of hydrogen peroxide-regulated gene expression in Arabidopsis reveals a high light-induced transcriptional cluster involved in anthocyanin biosynthesis. *Plant Physiol* **139**(2): 806-821.
- Verbelen JP, De Cnodder T, Le J, Vissenberg K, Baluska F. 2006. The Root Apex of Arabidopsis thaliana Consists of Four Distinct Zones of Growth Activities: Meristematic Zone, Transition Zone, Fast Elongation Zone and Growth Terminating Zone. *Plant Signal Behav* **1**(6): 296-304.
- Wagner U, Edwards R, Dixon DP, Mauch F. 2002. Probing the diversity of the Arabidopsis glutathione S-transferase gene family. *Plant Mol Biol* **49**(5): 515-532.
- Wang Y, Li R, Li D, Jia X, Zhou D, Li J, Lyi SM, Hou S, Huang Y, Kochian LV, et al. 2017. NIP1;2 is a plasma membrane-localized transporter mediating aluminum uptake, translocation, and tolerance in Arabidopsis. *Proc Natl Acad Sci U S A* **114**(19): 5047-5052.
- Wang Z, Ruan W, Shi J, Zhang L, Xiang D, Yang C, Li C, Wu Z, Liu Y, Yu Y, et al. 2014. Rice SPX1 and SPX2 inhibit phosphate starvation responses through interacting with PHR2 in a phosphate-dependent manner. *Proc Natl Acad Sci U S A* **111**(41): 14953-14958.
- Wang ZY, Nakano T, Gendron J, He J, Chen M, Vafeados D, Yang Y, Fujioka S, Yoshida S, Asami T, et al. 2002. Nuclear-localized BZR1 mediates brassinosteroid-induced growth and feedback suppression of brassinosteroid biosynthesis. *Dev Cell* **2**(4): 505-513.
- Ward JT, Lahner B, Yakubova E, Salt DE, Raghothama KG. 2008. The effect of iron on the primary root elongation of Arabidopsis during phosphate deficiency. *Plant Physiol* **147**(3): 1181-1191.
- Waszczak C, Carmody M, Kangasjarvi J. 2018. Reactive Oxygen Species in Plant Signaling. *Annu Rev Plant Biol* **69**: 209-236.
- Wendrich JR, Yang B, Vandamme N, Verstaen K, Smet W, Van de Velde C, Minne M, Wybouw B, Mor E, Arents HE, et al. 2020. Vascular transcription factors guide plant epidermal responses to limiting phosphate conditions. *Science* **370**(6518).
- Wild R, Gerasimaite R, Jung JY, Truffault V, Pavlovic I, Schmidt A, Saiardi A, Jessen HJ, Poirier Y, Hothorn M, et al. 2016. Control of eukaryotic phosphate homeostasis by inositol polyphosphate sensor domains. *Science* **352**(6288): 986-990.
- Willekens H, Inzé D, Van Montagu M, van Camp W. 1995. Catalases in plants. *Molecular Breeding* **1**(3): 207-228.

- Winterbourn CC. 2014.** The challenges of using fluorescent probes to detect and quantify specific reactive oxygen species in living cells. *Biochimica et biophysica acta* **1840**(2): 730-738.
- Winterbourn CC. 2015.** Are free radicals involved in thiol-based redox signaling? *Free Radic Biol Med* **80**: 164-170.
- Winterbourn CC. 2016.** Revisiting the reactions of superoxide with glutathione and other thiols. *Arch Biochem Biophys* **595**: 68-71.
- Winterbourn CC, Metodiewa D. 1994.** The reaction of superoxide with reduced glutathione. *Arch Biochem Biophys* **314**(2): 284-290.
- Xu B, Cheval C, Laohavisit A, Hocking B, Chiasson D, Olsson TSG, Shirasu K, Faulkner C, Gilliam M. 2017.** A calmodulin-like protein regulates plasmodesmal closure during bacterial immune responses. *New Phytol* **215**(1): 77-84.
- Yadav UP, Ivakov A, Feil R, Duan GY, Walther D, Giavalisco P, Piques M, Carillo P, Hubberten HM, Stitt M, et al. 2014.** The sucrose-trehalose 6-phosphate (Tre6P) nexus: specificity and mechanisms of sucrose signalling by Tre6P. *J Exp Bot* **65**(4): 1051-1068.
- Yamada M, Han X, Benfey PN. 2020.** RGF1 controls root meristem size through ROS signalling. *Nature* **577**(7788): 85-88.
- Yang S, Yu Q, Zhang Y, Jia Y, Wan S, Kong X, Ding Z. 2018.** ROS: The Fine-Tuner of Plant Stem Cell Fate. *Trends Plant Sci* **23**(10): 850-853.
- Yu Q, Tian H, Yue K, Liu J, Zhang B, Li X, Ding Z. 2016.** A P-Loop NTPase Regulates Quiescent Center Cell Division and Distal Stem Cell Identity through the Regulation of ROS Homeostasis in Arabidopsis Root. *PLoS Genet* **12**(9): e1006175.
- Yu X, Pasternak T, Eiblmeier M, Ditengou F, Kochersperger P, Sun J, Wang H, Rennenberg H, Teale W, Paponov I, et al. 2013.** Plastid-localized glutathione reductase2-regulated glutathione redox status is essential for Arabidopsis root apical meristem maintenance. *Plant Cell* **25**(11): 4451-4468.
- Zhang L, Chen L, Dong H. 2019.** Plant Aquaporins in Infection by and Immunity Against Pathogens - A Critical Review. *Front Plant Sci* **10**: 632.
- Zheng Z, Wang Z, Wang X, Liu D. 2019.** Blue Light-Triggered Chemical Reactions Underlie Phosphate Deficiency-Induced Inhibition of Root Elongation of Arabidopsis Seedlings Grown in Petri Dishes. *Mol Plant* **12**(11): 1515-1523.
- Zhou W, Lozano-Torres JL, Blilou I, Zhang X, Zhai Q, Smant G, Li C, Scheres B. 2019.** A Jasmonate Signaling Network Activates Root Stem Cells and Promotes Regeneration. *Cell* **177**(4): 942-956 e914.
- Zhu J, Kaepler SM, Lynch JP. 2005.** Topsoil foraging and phosphorus acquisition efficiency in maize (*Zea mays*). *Funct Plant Biol* **32**(8): 749-762.
- Ziegler J, Schmidt S, Chutia R, Muller J, Bottcher C, Strehmel N, Scheel D, Abel S. 2016.** Non-targeted profiling of semi-polar metabolites in Arabidopsis root exudates uncovers a role for coumarin secretion and lignification during the local response to phosphate limitation. *J Exp Bot* **67**(5): 1421-1432.

**Zielonka J, Kalyanaraman B. 2010.** Hydroethidine- and MitoSOX-derived red fluorescence is not a reliable indicator of intracellular superoxide formation: another inconvenient truth. *Free Radic Biol Med* **48**(8): 983-1001.

## 6. APPENDIX

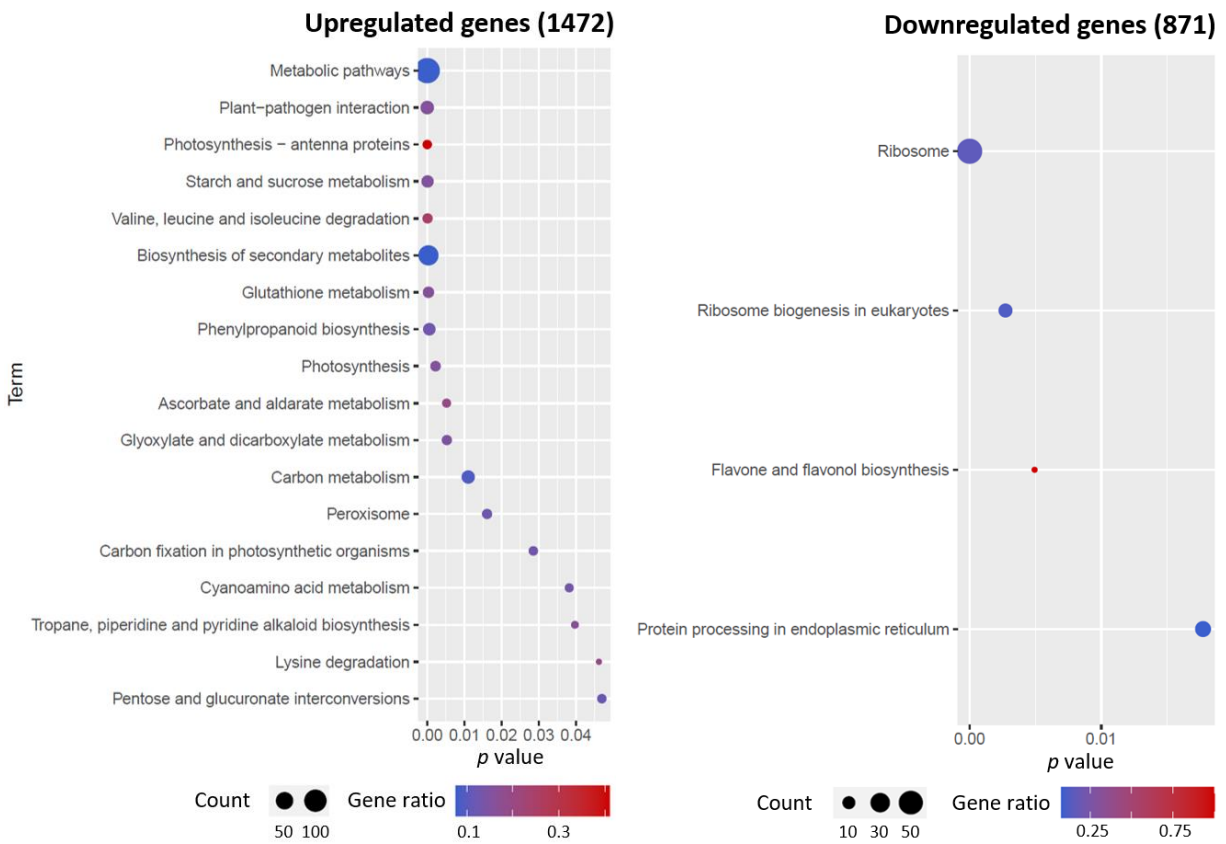


**Fig. S6-1: KEGG pathway analysis of Pi-responsive genes in *pdr2***

Pi deficiency induced genes (A) and repressed genes (B) (adjusted p-value < 0.05;  $-1 > \log_2FC > 1$ ) were analyzed for KEGG pathway enrichment. All significantly enriched pathways (p-value < 0.05) were included in the dot plot. Count: number of DEGs concerning this pathway. Gene ratio: ratio between the number of DEGs in each pathway and all the genes that can be found involved in this pathway in KEGG database.

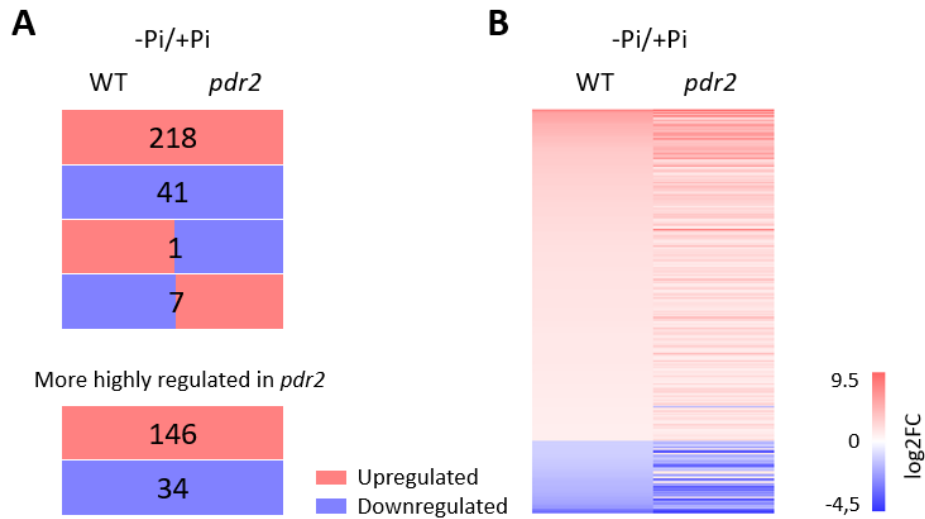


**Fig. S6-2: Analysis of low Pi-responsive genes that were shared between WT and *pdr2***

(A) Number of DEGs that were shared between WT and *pdr2* upon Pi limitation (adjusted p-value < 0.05;  $-1 > \log_2FC > 1$ ). 218 genes were upregulated, and 41 genes were downregulated in both WT and *pdr2*. One gene was upregulated in WT but downregulated in *pdr2*. Seven genes were downregulated in WT but upregulated in *pdr2*. 146 genes were more highly induced, and 34 genes were more highly suppressed in Pi-starved *pdr2* compared to the WT ( $-1 > (\log_2FC \text{ of } pdr2 / \log_2FC \text{ of } WT) > 1$ ). (B) A heatmap of 267 shared low Pi-responsive genes between WT and *pdr2*. Each row represents a gene with  $\log_2FC$  that was shown on a color scale. Blue = downregulated, red = upregulated.

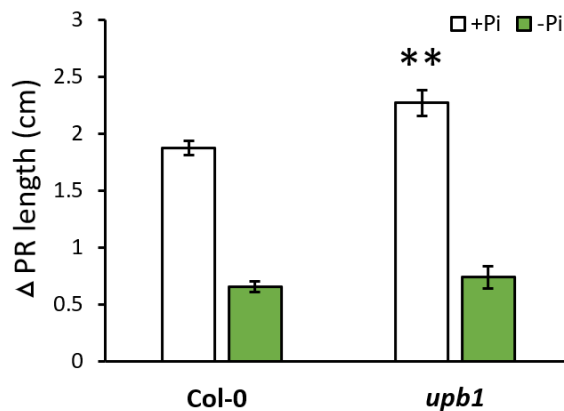


**Fig. S6-3: Comparison of primary root inhibition between *upb1* and WT**

Seeds were germinated on +Pi agar plates for 5 days, transferred to +Pi (50  $\mu\text{M}$  Fe, 2.5  $\mu\text{M}$  Al) or -Pi (50  $\mu\text{M}$  Fe, 2.5  $\mu\text{M}$  Al) conditions. After 3 days of transfer,  $\Delta$  primary root length was measured ( $\pm$ SD;  $n=10$ ). Asterisks indicate significant differences as determined by Student's t-test (two-tailed, equal variances,  $p < 0.001$ ) compared to Col-0 -Pi condition.

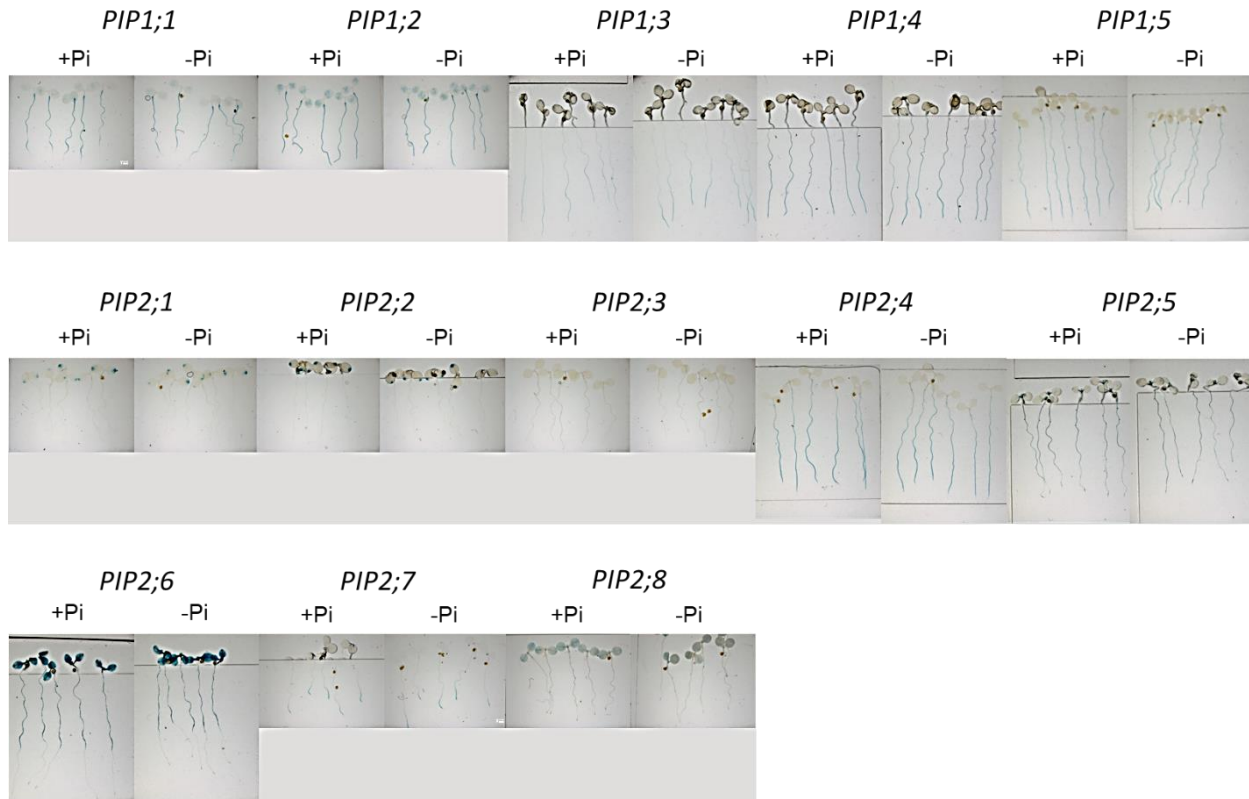


**Fig. S6-4: Expression analysis of *PIPs* in seedlings by GUS staining**

GUS staining of *pPIP::GFP-GUS* and *pPIP::GUS* reporter lines when grown under Pi-sufficient and Pi-deficient condition. Seeds were germinated on +Pi agar plates for 5 days and then transferred to +Pi (50  $\mu$ M Fe, 2.5  $\mu$ M Al) or -Pi (50  $\mu$ M Fe, 2.5  $\mu$ M Al) conditions. After 1 day of transfer, GUS staining was performed.

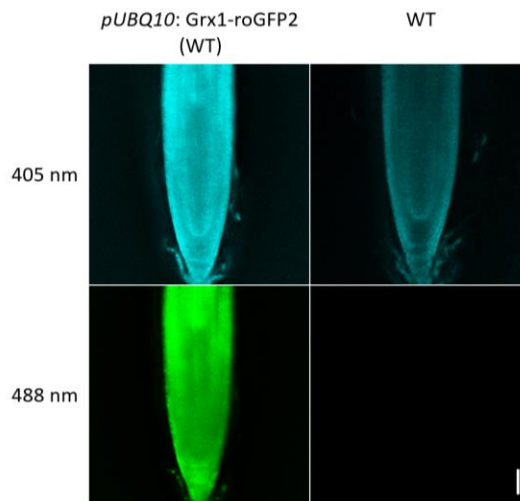


**Fig. S6-5: 405 nm triggered autofluorescence in root tips of WT**

Six-day-old seedlings of transgenic line (*pUBQ10:Grx1-roGFP2*) and WT were excited by 405 nm and 488 nm. Scale bars = 50  $\mu$ m.

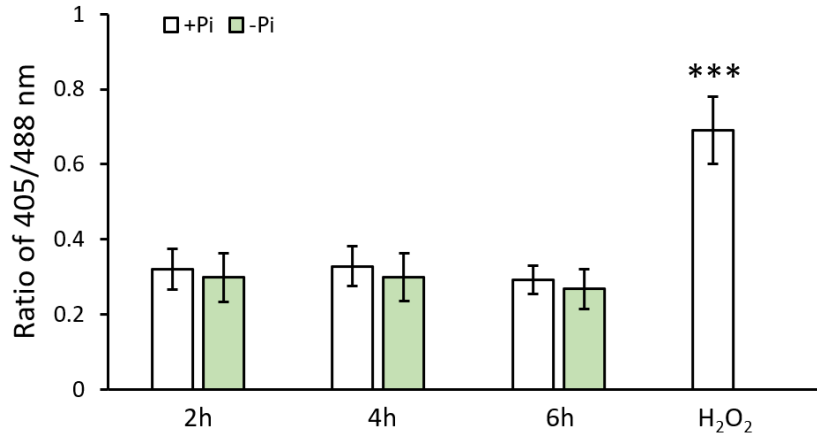


**Fig. S6-6: Response of cytosolic Grx1-roGFP2 to Pi deficiency in the QC of WT, related to Fig. 2-28**

Quantification of 405/488 nm ratio in the QC of WT after transfer from +Pi (25  $\mu$ M Fe) agar plates to +Pi (25  $\mu$ M Fe) or -Pi (25  $\mu$ M Fe) conditions (n=10-11 for +Pi and -Pi samples; n=5 for H<sub>2</sub>O<sub>2</sub> samples). To oxidize roGFP2, root tips were treated with 10 mM H<sub>2</sub>O<sub>2</sub> for 2 min before the images were taken. Asterisks indicate significant difference as determined by Student's t-test (two-tailed, equal variances, \*\*\* $p < 0.001$ ) compared to +Pi condition. Error bars represent  $\pm$  SD.

**Tab. S6-1: GO-enrichment analysis of 259 genes that were upregulated in *pdr2* vs. WT under +Pi condition**

GO Biological process	# of genes in upload list (259) (A)	# of genes in genome (18499) (B)	Gene ratio (A/B)	<i>P</i> value
response to oxidative stress	17	291	0.06	1.8E-07
response to bacterium	10	102	0.10	2.1E-06
hydrogen peroxide catabolic process	9	89	0.10	6.7E-06
oxidation-reduction process	34	1330	0.03	1.2E-05
cellular response to hypoxia	5	26	0.19	1.8E-04
cell wall macromolecule catabolic process	5	26	0.19	1.8E-04
amino sugar metabolic process	4	15	0.27	5.6E-04
aromatic compound biosynthetic process	4	15	0.27	5.6E-04
suberin biosynthetic process	4	19	0.21	1.2E-03
indole glucosinolate metabolic process	4	21	0.19	1.6E-03
chitin catabolic process	4	25	0.16	2.6E-03
response to insect	4	26	0.15	2.9E-03
defense response to bacterium	10	276	0.04	3.9E-03
response to salt	3	9	0.33	4.2E-03
glutathione metabolic process	5	62	0.08	5.0E-03
response to cold	10	299	0.03	6.5E-03
defense response	16	658	0.02	7.0E-03
response to wounding	8	199	0.04	7.0E-03
response to fungus	5	72	0.07	8.5E-03
response to abscisic acid	11	394	0.03	1.3E-02

toxin catabolic process	4	46	0.09	1.5E-02
response to chitin	6	133	0.05	1.7E-02
plant-type cell wall organization	5	91	0.05	1.9E-02
response to salt stress	12	484	0.02	2.0E-02
polysaccharide catabolic process	3	20	0.15	2.1E-02
selenate transport	2	2	1.00	2.2E-02
response to salicylic acid	6	155	0.04	3.0E-02
response to toxic substance	4	61	0.07	3.1E-02
methylation	7	212	0.03	3.2E-02
cellular response to ethylene stimulus	3	26	0.12	3.4E-02
defense response to fungus	11	464	0.02	3.6E-02
amino acid export	2	4	0.50	4.4E-02
cell differentiation	8	296	0.03	4.8E-02

**Tab. S6-2: GO-enrichment analysis of 288 genes that were upregulated in Pi-starved WT**

<b>GO Biological process</b>	<b># of genes in upload list (288) (A)</b>	<b># of genes in genome (18499) (B)</b>	<b>Gene ratio (A/B)</b>	<b><i>P</i> value</b>
trehalose metabolism in response to stress	5	21	0.24	6.7E-05
response to oxidative stress	13	291	0.04	7.7E-05
trehalose biosynthetic process	5	25	0.20	1.4E-04
glutamine metabolic process	5	35	0.14	5.2E-04
response to absence of light	4	26	0.15	2.7E-03
ethylene-activated signaling pathway	8	179	0.04	3.3E-03
cellular phosphate ion homeostasis	3	9	0.33	3.9E-03
response to wounding	8	199	0.04	5.8E-03
flavonoid glucuronidation	6	112	0.05	7.3E-03
syncytium formation	3	15	0.20	1.1E-02
response to chitin	6	133	0.05	1.5E-02
transcription, DNA-templated	31	1886	0.02	1.9E-02
response to hydrogen peroxide	4	54	0.07	2.0E-02
flavonoid biosynthetic process	6	145	0.04	2.0E-02
proline catabolic process	2	2	1.00	2.1E-02
cell wall biogenesis	4	60	0.07	2.7E-02
regulation of transcription, DNA-templated	33	2119	0.02	3.0E-02
proline catabolic process to glutamate	2	3	0.67	3.2E-02
glycerophospholipid catabolic process	2	3	0.67	3.2E-02
response to auxin	8	290	0.03	3.8E-02
cellular response to sucrose starvation	2	4	0.50	4.2E-02
inositol catabolic process	2	4	0.50	4.2E-02
response to karrikin	5	128	0.04	5.0E-02



**Tab. S6-3: GO-enrichment analysis of 85 genes that were downregulated in Pi-starved WT**

GO Biological process	# of genes in upload list (85) (A)	# of genes in genome (18499) (B)	Gene ratio (A/B)	<i>P</i> value
cellular response to blue light	3	6	0.50	1.8E-04
response to UV-B	4	61	0.07	1.2E-03
cellular response to far red light	2	2	1.00	6.9E-03
cellular response to red light	2	2	1.00	6.9E-03
cellular response to UV-A	2	5	0.40	1.7E-02
photoprotection	2	7	0.29	2.4E-02
cellular response to high light intensity	2	8	0.25	2.7E-02
fruit ripening	2	13	0.15	4.4E-02
regulation of chlorophyll biosynthetic process	2	14	0.14	4.7E-02

**Tab. S6-4: GO-enrichment analysis of 1472 genes that were upregulated in Pi-starved *pdr2***

GO Biological process	# of genes in upload list (1472) (A)	# of genes in genome (18499) (B)	Gene ratio (A/B)	<i>P</i> value
response to chitin	44	133	0.33	6.0E-22
defense response to bacterium	49	276	0.18	1.6E-12
defense response	76	658	0.12	2.6E-09
response to oxidative stress	44	291	0.15	4.6E-09
response to bacterium	24	102	0.24	6.9E-09
ethylene-activated signaling pathway	30	179	0.17	2.1E-07
photosynthesis, light harvesting in photosystem I	10	22	0.45	1.3E-06
photosynthesis	24	138	0.17	2.2E-06
plant-type hypersensitive response	17	74	0.23	2.4E-06
response to cold	38	299	0.13	4.6E-06
oxidation-reduction process	113	1330	0.08	6.3E-06
response to salicylic acid	24	155	0.15	1.6E-05
regulation of systemic acquired resistance	7	12	0.58	2.0E-05
response to karrikin	21	128	0.16	2.7E-05
hydrogen peroxide catabolic process	17	89	0.19	2.9E-05
photosynthesis, light harvesting	7	13	0.54	3.6E-05
signal transduction	47	450	0.10	5.4E-05
vasculature development	9	26	0.35	5.7E-05
trehalose metabolism in response to stress	8	21	0.38	9.5E-05
response to toxic substance	13	61	0.21	1.2E-04
defense response to bacterium, incompatible interaction	11	44	0.25	1.2E-04
protein-chromophore linkage	11	45	0.24	1.5E-04
response to water deprivation	32	279	0.11	2.0E-04

response to wounding	25	199	0.13	3.1E-04
metal ion transport	17	108	0.16	3.1E-04
trehalose biosynthetic process	8	25	0.32	3.2E-04
response to abscisic acid	40	394	0.10	3.7E-04
response to absence of light	8	26	0.31	4.2E-04
response to sucrose	11	52	0.21	5.1E-04
glutamine metabolic process	9	35	0.26	5.5E-04
glutathione metabolic process	12	62	0.19	5.7E-04
transcription, DNA-templated	138	1886	0.07	6.8E-04
response to other organism	11	55	0.20	8.2E-04
toxin catabolic process	10	46	0.22	8.5E-04
syncytium formation	6	15	0.40	1.0E-03
cation transmembrane transport	6	16	0.38	1.4E-03
cellular transition metal ion homeostasis	12	70	0.17	1.6E-03
developmental process involved in	6	17	0.35	1.9E-03
secondary shoot formation	6	18	0.33	2.5E-03
response to insect	7	26	0.27	2.6E-03
response to jasmonic acid	19	156	0.12	2.7E-03
response to high light intensity	10	55	0.18	3.1E-03
response to molecule of bacterial origin	6	19	0.32	3.2E-03
regulation of proteolysis	8	36	0.22	3.3E-03
response to auxin	29	290	0.10	3.4E-03
regulation of transcription, DNA-templated	147	2119	0.07	3.6E-03
sucrose biosynthetic process	6	20	0.30	4.1E-03
reductive pentose-phosphate cycle	6	20	0.30	4.1E-03
positive regulation of transcription, DNA-	23	217	0.11	4.9E-03
response to low light intensity stimulus	4	7	0.57	5.1E-03
aging	8	41	0.20	7.0E-03
defense response to fungus	40	464	0.09	7.0E-03
response to blue light	9	52	0.17	7.7E-03
glucose metabolic process	6	23	0.26	7.7E-03
positive regulation of leaf senescence	4	8	0.50	7.8E-03
response to salt stress	41	484	0.08	8.4E-03
cell death	8	44	0.18	1.0E-02
sucrose metabolic process	6	25	0.24	1.1E-02
oxidative photosynthetic carbon pathway	4	9	0.44	1.1E-02
cellular response to hypoxia	6	26	0.23	1.3E-02
leaf senescence	12	92	0.13	1.3E-02
camalexin biosynthetic process	4	10	0.40	1.5E-02
response to fructose	5	18	0.28	1.6E-02
inositol catabolic process	3	4	0.75	1.7E-02
transport of virus in host, tissue to tissue	3	4	0.75	1.7E-02
cellular response to sucrose starvation	3	4	0.75	1.7E-02
response to fungus	10	72	0.14	1.8E-02
response to ethylene	14	124	0.11	2.1E-02

flavonoid glucuronidation	13	112	0.12	2.2E-02
response to cadmium ion	29	342	0.08	2.7E-02
strigolactone biosynthetic process	3	5	0.60	2.8E-02
positive regulation of sequence-specific DNA binding transcription factor activity	3	5	0.60	2.8E-02
response to hydrogen peroxide	8	54	0.15	3.0E-02
plant-type cell wall organization	11	91	0.12	3.0E-02
response to glucose	6	32	0.19	3.1E-02
chaperone-mediated protein folding	6	32	0.19	3.1E-02
fruit ripening	4	13	0.31	3.2E-02
response to ozone	6	33	0.18	3.5E-02
peptidyl-proline modification	5	23	0.22	3.6E-02
multicellular organism development	31	384	0.08	3.9E-02
leucine catabolic process	3	6	0.50	4.0E-02
regulation of salicylic acid biosynthetic process	3	6	0.50	4.0E-02
lipid metabolic process	17	181	0.09	4.6E-02
cellular response to nitrogen starvation	5	25	0.20	4.8E-02

**Tab. S6-5: GO-enrichment analysis of 871 genes that were downregulated in Pi-starved *pdr2***

GO Biological process	# of genes in upload list (871) (A)	# of genes in genome (18499) (B)	Gene ratio (A/B)	<i>P value</i>
ribosome biogenesis	27	142	0.19	3.7E-13
cytoplasmic translation	16	52	0.31	4.0E-11
rRNA modification	15	71	0.21	3.9E-08
response to heat	21	160	0.13	1.7E-07
rRNA processing	14	77	0.18	8.0E-07
protein refolding	5	9	0.56	1.1E-04
translation	59	1121	0.05	1.6E-04
amino acid transmembrane transport	8	45	0.18	4.9E-04
amino acid transport	8	49	0.16	8.3E-04
regulation of growth	11	101	0.11	1.3E-03
maturation of LSU-rRNA	6	27	0.22	1.4E-03
ribosomal large subunit biogenesis	6	28	0.21	1.7E-03
response to cytokinin	15	183	0.08	2.1E-03
ribosomal small subunit assembly	7	45	0.16	2.8E-03
ribosomal large subunit assembly	6	35	0.17	4.6E-03
maturation of SSU-rRNA from tricistronic rRNA transcript (SSU-rRNA, 5.8S rRNA, LSU-rRNA)	6	41	0.15	9.1E-03
flavonoid glucuronidation	10	112	0.09	9.1E-03
xyloglucan metabolic process	6	42	0.14	1.0E-02
protein folding	18	288	0.06	1.0E-02
seed dormancy process	4	15	0.27	1.1E-02
aromatic compound biosynthetic process	4	15	0.27	1.1E-02

response to auxin	18	290	0.06	1.1E-02
root development	12	158	0.08	1.2E-02
cellular response to blue light	3	6	0.50	1.4E-02
purine nucleotide biosynthetic process	3	6	0.50	1.4E-02
response to karrikin	10	128	0.08	2.0E-02
polarity specification of adaxial/abaxial axis	4	23	0.17	3.5E-02
chaperone-mediated protein complex assembly	3	11	0.27	4.5E-02
cell wall macromolecule catabolic process	4	26	0.15	4.8E-02

**Tab. S6-6: GO-enrichment analysis of 14 genes that were upregulated in Pi-starved *lpr1lpr2***

GO Biological process	# of genes in upload list (14) (A)	# of genes in genome (18499) (B)	Gene ratio (A/B)	P value
cellular response to phosphate starvation	4	99	0.04	4.1E-05
phosphate ion transport	3	27	0.11	1.6E-04
cellular phosphate ion homeostasis	2	9	0.22	6.3E-03
transmembrane transport	3	212	0.01	9.4E-03

**Tab. S6-7: Differentially expressed oxidative stress responsive genes in Pi-starved WT and *pdr2* and in *pdr2* compared to WT under +Pi condition**

Gene ID	Gene name	WT -/+		<i>pdr2</i> -/+		<i>pdr2</i> /WT +		Gene description
		log <sub>2</sub> FC	p-value	log <sub>2</sub> FC	p-value	log <sub>2</sub> FC	p-value	
AT4G35770	STR15	5.59	2.2E-06	3.84	8.8E-15	2.70	5.7E-01	Rhodanese/Cell cycle control phosphatase superfamily protein
AT5G56550	OXS3	3.70	4.6E-03	4.01	4.6E-29	-0.82	1.0E+00	OXIDATIVE STRESS 3 (OXS3)
AT5G20250	DIN10	3.13	7.3E-05	3.03	3.1E-51	-0.02	1.0E+00	Probable galactinol--sucrose galactosyltransferase 6
AT5G16970	AER	3.05	8.7E-07	5.96	5.7E-59	0.49	1.0E+00	NADPH-dependent oxidoreductase 2-alkenal reductase
AT1G02930	GSTF6	2.45	2.0E-09	2.80	9.9E-21	4.44	1.6E-37	Glutathione S-transferase F6
AT3G30775	POX1	2.32	2.7E-05	2.41	5.4E-55	0.62	1.9E-01	Methylenetetrahydrofolate
AT3G20340	AT3G20340	2.25	6.9E-12	1.71	9.0E-28	0.35	1.0E+00	Protein expression protein
AT5G06730	PER54	2.05	1.9E-10	3.18	9.8E-38	0.18	1.0E+00	Peroxidase superfamily protein
AT2G19810	OZF1	1.91	4.7E-07	1.38	2.2E-05	-0.23	1.0E+00	Encodes Oxidation-related Zinc
AT1G21520	AT1G21520	1.88	4.3E-02	2.09	1.9E-05	2.02	5.8E-02	hypothetical protein
AT3G10020	AT3G10020	1.41	4.1E-05	4.10	3.0E-70	-0.96	5.4E-02	Uncharacterized protein
AT3G57520	SIP2	1.40	1.6E-09	1.97	2.0E-35	0.25	7.5E-01	Probable galactinol--sucrose galactosyltransferase 2
AT2G37130	PER21	1.03	2.4E-09	1.32	2.1E-12	0.27	8.3E-01	Peroxidase 21
AT1G34510	PER8	0.69	1.4E-01	1.41	2.3E-06	0.69	1.6E-01	Peroxidase 8
AT1G49570	PER10	-5.50	6.1E-01	5.52	1.7E-09	-3.19	1.0E+00	Peroxidase 10
AT1G71695	PER12	-0.51	3.5E-01	1.24	1.8E-09	0.44	7.1E-01	Peroxidase 12

AT2G41480	PER25	NA	NA	2.84	3.6E-03	0.79	1.0E+00	Peroxidase 25
AT3G49110	PER33	1.75	5.3E-01	3.00	8.4E-04	NA	NA	Peroxidase 33
AT4G08770	PER37	0.47	7.1E-02	1.26	8.7E-11	-0.18	1.0E+00	Peroxidase 37
AT4G08780	PER38	0.86	8.3E-01	2.93	2.4E-04	0.67	1.0E+00	Peroxidase 38
AT4G37520	PER50	0.62	5.1E-03	1.41	3.3E-18	-0.11	1.0E+00	Peroxidase 50
AT5G06720	PER53	NA	NA	5.80	3.8E-14	-1.35	1.0E+00	Peroxidase 53
AT5G19890	PER59	-3.36	8.2E-01	6.59	9.8E-05	-5.18	1.0E+00	Peroxidase 59
AT5G64110	PER70	0.86	6.6E-01	1.02	8.0E-03	2.73	1.4E-06	Peroxidase 70
AT5G05340	PER52	0.67	8.7E-01	4.78	5.3E-32	-0.04	1.0E+00	Peroxidase 52
AT4G35970	APX5	0.52	6.5E-01	2.06	1.1E-08	0.09	1.0E+00	Encodes a microsomal ascorbate
AT1G20630	CAT1	0.39	2.9E-01	2.42	2.5E-28	-0.58	1.6E-01	Catalase-1
AT4G25100	FSD1	1.74	1.9E-01	2.75	8.3E-04	3.15	4.6E-06	Superoxide dismutase [Fe] 1
AT1G35910	TPPD	0.77	3.5E-01	5.27	1.1E-146	0.11	1.0E+00	Probable trehalose-phosphate phosphatase D
AT3G15360	ATHM4	0.50	1.7E-01	1.06	1.4E-07	0.13	1.0E+00	Thiol-disulfide oxidoreductase
AT3G22200	POP2	0.55	3.5E-04	1.04	9.4E-17	0.18	7.9E-01	Pyridoxal phosphate (PLP)-dependent transferases superfamily protein
AT3G45640	MPK3	-0.02	9.9E-01	1.36	1.8E-12	0.25	1.0E+00	MPK3
AT3G46090	ZAT7	NA	NA	1.74	1.1E-02	4.22	1.6E-01	C2H2 and C2HC zinc fingers superfamily protein
AT1G13340	AT1G13340	1.20	2.8E-01	2.17	1.8E-10	0.82	8.2E-01	Regulator of Vps4 activity in the MVB pathway protein
AT1G27730	ZAT10	0.44	7.3E-01	2.27	3.5E-22	0.11	1.0E+00	Zinc finger protein ZAT10
AT1G58030	CAT2	-0.02	9.9E-01	1.10	1.0E-11	-0.13	1.0E+00	Cationic amino acid transporter 2
AT2G40000	HSPRO2	1.10	4.8E-01	2.45	1.1E-54	-0.60	1.0E+00	Nematode resistance protein-like HSPRO2
AT4G11830	PLDGAMMA	-0.67	6.3E-02	1.23	2.1E-04	-0.42	8.2E-01	Phospholipase D gamma 2
AT4G12720	AtNUDT7	0.50	6.0E-02	1.38	7.5E-22	0.67	2.2E-04	MutT/nudix family protein
AT5G20230	BCB	1.32	2.3E-01	3.86	1.1E-25	0.41	1.0E+00	Blue-copper-binding protein
AT5G39610	NAC92	NA	NA	2.58	4.6E-07	1.35	9.4E-01	NAC domain containing protein 6
AT1G11210	DUF761	-0.54	7.6E-01	1.80	2.6E-05	-0.02	1.0E+00	Cotton fiber protein, putative
AT5G59080	AT5G59080	0.02	1.0E+00	1.07	3.8E-02	0.00	1.0E+00	Unknown protein
AT2G04795	AT2G04795	-0.61	8.6E-01	2.05	4.2E-03	0.01	1.0E+00	Unknown protein
AT1G14540	PER4	-0.97	1.2E-02	-2.29	6.8E-36	1.16	2.6E-07	Peroxidase 49
AT3G49120	PER34	0.41	9.3E-01	-0.57	6.1E-01	2.28	8.0E-03	Peroxidase 34
AT1G14550	PER5	-1.64	1.3E-01	-4.42	4.6E-63	1.37	4.2E-07	Peroxidase 5
AT4G23190	CRK11	-0.01	1.0E+00	0.36	8.3E-02	1.08	5.8E-04	Cysteine-rich receptor-like protein kinase 11
AT4G02380	SAG21	-0.10	9.1E-01	0.47	6.1E-02	1.07	7.6E-08	senescence-associated gene 21
AT5G64120	PER71	-0.83	1.8E-01	-0.11	8.0E-01	2.24	1.6E-04	Peroxidase 71
AT2G21640	-	-0.30	7.7E-01	-1.29	1.2E-03	1.18	1.1E-02	Marker for oxidative stress response protein

AT2G18150	PER15	NA	NA	0.82	6.6E-02	6.56	3.7E-16	Peroxidase 15
AT1G52200	PCR8	-0.25	8.7E-01	0.01	9.9E-01	1.01	3.0E-02	Protein PLANT CADMIUM RESISTANCE 8
AT1G19020	-	0.50	6.2E-01	0.01	9.9E-01	1.56	8.8E-12	CDP-diacylglycerol-glycerol-3-phosphate 3-phosphatidyltransferase
AT4G37900	GRDP2	-0.25	8.9E-01	-0.02	9.6E-01	1.19	7.9E-03	Glycine-rich domain-containing protein 2
AT4G33420	-	-1.25	3.6E-01	-0.42	7.6E-01	1.51	1.1E-02	Peroxidase superfamily protein
AT5G39580	PER62	-0.84	7.6E-01	0.59	6.5E-02	2.28	5.3E-14	Peroxidase 62
AT4G36430	PER49	0.12	9.7E-01	1.30	7.3E-02	3.34	2.7E-03	Peroxidase 49
AT1G14540	PER4	-0.97	1.2E-02	-2.29	6.8E-36	1.16	2.6E-07	Peroxidase 4
AT3G01190	PER27	-0.24	5.9E-01	-1.35	2.7E-15	-0.22	1.0E+00	Peroxidase 27
AT5G40150	PER63	-0.04	9.7E-01	-1.00	1.1E-05	-0.04	1.0E+00	Peroxidase 63

Tab. S6-8: 5 clusters of genes that were identified in hierarchical clustering analysis

Cluster 1						
Gene ID	Gene name	WT -/+		<i>pdr2</i> -/+		Gene description
		log <sub>2</sub> FC	<i>p</i> -value	log <sub>2</sub> FC	<i>p</i> -value	
AT4G27590	-	2.23	3.5E-17	1.39	8.2E-09	Heavy metal transport/detoxification superfamily protein
AT3G20110	CYP705A20	1.38	4.2E-12	0.79	1.6E-06	Cytochrome P450, family 705, subfamily A, polypeptide 20
AT4G32950	-	2.18	1.4E-10	0.41	2.1E-01	Protein phosphatase 2C family protein
AT2G34655	-	2.17	1.4E-09	1.06	1.2E-03	NA
AT4G39780	ERF060	1.72	4.0E-08	1.17	1.6E-07	Ethylene-responsive transcription factor ERF060
AT3G07255	-	3.04	6.2E-08	1.40	2.3E-02	NA
AT5G66650	-	2.17	9.2E-08	1.41	2.6E-05	Calcium uniporter protein 3
AT5G44260	TZF5	1.42	2.5E-07	0.90	1.7E-03	Zinc finger C-x8-C-x5-C-x3-H type family protein
AT4G03510	RMA1	1.50	7.0E-07	0.89	3.5E-07	E3 ubiquitin-protein ligase RMA1
AT4G35770	STR15	5.59	2.2E-06	3.84	8.8E-15	Rhodanese/Cell cycle control phosphatase superfamily protein
AT4G00130	-	2.17	2.2E-06	0.72	1.9E-01	DNA-binding storekeeper protein-related transcriptional regulator
AT2G38210	PDX1L4	1.97	3.1E-06	1.29	5.6E-04	Pyridoxal 5'-phosphate synthase PDX1-like 4
AT2G42900	-	1.50	4.9E-06	0.70	1.8E-02	Plant basic secretory protein (BSP) family protein
AT4G27460	CBSX5	1.76	3.2E-05	0.91	4.5E-02	Cystathionine beta-synthase (CBS) family protein
AT3G48240	-	1.43	1.3E-04	0.60	7.7E-03	Octicosapeptide/Phox/Bem1p family protein
AT2G31085	CLE6	1.08	2.1E-04	0.41	7.9E-02	CLAVATA3/ESR (CLE)-related protein 6
AT1G62360	STM	6.40	3.0E-04	3.48	6.1E-04	KNOX/ELK homeobox transcription factor
AT2G05330	-	1.99	3.1E-04	0.52	4.1E-01	Putative BTB/POZ domain-containing protein
AT5G11410	-	6.38	3.8E-04	5.27	6.2E-07	Protein kinase superfamily protein
AT5G47740	-	1.51	1.0E-03	0.90	2.7E-02	Adenine nucleotide alpha hydrolases-like superfamily protein

AT2G16005	ROSY1	6.37	1.1E-03	2.38	2.5E-01	MD-2-related lipid recognition domain-containing protein
AT3G62690	ATL5	1.16	2.4E-03	0.58	2.4E-01	Encodes a RING-H2 zinc finger protein related to ATL2
AT4G22620	-	2.47	4.4E-03	1.48	7.1E-02	SAUR-like auxin-responsive protein family
AT2G44380	-	1.83	6.9E-03	1.07	1.3E-03	Cysteine/Histidine-rich C1 domain family protein
AT5G46360	KCO3	2.21	1.1E-02	0.90	2.3E-01	Potassium inward rectifier (Kir)-like channel 3
AT3G15170	NAC054	5.14	1.4E-02	2.98	4.9E-03	NAC (No Apical Meristem) domain transcriptional regulator superfamily protein
AT2G01913	-	1.45	2.5E-02	0.29	6.1E-01	NA
AT3G52770	ZPR3	1.34	3.2E-02	0.64	2.3E-01	Protein LITTLE ZIPPER 3
AT1G01570	-	1.07	3.6E-02	0.18	7.2E-01	transferase activity
AT4G35660	-	1.11	4.0E-02	0.70	1.9E-01	Selection/upkeep of intraepithelial T-cells protein, putative (DUF241)
<b>Cluster 2</b>						
Gene ID	Gene name	WT -/+		<i>pdr2</i> -/+		Gene description
		log <sub>2</sub> FC	<i>p</i> -value	log <sub>2</sub> FC	<i>p</i> -value	
AT3G22060	CRRSP38	1.38	3.8E-13	0.60	7.6E-03	Receptor-like protein kinase-related family protein
AT5G42720	-	1.42	4.4E-11	0.42	2.9E-01	Glycosyl hydrolase family 17 protein
AT3G45060	NRT2.6	5.60	5.8E-09	1.52	5.1E-02	High affinity nitrate transporter 2.6
AT3G48390	-	2.80	8.8E-09	3.01	8.2E-12	Uncharacterized protein T29H11_90
AT3G61060	AtPP2-A13	3.15	9.8E-08	1.90	1.2E-15	F-box protein PP2-A13
AT1G68440	-	1.36	4.1E-07	0.90	2.6E-07	Uncharacterized protein T2E12.1
AT2G19810	-	1.91	4.7E-07	1.38	2.2E-05	CCCH-type zinc finger family protein
AT4G37540	LBD39	1.28	1.1E-06	0.34	3.0E-02	LOB domain-containing protein 39 (LBD39)
AT3G48610	NPC6	1.27	4.5E-06	0.25	4.1E-01	Non-specific phospholipase C6 (NPC6)
AT2G43610	-	0.85	8.0E-06	1.14	1.5E-07	Chitinase family protein
AT3G52060	-	1.12	8.6E-06	0.56	2.2E-03	Core-2/l-branching beta-1,6-N-acetylglucosaminyltransferase family protein
AT1G72820	-	1.26	4.1E-05	0.63	2.1E-03	Mitochondrial substrate carrier family protein
AT1G64660	MGL	1.10	4.8E-05	0.29	3.6E-01	Methionine gamma-lyase
AT5G23360	-	1.38	6.0E-05	0.74	1.0E-03	GRAM domain-containing protein / ABA-responsive protein-related
AT1G11380	-	1.05	1.2E-04	0.56	2.8E-02	PLAC8 family protein
AT5G23370	-	1.47	2.8E-04	0.71	5.8E-03	GRAM domain-containing protein / ABA-responsive protein-related
AT3G51910	HSFA7A	2.81	1.6E-03	2.13	1.3E-23	Heat stress transcription factor A-7a
AT5G59590	UGT76E2	1.32	2.5E-03	0.55	1.6E-01	UDP-glucosyl transferase 76E2
AT4G12690	-	1.26	2.8E-03	0.85	1.2E-03	Plant protein of unknown function (DUF868)
AT5G18670	BAM9	2.38	3.1E-03	1.36	1.7E-09	Inactive beta-amylase 9
AT5G17960	-	1.52	4.8E-03	1.05	3.0E-02	Cysteine/Histidine-rich C1 domain family protein
AT5G26270	-	1.23	6.9E-03	0.80	1.2E-01	Unknown protein
AT5G61440	ACHT5	1.54	8.3E-03	1.02	2.0E-07	Atypical CYS HIS rich thioredoxin 5
AT2G15880	PEX3	1.79	1.5E-02	2.23	4.2E-04	Pollen-specific leucine-rich repeat extensin-like protein 3
AT2G34180	CIPK13	2.60	1.6E-02	1.92	4.4E-14	CBL-interacting serine/threonine-protein kinase 13

AT5G61590	ERF107	1.29	2.4E-02	1.29	2.3E-02	Ethylene-responsive transcription factor ERF107
AT1G13260	RAV1	1.51	1.3E-01	1.15	4.2E-09	AP2/ERF and B3 domain-containing transcription factor RAV1
AT2G25900	ATCTH	1.72	1.4E-01	2.22	5.2E-14	Putative Cys3His zinc finger protein (ATCTH) mRNA, complete
AT5G21940	-	2.00	1.8E-01	1.93	1.7E-20	Hybrid signal transduction histidine kinase M-like protein
AT2G17880	-	1.84	2.1E-01	1.34	3.3E-06	Chaperone DnaJ-domain superfamily protein
AT4G37610	BT5	1.51	3.4E-01	1.28	1.2E-09	BTB/POZ and TAZ domain-containing protein 5
<b>Cluster 3</b>						
Gene ID	Gene name	WT -/+		<i>pdr2</i> -/+		Gene description
		log <sub>2</sub> FC	<i>p</i> -value	log <sub>2</sub> FC	<i>p</i> -value	
AT5G57540	XTH13	1.05	5.4E-13	0.35	1.5E-01	Putative xyloglucan endotransglucosylase/hydrolase protein 13
AT2G02990	RNS1	1.87	1.1E-12	1.77	2.5E-15	Member of the ribonuclease T2 family
AT1G02930	GSTF6	2.45	2.0E-09	2.80	9.9E-21	Glutathione S-transferase F6
AT5G18840	-	1.31	5.2E-09	1.30	1.5E-09	Major facilitator superfamily protein
AT2G43620	-	3.15	1.4E-08	2.32	1.5E-06	Chitinase family protein
AT4G37390	YDK1	2.89	4.9E-05	0.96	4.3E-02	Indole-3-acetic acid-amido synthetase GH3.2
AT4G34950	-	1.23	6.0E-05	0.60	1.1E-02	Major facilitator superfamily protein
AT5G65870	PSK5	1.64	6.7E-05	1.88	6.2E-09	Phytosulfokine 5 precursor
AT1G09932	-	1.83	9.4E-04	1.10	8.6E-06	Phosphoglycerate mutase family protein
AT1G25240	-	1.41	1.2E-03	0.54	7.4E-02	Putative clathrin assembly protein At1g25240
AT5G40010	AATP1	2.86	2.0E-03	1.27	9.2E-03	AAA-ATPase ASD, mitochondrial
AT4G18170	WRKY28	3.65	3.6E-03	4.33	8.3E-27	Probable WRKY transcription factor 28
AT4G17980	anac071	5.38	4.9E-03	3.01	2.3E-06	NAC domain containing protein 71
AT3G50950	RPP13L4	1.45	6.3E-03	2.58	1.0E-40	Disease resistance RPP13-like protein 4
AT5G45630	-	1.90	6.5E-03	2.12	7.6E-19	Plant protein of unknown function
AT1G17147	VQ1	1.20	1.6E-02	0.78	1.3E-01	VQ motif-containing protein 1
AT4G15490	UGT84A3	2.90	1.6E-02	2.88	4.3E-05	UDP-Glycosyltransferase superfamily protein
AT5G39670	CML46	2.98	1.6E-02	3.79	1.2E-30	Calcium-binding EF-hand family protein
AT1G65500	-	5.44	1.7E-02	2.71	5.3E-03	Unknown protein
AT4G30370	ATL14	1.45	2.1E-02	1.56	1.3E-05	RING/U-box superfamily protein
AT4G35180	LHT7	1.69	2.5E-02	1.21	3.1E-03	Lysine histidine transporter-like 7
AT2G26480	UGT76D1	1.04	3.4E-02	0.88	4.1E-04	UDP-glucosyl transferase 76D1
AT2G18470	PERK4	5.28	4.2E-02	4.17	1.4E-05	Proline-rich receptor-like protein kinase PERK4
AT1G21520	-	1.88	4.3E-02	2.09	1.9E-05	Uncharacterized protein At1g21520/F24J8_4
AT2G32960	DSP2	1.09	4.4E-02	0.78	3.4E-02	Phosphotyrosine protein phosphatases superfamily protein
AT5G43175	BHLH139	1.88	5.2E-02	2.05	5.9E-06	Basic helix-loop-helix (bHLH) DNA-binding superfamily protein
AT3G20570	ENODL9	1.17	6.3E-02	1.23	2.8E-05	Predicted GPI-anchored protein
AT2G27505	-	4.54	6.6E-02	2.10	3.9E-03	FBD-like domain family protein
AT3G51890	-	0.98	7.6E-02	1.27	1.4E-06	Clathrin light chain protein
AT1G31290	AGO3	4.37	8.5E-02	5.00	3.3E-18	Protein argonaute 3



AT2G47560	ATL64	2.98	9.6E-02	2.37	1.4E-04	RING/U-box superfamily protein
AT5G46530	-	1.17	1.4E-01	1.60	6.4E-05	AWPM-19-like family protein
AT4G02520	GSTF2	0.93	1.4E-01	2.08	1.1E-11	Glutathione S-transferase PHI 2
AT5G38770	GDU7	3.21	1.5E-01	1.97	1.6E-02	GDU (glutamine dumper) family protein
AT5G62490	HVA22B	1.96	1.5E-01	2.19	2.2E-03	HVA22-like protein b
AT5G16010	-	0.67	1.6E-01	1.34	4.0E-05	3-oxo-5-alpha-steroid 4-dehydrogenase family protein
AT4G25100	FSD1	1.74	1.9E-01	2.75	8.3E-04	Superoxide dismutase [Fe] 1, chloroplastic
AT2G34540	-	1.90	2.0E-01	1.83	5.5E-03	Uncharacterized protein At2g34540
AT4G24260	KOR3	3.32	2.5E-01	2.86	3.4E-06	Glycosyl hydrolase 9A3
AT2G05940	RIPK	0.65	2.7E-01	1.10	9.9E-08	Serine/threonine-protein kinase RIPK
AT1G69920	GSTU12	2.35	3.1E-01	2.48	3.7E-09	Glutathione S-transferase TAU 12
AT1G02920	GSTF7	2.02	3.1E-01	1.75	1.5E-05	Glutathione S-transferase F7
AT1G24140	3MMP	2.17	3.4E-01	2.33	2.6E-05	Metalloendoproteinase 3-MMP
AT3G04220	-	1.52	4.1E-01	1.78	1.1E-05	Disease resistance protein (TIR-NBS-LRR class) family
AT3G26830	PAD3	0.78	4.5E-01	1.91	6.4E-11	Bifunctional dihydrocamalexate synthase/camalexin synthase
AT5G25190	ERF003	0.90	4.7E-01	1.43	5.1E-04	Ethylene-responsive transcription factor ERF003
AT4G23880	-	1.42	4.8E-01	1.17	4.7E-02	Uncharacterized protein
AT1G73330	ATDR4	2.20	5.1E-01	2.25	1.5E-02	plant-specific protease inhibitor-like protein
AT1G15010	-	1.04	5.6E-01	1.45	5.0E-04	Mediator of RNA polymerase II transcription subunit
AT3G21530	-	0.98	5.6E-01	1.39	8.4E-04	Uncharacterized protein
AT3G51540	-	0.68	5.9E-01	1.30	3.0E-07	Uncharacterized protein F26O13.180
AT3G14620	CYP72A8	1.54	6.2E-01	2.54	1.5E-08	Cytochrome P450, family 72, subfamily A, polypeptide 8
AT1G67470	-	1.26	6.4E-01	1.75	1.9E-04	Inactive serine/threonine-protein kinase At1g67470
AT5G22540	-	1.25	6.5E-01	1.91	2.0E-03	Plant protein of unknown function
AT1G10340	-	1.19	6.5E-01	1.18	5.0E-04	Ankyrin repeat family protein
AT1G66090	-	0.76	6.5E-01	2.27	2.0E-14	Disease resistance protein (TIR-NBS class)
AT5G64110	PER70	0.86	6.6E-01	1.02	8.0E-03	Peroxidase superfamily protein
AT3G63540	-	1.01	6.7E-01	1.27	4.6E-02	Mog1/PsbP/DUF1795-like photosystem II reaction center PsbP family protein
AT5G41740	-	1.43	6.9E-01	2.06	4.4E-05	Disease resistance protein (TIR-NBS-LRR class) family
AT2G25940	ALPHA-VPE	0.67	6.9E-01	1.17	5.9E-03	Vacuolar-processing enzyme alpha-isozyme
AT2G09735	-	1.11	6.9E-01	1.76	6.5E-03	NA
AT1G70800	CAR6	0.80	7.2E-01	1.19	5.6E-03	Calcium-dependent lipid-binding (CaLB domain) family protein
AT5G48690	-	0.87	7.3E-01	1.29	4.5E-02	Plant protein of unknown function
AT1G20520	-	0.99	8.1E-01	1.71	2.5E-02	Arabidopsis protein of unknown function (DUF241)
AT4G19840	PP2A1	0.51	8.6E-01	1.33	6.7E-05	Protein PHLOEM PROTEIN 2-LIKE A1
AT3G04070	NAC047	0.76	8.8E-01	1.41	1.4E-04	NAC domain containing protein 47
AT1G07680	-	NA	NA	1.39	3.6E-02	Unknown protein
AT1G24147	-	NA	NA	5.87	2.6E-04	Unknown protein
AT1G30190	-	NA	NA	6.05	2.0E-09	Uncharacterized protein T2H7.2
AT1G52342	-	NA	NA	2.43	1.1E-03	Unknown protein
AT1G56060	-	NA	NA	5.58	1.4E-07	Unknown protein

AT1G57630	-	NA	NA	2.15	4.4E-03	Toll-Interleukin-Resistance (TIR) domain family protein
AT2G04515	-	NA	NA	2.25	1.8E-03	Unknown protein
AT3G05015	-	NA	NA	2.46	1.6E-02	NA
AT3G09525	-	NA	NA	1.98	5.0E-02	NA
AT3G14060	-	NA	NA	3.37	6.7E-05	NA
AT3G27027	-	NA	NA	2.33	3.5E-02	Protein of unknown function
AT3G27400	-	NA	NA	3.39	2.7E-06	Pectin lyase-like superfamily protein
AT4G21903	-	NA	NA	2.07	5.4E-03	MATE efflux family protein
AT4G33930	-	NA	NA	2.93	5.9E-03	Uncharacterized protein
AT5G07165	-	NA	NA	4.46	2.0E-04	NA
AT5G22460	-	NA	NA	3.78	5.2E-04	alpha/beta-Hydrolases superfamily protein
AT5G22530	-	NA	NA	4.42	1.8E-16	Uncharacterized protein
AT5G43064	-	NA	NA	3.18	8.0E-03	NA
AT4G09120	ATL36	NA	NA	2.35	2.6E-02	Putative RING-H2 finger protein ATL36
AT3G23120	AtRLP38	NA	NA	4.36	1.1E-05	Disease resistance protein
AT3G14210	ESM1	NA	NA	2.81	2.6E-07	Epithiospecifier modifier 1
AT1G01680	PUB54	NA	NA	6.92	6.9E-07	U-box domain-containing protein 54
AT4G39770	TPPH	NA	NA	4.30	4.6E-04	Haloacid dehalogenase-like hydrolase (HAD) superfamily protein
AT3G46090	ZAT7	NA	NA	1.74	1.1E-02	C2H2 and C2HC zinc fingers superfamily protein
<b>Cluster 4</b>						
Gene ID	Gene name	WT -/+		<i>pdr2</i> -/+		Gene description
		log <sub>2</sub> FC	<i>p</i> -value	log <sub>2</sub> FC	<i>p</i> -value	
AT5G49520	WRKY48	3.30	7.9E-22	4.75	7.0E-89	WRKY Transcription Factor 48
AT3G25717	RTFL16	1.72	1.1E-14	2.04	6.4E-17	ROTUNDIFOLIA like 16 (RTFL16)
AT1G14860	NUDT18	1.53	1.0E-10	1.67	5.6E-20	Nudix hydrolase 18
AT2G37130	PER21	1.03	2.4E-09	1.32	2.1E-12	Peroxidase superfamily protein
AT1G23800	ALDH2B7	2.20	3.9E-09	2.56	1.1E-29	Aldehyde dehydrogenase family 2 member B7
AT5G17760	-	1.12	8.2E-08	3.18	1.4E-90	P-loop containing nucleoside triphosphate hydrolases superfamily protein
AT1G21680	-	1.93	2.5E-07	2.15	4.5E-09	DPP6 N-terminal domain-like protein
AT3G11340	UGT76B1	1.04	6.4E-06	1.32	2.4E-18	UDP-Glycosyltransferase superfamily protein
AT3G22910	ACA13	1.74	6.6E-06	4.43	5.8E-60	ATPase E1-E2 type family protein / haloacid dehalogenase-like hydrolase family protein
AT3G60690	-	1.18	1.3E-05	0.85	3.5E-04	SAUR-like auxin-responsive protein family
AT3G22930	CML11	1.10	1.4E-05	1.91	2.3E-37	Encodes a calmodulin-like protein
AT5G65660	-	0.96	2.0E-05	1.19	7.9E-18	Hydroxyproline-rich glycoprotein family protein
AT5G49450	BZIP1	2.25	2.0E-05	3.58	1.3E-27	Basic leucine zipper 1
AT4G23700	CHX17	1.62	3.6E-05	2.44	2.9E-26	Cation/H(+) antiporter 17
AT5G43980	CRRSP56	3.23	6.8E-05	3.79	2.3E-14	Cysteine-rich repeat secretory protein 56
AT5G06370	-	0.77	1.6E-04	1.12	8.9E-08	NC domain-containing protein-related
AT5G65140	TPPJ	1.21	1.8E-04	2.75	6.4E-26	Haloacid dehalogenase-like hydrolase (HAD) superfamily protein
AT4G19700	BOI	0.91	1.8E-04	1.58	1.1E-14	SBP (S-ribonuclease binding protein) family protein
AT3G51860	CAX3	1.47	2.3E-04	2.40	1.7E-34	Vacuolar cation/proton exchanger 3

AT5G20830	SUS1	0.85	3.1E-04	2.59	7.1E-41	Sucrose synthase 1
AT3G22200	POP2	0.55	3.5E-04	1.04	9.4E-17	Pyridoxal phosphate (PLP)-dependent transferases superfamily protein
AT1G27290	-	0.93	5.8E-04	1.22	1.6E-13	Uncharacterized protein
AT5G02020	SIS	1.48	6.3E-04	1.82	2.2E-07	E3 ubiquitin-protein ligase RLIM-like protein
AT5G17980	-	0.97	7.2E-04	1.98	9.2E-31	C2 calcium/lipid-binding plant phosphoribosyltransferase family protein
AT1G67900	-	0.99	8.7E-04	1.10	9.9E-07	BTB/POZ domain-containing protein
AT5G16120	-	0.75	2.5E-03	1.62	3.1E-13	alpha/beta-Hydrolases superfamily protein
AT3G24770	CLE41	1.21	3.1E-03	2.50	3.1E-18	CLAVATA3/ESR (CLE)-related protein 41
AT5G21120	EIL2	1.27	3.2E-03	0.95	2.3E-03	ETHYLENE INSENSITIVE 3-like 2 protein
AT2G39660	BIK1	0.74	6.6E-03	1.35	2.0E-13	Serine/threonine-protein kinase BIK1
AT2G47260	WRKY23	1.43	6.8E-03	3.17	1.9E-28	Probable WRKY transcription factor 23
AT5G61890	ERF114	5.65	8.3E-03	9.90	7.1E-15	Ethylene-responsive transcription factor ERF114
AT2G23320	WRKY15	0.75	8.7E-03	1.91	9.7E-28	Probable WRKY transcription factor 15
AT1G77640	ERF013	1.21	9.3E-03	2.39	5.3E-23	Ethylene-responsive transcription factor ERF013
AT5G54500	FQR1	0.41	9.9E-03	1.02	2.3E-09	flavin mononucleotide-binding flavodoxin-like quinone reductase
AT1G19380	-	0.98	1.1E-02	1.88	8.0E-22	Protein of unknown function
AT4G19160	-	0.70	1.1E-02	2.03	2.2E-18	Transglutaminase family protein
AT3G10985	SAG20	0.57	1.2E-02	1.35	8.6E-13	A senescence-associated gene
AT5G64410	OPT4	0.87	1.3E-02	2.09	1.2E-22	Oligopeptide transporter 4
AT3G60670	-	2.63	1.5E-02	3.11	1.6E-08	PLATZ transcription factor family protein
AT4G21120	CAT1	1.39	1.7E-02	3.18	8.5E-22	Cationic amino acid transporter 1
AT5G22520	-	5.59	1.7E-02	8.83	1.3E-11	Uncharacterized protein
AT1G50570	-	0.54	1.7E-02	1.28	2.9E-13	Calcium-dependent lipid-binding (CaLB domain) family protein
AT1G60010	-	0.82	2.4E-02	1.04	1.7E-05	Uncharacterized protein
AT1G34300	-	0.51	2.6E-02	1.09	6.0E-08	G-type lectin S-receptor-like serine/threonine-protein kinase
AT3G11260	WOX5	2.50	2.7E-02	3.27	1.8E-09	WUSCHEL related homeobox 5
AT2G22880	-	1.43	2.8E-02	2.10	3.0E-08	Uncharacterized protein
AT5G47070	PBL19	1.01	2.8E-02	2.43	1.9E-32	Probable serine/threonine-protein kinase PBL19
AT5G62350	-	0.63	2.8E-02	1.56	1.8E-15	Plant invertase/pectin methylesterase inhibitor superfamily protein
AT1G02850	BGLU11	0.60	2.8E-02	1.75	2.7E-17	Beta glucosidase 11 (BGLU11)
AT3G47480	CML47	2.14	2.9E-02	7.92	3.4E-30	Calcium-binding EF-hand family protein
AT5G57560	XTH22	1.16	3.0E-02	3.14	2.3E-34	Xyloglucan endotransglucosylase/hydrolase family protein
AT3G19660	-	1.08	3.8E-02	1.69	1.8E-06	Uncharacterized protein
AT2G36950	HIPP05	0.84	3.8E-02	1.51	1.9E-12	Heavy metal transport/detoxification superfamily protein
AT3G48440	-	0.73	4.0E-02	1.41	9.3E-13	Zinc finger C-x8-C-x5-C-x3-H type family protein
AT4G34220	-	0.96	4.3E-02	2.37	6.3E-27	Leucine-rich repeat protein kinase family protein
AT1G21910	ERF012	0.72	4.5E-02	1.56	1.8E-13	Ethylene-responsive transcription factor ERF012

AT5G01380	GT-3A	1.53	5.8E-02	3.23	9.7E-30	Homeodomain-like superfamily protein
AT3G49700	ACS9	3.96	5.8E-02	3.35	1.2E-06	1-aminocyclopropane-1-carboxylate (ACC) synthase
AT2G30500	NET4B	0.49	6.5E-02	1.14	6.2E-11	Kinase interacting (KIP1-like) family protein
AT3G53210	-	0.54	6.6E-02	1.09	2.2E-07	Nodulin MtN21 /EamA-like transporter family protein
AT1G34180	anac016	1.70	6.9E-02	2.63	6.5E-10	NAC domain containing protein 16
AT1G34540	CYP94D1	1.01	7.3E-02	1.33	8.7E-05	Cytochrome P450, family 94, subfamily D, polypeptide 1
AT5G04080	-	0.93	7.3E-02	1.39	9.2E-07	Cysteine-rich TM module stress tolerance protein
AT1G78080	RAP2-4	0.41	7.5E-02	1.06	8.4E-13	Ethylene-responsive transcription factor RAP2-4
AT3G03310	LCAT3	0.47	7.6E-02	1.19	6.0E-11	Lecithin:cholesterol acyltransferase 3
AT1G58360	AAP1	0.63	7.9E-02	1.17	4.8E-05	Amino acid permease 1
AT1G32700	-	0.55	7.9E-02	1.09	1.6E-11	PLATZ transcription factor family protein
AT1G62422	-	0.90	8.0E-02	1.26	3.0E-05	Uncharacterized protein
AT3G14260	-	1.70	8.3E-02	2.42	8.9E-08	Uncharacterized protein
AT5G40780	LHT1	0.43	8.6E-02	1.22	4.6E-27	Lysine histidine transporter 1
AT1G71040	LPR2	0.63	8.7E-02	1.41	1.5E-15	Cupredoxin superfamily protein
AT5G44005	-	1.84	9.2E-02	1.60	6.0E-03	NA
AT4G17490	ERF6	0.55	1.0E-01	1.74	2.1E-09	Ethylene responsive element binding factor 6
AT1G50420	SCL3	0.42	1.0E-01	1.29	9.6E-09	scarecrow-like protein (SCL3) Putative transcription factor
AT1G60030	NAT7	1.04	1.1E-01	1.98	5.1E-10	Nucleobase-ascorbate transporter 7
AT3G09070	OPS	0.52	1.1E-01	1.59	1.4E-12	Uncharacterized protein
AT1G50090	BCAT7	1.14	1.1E-01	1.51	2.6E-04	D-aminoacid aminotransferase-like PLP-dependent enzymes superfamily protein
AT1G33560	ADR1	0.48	1.1E-01	1.55	3.7E-23	Disease resistance protein (CC-NBS-LRR class) family
AT1G06573	-	1.14	1.2E-01	1.14	2.9E-03	NA
AT1G51700	DOF1.7	1.98	1.2E-01	4.08	1.6E-29	Dof zinc finger protein DOF1.7
AT1G29930	LHCB1.3	0.93	1.2E-01	2.25	2.2E-11	Chlorophyll a-b binding protein 1
AT5G20970	-	0.64	1.3E-01	1.39	2.0E-06	HSP20-like chaperones superfamily protein
AT3G61198	-	1.04	1.3E-01	1.50	9.6E-05	NA
AT3G07040	RPM1	1.22	1.4E-01	2.01	4.1E-10	NB-ARC domain-containing disease resistance protein
AT4G28040	-	0.87	1.4E-01	2.12	3.5E-27	Nodulin MtN21 /EamA-like transporter family protein
AT1G34510	PER8	0.69	1.4E-01	1.41	2.3E-06	Peroxidase superfamily protein
AT2G41190	AVT1A	0.55	1.5E-01	1.13	1.7E-05	Transmembrane amino acid transporter family protein
AT2G37760	AKR4C8	0.44	1.5E-01	1.03	6.8E-06	NAD(P)-linked oxidoreductase superfamily protein
AT3G56400	WRKY70	0.99	1.5E-01	3.75	2.3E-10	Member of WRKY Transcription Factor
AT1G73500	MKK9	0.51	1.6E-01	1.42	1.3E-06	Mitogen-activated protein kinase kinase 9
AT5G53880	-	1.57	1.7E-01	4.17	6.8E-25	Uncharacterized protein
AT3G15360	TRX-M4	0.50	1.7E-01	1.06	1.4E-07	Thioredoxin M4, chloroplastic
AT5G47050	-	0.44	1.8E-01	1.41	3.4E-14	SBP (S-ribonuclease binding protein) family protein
AT1G26930	-	0.36	1.8E-01	1.15	1.1E-18	Galactose oxidase/kelch repeat superfamily protein
AT4G35480	ATL45	1.01	2.0E-01	2.04	2.0E-06	Probable E3 ubiquitin-protein ligase ATL45
AT3G46600	SCL30	0.38	2.0E-01	1.08	3.3E-09	GRAS family transcription factor
AT1G14890	-	0.88	2.1E-01	1.10	9.6E-03	Plant invertase/pectin methylesterase inhibitor superfamily protein

AT4G28390	AAC3	0.65	2.2E-01	1.13	7.9E-05	mitochondrial ADP/ATP carrier protein
AT5G02790	GSTL3	0.71	2.2E-01	1.76	5.2E-09	Glutathione S-transferase family protein
AT3G46110	-	1.78	2.3E-01	3.02	2.7E-13	Uncharacterized protein
AT5G20230	BCB	1.32	2.3E-01	3.86	1.1E-25	Blue-copper-binding protein
AT1G49730	-	0.43	2.3E-01	1.36	2.5E-06	Probable receptor-like protein kinase
AT5G58787	-	0.51	2.3E-01	1.49	8.2E-14	Uncharacterized protein
AT2G46400	WRKY46	1.62	2.5E-01	5.68	2.0E-65	Probable WRKY transcription factor 46
AT1G28260	SMG7L	1.24	2.5E-01	2.38	8.9E-12	Telomerase activating protein Est1
AT1G65510	-	0.81	2.7E-01	1.72	3.4E-10	Unknown protein
AT4G33467	-	1.35	2.7E-01	1.21	2.0E-02	Unknown protein
AT1G13340	-	1.20	2.8E-01	2.17	1.8E-10	Regulator of Vps4 activity in the MVB pathway protein
AT4G18880	HSFA4A	0.66	2.8E-01	2.07	5.4E-23	Heat stress transcription factor A-4a
AT2G46950	CYP709B2	0.54	2.8E-01	1.30	4.5E-10	Cytochrome P450, family 709, subfamily B, polypeptide 2
AT5G60270	LECRK17	1.03	2.9E-01	2.75	4.9E-13	Concanavalin A-like lectin protein kinase family protein
AT4G33490	-	0.53	3.1E-01	1.17	1.8E-08	Eukaryotic aspartyl protease family protein
AT4G13030	-	1.51	3.2E-01	3.12	4.4E-09	P-loop containing nucleoside triphosphate hydrolases superfamily protein
AT2G30140	UGT87A2	0.53	3.2E-01	1.71	1.4E-15	UDP-Glycosyltransferase superfamily protein
AT4G01026	PYL7	0.84	3.2E-01	2.23	1.1E-13	Abscisic acid receptor PYL7
AT5G54080	HGO	0.42	3.3E-01	1.14	8.0E-10	Homogentisate 1,2-dioxygenase
AT5G41610	CHX18	0.43	3.4E-01	1.08	2.5E-06	Cation/H(+) antiporter 18
AT1G61520	LHCA3	0.68	3.6E-01	1.43	2.9E-05	Photosystem I chlorophyll a/b-binding protein 3-1
AT1G63600	-	0.57	3.7E-01	1.03	9.6E-04	Receptor-like protein kinase-related family protein
AT3G02840	-	1.74	3.8E-01	2.91	2.1E-06	Uncharacterized protein
AT1G10140	-	0.68	3.9E-01	1.12	2.1E-04	Uncharacterized protein
AT3G13590	-	1.34	4.0E-01	2.02	1.2E-03	Cysteine/Histidine-rich C1 domain family protein
AT1G76040	CPK29	0.41	4.2E-01	1.16	7.6E-07	Calcium-dependent protein kinase 29
AT2G41010	CAMBP25	0.94	4.2E-01	2.16	2.8E-14	Calmodulin (CAM)-binding protein of 25 kDa
AT1G21550	CML44	0.89	4.2E-01	1.87	1.2E-04	Calcium-binding EF-hand family protein
AT1G01480	ACS2	0.52	4.2E-01	1.53	3.8E-06	1-amino-cyclopropane-1-carboxylate synthase 2
AT4G37730	AtbZIP7	0.73	4.3E-01	1.11	2.1E-03	BZIP transcription factor-like protein
AT2G27140	-	0.44	4.4E-01	1.47	1.4E-06	HSP20-like chaperones superfamily protein
AT5G01760	TOL7	1.22	4.4E-01	2.31	5.1E-06	ENTH/VHS/GAT family protein
AT2G42820	HVA22F	0.70	4.4E-01	1.47	9.2E-04	HVA22-like protein F (HVA22F)
AT4G27730	OPT6	0.71	4.4E-01	1.89	2.2E-08	Oligopeptide transporter 6
AT4G22780	ACR7	0.65	4.5E-01	1.50	2.1E-07	ACT domain containing protein
AT3G04530	PPCK2	0.81	4.5E-01	1.04	2.2E-02	phosphoenolpyruvate carboxylase kinase
ATMG00030	ORF107A	0.84	4.5E-01	1.72	6.0E-04	Uncharacterized mitochondrial protein
AT1G73270	SCPL6	0.68	4.5E-01	1.43	4.7E-04	Serine carboxypeptidase-like 6
AT5G39330	-	0.69	4.5E-01	1.07	6.3E-04	Transmembrane protein
AT1G75160	-	0.64	4.5E-01	1.57	2.5E-06	Protein of unknown function
AT3G62150	ABCB21	1.54	4.6E-01	2.99	2.1E-07	ABC transporter B family member 21
AT1G69430	-	0.90	4.6E-01	1.36	4.4E-03	Uncharacterized protein

AT5G16400	TRXF2	0.90	4.7E-01	1.06	3.2E-02	Thioredoxin F2, chloroplastic
AT1G33030	-	1.46	4.9E-01	2.53	1.0E-04	O-methyltransferase family protein
AT5G64870	FLOT3	1.62	4.9E-01	3.27	7.5E-10	SPFH/Band 7/PHB domain-containing membrane-associated protein family
AT2G44840	ERF13	1.04	5.0E-01	1.69	8.3E-05	Ethylene-responsive element binding factor 13
AT3G15770	-	0.48	5.2E-01	1.26	1.9E-06	Unknown protein
AT1G28370	ERF11	0.97	5.6E-01	1.46	1.1E-02	Ethylene-responsive transcription factor 11
AT5G17850	CCX2	0.68	5.6E-01	1.37	7.2E-06	Sodium/calcium exchanger family protein
AT2G38465	-	1.44	5.6E-01	1.83	3.9E-02	Uncharacterized protein At2g38465
AT5G64040	PSAN	0.61	5.6E-01	1.75	3.1E-09	Photosystem I reaction center subunit PSI-N
AT3G17380	-	0.57	5.7E-01	1.59	4.1E-05	TRAF-like family protein
AT3G49380	iqd15	0.69	5.8E-01	1.27	3.2E-03	Putative calmodulin-binding protein
AT3G10510	-	1.18	5.9E-01	1.72	1.5E-02	Galactose oxidase/kelch repeat superfamily protein
AT2G47450	CAO	0.39	6.0E-01	1.22	4.9E-06	Signal recognition particle 43 kDa protein
AT2G39400	-	0.99	6.2E-01	2.09	2.6E-03	alpha/beta-Hydrolases superfamily protein
AT1G51400	-	0.71	6.2E-01	1.25	1.6E-02	Uncharacterized protein
AT4G17250	-	0.87	6.2E-01	2.90	1.3E-09	Unknown protein
AT2G16700	ADF5	0.53	6.3E-01	1.51	9.4E-06	Actin-depolymerizing factor 5
AT1G12900	GAPA-2	1.17	6.3E-01	2.22	8.5E-04	Glyceraldehyde-3-phosphate dehydrogenase GAPA2
AT5G58830	SBT4.8	1.28	6.3E-01	1.94	2.3E-02	Subtilisin-like serine endopeptidase family protein
AT2G37925	COPT4	0.88	6.4E-01	1.28	4.1E-02	copper transporter family
AT2G09500	-	0.62	6.4E-01	1.09	3.6E-02	NA
AT4G19390	-	0.70	6.5E-01	2.13	3.2E-07	Uncharacterised protein family
AT5G65130	-	1.10	6.5E-01	2.29	9.4E-04	Ethylene-responsive transcription factor ERF057
AT1G28480	GRXC9	0.50	6.5E-01	1.16	6.4E-04	Thioredoxin superfamily protein
AT1G17020	SRG1	1.28	6.6E-01	2.62	1.8E-04	Senescence-related gene 1
AT4G03270	CYCD6-1	0.55	6.7E-01	1.10	4.6E-02	Putative cyclin-D6-1
AT4G03280	PETC	0.67	6.7E-01	2.46	3.1E-10	Cytochrome b6-f complex iron-sulfur subunit, chloroplastic
AT1G70420	-	0.54	6.8E-01	1.51	8.2E-06	DNA ligase-like protein
AT3G44880	PAO	0.35	6.9E-01	1.03	1.9E-03	Pheophorbide a oxygenase family protein with Rieske [2Fe-2S] domain
AT2G44578	-	0.59	6.9E-01	2.02	1.0E-04	RING/U-box superfamily protein
AT3G18950	-	0.74	7.0E-01	2.04	4.8E-05	Transducin/WD40 repeat-like superfamily protein
AT4G39580	-	0.51	7.0E-01	1.03	2.6E-02	Galactose oxidase/kelch repeat superfamily protein
AT4G04640	ATPC1	0.35	7.1E-01	1.00	2.0E-03	ATP synthase gamma chain 1, chloroplastic
AT2G34530	-	0.57	7.4E-01	1.48	1.1E-03	Unknown protein
AT3G02150	TCP13	1.44	7.4E-01	2.82	5.2E-03	Plastid transcription factor 1
AT1G77700	-	0.38	7.5E-01	1.29	4.3E-04	Pathogenesis-related thaumatin superfamily protein
AT1G60360	-	0.71	7.5E-01	2.07	7.3E-04	RING/U-box superfamily protein
AT1G75060	-	0.52	7.6E-01	1.36	1.4E-02	Histone deacetylase complex subunit
AT3G59930	-	0.58	7.7E-01	1.56	2.8E-02	Encodes a defensin-like (DEFL) family protein
AT3G57760	-	0.50	7.7E-01	1.21	3.5E-03	Protein kinase superfamily protein
AT2G46940	-	0.67	7.7E-01	1.41	8.0E-03	Unknown protein
AT5G13790	AGL15	0.64	7.8E-01	1.40	2.2E-02	AGAMOUS-Like 15

AT5G05735	-	0.41	7.9E-01	1.09	1.2E-02	NA
AT1G07135	-	0.65	7.9E-01	1.38	9.5E-07	Predicted GPI-anchored protein
AT5G25910	AtRLP52	0.90	8.0E-01	2.57	2.3E-04	Receptor like protein 52
AT1G02450	NIMIN-1	0.65	8.0E-01	1.93	1.2E-03	Protein NIM1-INTERACTING 1
AT4G08780	PER38	0.86	8.3E-01	2.93	2.4E-04	Peroxidase superfamily protein
AT5G22555	-	0.45	8.4E-01	1.49	1.3E-02	Unknown protein
AT5G03890	-	0.41	8.4E-01	1.35	7.7E-03	Uncharacterized protein
AT4G25434	ATNUDT10	0.60	8.5E-01	2.18	1.0E-03	Nudix hydrolase homolog 10
AT3G02850	SKOR	0.65	8.6E-01	1.85	3.5E-02	STELAR K <sup>+</sup> outward rectifier
AT5G67550	-	0.71	8.6E-01	2.48	2.0E-04	Unknown protein
AT3G02480	-	0.52	8.6E-01	1.65	1.1E-02	Late embryogenesis abundant protein (LEA) family protein
AT2G45760	BAP2	0.73	8.7E-01	2.22	2.6E-03	BON association protein 2
AT1G52315	-	0.55	8.7E-01	1.99	2.2E-03	Regulator of Vps4 activity in the MVB pathway protein
AT5G56510	APUM12	NA	NA	7.34	2.8E-15	Pumilio homolog 12
AT5G24316	-	NA	NA	2.56	8.7E-03	Proline-rich family protein
AT4G35485	-	NA	NA	2.27	2.4E-02	NA
AT3G61470	LHCA2	NA	NA	2.32	3.6E-02	Photosystem I chlorophyll a/b-binding protein 2
AT3G01175	-	NA	NA	3.89	1.5E-06	Protein of unknown function
AT2G28500	LBD11	NA	NA	6.16	3.6E-10	LOB domain-containing protein 11
AT5G10380	ATL55	NA	NA	4.52	6.7E-11	RING finger domain protein
AT1G30560	-	NA	NA	3.58	9.7E-05	Putative glycerol-3-phosphate transporter 3
AT4G11655	-	NA	NA	4.73	8.8E-08	Uncharacterised protein family
<b>Cluster 5</b>						
Gene ID	Gene name	WT +/-		<i>pdr2</i> +/-		Gene description
		log <sub>2</sub> FC	<i>p</i> -value	log <sub>2</sub> FC	<i>p</i> -value	
AT5G22580	-	2.76	3.3E-48	2.23	4.1E-14	Stress-response A/B barrel domain-containing protein
AT4G35750	-	1.97	9.9E-47	1.69	3.1E-30	SEC14 cytosolic factor family protein / phosphoglyceride transfer family protein
AT5G01600	FER1	1.65	9.7E-41	1.81	4.5E-21	Ferritin-1, chloroplastic
AT1G33790	JAL4	3.19	2.8E-29	6.48	2.3E-120	Jacalin lectin family protein
AT1G68290	ENDO2	4.56	2.0E-19	4.92	6.0E-35	Endonuclease 2
AT1G55200	-	2.37	6.8E-17	2.95	6.6E-19	Protein kinase protein with adenine nucleotide alpha hydrolases-like domain
AT5G46590	anac096	2.67	2.1E-16	3.27	3.8E-52	NAC domain containing protein 96
AT5G51550	EXL3	1.67	3.4E-16	1.56	2.6E-12	Protein EXORDIUM-like 3
AT3G47340	ASN1	5.85	6.8E-16	8.02	3.8E-56	Glutamine-dependent asparagine synthetase
AT1G14960	-	1.65	2.2E-15	1.94	8.5E-17	Polyketide cyclase/dehydrase and lipid transport superfamily protein
AT3G07540	FH10	2.68	6.6E-15	3.92	3.8E-52	Actin-binding FH2 (formin homology 2) family protein
AT5G38710	POX2	2.85	1.5E-14	2.91	1.1E-29	Methylenetetrahydrofolate reductase family protein
AT2G33830	DRMH1	3.25	1.9E-14	6.15	3.4E-10	Dormancy/auxin associated family protein
AT3G22120	CWLP	1.75	3.9E-13	2.47	1.3E-10	Cell wall-plasma membrane linker protein homolog (CWLP)
AT2G22430	ATHB-6	1.09	5.2E-13	1.34	5.7E-23	Homeobox-leucine zipper protein ATHB-6

AT2G39570	ACR9	1.66	1.1E-12	1.92	1.3E-25	ACT domain-containing protein ACR9
AT4G19980	-	2.20	5.8E-12	2.01	2.6E-13	Unknown protein
AT1G18460	-	1.39	5.9E-12	1.05	6.7E-07	alpha/beta-Hydrolases superfamily protein
AT3G20340	-	2.25	6.9E-12	1.71	9.0E-28	Protein expression protein
AT3G04350	-	1.36	2.8E-11	1.09	1.4E-10	Uncharacterized protein
AT5G54490	PBP1	1.74	2.8E-11	2.56	3.8E-24	Calcium-binding protein PBP1
AT2G32150	-	2.25	3.3E-11	3.09	8.5E-57	Haloacid dehalogenase-like hydrolase (HAD) superfamily protein
AT5G06730	PER54	2.05	1.9E-10	3.18	9.8E-38	Peroxidase superfamily protein
AT1G70290	TPS8	1.66	1.9E-10	3.03	9.3E-46	Probable alpha,alpha-trehalose-phosphate synthase [UDP-forming] 8
AT1G22400	UGT85A1	1.20	2.0E-10	1.00	1.8E-11	UDP-Glycosyltransferase superfamily protein
AT1G76990	ACR3	1.19	2.0E-10	1.29	3.3E-20	ACT domain-containing protein ACR3
AT5G14180	LIP2	2.03	2.2E-10	2.92	5.2E-38	Myzus persicae-induced lipase 1
AT1G32510	ANAC011	4.75	3.0E-10	6.72	1.9E-16	NAC domain containing protein 11
AT1G80380	GLYK	1.87	3.6E-10	1.96	9.5E-15	P-loop containing nucleoside triphosphate hydrolases superfamily protein
AT2G15890	MEE14	1.81	4.8E-10	2.37	6.5E-26	Maternal effect embryo arrest 14
AT3G57520	RFS2	1.40	1.6E-09	1.97	2.0E-35	Probable galactinol--sucrose galactosyltransferase 2
AT1G30820	-	1.49	2.5E-09	2.36	3.1E-27	CTP synthase family protein
AT5G63450	CYP94B1	2.08	2.9E-09	2.00	1.6E-08	Cytochrome P450, family 94, subfamily B, polypeptide 1
AT4G38470	STY46	1.69	4.0E-09	2.05	1.4E-20	ACT-like protein tyrosine kinase family protein
AT5G14920	GASA14	1.23	4.3E-09	1.34	6.9E-08	Gibberellin-regulated family protein
AT5G28770	BZIP63	1.59	5.4E-09	1.95	2.0E-13	bZIP transcription factor family protein
AT1G78830	-	1.61	7.8E-09	1.88	9.3E-11	Curculin-like (mannose-binding) lectin family protein
AT3G26740	CCL	5.28	7.8E-09	5.28	2.2E-17	Light-regulated protein 1, chloroplastic
AT4G24230	ACBP3	1.84	1.7E-08	2.38	6.4E-34	acyl-CoA-binding protein ACBP3
AT3G53620	PPA4	0.92	2.3E-08	1.27	2.6E-21	Soluble inorganic pyrophosphatase 4
AT1G15040	GAT1_2.1	4.63	2.6E-08	4.56	2.6E-83	Class I glutamine amidotransferase-like superfamily protein
AT5G01370	ACI1	1.78	6.2E-08	2.28	2.3E-18	Uncharacterized protein
AT1G09460	-	1.08	6.4E-08	0.77	3.5E-04	Carbohydrate-binding X8 domain superfamily protein
AT4G02050	STP7	1.16	7.8E-08	1.29	2.3E-13	Sugar transporter protein 7
AT1G73260	KTI1	2.58	7.8E-08	3.80	1.6E-14	Kunitz trypsin inhibitor 1
AT1G23870	TPS9	1.41	7.9E-08	1.65	2.9E-31	Probable alpha,alpha-trehalose-phosphate synthase [UDP-forming] 9
AT5G10510	AIL6	0.91	8.2E-08	1.62	6.0E-33	AP2-like ethylene-responsive transcription factor AIL6
AT3G25130	-	3.66	8.9E-08	3.78	1.4E-09	Acidic leucine-rich nuclear phosphoprotein 32 family B protein
AT5G08000	E13L3	4.78	1.2E-07	4.94	4.7E-12	Glucan endo-1,3-beta-glucosidase-like protein 3
AT2G39700	EXPA4	0.94	1.3E-07	1.58	2.9E-21	Expansin-A4
AT4G18340	-	1.37	1.7E-07	1.67	1.7E-29	Glycosyl hydrolase superfamily protein
AT3G43270	PME32	1.11	1.9E-07	2.02	3.1E-27	Plant invertase/pectin methylesterase inhibitor superfamily



AT5G24490	-	1.59	1.9E-07	2.42	1.2E-27	Uncharacterized protein
AT3G19200	-	1.36	2.2E-07	2.07	7.4E-15	Unknown protein
AT1G62770	PMEI9	1.05	2.9E-07	1.26	2.7E-12	Plant invertase/pectin methylesterase inhibitor superfamily protein
AT2G43535	ATTI4	1.02	3.1E-07	1.38	4.5E-12	Scorpion toxin-like knottin superfamily protein
AT2G18700	TPS11	1.56	4.4E-07	2.53	7.2E-59	Probable alpha,alpha-trehalose-phosphate synthase [UDP-forming] 11
AT1G25400	-	1.42	6.1E-07	1.24	8.1E-11	Uncharacterized protein
AT3G04300	-	3.44	7.7E-07	4.85	4.1E-35	RmlC-like cupins superfamily protein
AT5G16970	AER	3.05	8.7E-07	5.96	5.7E-59	NADPH-dependent oxidoreductase 2-alkenal reductase
AT1G21830	-	1.40	1.1E-06	1.26	2.8E-08	Uncharacterized protein
AT4G32300	SD25	1.05	1.1E-06	1.15	1.6E-07	G-type lectin S-receptor-like serine/threonine-protein kinase SD2-5
AT5G27920	-	1.24	1.3E-06	1.11	1.0E-08	Uncharacterized protein
AT4G38210	EXPA20	1.14	1.3E-06	1.85	1.8E-11	Expansin-A20
AT3G03150	-	0.86	1.5E-06	1.34	1.3E-13	Uncharacterized protein
AT3G43430	-	1.44	1.6E-06	2.14	1.1E-27	Uncharacterized protein
AT2G24560	-	3.85	2.5E-06	3.59	9.6E-10	GDSL-like Lipase/Acylhydrolase family protein
AT1G62500	-	1.40	3.0E-06	0.99	1.8E-05	Bifunctional inhibitor/lipid-transfer protein/seed storage 2S albumin superfamily protein
AT3G23570	-	1.17	3.7E-06	1.96	4.7E-18	alpha/beta-Hydrolases superfamily protein
AT1G05147	-	3.97	3.8E-06	4.21	1.9E-16	NA
AT5G65690	PCK2	2.42	3.8E-06	2.57	2.3E-33	Putative phosphoenolpyruvate carboxykinase
AT2G38230	PDX11	1.74	4.4E-06	1.40	1.2E-09	Pyridoxal 5'-phosphate synthase subunit PDX1.1
AT1G30720	-	1.66	4.9E-06	1.27	3.6E-06	FAD-binding Berberine family protein
AT5G07310	ERF115	7.23	6.2E-06	9.28	1.3E-12	Ethylene-responsive transcription factor ERF115
AT3G21670	NPF6.4	1.72	6.6E-06	1.31	4.7E-05	Major facilitator superfamily protein
AT1G22710	SUC2	1.54	6.9E-06	1.42	3.4E-09	Sucrose transport protein SUC2
AT3G19930	STP4	1.00	6.9E-06	1.41	1.8E-10	Sugar transport protein 4
AT5G16110	-	1.11	7.9E-06	1.41	3.8E-31	Uncharacterized protein
AT3G07310	-	2.06	9.1E-06	1.99	3.0E-06	Phosphoserine aminotransferase, putative
AT5G07440	GDH2	0.98	1.5E-05	1.57	6.7E-33	Glutamate dehydrogenase 2
AT3G07350	-	1.44	1.7E-05	2.27	2.2E-10	Sulfate/thiosulfate import ATP-binding protein, putative
AT4G22590	TPPG	1.10	1.8E-05	1.47	1.6E-12	Haloacid dehalogenase-like hydrolase (HAD) superfamily protein
AT3G46690	UGT76E4	1.29	2.0E-05	1.33	2.6E-11	UDP-Glycosyltransferase superfamily protein
AT3G13430	-	1.14	2.0E-05	0.87	1.1E-07	RING/U-box superfamily protein
AT3G30775	EDR5	2.32	2.7E-05	2.41	5.4E-55	Methylenetetrahydrofolate reductase family protein
AT5G08350	-	1.38	3.2E-05	1.17	7.4E-07	GRAM domain-containing proteind
AT3G10020	-	1.41	4.1E-05	4.10	3.0E-70	Uncharacterized protein
AT1G68840	RAV2	0.81	4.8E-05	1.31	2.1E-13	AP2/ERF and B3 domain-containing transcription repressor RAV2
AT2G19800	MIOX2	2.50	4.9E-05	3.06	3.2E-48	Myo-inositol oxygenase 2

AT1G15085	-	1.64	5.1E-05	1.64	1.4E-05	NA
AT4G22730	-	1.84	5.8E-05	2.76	1.8E-15	Leucine-rich repeat protein kinase family protein
AT2G41430	ERD15	0.76	6.2E-05	1.05	1.4E-21	Protein EARLY RESPONSIVE TO DEHYDRATION 15
AT4G27970	SLAH2	1.26	7.1E-05	2.49	3.0E-41	S-type anion channel SLAH2
AT5G20250	DIN10	3.13	7.3E-05	3.03	3.1E-51	Probable galactinol--sucrose galactosyltransferase 6
AT2G20520	FLA6	1.09	7.4E-05	1.05	3.8E-04	Fasciclin-like arabinogalactan-protein 6 (Fla6)
AT2G43510	ATTI1	3.97	8.6E-05	7.68	5.6E-22	Trypsin inhibitor protein 1
AT1G19850	ARF5	0.66	9.2E-05	1.36	2.2E-28	Transcriptional factor B3 family protein
AT5G22920	RZPF34	2.62	9.9E-05	2.21	1.8E-24	CHY-type/CTCHY-type/RING-type Zinc finger protein
AT3G16350	-	0.81	1.0E-04	1.03	6.9E-08	Homeodomain-like superfamily protein
AT1G69490	NAC029	1.91	1.1E-04	4.09	2.1E-36	NAC-like, activated by AP3/PI
AT1G31650	ROPGEF14	0.78	1.1E-04	1.81	2.3E-28	Rop guanine nucleotide exchange factor 14
AT4G16190	RD19C	0.90	1.1E-04	1.60	1.4E-10	Probable cysteine protease RD19C
AT3G48360	BT2	2.90	1.1E-04	2.84	4.3E-24	BTB/POZ and TAZ domain-containing protein 2
AT5G19650	OFP8	2.09	1.2E-04	3.27	4.4E-19	Transcription repressor OFP8
AT1G32460	-	0.97	1.3E-04	1.05	8.7E-16	Uncharacterized protein
AT4G32480	-	3.00	1.5E-04	2.42	7.9E-37	Putative sugar phosphate exchanger
AT1G25550	HHO3	0.84	1.9E-04	1.06	5.1E-07	Myb-like transcription factor family protein
AT2G19970	-	3.21	1.9E-04	4.70	3.1E-09	CAP (Cysteine-rich secretory proteins, Antigen 5, and Pathogenesis-related 1 protein) superfamily protein
AT1G55650	HMGB11	6.50	2.0E-04	5.30	4.2E-03	HMG (high mobility group) box protein with ARID/BRIGHT DNA-binding domain
AT3G63210	MARD1	0.67	2.3E-04	1.03	4.3E-07	Uncharacterized protein
AT1G52245	-	2.34	2.3E-04	2.04	1.9E-31	NA
AT5G02580	-	1.01	2.4E-04	0.93	6.3E-05	Uncharacterized protein
AT1G71520	ERF020	1.45	2.7E-04	1.23	9.2E-04	Ethylene-responsive transcription factor ERF020
AT3G07650	COL9	0.83	2.9E-04	1.53	1.3E-08	Zinc finger protein CONSTANS-LIKE 9
AT3G47380	PMEI11	0.92	3.5E-04	1.71	1.3E-10	Plant invertase/pectin methylesterase inhibitor superfamily protein
AT4G34138	UGT73B1	0.77	4.1E-04	1.48	8.5E-18	UDP-glucosyl transferase 73B1
AT5G04040	SDP1	0.92	4.1E-04	1.09	5.6E-10	Patatin-like phospholipase family protein
AT1G23390	-	1.16	4.7E-04	1.99	5.1E-15	Kelch repeat-containing F-box family protein
AT4G08950	EXO	0.95	5.0E-04	2.26	1.1E-29	Phosphate-responsive 1 family protein
AT1G67480	-	0.63	5.2E-04	1.07	6.8E-21	Galactose oxidase/kelch repeat superfamily protein
AT2G02710	TLP1	2.02	5.4E-04	2.53	2.6E-29	Protein TWIN LOV 1
AT3G20660	OCT4	0.86	5.7E-04	1.83	1.3E-22	Organic cation/carnitine transporter 4
AT5G05770	WOX7	4.17	7.0E-04	5.79	4.1E-22	WUSCHEL-related homeobox gene family member
AT5G19090	HIPP33	0.60	7.2E-04	1.27	1.2E-20	Heavy metal transport/detoxification superfamily protein
AT4G24040	TRE1	1.30	7.5E-04	2.31	2.4E-26	Trehalase 1
AT3G06850	BCE2	1.10	7.8E-04	2.21	9.8E-21	2-oxoacid dehydrogenases acyltransferase family protein
AT3G24450	-	0.96	8.3E-04	1.44	3.6E-13	Heavy metal transport/detoxification superfamily protein
AT4G37260	MYB73	0.63	8.6E-04	1.13	1.4E-10	Transcription factor MYB73

AT4G29610	CDA6	1.20	8.9E-04	2.00	1.5E-10	Cytidine/deoxycytidylate deaminase family protein
AT5G41080	GDPD2	1.63	1.0E-03	1.52	1.7E-06	PLC-like phosphodiesterases superfamily protein
AT1G28330	DRM1	2.31	1.1E-03	3.51	3.0E-56	Dormancy-associated protein (DRM1)
AT1G28190	-	1.43	1.1E-03	1.96	1.8E-08	Unknown protein
AT2G42960	-	0.79	1.2E-03	1.41	2.5E-09	Probable receptor-like protein kinase
AT3G42725	-	3.34	1.4E-03	4.18	9.0E-09	Uncharacterized protein
AT3G54880	-	0.76	1.5E-03	1.39	1.0E-07	Uncharacterized protein
AT2G25090	CIPK16	1.74	1.5E-03	1.53	3.2E-04	CBL-interacting serine/threonine-protein kinase 16
AT1G25560	TEM1	0.67	1.8E-03	1.32	5.5E-12	AP2/ERF and B3 domain-containing transcription repressor TEM1
AT2G33020	AtRLP24	3.29	2.1E-03	6.61	1.9E-21	Putative leucine-rich repeat disease resistance protein
AT3G49160	PKP4	0.77	2.2E-03	1.38	5.1E-12	Plastidial pyruvate kinase 4
AT2G20670	-	2.80	2.5E-03	2.52	5.6E-33	Sugar phosphate exchanger, putative
AT2G40420	AVT6D	0.86	2.5E-03	1.38	2.6E-10	Encodes a putative amino acid transporter
AT4G00200	AHL7	0.79	3.0E-03	1.13	1.0E-07	AT-hook motif nuclear-localized protein 7
AT5G12890	UGT92A1	1.34	3.1E-03	1.93	2.1E-07	UDP-Glycosyltransferase superfamily protein
AT2G19460	-	0.79	3.2E-03	1.03	3.9E-10	Uncharacterized protein
AT1G12890	ERF088	3.42	3.3E-03	5.04	6.7E-10	Ethylene-responsive transcription factor ERF088
AT1G11440	-	1.13	3.8E-03	1.16	6.0E-05	Putative serine/threonine protein kinase
AT2G17440	PIRL5	0.66	3.8E-03	1.16	9.6E-17	Intracellular Ras-group-related LRRs (Leucine rich repeat proteins)
AT1G72610	GLP1	1.30	3.9E-03	1.55	3.2E-05	Germin-like protein subfamily 3 member 1
AT3G47160	-	0.75	4.0E-03	1.33	1.2E-19	RING/U-box superfamily protein
AT1G30730	-	1.83	4.1E-03	1.83	1.1E-15	FAD-binding Berberine family protein
AT1G13245	RTFL17	1.22	4.2E-03	0.86	3.9E-02	Uncharacterized protein
AT1G13250	GATL3	1.05	4.3E-03	1.02	1.8E-05	Probable galacturonosyltransferase-like 3
AT1G16110	WAKL6	1.57	4.4E-03	2.74	1.6E-10	Wall-associated receptor kinase-like 6
AT5G65207	-	1.27	4.6E-03	1.07	3.4E-04	Uncharacterized protein
AT5G56550	OXS3	3.70	4.6E-03	4.01	4.6E-29	Uncharacterized protein At5g56550
AT3G23880	-	1.89	4.9E-03	2.21	6.7E-05	F-box and associated interaction domains-containing protein
AT4G37520	PER50	0.62	5.1E-03	1.41	3.3E-18	Peroxidase superfamily protein
AT5G26340	STP13	0.78	5.1E-03	1.30	7.6E-10	Major facilitator superfamily protein
AT5G53490	-	2.85	5.4E-03	2.07	2.5E-02	Tetratricopeptide repeat (TPR)-like superfamily protein
AT3G15630	-	2.54	5.4E-03	3.06	1.3E-44	NA
AT4G18890	BEH3	0.70	5.5E-03	1.01	6.1E-07	BES1/BZR1 homolog 3 (BEH3)
AT4G34560	-	1.36	5.6E-03	1.11	2.1E-03	Uncharacterized protein
AT5G19120	-	2.41	6.4E-03	2.30	3.7E-17	Eukaryotic aspartyl protease family protein
AT3G16120	-	4.41	6.6E-03	6.17	8.5E-13	Dynein light chain type 1 family protein
AT5G58650	PSY1	2.33	6.9E-03	2.45	1.5E-26	18-aa tyrosine-sulfated glycopeptide
AT4G34139	-	1.18	8.0E-03	1.61	6.8E-05	NA
AT1G66890	-	1.08	8.8E-03	0.85	7.3E-03	Uncharacterized protein
AT4G28170	-	1.44	1.0E-02	1.67	1.3E-05	Unknown protein

AT4G38580	HIPP26	0.78	1.1E-02	1.75	5.1E-12	Heavy metal-associated isoprenylated plant protein 26
AT3G60140	BGLU30	3.20	1.2E-02	3.76	1.1E-05	Glycosyl hydrolase superfamily protein
AT5G16370	AAE5	1.96	1.2E-02	1.86	4.6E-22	Probable acyl-activating enzyme 5
AT3G23230	ERF098	4.48	1.3E-02	3.90	3.2E-04	Ethylene-responsive transcription factor ERF098
AT5G47240	atnudt8	1.04	1.3E-02	0.76	7.9E-03	Nudix hydrolase homolog 8
AT1G03600	PSB27-1	1.74	1.4E-02	1.80	1.7E-03	Photosystem II repair protein PSB27-H1
AT1G68020	ATPS6	0.75	1.5E-02	1.47	5.1E-14	UDP-Glycosyltransferase / trehalose-phosphatase family protein
AT5G49320	-	1.44	1.5E-02	1.27	7.4E-03	Putative transmembrane protein
AT3G15370	ATEXPA12	0.80	1.5E-02	1.44	4.2E-12	Expansin-A12
AT3G50740	UGT72E1	0.90	1.5E-02	1.41	2.1E-04	UDP-glucosyl transferase 72E1
AT3G15450	-	3.06	1.6E-02	3.82	1.9E-49	Aluminium induced protein with YGL and LRDR motifs
AT5G62940	DOF5.6	1.39	1.7E-02	1.50	4.3E-05	Dof-type zinc finger DNA-binding family protein
AT5G66050	-	0.99	1.7E-02	1.45	8.4E-09	Uncharacterized protein
AT1G58180	BCA6	1.03	1.7E-02	1.76	4.2E-11	Beta carbonic anhydrase 6, mitochondrial
AT1G03610	-	0.77	1.8E-02	1.17	3.6E-09	Uncharacterized protein
AT5G14360	-	1.06	2.0E-02	2.16	2.4E-07	Ubiquitin-like superfamily protein
AT3G15440	-	4.00	2.2E-02	3.87	3.1E-03	NA
AT1G80920	ATJ8	1.91	2.2E-02	1.99	6.6E-43	Chaperone DnaJ-domain superfamily protein
AT5G39080	-	1.51	2.3E-02	3.23	4.9E-09	HXXXD-type acyl-transferase family protein
AT5G14470	GLCAK2	2.43	2.5E-02	2.71	7.4E-08	GHMP kinase family protein
AT3G01940	-	1.63	2.6E-02	1.31	1.7E-02	Transmembrane protein, putative
AT3G53232	RTFL1	4.31	2.7E-02	6.33	3.3E-07	ROTUNDIFOLIA like 1
AT5G28650	WRKY74	1.73	3.0E-02	2.24	9.6E-07	Probable WRKY transcription factor 74
AT3G22740	HMT3	0.85	3.1E-02	1.26	2.2E-06	Homocysteine S-methyltransferase 3
AT1G23052	-	1.69	3.1E-02	1.35	3.9E-03	NA
AT1G80840	WRKY40	1.37	3.1E-02	2.32	1.1E-14	Probable WRKY transcription factor 40
AT1G72890	-	1.73	3.2E-02	2.57	7.5E-10	Disease resistance protein (TIR-NBS class)
AT2G05380	GRP3S	2.19	3.3E-02	3.66	4.7E-09	Glycine-rich protein 3 short isoform (GRP3S) mRNA, complete
AT5G22570	WRKY38	1.20	3.3E-02	2.68	1.4E-12	Probable WRKY transcription factor 38
AT5G49120	FLZ15	1.11	3.4E-02	1.23	7.7E-05	DUF581 family protein, putative
AT3G45730	-	2.75	3.5E-02	3.70	4.4E-27	Uncharacterized protein
AT4G27450	-	1.08	3.5E-02	2.96	5.1E-21	Aluminium induced protein with YGL and LRDR motifs
AT5G03230	-	0.92	3.5E-02	1.77	2.8E-10	NA
AT3G46490	-	0.94	3.8E-02	1.05	9.6E-03	2-oxoglutarate (2OG) and Fe(II)-dependent oxygenase superfamily protein
AT5G59570	BOA	0.73	3.8E-02	1.67	2.8E-09	Homeodomain-like superfamily protein
AT4G38932	-	0.69	4.2E-02	1.05	5.1E-08	NA
AT4G29190	-	0.95	4.3E-02	2.14	7.3E-10	Zinc finger C-x8-C-x5-C-x3-H type family protein
AT4G11370	RHA1A	1.43	4.6E-02	1.21	4.0E-02	Probable E3 ubiquitin-protein ligase RHA1A
AT5G12270	-	1.28	4.6E-02	1.23	8.9E-03	2-oxoglutarate (2OG) and Fe(II)-dependent oxygenase superfamily protein
AT1G80160	-	2.78	4.7E-02	4.26	2.6E-09	Lactoylglutathione lyase / glyoxalase I family protein

AT1G15330	PV42A	4.66	4.8E-02	4.85	7.2E-26	SNF1-related protein kinase regulatory subunit gamma-like PV42a
AT5G48175	-	0.89	5.0E-02	2.37	3.6E-19	Transmembrane protein
AT2G43540	-	0.56	5.6E-02	1.07	8.8E-04	Unknown protein
AT1G76600	-	1.52	6.0E-02	1.38	2.7E-11	Uncharacterized protein
AT3G49790	-	1.03	6.1E-02	1.04	2.4E-03	Uncharacterized protein
AT1G56220	-	0.67	6.2E-02	1.21	1.7E-12	Dormancy/auxin associated family protein
AT4G01250	WRKY22	1.13	6.3E-02	1.55	3.8E-06	WRKY family transcription factor
AT4G39650	GGT2	1.31	6.9E-02	1.71	5.0E-03	Gamma-glutamyl transpeptidase 2
AT5G23350	-	1.68	7.2E-02	1.18	1.4E-07	GRAM domain-containing protein
AT1G25230	-	0.63	7.2E-02	1.26	8.2E-07	Calcineurin-like metallo-phosphoesterase superfamily protein
AT5G58660	-	0.99	7.7E-02	1.51	9.1E-07	2-oxoglutarate (2OG) and Fe(II)-dependent oxygenase superfamily protein
AT4G36820	-	1.61	8.5E-02	1.64	2.8E-03	Calcium uniporter protein 1, mitochondrial
AT2G37640	EXPA3	1.02	8.9E-02	1.82	2.8E-06	Barwin-like endoglucanases superfamily protein
AT2G18670	ATL56	1.12	9.0E-02	1.73	4.2E-05	RING/U-box superfamily protein
AT3G54780	-	1.01	9.0E-02	1.51	2.5E-05	Zinc finger (C3HC4-type RING finger) family protein
AT1G15670	-	0.52	9.2E-02	1.03	2.6E-06	Galactose oxidase/kelch repeat superfamily protein
AT2G38530	LTP2	2.53	9.4E-02	4.83	2.2E-10	Non-specific lipid-transfer protein 2
AT2G31160	LSH3	1.22	9.7E-02	1.38	4.9E-03	Protein LIGHT-DEPENDENT SHORT HYPOCOTYLS 3
AT1G10690	SMR8	0.67	1.0E-01	1.03	8.5E-05	Cyclin-dependent protein kinase inhibitor SMR8
AT5G42900	COR27	0.87	1.1E-01	2.29	5.3E-03	Uncharacterized protein
AT4G10500	DLO1	0.98	1.1E-01	1.55	2.1E-04	2-oxoglutarate (2OG) and Fe(II)-dependent oxygenase superfamily protein
AT5G44460	CML43	0.73	1.1E-01	1.42	2.0E-04	Probable calcium-binding protein CML43
AT4G23410	TET5	0.93	1.2E-01	1.41	6.7E-05	Tetraspanin-5
AT1G60870	MEE9	1.20	1.2E-01	2.63	8.8E-09	Uncharacterized protein
AT4G02770	PSAD1	0.84	1.2E-01	1.56	5.4E-10	Photosystem I reaction center subunit II-1
AT1G26800	MPSR1	1.25	1.4E-01	1.20	2.1E-02	RING/U-box superfamily protein
AT4G36040	ATJ11	1.90	1.5E-01	2.54	2.2E-24	Chaperone DnaJ-domain superfamily protein
AT2G34140	CDF4	0.70	1.6E-01	1.17	1.4E-04	Dof-type zinc finger DNA-binding family protein
AT5G13080	WRKY75	1.15	1.7E-01	2.26	1.5E-09	WRKY transcription factor 75
AT3G50410	DOF3.4	2.28	1.7E-01	4.53	4.8E-11	Dof zinc finger protein DOF3.4
AT2G39920	-	1.18	1.7E-01	2.45	2.5E-07	HAD superfamily, subfamily IIIB acid phosphatase
AT3G47180	-	1.25	1.8E-01	1.97	3.4E-03	RING/U-box superfamily protein
AT1G25440	COL16	2.02	1.9E-01	1.62	4.3E-02	B-box type zinc finger protein with CCT domain
AT3G59940	SKIP20	0.92	2.0E-01	2.02	2.0E-12	Galactose oxidase/kelch repeat superfamily protein
AT2G13610	ABCG5	1.42	2.1E-01	2.62	1.5E-06	ABC-2 type transporter family protein
AT1G32928	-	1.66	2.3E-01	1.96	1.1E-09	Avr9/Cf-9 rapidly elicited protein
AT5G02030	BLH9	1.59	2.3E-01	2.00	7.2E-04	POX (plant homeobox) family protein
AT1G01240	-	0.62	2.4E-01	1.51	2.8E-06	Uncharacterized protein
AT1G05562	-	0.61	2.4E-01	1.03	2.8E-03	NA
AT3G03200	NAC045	0.92	2.4E-01	1.89	3.6E-05	NAC domain containing protein 45

AT4G23670	-	1.25	2.4E-01	1.56	1.5E-02	Polyketide cyclase/dehydrase and lipid transport superfamily protein
AT1G11530	CXXS1	0.98	2.5E-01	2.21	6.8E-08	C-terminal cysteine residue is changed to a serine 1
AT1G74000	SSL11	0.65	2.5E-01	1.30	3.2E-04	A protein similar to strictosidine synthase
AT1G62290	APA2	1.10	2.5E-01	2.01	6.4E-05	Sapoin-like aspartyl protease family protein
AT1G74440	-	0.76	2.5E-01	1.19	2.1E-04	ER membrane protein, putative
AT4G00210	LBD31	1.92	2.6E-01	2.25	6.9E-03	LOB domain-containing protein 31 (LBD31)
AT5G53950	NAC098	1.56	2.8E-01	3.71	3.5E-08	NAC domain containing protein 98
AT3G08940	LHCB4.2	0.62	2.9E-01	1.10	7.5E-04	Chlorophyll a-b binding protein CP29.2
AT5G60680	-	0.96	3.0E-01	1.15	2.5E-06	Protein of unknown function
AT3G26580	-	0.66	3.0E-01	1.20	7.6E-04	Tetratricopeptide repeat (TPR)-like superfamily protein
AT1G75960	AAE8	1.71	3.4E-01	2.12	2.9E-03	AMP-dependent synthetase and ligase family protein
AT3G06360	AGP27	0.83	3.5E-01	1.14	1.2E-02	Classical arabinogalactan protein 27
AT5G48590	-	0.60	3.5E-01	1.06	2.7E-04	Putative phosphoserine aminotransferase
AT1G23850	-	0.48	3.5E-01	1.04	6.3E-06	Uncharacterized protein
AT3G16770	RAP2-3	0.68	3.5E-01	1.03	3.2E-03	Ethylene-responsive transcription factor RAP2-3
AT4G09770	-	0.63	3.6E-01	1.19	2.2E-03	TRAF-like family protein
AT3G22121	-	1.11	3.6E-01	2.11	1.3E-03	NA
AT4G28240	-	1.29	3.6E-01	1.56	4.4E-11	Wound-responsive family protein
AT4G30090	-	0.77	3.8E-01	1.02	1.4E-02	Golgin family A protein
AT5G38850	-	0.48	4.1E-01	1.00	2.8E-04	Disease resistance protein (TIR-NBS-LRR class)
AT2G30570	PSBW	1.23	4.2E-01	2.37	1.7E-07	Photosystem II reaction center W protein
AT1G05575	-	0.82	4.2E-01	1.36	1.2E-02	Uncharacterized protein
AT1G80650	RTL1	0.82	4.3E-01	1.74	6.8E-05	RNAse THREE-like protein 1
AT4G16745	-	0.68	4.4E-01	1.06	6.4E-03	Exostosin family protein
AT1G20340	DRT112	0.47	4.4E-01	1.05	1.1E-06	Plastocyanin major isoform, chloroplastic
AT4G14830	HSP1	0.75	4.6E-01	1.14	6.1E-03	17.6 kDa class II heat shock protein
AT2G18500	OFP7	1.34	4.6E-01	2.08	1.9E-03	Transcription repressor OFP7
AT2G32670	VAMP725	1.20	4.7E-01	1.89	1.3E-02	Vesicle-associated membrane protein 725
AT5G02160	-	0.59	4.7E-01	1.05	8.2E-03	Uncharacterized protein
AT3G52070	-	1.07	4.7E-01	2.76	3.7E-06	RNA/RNP complex-1-interacting phosphatase
AT5G17260	NAC086	0.75	4.8E-01	1.45	1.1E-03	NAC domain containing protein 86
AT2G40000	HSPRO2	1.10	4.8E-01	2.45	1.1E-54	Nematode resistance protein-like HSPRO2
AT3G28540	-	0.92	5.0E-01	2.08	2.6E-04	P-loop containing nucleoside triphosphate hydrolases superfamily protein
AT4G24110	-	1.06	5.0E-01	2.51	5.2E-31	NADP-specific glutamate dehydrogenase
AT3G49110	PER33	1.75	5.3E-01	3.00	8.4E-04	Peroxidase 33
AT2G19210	-	1.30	5.3E-01	2.88	8.7E-06	Leucine-rich repeat transmembrane protein kinase protein
AT4G30140	CDEF1	1.08	5.4E-01	1.93	9.7E-04	GDSL-like Lipase/Acylhydrolase superfamily protein
AT3G09050	-	0.83	5.4E-01	1.69	1.9E-03	Uncharacterized protein
AT3G30580	-	1.17	6.0E-01	1.93	1.4E-02	Unknown protein
AT5G03668	-	0.89	6.4E-01	2.01	1.1E-03	NA
AT1G69572	-	0.76	6.5E-01	1.46	4.3E-02	NA

AT1G66783	MIR157A	1.18	6.6E-01	1.81	3.9E-02	NA
AT4G27440	PORB	0.59	7.1E-01	1.40	2.5E-02	Protochlorophyllide reductase B
AT4G39795	FLZ7	NA	NA	2.12	4.9E-02	Uncharacterized protein
AT4G29305	LCR25	NA	NA	4.69	3.9E-02	Low-molecular-weight cysteine-rich 25
AT3G45490	-	NA	NA	3.56	2.1E-02	Reverse transcriptase-like protein
AT1G15610	-	NA	NA	3.81	8.2E-03	Unknown protein
AT1G19530	-	NA	NA	4.79	7.8E-03	DNA polymerase epsilon catalytic subunit A
AT4G22630	-	NA	NA	3.80	7.3E-03	Bifunctional inhibitor/lipid-transfer protein/seed storage 2S albumin superfamily protein
AT5G22545	-	NA	NA	5.14	2.2E-03	Uncharacterized protein
AT1G22630	-	NA	NA	5.66	1.3E-03	Unknown protein
AT5G43650	BHLH92	NA	NA	6.03	2.2E-04	Basic helix-loop-helix (bHLH) DNA-binding superfamily protein
AT5G06775	-	NA	NA	6.25	1.3E-04	NA
AT2G29310	-	NA	NA	6.20	1.1E-04	NAD(P)-binding Rossmann-fold superfamily protein
AT1G75490	DREB2D	NA	NA	6.22	1.6E-05	Dehydration-responsive element-binding protein 2D
AT2G25370	-	NA	NA	7.07	1.0E-06	RING/U-box superfamily protein
AT5G52760	HIPP14	NA	NA	10.88	6.9E-18	Heavy metal-associated isoprenylated plant protein 14
AT3G60415	-	NA	NA	11.00	5.0E-18	Uncharacterized protein

**Tab. S6-9: 68 differentially expressed ROS related transcription factors in Pi-starved WT and *pdr2* and expression level of *PSK5* and *WOX5***

Gene ID	Gene name	WT -/+		<i>pdr2</i> -/+		Gene description
		log <sub>2</sub> FC	<i>p</i> -value	log <sub>2</sub> FC	<i>p</i> -value	
AT5G49520	WRKY48	3.30	7.9E-22	4.75	7.0E-89	Probable WRKY transcription factor 48
AT5G07310	ERF115	7.23	6.2E-06	9.28	1.3E-12	Ethylene-responsive transcription factor ERF115
AT1G25550	HHO3	0.84	1.9E-04	1.06	5.1E-07	Transcription factor HHO3
AT4G18170	WRKY28	3.65	3.6E-03	4.33	8.3E-27	WRKY transcription factor
AT4G18890	BEH3	0.70	5.5E-03	1.01	6.1E-07	BES1/BZR1 homolog protein 3
AT2G23320	WRKY15	0.75	8.7E-03	1.91	9.7E-28	Probable WRKY transcription factor 15
AT1G77640	ERF013	1.21	9.3E-03	2.39	5.3E-23	Ethylene-responsive transcription factor ERF013
AT3G23230	ERF098	4.48	1.3E-02	3.90	3.2E-04	Ethylene-responsive transcription factor ERF098
AT1G62300	WRKY6	0.57	1.4E-02	0.93	1.1E-11	Uncharacterized protein
AT1G80840	WRKY40	1.37	3.1E-02	2.32	1.1E-14	Probable WRKY transcription factor 40
AT5G22570	WRKY38	1.20	3.3E-02	2.68	1.4E-12	Probable WRKY transcription factor 38
AT5G61890	ERF114	5.65	8.3E-03	9.90	7.1E-15	Ethylene-responsive transcription factor ERF114
AT5G01380	GT-3A	1.53	5.8E-02	3.23	9.7E-30	Trihelix transcription factor GT-3a
AT4G01250	WRKY22	1.13	6.3E-02	1.55	3.8E-06	WRKY transcription factor 22
AT4G17490	ERF6	0.55	1.0E-01	1.74	2.1E-09	Ethylene-responsive transcription factor 6
AT1G51700	DOF1.7	1.98	1.2E-01	4.08	1.6E-29	Dof zinc finger protein DOF1.7
AT1G13260	RAV1	1.51	1.3E-01	1.15	4.2E-09	AP2/ERF and B3 domain-containing transcription factor RAV1
AT5G59820	ZAT12	0.58	1.3E-01	0.85	5.2E-05	Zinc finger protein ZAT12

AT4G23550	WRKY29	-1.26	1.3E-01	-2.00	1.0E-08	WRKY29
AT3G56400	WRKY70	0.99	1.5E-01	3.75	2.3E-10	Probable WRKY transcription factor 70
AT5G13080	WRKY75	1.15	1.7E-01	2.26	1.5E-09	WRKY75
AT3G46600	SCL30	0.38	2.0E-01	1.08	3.3E-09	Scarecrow-like protein 30
AT4G31800	WRKY18	0.71	2.3E-01	2.71	1.5E-55	WRKY like transcription factor
AT4G17230	SCL13	0.38	2.4E-01	0.82	6.7E-07	SCARECROW-like 13
AT2G46400	WRKY46	1.62	2.5E-01	5.68	2.0E-65	Probable WRKY transcription factor 46
AT4G18880	HSFA4A	0.66	2.8E-01	2.07	5.4E-23	HSF A4A
AT3G55980	SZF1	0.58	3.3E-01	1.74	4.0E-17	Salt-inducible zinc finger 1
AT2G42280	-	0.38	4.7E-01	0.71	1.1E-03	basic helix-loop-helix (bHLH) DNA-binding superfamily protein
AT2G44840	ERF13	1.04	5.0E-01	1.69	8.3E-05	Ethylene-responsive transcription factor 13
AT1G28370	ERF11	0.97	5.6E-01	1.46	1.1E-02	ERF domain protein 11
AT2G40140	CZF1	0.25	5.8E-01	1.20	2.6E-07	Zinc finger CCCH domain-containing protein 29
AT2G38470	WRKY33	0.35	5.9E-01	1.61	1.0E-18	WRKY33
AT2G26150	HSFA2	-0.41	6.3E-01	-2.65	3.4E-15	Heat stress transcription factor A-2
AT5G66730	ENY	0.16	6.6E-01	0.79	2.2E-08	IDD1
AT3G19290	ABF4	-0.25	6.8E-01	0.83	1.4E-05	ABRE binding factor 4
AT5G24590	NAC091	0.24	6.9E-01	0.80	5.3E-07	NAC domain-containing protein 91
AT4G17500	ERF1A	0.39	7.1E-01	1.90	5.5E-17	Ethylene-responsive transcription factor 1A
AT1G27730	ZAT10	0.44	7.3E-01	2.27	3.5E-22	Zinc finger protein ZAT10
AT5G47220	ERF2	0.79	7.7E-01	5.09	2.9E-31	ERF2
AT5G24110	WRKY30	0.66	7.7E-01	-1.84	7.9E-04	Probable WRKY transcription factor 30
AT1G67970	HSFA8	0.24	7.8E-01	1.13	3.6E-05	Heat stress transcription factor A-8
AT5G13790	AGL15	0.64	7.8E-01	1.40	2.2E-02	AGL15
AT5G64060	anac103	-0.28	7.8E-01	-1.41	9.3E-04	NAC domain containing protein 103
AT5G46350	WRKY8	0.56	7.9E-01	2.50	4.3E-13	WRKY transcription factor 8
AT1G74080	MYB122	-0.61	7.9E-01	2.92	3.0E-18	Transcription factor MYB122
AT1G01010	NAC001	-0.24	7.9E-01	0.79	2.9E-05	NAC domain-containing protein 1
AT4G36990	HSFB1	0.19	8.0E-01	0.73	2.6E-03	Heat stress transcription factor B-1
AT1G54330	ANAC020	0.36	8.1E-01	-1.31	3.6E-02	NAC domain containing protein 20
AT5G13330	ERF113	0.16	8.1E-01	1.61	2.8E-34	Rap2.6L
AT3G15500	NAC055	0.43	8.5E-01	1.51	1.0E-02	NAC3
AT4G36780	BEH2	0.11	8.5E-01	0.88	4.3E-07	BES1/BZR1 homolog 2
AT1G02220	NAC003	0.20	8.5E-01	1.17	4.3E-04	NAC domain-containing protein 3
AT2G33860	ARF3	-0.12	8.6E-01	-1.18	1.0E-07	Auxin response factor 3
AT1G18570	MYB51	0.22	8.9E-01	1.21	1.0E-08	Transcription factor MYB51
AT3G23250	MYB15	0.60	9.2E-01	2.65	4.6E-27	Transcription factor MYB15
AT2G46510	AIB	-0.11	9.5E-01	0.69	3.3E-02	Transcription factor ABA-INDUCIBLE bHLH-TYPE
AT3G15210	ERF4	0.14	9.6E-01	0.77	5.1E-05	Ethylene-responsive transcription factor 4
AT1G18860	WRKY61	-0.09	9.6E-01	-0.75	8.0E-03	WRKY DNA-binding protein 61
AT5G51190	ERF105	0.15	9.7E-01	2.65	1.8E-12	Ethylene-responsive transcription factor ERF105
AT2G31230	ERF15	0.07	9.7E-01	-1.02	4.3E-04	Ethylene-responsive transcription factor 15
AT3G49530	NAC062	0.04	9.7E-01	1.21	3.7E-18	NAC domain-containing protein 62



AT5G57150	-	-0.05	9.8E-01	0.93	7.0E-06	Basic helix-loop-helix (BHLH) DNA-binding superfamily protein
AT4G34410	ERF109	0.06	9.9E-01	1.27	2.9E-03	Ethylene-responsive transcription factor ERF109
AT3G01970	WRKY45	-0.04	9.9E-01	2.92	1.4E-14	Probable WRKY transcription factor 45
AT2G38250	GT-3B	-0.03	9.9E-01	2.14	1.3E-09	Trihelix transcription factor GT-3b
AT1G77920	TGA7	0.00	1.0E+00	0.67	1.5E-04	Transcription factor TGA7
AT3G44350	anac061	NA	NA	6.88	8.5E-07	NAC domain containing protein 61
AT2G47190	ATMYB2	NA	NA	4.52	1.1E-02	ATMYB2
AT3G23240	ERF1B	NA	NA	5.69	2.5E-03	Ethylene-responsive transcription factor 1B
AT3G11260	WOX5	2.50	2.7E-02	3.27	1.8E-09	WUSCHEL-related homeobox 5
AT5G65870	PSK5	1.64	6.7E-05	1.88	6.2E-09	Phytosulfokines 5

**Tab. S6-10: 42 predicted differentially expressed transcription factors in Pi-starved WT and *pdr2* that may regulate PRXs**

Gene ID	Gene name	WT -/+		<i>pdr2</i> -/+		Gene description
		log <sub>2</sub> FC	<i>p</i> -value	log <sub>2</sub> FC	<i>p</i> -value	
AT5G49520	WRKY48	3.30	7.9E-22	4.75	7.0E-89	Probable WRKY transcription factor 48
AT2G22430	ATHB-6	1.09	5.2E-13	1.34	5.7E-23	Homeobox-leucine zipper protein ATHB-6
AT3G16350	-	0.81	1.0E-04	1.03	6.9E-08	NA
AT1G69490	NAC029	1.91	1.1E-04	4.09	2.1E-36	NAC DOMAIN CONTAINING PROTEIN 29
AT1G62360	STM	6.40	3.0E-04	3.48	6.1E-04	Homeobox protein SHOOT MERISTEMLESS
AT1G25560	TEM1	0.67	1.8E-03	1.32	5.5E-12	AP2/ERF and B3 domain-containing transcription repressor TEM1
AT5G21120	EIL2	1.27	3.2E-03	0.95	2.3E-03	ETHYLENE-INSENSITIVE3-like 2
AT4G18170	WRKY28	3.65	3.6E-03	4.33	8.3E-27	WRKY transcription factor
AT2G47260	WRKY23	1.43	6.8E-03	3.17	1.9E-28	WRKY transcription factor 23
AT2G23320	WRKY15	0.75	8.7E-03	1.91	9.7E-28	Probable WRKY transcription factor 15
AT5G62940	DOF5.6	1.39	1.7E-02	1.50	4.3E-05	HCA2
AT5G28650	WRKY74	1.73	3.0E-02	2.24	9.6E-07	Probable WRKY transcription factor 74
AT1G80840	WRKY40	1.37	3.1E-02	2.32	1.1E-14	Probable WRKY transcription factor 40
AT5G22570	WRKY38	1.20	3.3E-02	2.68	1.4E-12	Probable WRKY transcription factor 38
AT4G36740	HB-5	-2.95	3.8E-02	-1.77	1.6E-01	homeobox protein 40
AT5G01380	GT-3A	1.53	5.8E-02	3.23	9.7E-30	Trihelix transcription factor GT-3a
AT4G01250	WRKY22	1.13	6.3E-02	1.55	3.8E-06	WRKY transcription factor 22
AT1G51700	DOF1.7	1.98	1.2E-01	4.08	1.6E-29	Dof zinc finger protein DOF1.7
AT1G13260	RAV1	1.51	1.3E-01	1.15	4.2E-09	AP2/ERF and B3 domain-containing transcription factor RAV1
AT3G56400	WRKY70	0.99	1.5E-01	3.75	2.3E-10	Probable WRKY transcription factor 70
AT2G34140	CDF4	0.70	1.6E-01	1.17	1.4E-04	Cyclic dof factor 4
AT5G13080	WRKY75	1.15	1.7E-01	2.26	1.5E-09	WRKY75
AT3G50410	DOF3.4	2.28	1.7E-01	4.53	4.8E-11	DOF PROTEIN 3.4
AT4G31800	WRKY18	0.71	2.3E-01	2.71	1.5E-55	WRKY like transcription factor
AT2G46400	WRKY46	1.62	2.5E-01	5.68	2.0E-65	Probable WRKY transcription factor 46
AT5G38140	NFYC10	-1.02	3.5E-01	1.38	2.5E-02	Nuclear transcription factor Y subunit C-10

AT5G66700	ATHB-53	1.53	5.4E-01	7.80	5.7E-23	Homeobox-leucine zipper protein ATHB-53
AT5G62430	CDF1	-0.66	5.8E-01	-1.02	3.6E-02	Cyclic dof factor 1
AT2G38470	WRKY33	0.35	5.9E-01	1.61	1.0E-18	WRKY33
AT4G04450	WRKY42	0.40	6.2E-01	1.39	3.0E-06	WRKY transcription factor 42
AT5G02460	DOF5.1	0.44	6.7E-01	-1.37	5.4E-03	Dof zinc finger protein DOF5.1
AT5G24110	WRKY30	0.66	7.7E-01	-1.84	7.9E-04	Probable WRKY transcription factor 30
AT5G46350	WRKY8	0.56	7.9E-01	2.50	4.3E-13	WRKY transcription factor 8
AT1G69570	CDF5	0.33	8.2E-01	1.10	4.6E-02	Cyclic dof factor 5
AT3G15500	NAC055	0.43	8.5E-01	1.51	1.0E-02	NAC DOMAIN CONTAINING PROTEIN 55
AT3G04070	NAC047	0.76	8.8E-01	1.41	1.4E-04	NAC DOMAIN CONTAINING PROTEIN 47
AT1G68640	PAN	0.13	9.0E-01	-1.81	5.7E-07	Transcription factor PERIANTHIA
AT5G12330	LRP1	0.11	9.4E-01	1.54	7.3E-10	Lateral root primordium (LRP) protein-related
AT3G50870	GATA18	0.10	9.4E-01	-2.71	1.7E-16	GATA transcription factor 18
AT3G52440	-	0.17	9.5E-01	-1.84	1.3E-02	Dof-type zinc finger DNA-binding family protein (Fragment)
AT2G37590	DOF2.4	0.10	9.6E-01	-1.13	2.8E-02	Dof zinc finger protein DOF2.4
AT3G01970	WRKY45	-0.04	9.9E-01	2.92	1.4E-14	Probable WRKY transcription factor 45

Tab. S6-11: Expression levels of 13 PIPs in WT, *pdr2* and *lpr1lpr2*

Gene ID	Gene name	WT -/+		<i>pdr2</i> -/+		<i>lpr1lpr2</i> -/+		FPKM average					
		log <sub>2</sub> FC	p-value	log <sub>2</sub> FC	p-value	log <sub>2</sub> FC	p-value	WT+	WT-	<i>pdr2</i> +	<i>pdr2</i> -	<i>lpr1lpr2</i> +	<i>lpr1lpr2</i> -
AT3G61430	<i>PIP1;1</i>	-0.42	1.5E-01	-0.44	3.6E-02	-0.14	1.0E+00	159	117	166	136	216	189
AT2G45960	<i>PIP1;2</i>	0.00	1.0E+00	-0.55	2.1E-05	-0.11	1.0E+00	490	479	491	374	584	527
AT1G01620	<i>PIP1;3</i>	0.40	8.2E-02	0.30	7.4E-02	0.22	1.0E+00	232	299	196	271	237	266
AT4G00430	<i>PIP1;4</i>	0.14	7.5E-01	-0.28	1.6E-01	0.03	1.0E+00	59	63	51	47	60	59
AT4G23400	<i>PIP1;5</i>	-0.14	7.7E-01	-0.82	2.7E-09	-0.03	1.0E+00	79	70	81	51	78	74
AT3G53420	<i>PIP2;1</i>	-0.06	9.6E-01	-0.05	8.7E-01	-0.20	1.0E+00	231	218	306	327	301	253
AT2G37170	<i>PIP2;2</i>	-0.08	9.0E-01	-0.18	3.7E-01	-0.18	1.0E+00	175	162	185	182	219	186
AT2G37180	<i>PIP2;3</i>	-0.13	9.0E-01	-0.74	1.0E-06	-0.23	1.0E+00	21	19	30	20	33	27
AT5G60660	<i>PIP2;4</i>	-0.72	1.4E-08	-1.33	3.8E-26	-0.10	1.0E+00	89	53	70	31	86	78
AT3G54820	<i>PIP2;5</i>	1.11	7.8E-01	0.67	5.1E-01	-0.35	1.0E+00	0	0	0	0	0	0
AT2G39010	<i>PIP2;6</i>	0.82	1.1E-03	-0.22	3.7E-01	0.07	1.0E+00	9	15	12	11	8	8
AT4G35100	<i>PIP2;7</i>	-0.07	9.1E-01	-1.17	6.4E-22	0.08	1.0E+00	504	471	462	230	501	514
AT2G16850	<i>PIP2;8</i>	0.26	6.6E-01	-1.60	3.7E-09	-0.01	1.0E+00	6	7	6	2	6	5

Tab. S6-12: Differentially expressed callose related genes in Pi-starved WT and *pdr2*

Gene ID	Gene name	WT -/+		<i>pdr2</i> -/+		<i>lpr1lpr2</i> -/+		Gene description
		log <sub>2</sub> FC	p-value	log <sub>2</sub> FC	p-value	log <sub>2</sub> FC	p-value	
AT1G05570	<i>CALS1</i>	-0.60	5.2E-02	0.52	3.3E-02	-0.23	1.0E+00	Callose synthase 1
AT2G31960	<i>CALS2</i>	-0.34	2.5E-01	0.32	7.3E-02	-0.14	1.0E+00	Callose synthase 2
AT5G13000	<i>CALS3</i>	-0.17	6.4E-01	0.32	1.6E-02	0.00	1.0E+00	Callose synthase 3
AT5G36870	<i>CALS4</i>	-1.02	7.4E-01	0.19	9.2E-01	0.32	1.0E+00	Callose synthase 4
AT2G13680	<i>CALS5</i>	0.51	8.3E-01	-0.70	3.9E-01	0.54	1.0E+00	Callose synthase 5
AT3G59100	<i>CALS6</i>	-0.32	6.1E-01	0.69	1.5E-03	-0.15	1.0E+00	Putative callose synthase 6

AT1G06490	<i>CALS7</i>	-0.27	8.1E-01	0.70	2.0E-03	-0.22	1.0E+00	Callose synthase 7
AT3G14570	<i>CALS8</i>	-0.51	2.3E-01	0.09	8.4E-01	-0.11	1.0E+00	Putative callose synthase 8
AT3G07160	<i>CALS9</i>	-0.31	3.4E-01	0.63	5.5E-06	-0.03	1.0E+00	Glucan synthase-like 10
AT2G36850	<i>CALS10</i>	-0.28	4.1E-01	0.32	1.4E-02	-0.06	1.0E+00	Callose synthase 10
AT4G04970	<i>CALS11</i>	-0.10	8.6E-01	-0.14	4.3E-01	-0.09	1.0E+00	Callose synthase 11
AT4G03550	<i>CALS12</i>	-0.09	8.5E-01	0.08	6.4E-01	-0.02	1.0E+00	Callose synthase 12
AT5G42100	<i>BG_PPAP</i>	0.15	6.9E-01	-0.28	4.0E-02	0.11	1.0E+00	Glucan endo-1,3-beta-glucosidase 10
AT5G43980	<i>PDLP1</i>	3.23	6.8E-05	3.79	2.3E-14	0.45	1.0E+00	Plasmodesmata-located protein 1
AT1G04520	<i>PDLP2</i>	0.08	8.8E-01	-0.79	2.2E-07	-0.04	1.0E+00	Plasmodesmata-located protein 2
AT2G33330	<i>PDLP3</i>	0.33	7.0E-01	0.69	3.8E-02	0.00	1.0E+00	Plasmodesmata-located protein 3
AT3G04370	<i>PDLP4</i>	NA	NA	1.62	5.4E-01	1.84	1.0E+00	Plasmodesmata-located protein 4
AT1G70690	<i>PDLP5</i>	-0.28	8.4E-01	-0.57	1.6E-01	0.35	1.0E+00	Plasmodesmata-located protein 5
AT2G01660	<i>PDLP6</i>	-0.48	5.7E-01	-0.31	3.9E-01	0.06	1.0E+00	Cysteine-rich repeat secretory protein
AT5G37660	<i>PDLP7</i>	-0.03	9.7E-01	-0.51	1.6E-03	-0.20	1.0E+00	Cysteine-rich repeat secretory protein
AT3G60720	<i>PDLP8</i>	-0.32	8.5E-01	0.72	1.5E-01	-0.06	1.0E+00	Plasmodesmata-located protein 8
AT5G61130	<i>PDCB1</i>	0.16	7.5E-01	-0.19	3.7E-01	0.17	1.0E+00	Plasmodesmata callose-binding
AT5G08000	<i>PDCB2</i>	4.78	1.2E-07	4.94	4.7E-12	3.40	1.0E+00	Plasmodesmata callose-binding
AT1G18650	<i>PDCB3</i>	0.56	2.3E-01	-0.05	9.2E-01	0.05	1.0E+00	Plasmodesmata callose-binding
AT1G69295	<i>PDCB4</i>	-0.01	9.9E-01	-0.35	1.1E-02	0.04	1.0E+00	Plasmodesmata callose-binding
AT3G58100	<i>PDCB5</i>	0.11	8.7E-01	-0.72	1.1E-03	0.31	1.0E+00	Plasmodesmata callose-binding
AT3G50770	<i>CML41</i>	-0.01	1.0E+00	7.26	1.2E-65	-0.27	1.0E+00	Probable calcium-binding protein

Tab. S6-13: Differentially expressed *TPS* and *TPP* in WT and *pdr2*

Gene ID	Gene name	WT -/+		<i>pdr2</i> -/+		Gene description
		log <sub>2</sub> FC	<i>p</i> -value	log <sub>2</sub> FC	<i>p</i> -value	
AT1G68020	<i>TPS6</i>	0.75	1.5E-02	1.47	5.1E-14	Trehalose-6-phosphatase synthase S6
AT1G70290	<i>TPS8</i>	1.66	1.9E-10	3.03	9.3E-46	Trehalose-6-phosphatase synthase S8
AT1G23870	<i>TPS9</i>	1.41	7.9E-08	1.65	2.9E-31	Trehalose-6-phosphatase synthase S9
AT2G18700	<i>TPS11</i>	1.56	4.4E-07	2.53	7.2E-59	Trehalose-6-phosphatase synthase 11
AT1G78090	<i>TPPB</i>	-0.21	8.8E-01	0.73	1.4E-03	Trehalose-6-phosphate phosphatase B
AT1G35910	<i>TPPD</i>	0.77	3.5E-01	5.27	1.1E-146	Trehalose-7-phosphate phosphatase D
AT2G22190	<i>TPPE</i>	NA	NA	2.96	2.6E-01	Trehalose-8-phosphate phosphatase E
AT4G22590	<i>TPPG</i>	1.10	1.8E-05	1.47	1.6E-12	Trehalose-9-phosphate phosphatase G
AT4G39770	<i>TPPH</i>	NA	NA	4.30	4.6E-04	Trehalose-10-phosphate phosphatase H
AT5G10100	<i>TPPI</i>	-1.07	4.7E-03	-1.74	1.3E-10	Trehalose-11-phosphate phosphatase I
AT5G65140	<i>TPPJ</i>	1.21	1.8E-04	2.75	6.4E-26	Trehalose-12-phosphate phosphatase J
AT4G24040	<i>TRE1</i>	1.30	7.5E-04	2.31	2.4E-26	Trehalase 1

Tab. S6-14: Expression levels of select local and systemic low Pi responsive genes in WT, *pdr2* and *lpr1lpr2*

Gene ID	Gene name	WT -/+		<i>pdr2</i> -/+		<i>lpr1lpr2</i> -/+		FPKM average					
		log <sub>2</sub> FC	<i>p</i> -value	log <sub>2</sub> FC	<i>p</i> -value	log <sub>2</sub> FC	<i>p</i> -value	WT +	WT -	<i>pdr2</i> +	<i>pdr2</i> -	<i>lpr1lpr2</i> +	<i>lpr1lpr2</i> -
AT5G23630	<i>PDR2</i>	-0.25	3.7E-01	-0.24	1.7E-01	0.01	1.0E+00	32.61	26.70	30.34	28.89	29.68	28.79
AT1G23010	<i>LPR1</i>	-0.46	3.8E-01	0.41	3.5E-01	-0.97	1.0E+00	3.06	2.16	2.97	4.32	0.39	0.20

AT1G71040	<i>LPR2</i>	0.63	8.7E-02	1.41	1.5E-15	-0.05	1.0E+00	3.09	4.66	3.57	10.57	0.54	0.51
AT1G34370	<i>STOP1</i>	0.14	6.7E-01	0.34	4.5E-02	-0.11	1.0E+00	53.89	57.83	60.90	85.81	60.38	54.18
AT1G08430	<i>ALMT1</i>	1.40	5.4E-01	2.92	2.4E-07	3.03	7.5E-05	0.18	0.47	0.30	2.56	0.21	1.66
AT1G08650	<i>PPCK1</i>	1.02	7.2E-06	0.11	6.9E-01	0.21	1.0E+00	34.83	68.24	31.45	38.21	35.86	40.18
AT3G04530	<i>PPCK2</i>	0.81	4.5E-01	1.04	2.2E-02	0.88	1.0E+00	0.71	1.21	0.90	2.06	0.76	1.32
AT5G20150	<i>SPX1</i>	3.09	5.9E-37	1.89	1.3E-22	2.06	1.8E-14	6.09	50.26	5.23	21.57	7.00	27.72
AT5G03545	<i>AT4</i>	4.09	1.2E-25	2.69	2.5E-15	4.14	1.2E-26	1.03	17.08	1.75	12.42	1.20	19.97
AT3G09922	<i>IPS1</i>	2.62	1.5E-01	2.01	5.0E-02	3.64	6.1E-04	0.25	1.46	0.47	2.03	0.32	3.67
AT1G25550	<i>HHO3</i>	0.84	1.9E-04	1.06	5.1E-07	0.06	1.0E+00	24.66	42.73	24.53	57.51	29.79	29.66
AT3G17790	<i>PAP17</i>	4.30	1.0E-07	2.44	6.5E-06	4.30	1.8E-30	0.47	8.85	0.73	4.35	0.36	6.74
AT1G68740	<i>PHO1-H1</i>	0.05	9.9E-01	1.37	3.1E-03	-0.09	1.0E+00	0.21	0.20	0.51	1.44	0.69	0.60
AT2G03240	<i>PHO1-H5</i>	0.33	4.9E-01	1.13	4.8E-17	-0.12	1.0E+00	7.42	9.00	8.07	19.86	7.42	6.55
AT1G26730	<i>PHO1-H7</i>	0.09	9.7E-01	1.85	9.3E-08	-0.34	1.0E+00	0.45	0.46	0.41	1.66	0.42	0.32
AT5G43370	<i>PHT1-2</i>	3.47	9.7E-06	0.65	6.3E-01	4.48	1.4E-17	0.18	1.92	0.13	0.22	0.21	4.41
AT2G38940	<i>PHT1-4</i>	1.38	1.8E-08	0.40	1.6E-01	1.15	2.8E-03	18.71	47.80	19.97	29.20	17.97	38.80
AT5G20380	<i>PHT4;5</i>	-0.47	5.8E-01	1.18	1.2E-03	-0.45	1.0E+00	1.92	1.34	1.71	4.34	2.14	1.50

**Tab. S6-15: KEGG pathway analysis of up- and down-regulated genes in Pi-starved WT**

Analysis of the upregulated genes			
KEGG pathway term	# of genes in upload list (288)	# of genes in genome (4727)	<i>P</i> value
Starch and sucrose metabolism	6	125	3.7E-03
Ascorbate and aldarate metabolism	4	41	4.8E-03
Plant hormone signal transduction	6	265	7.1E-02
Arginine and proline metabolism	3	53	7.3E-02
Analysis of the downregulated genes			
KEGG pathway term	# of genes in upload list (85)	# of genes in genome (4727)	<i>P</i> value
Cysteine and methionine metabolism	3	99	3.8E-02

**Tab. S6-16: GO-enrichment analysis of 218 genes that were upregulated in both WT and *pdr2* upon Pi limitation**

GO Biological process	# of genes in upload list (218)	# of genes in genome (18499)	<i>P</i> value
response to oxidative stress	13	291	6.0E-06
trehalose metabolism in response to stress	5	21	2.5E-05
trehalose biosynthetic process	5	25	5.1E-05
glutamine metabolic process	5	35	2.0E-04
response to absence of light	4	26	1.3E-03
ethylene-activated signaling pathway	7	179	3.9E-03
response to chitin	6	133	5.1E-03
response to wounding	7	199	6.5E-03
transcription, DNA-templated	27	1886	6.9E-03
regulation of transcription, DNA-templated	29	2119	8.9E-03

proline catabolic process	2	2	1.7E-02
proline catabolic process to glutamate	2	3	2.5E-02
defense response to bacterium	7	276	2.8E-02
response to water deprivation	7	279	2.9E-02
cellular response to sucrose starvation	2	4	3.3E-02
pyridoxal phosphate biosynthetic process	2	5	4.1E-02
vitamin B6 biosynthetic process	2	5	4.1E-02
glutamate biosynthetic process	2	5	4.1E-02

**Tab. S6-17: GO-enrichment analysis of 146 genes that were more highly induced in Pi-starved *pdr2* compared to WT**

GO Biological process	# of genes in upload list (146)	# of genes in genome (18499)	<i>P</i> value
trehalose metabolism in response to stress	5	21	6.32E-06
trehalose biosynthetic process	5	25	1.31E-05
response to oxidative stress	9	291	3.28E-04
response to absence of light	4	26	4.69E-04
glutamine metabolic process	4	35	1.14E-03
defense response to bacterium	7	276	5.88E-03
proline catabolic process	2	2	1.18E-02
transcription, DNA-templated	20	1886	1.38E-02
proline catabolic process to glutamate	2	3	1.76E-02
response to bacterium	4	102	2.24E-02
cellular response to sucrose starvation	2	4	2.34E-02
glutamate biosynthetic process	2	5	2.91E-02
response to sucrose	3	52	3.77E-02
regulation of transcription, DNA-templated	20	2119	4.05E-02

**Tab. S6-18: Primers used for genotyping**

LP, RP, F and R denotes left primer, right primer, forward and reverse primers, respectively. Unless otherwise indicated, the T-DNA border primer used is LBb1.3.

For T-DNA insertion line				
Gene name	Gene ID	T-DNA insertion line	Primer	5'→3' sequence
<i>PIP1;1</i>	AT3G61430	GABI_437B11	PIP1;1-F	CAGAGCTTTACAATTTCTCTCTACA
			PIP1;1-R	CACAGTGTTAGCTCCTCCTCT
			GABI_LB2	CCCATTTGGACGTGAATGTAGACAC
<i>PIP1;2</i>	AT2G45960	SALK_019794	PIP1;2-F	CTGGTTTCTCCGATCTAACGA
			PIP1;2-R	GCATTTTGATCCGATGTTACAA
			LBa1	GGTTCACGTAGTGGGCCATC
<i>PIP1;3</i>	AT1G01620	SALK_051107	LP-PIP1;3	TAACGTGGCCCATAAAGAGTG
			RP-PIP1;3	AATTGGTCTTTTGTTCATGC
			LBa1	GGTTCACGTAGTGGGCCATC
<i>PIP1;4</i>	AT4G00430	SAIL_808_A10	PIP1;4-F	TTGTTGATTCAATTCGGTCTGT
			PIP1;4-R	CTCAGCTATCCGGCTCTGT

## Appendix

			SAIL_L	TTCATAACCAATCTCGATACAC
<i>PIP1;5</i>	AT4G23400	SALK_056898	LP-PIP1;5	CTTGCTGCTCTGTACCATCAG
			RP-PIP1;5	GGGTTTTGTTTTGTATTGCAAG
<i>PIP2;1</i>	AT3G53420	SM_3_35928	PIP2;1-F	AACATATAACGTTGGCAAAAAaaa
			PIP2;1-R	TGGTTAAGACAGGGTTAGTCA
			dSpm1	CTTATTTAGTAAGAGTGTGGGGTTTTGG
<i>PIP2;2</i>	AT2G37170	SAIL_169_A03	primer pairs for verification on genomic DNA	
			PIP2;2-F	AAGTTATAGAAATGGCCAAAGAC
			PIP2;2-R	CTCAAACGTTGGCTGCACTTCTG
			primer pairs for identifying T-DNA insertion	
			SAIL_L	TTCATAACCAATCTCGATACAC
			SAIL_169A03-R	ACCGGAACGTGGGAGTCTC
<i>PIP2;3</i>	AT2G37180	SAIL_1215_D03	PIP2;3-F	GGAATCGCGGCAGAGATCA
			PIP2;3-R	GAAGAAAAAGTTGTCTTTCTC
			SAIL_L	TTCATAACCAATCTCGATACAC
<i>PIP2;4</i>	AT5G60660	SAIL_535_D05	LP-PIP2;4	AGCCGGATTTATATGACCACC
			RP-PIP2;4	TGGTGTAGACAAAGGATTGGC
<i>PIP2;5</i>	AT3G54820	SAIL_452H09	PIP2;5-F	CGAAGGAAGTGGTTGGTGATA
			PIP2;5-R	AGGCACTGAGCCACCATGTA
			SAIL_L	TTCATAACCAATCTCGATACAC
<i>PIP2;6</i>	AT2G39010	SALK_092140	PIP2;6-F	CTATCTCATCTGGATCAGCTGGTT
			PIP2;6-R	TACACACAAACCTCCCCACA
			LBa1	GGTTCACGTAGTGGGCCATC
<i>PIP2;7</i>	AT4G35100	CSHL_GT19652	PIP2;7-F	GCTGTGACTTTCGGTCTGTTC
			PIP2;7-R	AAACCAAAGGCAAACGATTAAC
			CSHL_Ds3-4	CCGTCCCGCAAGTTAAATATG
<i>PIP2;8</i>	AT2G16850	SALK_099098	PIP2;8-F	AAATACCTTTTTAGCAAGTTGG
			PIP2;8-R	AACTGGTTTGCAAAGTTTTACT
			LBa1	GGTTCACGTAGTGGGCCATC
<i>DIN10</i>	AT5G20250	SALK_066490C	LP-DIN10-1	TTGCTTCGAGCAGTAAAGAGC
			RP-DIN10-1	GAGAAATGGGCCGAGATATTC
<i>AER</i>	AT5G16970	SALK_005324C	LP-AER-1	TTGGATTGGCTACACAAAAC
			RP-AER-1	ATCAATTGGCAAAGTGGACTG
<i>GSTF6</i>	AT1G02930	SALK_026398	LP-GSTF6	CTCGAGCATCTAACGATCCAC
			RP-GSTF6	TGAACCAACTGGGTCAAATC
<i>ERD5</i>	AT3G30775	SALK_119334C	LP-ERD5-1	CGTGGGTCTAGAGCTCTAAAC
			RP-ERD5-1	TAAACGATTGGTCGGTCTTTG
<i>OZF1</i>	AT2G19810	SALK_151571C	LP-OZF1-1	TCACATCACCAGCACTTTACG
			RP-OZF1-1	GTTGTTGCAAGAGAGGAGACG
<i>SIP2</i>	AT3G57520	SALK_038166C	LP-SIP2-1	TCGAATTGTTGGCTAAGACG
			RP-SIP2-1	GCTTCAATTCCTCTCACCTC
<i>FSD1</i>	AT4G25100	SALK_029455	LP-FSD1-1	TTTGTGGTCTCCCAACAAC
			RP-FSD1-1	GTTGAAAGCAGGGAGGAGATC
<i>TPPD</i>	AT1G35910	SALK_120962C	LP-TPPD-1	CATAGGCAAAAACCTATTTCGC
			RP-TPPD-1	TGTCTTTCTCACACCAAACCC

<i>LPR1</i>	AT1G23010	SALK_016297	mod.lpr1_LP mod.lpr1_RP	CGGCGTGGTGGCGAAGAATAT GTCAGAAACACACACACACAC
<i>LPR2</i>	AT1G71040	SALK_091930	mod.lpr2_LP mod.lpr2_RP	GTGGTAAACATAGCCTGGCTC CCGGTTTGTAGGCTCTTACA
For other lines				
			Primer	5'→3' sequence
GFP			GFP_rev GFP_for	AAGTCGTGCTGCTTCATGTG ACGTAAACGGCCACAAGTTC
GUS			GUS L7 GUS R1791	CGTCCTGTAGAAACCCCAAC CGGTTTTTCACCGAAGTTCA
<i>pdr2</i>	AT5G23630		pdr2 LP (for dCAPS) pdr2 RP (for dCAPS)	TTATCCTTCTTTCATGATTCCAGGTGATGATAT TGA CTGCACCTGTAGGGGATG

## Supplementary methods

### 1. R script for Principal component analysis (PCA)

```
# set working directory and load data
setwd('P:/project/directions/RNA-seq/Results/data_processing/hcluster_PCA')
gene_exp <- read.table(file = 'P:/project/directions/RNA-
seq/Results/data_processing/hcluster_PCA/fpkm all samples.txt',
                      sep = '\t', header = T, row.names = 1)
sample_info <- read.table(file = 'P:/project/directions/RNA-
seq/Results/data_processing/hcluster_PCA/sample information.txt',
                          sep = '\t', header = T, row.names = 1)
#log2 transformation of data
##replace 0 with the minimum value in the data set
gene_exp_1 <- gene_exp
gene_exp_1[gene_exp_1==0] <- NA
gene_exp_1[is.na(gene_exp_1)] <- min(gene_exp_1,na.rm = T)
##log2 transformation
gene_exp_1 <- log2(gene_exp_1)

#PCA
install.packages("PCAtools")
library(PCAtools)
## PC analysis
```

```

p <- pca(gene_exp_1, metadata = sample_info, removeVar = 0.05, scale = T)
pca_loadings <- p$loadings
pca_rotated <- p$rotated
## Plot the result
screplot(p)
biplot(p,
  x= 'PC1',
  y= 'PC2',
  colby = 'genotype',
  shape = 'treatment',
  legendPosition = 'top')
## find out genes that influence PCs
plotloadings(p)

# save results
write.table(pca_loadings, file = "P:/project/directions/RNA-
seq/Results/data_processing/hcluster_PCA/pca_loadings.txt", sep = "\t")
write.table(pca_rotated, file = "P:/project/directions/RNA-
seq/Results/data_processing/hcluster_PCA/pca_rotated.xlsx", sep = "\t")
pca_rotated_3_columns <- pca_rotated[,1:3]
write.table(pca_rotated_3_columns, file = "P:/project/directions/RNA-
seq/Results/data_processing/hcluster_PCA/pca_rotated_3_columns.txt", sep = "\t")

```

Example tables used in the script:

“fpkm all samples.txt”

Table need to save as Text (Tab delimited) file.

gene_id	WT_P1	WT_nP1	WT_P2	WT_nP2	WT_P3	WT_nP3	pdr2_P1	pdr2_nP1	pdr2_P2	pdr2_nP2	pdr2_P3	pdr2_nP3	I112_P1	I112_nP1	I112_P2	I112_nP2	I112_P3	I112_nP3
AT3G56890	1.425375	1.173341	1.099193	1.470374	1.232845	1.301208	0.961464	0.878078	0.916671	0.687542	1.141658	1.200796	1.161702	0.311264	0.591403	0.385392	0.976371	1.090656
AT3G18870	0.909624	0.693319	1.794686	1.140344	0.600996	0.73812	1.43806	1.141471	1.051448	1.551189	1.655832	0.9391	0.921278	0.99319	0.366929	0.634379	0.649047	0.814056
AT3G59440	1.319997	1.293567	0.956701	1.891207	1.019376	1.090247	0.662487	1.677953	1.188938	1.51598	0.114422	1.245962	0.674071	0.823579	0.782401	0.91046	0.740035	0.126569
AT2G38823	0.676028	0.28984	0.471594	0.090803	0.365447	0.578567	1.692201	1.041139	1.358624	1.574855	1.230605	1.151591	1.721791	1.983734	1.88455	0.979201	0.22611	0.723167
AT4G19560	0.789847	0.884608	1.144922	1.121538	1.067437	0.978557	0.862197	0.839915	0.720318	1.236978	1.181046	1.642532	1.058778	1.078011	1.053372	0.490313	0.845374	1.050828
AT5G52900	0.736821	0.689247	0.985527	1.367573	0.724201	1.008953	0.988374	0.687737	0.791872	1.358496	0.914503	1.659704	0.861991	1.243337	1.250652	1.261305	0.573542	0.944153
AT5G60350	0.185681	0.655067	0.376815	0.718286	0.401501	0.101704	1.878722	3.202798	1.40486	3.094057	1.892822	2.300375	0.318596	0.081096	0.577808	0.215162	0.357722	0.299111
AT4G34345	0.410701	1.609911	0.625098	1.213629	2.109158	0.749848	0.97394	1.05419	1.16526	0.22512	1.214881	0.508812	0.550539	1.233188	1.491038	0.991475	1.318721	0.620244

“sample information.txt”

Table need to save as Text (Tab delimited) file.



sample	genotype	treatment
WT_P1	WT	+Pi
WT_nP1	WT	-Pi
WT_P2	WT	+Pi
WT_nP2	WT	-Pi
WT_P3	WT	+Pi
WT_nP3	WT	-Pi
pdr2_P1	pdr2	+Pi
pdr2_nP1	pdr2	-Pi
pdr2_P2	pdr2	+Pi
pdr2_nP2	pdr2	-Pi
pdr2_P3	pdr2	+Pi
pdr2_nP3	pdr2	-Pi
l1l2_P1	lpr1lpr2	+Pi
l1l2_nP1	lpr1lpr2	-Pi
l1l2_P2	lpr1lpr2	+Pi
l1l2_nP2	lpr1lpr2	-Pi
l1l2_P3	lpr1lpr2	+Pi
l1l2_nP3	lpr1lpr2	-Pi

## 2. Macro script for converting images into 8-bit images

```
// Select images folder
dir = getDirectory("Choose a Directory ");

// Folder management
getDateAndTime(year, month, dayOfWeek, dayOfMonth, hour, minute, second, msec);
MonthNames = newArray("Jan", "Feb", "Mar", "Apr", "May", "Jun", "Jul", "Aug", "Sep", "Oct", "Nov", "Dec");
DayNames = newArray("Sun", "Mon", "Tue", "Wed", "Thu", "Fri", "Sat");
if (hour<10) {hours = "0"+hour;}
else {hours=hour;}
if (minute<10) {minutes = "0"+minute;}
else {minutes=minute;}
if (month<10) {months = "0"+(month+1);}
else {months=month+1;}
if (dayOfMonth<10) {dayOfMonths = "0"+dayOfMonth;}
else {dayOfMonths=dayOfMonth;}
results_Dir = dir + "Results"+year+"-"+months+"-"+dayOfMonths+" "+hours+"h"+minutes+
File.separator;
File.makeDirectory(results_Dir);
// change image type and save as tiff
listdir = getFileList(dir);
var s = 0;
for (i = 0; i < listdir.length; i++) {
    if (endsWith(listdir[i], ".JPG")) {
```

```

        open(dir + listdir[i]);
        selectWindow(listdir[i]);
        run("8-bit");
        saveAs("tiff", results_Dir + listdir[i]);
        close();
    }}

```

### 3. Macro script for GRX1-roGPF2 images processing

```

// Select images folder
dir = getDirectory("Choose a Directory ");
time0 = getTime();
setBatchMode(true);
// Folder management
getDateAndTime(year, month, dayOfWeek, dayOfMonth, hour, minute, second, msec);
MonthNames = newArray("Jan", "Feb", "Mar", "Apr", "May", "Jun", "Jul", "Aug", "Sep", "Oct", "Nov", "Dec");
DayNames = newArray("Sun", "Mon", "Tue", "Wed", "Thu", "Fri", "Sat");
if (hour<10) {hours = "0"+hour;}
else {hours=hour;}
if (minute<10) {minutes = "0"+minute;}
else {minutes=minute;}
if (month<10) {months = "0"+(month+1);}
else {months=month+1;}
if (dayOfMonth<10) {dayOfMonths = "0"+dayOfMonth;}
else {dayOfMonths=dayOfMonth;}
results_Dir = dir + "Results"+year+"-"+months+"-"+dayOfMonths+" "+hours+"h"+minutes+
File.separator;
File.makeDirectory(results_Dir);
images_405_Dir = results_Dir + "Images 405" + File.separator;
File.makeDirectory(images_405_Dir);
images_488_Dir = results_Dir + "Images 488" + File.separator;
File.makeDirectory(images_488_Dir);
images_ratio_Dir = results_Dir + "ratio images" + File.separator;
File.makeDirectory(images_ratio_Dir);

```



```
open(images_488_Dir+list488[j]);  
Image2=getTitle();  
imageCalculator("Divide create 32-bit", Image1, Image2);  
saveAs("tiff", images_ratio_Dir + list405[h]+"vs"+list488[j]);  
}
```

## 7. ACKNOWLEDGEMENT

I would like to express my gratitude to many individuals who helped and supported me during my thesis process, which made this work possible.

First of all, I would like to express my deepest appreciation to Prof. Dr. Steffen Abel for giving me the opportunity to pursue my PhD in his lab. Without his invaluable supervision, suggestions, and support, I could not have undertaken this journey. I am very grateful to him for editing my thesis and for his patience with my writing.

Furthermore, I would like to express my sincere appreciation to the thesis assessors for investing their precious time to review my thesis. I also would like to extend my gratitude to the thesis committee for evaluating my PhD work.

I greatly acknowledge China Scholar Council (CSC) for funding my study in Germany. I would also like to thank MLU, Halle-Wittenberg and Deutscher Akademischer Austauschdienst (DAAD) for supporting me with PhD finalization grant.

I would like to thank Prof. Dr. Sabine Rosahl for accompanying and supporting me as my co-supervisor. Her guidance and suggestions have given me a lot of strength to face all the difficulties throughout my doctorate studies. I am also thankful to her for editing my thesis. Moreover, I would like to extend my sincere thanks to my research supervisor Dr. Christin Naumann for her constant support, encouragement, and discussions of my project. Many thanks to her for reading my thesis and providing feedback that helped in improving it.

Sincere thanks should also go to PD Dr. Anton R Schäffner for kindly sharing all the *pip* mutants and GUS/GFP lines, Dr. Khabat Vahabi for getting me started with RNA-seq data analysis and numerous supports during the analysis, Dr. Rainer Waadt for sharing the GRX1-roGFP seeds and plasmids, and for helping with the troubleshooting, Prof. Dr. Bettina Hause and Hagen Stellmach for the support with the GRX1-roGFP experiment setup and other technical support in microscopy.

I would like to thank each of my former and present colleagues and friends in the nutrient signaling group for their support. Special thanks to Dr. Jörg Ziegler for fruitful discussions and valuable advice that improved my scientific thinking and this thesis, Pinelopi for excellent corporation on the RNA-seq experiment and for accompanying and encouraging me all the time, Ranju for helping me whenever I

needed, Caro for the concern and support, Samuel for all the interesting discussions, Birgit for her kind help and care, Kathrin and Nancy for their help with experiments.

Many thanks to Dr. Debora Gasperini, Dr. Katharina Bürstenbinder, and Dr. Selma P. Gago Zachert for the helpful suggestions on my project and for sharing materials and protocols with me. Thanks should also go to every colleague from the MSV department for the discussions during my presentations and for the pleasant working atmosphere. I also want to thank Alexandra for helping me with all the paperwork.

I am grateful to all my friends for their company, encouragement, and help. Especially I want to thank Xiyuan, Jiejie, Yunjing, Lijie, and Mingming for always supporting me, giving me advice, sharing experience, and lifting my spirit up during the hard times of my PhD. I am so blessed to have them by my side.

Lastly, I want to send my deepest gratitude to my parents, brother, and sister-in-law for their love, understanding, and constant support, and for always believing in me. I also want to thank my lovely nephew for bringing me a lot of joy.

## 8. CURRICULUM VITAE

Name: Mingdan Deng  
 Nationality: Chinese  
 Date of birth: 08.05.1990  
 Gender: Female  
 Place of birth: Taiyuan, Shanxi, China  
 Email: mingdandeng@gmail.com  
 Current address: Bernburger Str. 18, 06108, Halle (saale)

### Education

2017-present	<b>PhD Candidate</b> Leibniz Institute of Plant Biochemistry, Halle (Saale) Dissertation thesis: Insights into the transcriptome and ROS signaling of Arabidopsis thaliana root tips during Pi deficiency response Supervisor: Prof. Dr. Steffen Abel
2014-2017	<b>Master of Agriculture (Horticulture)</b> Zhejiang University, Hangzhou, China Thesis: Studies on glucosinolate biosynthetic pathway genes and the regulation by postharvest light treatments in Chinese kale sprouts Supervisor: Prof. Dr. Qiaomei Wang
2009-2013	<b>Bachelor of Agriculture (Horticulture)</b> Shanxi Agricultural University, Shanxi, China Thesis: Observation and hormone regulation of the characteristics of stomas on jujube peel

### Conference attendances

14 <sup>th</sup> Plant Science Student Conference	IPK, Gatersleben, Germany, 19.-22.06.2018
15 <sup>th</sup> Plant Science Student Conference	IPB, Halle, Germany, 18.-21.06.2019

### List of publications

- 1) Cai C, Yuan W, Miao H, **Deng M**, Wang M, Lin J, Zeng W, Wang Q. Functional Characterization of BoaMYB51s as Central Regulators of Indole Glucosinolate Biosynthesis in Brassica oleracea var. alboglabra Bailey. *Frontiers in plant science*. 2018; 9: 1599. DOI: 10.3389/fpls.2018.01599.
- 2) **Deng M**, Qian H, Miao H, Cai C, Wang Q. Influence of pre-harvest red light irradiation on main phytochemicals and antioxidant activity of Chinese kale sprouts. *Food chemistry*. 2016; 222: 1-5. DOI: 10.1016/j.foodchem.2016.11.157
- 3) Qian H, Liu T, **Deng M**, Miao H, Cai C, Shen W, Wang Q. Effects of light quality on main health-promoting compounds and antioxidant capacity of Chinese kale sprouts. *Food chemistry*. 2015; 196:1230-1238. DOI: 10.1016/j.foodchem.2015.10.055

## 9. STATUTORY DECLARATION

### **Eidesstattliche Erklärung / *Declaration under Oath***

Ich erkläre an Eides statt, dass ich die Arbeit selbstständig und ohne fremde Hilfe verfasst, keine anderen als die von mir angegebenen Quellen und Hilfsmittel benutzt und die den benutzten Werken wörtlich oder inhaltlich entnommenen Stellen als solche kenntlich gemacht habe.

*I declare under penalty of perjury that this thesis is my own work entirely and has been written without any help from other people. I used only the sources mentioned and included all the citations correctly both in word or content.*

---

Datum / Date

---

Unterschrift des Antragstellers / Signature of the applicant